

Optimum delivery of topical actives and investigation of skin permeability assays

Yanling Zhang

December 2019

**Thesis submitted in accordance with the requirements of
UCL School of Pharmacy for the degree of Doctor of Philosophy**

UCL School of Pharmacy

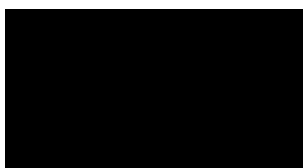
29-39 Brunswick Square

London

WC1N 1AX

Declaration

This thesis is based on the research performed in the School of Pharmacy, University College London between 2016 and 2019 under the supervision of Dr. Majella Lane and Prof. Michael Heinrich. I confirm the research described here is original. I also certify that I have written all the text herein and I have acknowledged the work of other people.



.....
Signature

.....
Date

Abstract

A wide range of actives target the skin for therapeutic or cosmetic purposes, and the stratum corneum (SC) is recognized as the major barrier to the percutaneous absorption of drugs and xenobiotics. *In vitro* skin penetration is usually assessed in human or animal tissue. However, there are ethical and practical concerns associated with sourcing these materials. Hence, a reliable, robust, more accessible and efficient surrogate for evaluating permeation behavior would be beneficial. Niacinamide is the amide form of vitamin B3 and its dermal application has been shown to improve skin conditions including melanogenesis, atopic dermatitis, ultraviolet-induced DNA damage, acne and inflammation. Phenylethyl resorcinol is a tyrosinase inhibitor and has been used in the personal care industry as a novel skin lightening ingredient. Rational formulations of both actives are desirable. In this work, followed by characterization, both model actives were initially formulated into simple solutions based on their physicochemical properties. The permeation behavior was investigated using porcine and human skin, and a recently developed Parallel Artificial Membrane Permeation Assay (PAMPA) model under varying dose conditions. The feasibility of the Skin PAMPA model for prediction of human skin permeability was confirmed under clinically relevant dose conditions. Binary and ternary solvent systems were subsequently developed and evaluated using the three models under finite dose conditions. Skin penetration enhancement was evident for binary systems composed of propylene glycol and fatty acids. Finally, *in vivo* studies using confocal Raman spectroscopy (CRS) and tape stripping were conducted on human subjects. *In vivo-in vitro* correlation in skin permeation was observed for niacinamide. Overall PAMPA demonstrated its potential as a screening tool for simple topical formulations. The efficacy of topical formulations was also demonstrated to be enhanced by a rational selection of solvents; CRS is proposed as a suitable method for evaluation of *in vivo* permeation kinetic studies.

Impact statement

To our knowledge, this was the first systematic characterization of phenylethyl resorcinol (PR). We reported its physicochemical properties, melting point, solubility and stability results. A new quantitative analysis method was developed and validated. The permeation behavior of PR in porcine skin and human skin was reported. Promising vehicles for maximum PR delivery to human skin were identified. These findings will benefit the researchers working in related fields in academia and the formulation scientists working in pharmaceutical and cosmetic industries.

There is limited information about the skin delivery and deposition of niacinamide (NIA) in human skin. In this work, a detailed analysis of NIA topical delivery was undertaken which will be valuable to researchers working in this field.

The applications of a recently developed skin permeability assay, parallel artificial membrane permeability assay (PAMPA) model was probed in this study. The appropriate experimental conditions were developed and confirmed. A good correlation was obtained for permeation data from the Skin PAMPA model and human skin under clinically relevant dose conditions. The results suggested that the Skin PAMPA model is a promising screening tool for simple solutions; potential interactions between the PAMPA membrane and certain excipients were evident. The findings add to our knowledge of the potential uses of Skin PAMPA for screening dermal/transdermal preparations. The results outlined in this work will be of interest to academic scientists as well as industrial scientists.

Confocal Raman spectroscopy (CRS) is a non-invasive approach which has been used to determine stratum corneum thickness and to profile endogenous skin components. However, the application of this technique in therapeutic equivalence tests of topical/transdermal products has not been fully explored. In this thesis, *in vivo* distribution of both actives and excipients was measured using CRS and a well-established tape stripping technique. The CRS data correlated well with the results obtained from tape stripping. A good *in vivo-in vitro* correlation was observed for skin uptake of NIA. We propose CRS as a non-invasive method for conducting permeation kinetic studies. These findings should deliver

considerable benefits for not only the personal care sector, the pharmaceutical industry, but also the government, patients and consumers.

Acknowledgements

This dissertation and my PhD project would not be possible without the generous support of so many people in so many ways. I would like to express my appreciation for all the help I have received in the acknowledgements.

First and foremost, my heartfelt gratitude goes to my PhD supervisor, Dr. Majella Lane. I sincerely thank her for giving me the opportunity to join the Skin Research Group and work on this exciting research project. Her patience, continuous support, warm encouragement, immense knowledge and guidance helped and inspired me throughout the time. I would like to extend my gratitude to Prof. Jonathan Hadgraft for giving insightful comments and constructive suggestions which enhanced this research project. I thank my second supervisor Prof. Michael Heinrich for his advice and feedback. This project was also made possible by support from Dr. Balint Sinko, and I would like to express my appreciation to him.

I want to thank my colleagues from the Skin Research Group, past and present, for keeping me company during these memorable years, with the special thanks to Dr. Miguel Paz Alvarez, Dr. Bruno Sil Dos Santos and Dr. Lin Luo. I also want to thank Dr. Nattika Nimmano, Ms Helena Yong, my cohorts and all my friends at UCL School of Pharmacy. They formed an important part of my life in London. Thanks also to all the MPharm and MSc students that I had the pleasure to supervise and to work with.

Finally, I would like to thank my families. I am very grateful to my parents for their unconditional support and nonstop love. They are the infinite strength behind me. There is a special person I need to thank. Ken, I would not be able to complete this journey without you. Thank you for being by my side and I cannot wait to start the new adventure with you. I also feel grateful to Ken's parents, for their support and everything. This thesis is dedicated to Ken and our families.

Table contents

Declaration.....	1
Abstract.....	2
Impact statement.....	3
Acknowledgements	5
Table contents	6
List of figures.....	11
List of tables	18
List of symbols and abbreviations	20
Chapter 1.....	21
Introduction.....	21
1.1 Structure of human skin.....	22
1.1.1 Hypodermis.....	23
1.1.2 Dermis	23
1.1.3 Epidermis.....	24
1.1.4 Stratum corneum.....	25
1.2 Skin permeation.....	26
1.3 Fick's diffusion law (physicochemical determinants of topical delivery)	27
1.4 Skin penetration enhancement	28
1.4.1 Passive enhancement strategies.....	28
1.4.1.1 Chemical penetration enhancers.....	28
1.4.1.2 Supersaturated systems.....	30
1.4.2 Physical enhancement strategies	30
1.4.2.1 Microneedle technology	30
1.4.2.2 Other physical methods	31
1.5 <i>In vitro</i> skin permeation assessment	32
1.5.1 Diffusion cells.....	32
1.5.2 Skin model membranes.....	33
1.5.3 The Skin Parallel Artificial Membrane Permeability Assay (PAMPA) model	35
1.5.4 Human skin equivalents (HSEs)	36
1.6 <i>In vivo</i> skin permeation assessment	36
1.6.1 Tape stripping and the measurement of transepidermal water loss (TEWL) ..	36
1.6.2 Confocal Raman spectroscopy (CRS).....	37
1.7 Model actives.....	38
1.7.1 Niacinamide.....	38
1.7.2 Phenylethyl resorcinol.....	39
1.8 Aims and objectives	41
Chapter 2.....	42
Development and evaluation of simple formulations of NIA using mammalian skin and the Skin PAMPA model	42
2.1 Introduction	43

2.2 Materials and methods	45
2.2.1 Development and validation of HPLC method of NIA	45
2.2.2 Solubility and stability studies of NIA	46
2.2.3 Preparation of NIA solutions	47
2.2.4 Dynamic vapour sorption (DVS) studies of single solvent formulations	47
2.2.5 Permeation studies of NIA from single solvent formulations using porcine skin	47
2.2.6 Permeation studies of NIA from single solvent formulations using human skin	50
2.2.7 The development of the Skin PAMPA method	50
2.2.8 Permeation studies using the Skin PAMPA model	52
2.2.9 Statistical analysis	52
2.3 Results and discussion	53
2.3.1 Development and validation of HPLC assay method of NIA.....	53
2.3.2 Solubility and stability studies of NIA	55
2.3.3 DVS.....	57
2.3.4 Permeation studies of NIA using porcine skin under infinite dose conditions	58
2.3.5 Permeation studies of NIA using porcine skin under finite dose conditions ..	61
2.3.6 Permeation studies of NIA using human skin under infinite dose conditions	63
2.3.7 Permeation studies of NIA in human skin under finite dose conditions	65
2.3.8 The development of the Skin PAMPA method for NIA.....	68
2.3.9 Permeation studies of NIA using the Skin PAMPA model.....	71
2.4 Conclusion	76
Chapter 3.....	78
Development and evaluation of simple formulations of PR using mammalian skin and the Skin PAMPA model	78
3.1 Introduction	79
3.2 Materials and methods	80
3.2.1 Materials	80
3.2.2 Methods.....	81
3.2.2.1 Development and validation of the HPLC method for PR.....	81
3.2.2.2 Solubility and stability studies of PR.....	81
3.2.2.3 LogP _(octanol/water) measurement	81
3.2.2.4 Thermal analysis.....	82
3.2.2.5 Preparation of PR solutions.....	82
3.2.2.6 Dynamic vapour sorption (DVS) studies	83
3.2.2.7 Permeation and mass balance studies of PR using porcine skin.....	83
3.2.2.8 Permeation and mass balance studies of PR using human skin.....	84
3.2.3.9 Permeation studies of PR using the Skin PAMPA model	84
3.2.3.10 Statistical analysis	85
3.3 Results and discussion	85
3.3.1 Development and validation of HPLC method for PR.....	85
3.3.2 Solubility and stability studies of PR	87

3.3.3 LogP _(octanol/water) measurement.....	89
3.3.4 Thermal analysis.....	89
3.3.5 DVS studies.....	90
3.3.6 Permeation and mass balance studies of PR in porcine skin under infinite dose conditions	91
3.3.7 Permeation and mass balance studies of PR in porcine skin under finite dose conditions	94
3.3.8 Permeation and mass balance studies of PR in human skin under finite dose conditions	97
3.3.9 Permeation studies of PR using the Skin PAMPA model.....	102
3.4 Conclusion	108
Chapter 4.....	110
<i>In vitro</i> evaluation of NIA from binary and ternary systems.....	110
4.1 Introduction	111
4.2 Materials and methods	112
4.2.1 Materials	112
4.2.2 Methods.....	112
4.2.2.1 Evaluation of binary vehicle formulations of NIA using the Skin PAMPA model.....	112
4.2.2.2 Evaluation of binary vehicle formulations of NIA in porcine skin.....	114
4.2.2.3 Evaluation of binary vehicle formulations of NIA in human skin.....	115
4.2.2.4 Evaluation of ternary vehicle formulations of NIA in the Skin PAMPA model and mammalian skin.....	115
4.3 Results and discussion.....	115
4.3.1 Evaluation of binary and ternary vehicle systems of NIA in the Skin PAMPA model	115
4.3.1.1 Binary vehicles of NIA composed of PG and other solvents in the Skin PAMPA model.....	115
4.3.1.2 Binary vehicles of NIA composed of TC and other solvents in the Skin PAMPA model.....	117
4.3.1.3 Binary vehicles composed of T-BA and other solvents in the Skin PAMPA model.....	119
4.3.1.4 Ternary formulations of NIA in the Skin PAMPA model.....	120
4.3.2 Evaluation of binary and ternary vehicle systems of NIA in porcine skin.....	122
4.3.2.1 Binary systems composed of PG and other solvents in porcine skin.....	122
4.3.2.2 Binary systems composed of TC and other solvents.....	125
4.3.2.3 Binary systems composed of T-BA and other solvents.....	126
4.3.2.4 Ternary systems of NIA evaluated in porcine skin.....	128
4.3.2.5 Comparisons of NIA binary and ternary vehicles in the Skin PAMPA model and porcine skin	130
4.3.3 Evaluations of binary and ternary systems for NIA in human skin	132
4.3.3.1 Binary vehicle systems composed of PG and other solvents.....	132
4.3.3.2 Binary systems composed of TC/T-BA and other solvents.....	135
4.3.3.3 Ternary vehicle systems of NIA	137

4.3.3.4 Comparisons of NIA binary and ternary vehicle formulations in the Skin PAMPA model and human skin	139
4.4 Conclusions	141
Chapter 5.....	143
<i>In vitro</i> evaluation of PR from binary and ternary solvent systems.....	143
5.1 Introduction	144
5.2 Materials and methods	145
5.2.1 Materials	145
5.2.2 Methods.....	145
5.2.2.1 Evaluation of binary vehicle formulations of PR using the Skin PAMPA model.....	145
5.2.2.2 Evaluation of binary formulations of PR in porcine skin.....	145
5.2.2.3 Evaluation of binary vehicle formulations of PR in human skin	146
5.2.2.4 Evaluation of ternary vehicle formulations of PR using the Skin PAMPA model and mammalian skin.....	146
5.3 Results and discussion.....	146
5.3.1 Evaluation of PR in the Skin PAMPA model	146
5.3.2.1 Binary systems of PR composed of PG and other solvents.....	146
5.3.3.2 Binary systems of PR composed of TC or DMI and other solvents	148
5.3.3.2 Ternary systems of PR composed of TC, PG and IPM.....	149
5.3.2 Evaluation of PR in porcine skin	151
5.3.2.1 Binary systems of PR composed of PG and other solvents.....	151
5.3.2.2 Binary systems of PR composed of TC or DMI and other solvents	152
5.3.2.3 Ternary systems of PR composed of TC, PG and IPM.....	154
5.3.2.4 Comparison of PR permeation from binary and ternary systems in the Skin PAMPA model and porcine skin.....	156
5.3.3 Evaluation of binary and ternary systems of PR in human skin.....	157
5.3.3.1 Binary systems of PR evaluated in human skin.....	157
5.3.3.2 Ternary systems of PR composed of PG, TC and IPM.....	160
5.3.3.3 Comparison of PR permeation from binary and ternary systems in the Skin PAMPA model and mammalian skin	161
5.4 Conclusions.....	163
Chapter 6.....	164
<i>In vivo</i> evaluation of NIA and PR formulations	164
6.1 Introduction	165
6.2 Materials and methods	166
6.2.1 Materials	166
6.2.2 Volunteer recruitment.....	166
6.2.3 Confocal Raman spectroscopy (CRS) studies.....	167
6.2.3.1 Confocal Raman spectroscopy.....	167
6.2.3.2 Preparation of standards and reference spectra.....	169
6.2.3.3 <i>In vivo</i> determination of water profile for human skin	169
6.2.3.4 Preparation of formulations and <i>in vivo</i> evaluation of skin penetration	170

6.2.3.5 Data analysis.....	171
6.2.4 Tape stripping.....	172
6.2.4.1 Tape stripping studies.....	172
6.2.4.2 Trans Epidermal Water Loss (TEWL) and SC protein content measurement	172
6.3 Results and discussion.....	173
6.3.1 Confocal Raman spectroscopy studies	173
6.3.1.1 Model actives and vehicle reference spectra	173
6.3.1.2 Stratum corneum thickness determined using CRS.....	176
6.3.1.3 <i>In vivo</i> evaluation of NIA using CRS.....	176
6.3.1.4 <i>In vivo</i> evaluation of solvents in NIA formulations using CRS.....	178
6.3.1.5 <i>In vivo</i> evaluation of PR using CRS	182
6.3.1.6 <i>In vivo</i> evaluation of solvents in PR formulations using CRS	184
6.3.2 Tape stripping studies.....	189
6.3.2.1 Stratum corneum thickness.....	189
6.3.2.2 <i>In vivo</i> permeation of NIA evaluated using tape stripping	190
6.3.2.3 <i>In vivo</i> permeation of PR evaluated using tape stripping.....	192
6.3.3 <i>In vivo</i> - <i>in vitro</i> correlation in skin permeation	194
6.4 Conclusions.....	197
Chapter 7.....	199
Conclusions and future work.....	199
7.1 Conclusions.....	200
7.2 Future work	203
Appendices.....	204
Appendix 1. TEWL measurement of porcine skin after the application of T-BA.....	205
Appendix 2. DVS measurement of TC under infinite dose conditions.....	206
Appendix 3. Miscibility determination of binary and ternary vehicle systems	207
Appendix 4. Consent form used in the <i>in vivo</i> study	209
References.....	212

List of figures

Figure 1. 1 Cross-section of human skin adapted from Benson (2005).....	22
Figure 1. 2 Schematic representation of the structure of human epidermis. Adapted from Gould (2018)	24
Figure 1. 3 Schematic representation of the possible penetration pathways through the stratum corneum (Hadgraft and Lane, 2011). Route 1 (highlighted in red) represents the possible transappendageal pathway; route 2 (highlighted in blue) shows the transcellular pathway and route 3 (highlight in orange) illustrates the intercellular pathway.....	27
Figure 1. 4 Vertical Franz diffusion cell used in the present work.	33
Figure 1. 5 Schematic diagram of the Skin PAMPA system. The donor compartment (A), applied formulations (B), pre-coated lipid membrane (C), receptor phase (D), individual stirrer (E) and the receptor plate (F) are indicated in the figure.	35
Figure 1. 6 The structure of PR.....	40
Figure 2. 1 Schematic view of vertical Franz diffusion cell. The donor compartment (A), skin membrane (B), and the receptor compartment (C) are indicated in the figure.	49
Figure 2. 2 Schematic view of the Skin PAMPA system. The donor compartment (A), formulations (B), pre-coated lipid membrane (C), receptor phase (D), individual stirrer (E) and the receptor plate (F) are indicated in the figure.	51
Figure 2. 3 The calibration curve for NIA	55
Figure 2. 4 The stability of NIA in a series of tested solvents (mean \pm SD, n=3).	57
Figure 2. 5 Percentage weight loss over 1440 min for 5 % (w/v) NIA in PG, DMI, TC, T-BA, PEG 400 and PEG 600 (n=3, mean \pm SD).	58
Figure 2. 6 Permeation profiles of NIA from Olay [®] , T-BA, PG, TC and DMI in porcine skin following the application of 50 $\mu\text{L}/\text{cm}^2$. Each data point represents the mean \pm SD, $3 \leq n \leq 5$	60
Figure 2. 7 Percent of NIA permeated from Olay [®] , T-BA, PG, TC and DMI in porcine skin following the application of 50 $\mu\text{L}/\text{cm}^2$. Each data point represents the mean \pm SD, $3 \leq n \leq 5$	60
Figure 2. 8 Permeation profiles of NIA that permeated from Olay [®] , T-BA, PG, TC and DMI in porcine skin following the application of 5 $\mu\text{L}/\text{cm}^2$. Each data point represents the mean \pm SD, $3 \leq n \leq 5$	62
Figure 2. 9 Percentages of NIA that permeated from Olay [®] , T-BA, PG, TC and DMI in porcine skin following the application of 5 $\mu\text{L}/\text{cm}^2$. Each data point represents the mean \pm SD, $3 \leq n \leq 5$	62
Figure 2. 10 Permeation profiles of NIA that permeated from Olay [®] , T-BA, PG, TC and DMI in human skin following the application of 50 $\mu\text{L}/\text{cm}^2$ of formulations. Each data point represents the mean \pm SD, $3 \leq n \leq 5$	64
Figure 2. 11 Percentages of NIA that permeated from Olay [®] , T-BA, PG, TC and DMI in	

human skin following the application of 50 $\mu\text{L}/\text{cm}^2$ of formulations. Each data point represents the mean \pm SD, $3 \leq n \leq 5$	64
Figure 2. 12 Permeation profiles of NIA from Olay [®] , T-BA, PG, TC and DMI in human skin following the application of 5 $\mu\text{L}/\text{cm}^2$ of formulations. Each data point represents the mean \pm SD, $3 \leq n \leq 5$	66
Figure 2. 13 Percentages of NIA that permeated from Olay [®] , T-BA, PG, TC and DMI in human skin following the application of 5 $\mu\text{L}/\text{cm}^2$ of formulations. Each data point represents the mean \pm SD, $3 \leq n \leq 5$	66
Figure 2. 14 The PAMPA permeation profiles of NIA from DMI, PG, Olay [®] , PEG 400 and PEG 600 following the application of 1 μL of formulation. Each data point represents the mean \pm SD, $n=6$	69
Figure 2. 15 The percentage permeation of NIA from DMI, PG Olay, PEG 400 and PEG 600 following the application of 1 μL of formulation. Each data point represents the mean \pm SD, $n=6$	69
Figure 2. 16 PAMPA permeation profiles of NIA from DMI, PG, Olay [®] , PEG 400 and PEG 600 following the application of 17 μL of formulation. Each data point represents the mean \pm SD, $n=6$	70
Figure 2. 17 Percentage NIA permeation from DMI, PG Olay, PEG 400 and PEG 600 following the application of 17 μL of formulation. Each data point represents the mean \pm SD, $n=6$	71
Figure 2. 18 PAMPA permeation profiles of NIA from T-BA, TC, DMI, PG, Olay [®] , PEG 400 and PEG 600 following the application of 1 μL of formulation. Each data point represents the mean \pm SD, $n=4$	72
Figure 2. 19 The percentage permeation of NIA from TC, T-BA, DMI, PG, Olay, PEG 400 and PEG 600 following the application of 1 μL of formulation. Each data point represents the mean \pm SD, $n=4$	73
Figure 2. 20 PAMPA permeation profiles of NIA from T-BA, TC, DMI, PG, Olay [®] , PEG 400 and PEG 600 following the application of 30 μL . Each data point represents the mean \pm SD, $n=4$	74
Figure 2. 21 The percentage of NIA permeation from TC, T-BA, DMI, PG, Olay, PEG 400 and PEG 600 following the application of 30 μL of formulation. Each data point represents the mean \pm SD, $n=4$	75
Figure 2. 22 Correlations between the cumulative amounts of NIA that permeated through (A) porcine skin and the Skin PAMPA model and (B) human skin and the Skin PAMPA model under finite dose conditions.....	76
Figure 3. 1 The calibration curve for PR	86
Figure 3. 2 The stability of PR in various solvents at 32 ± 1 °C (mean \pm SD, $n=3$).	89
Figure 3. 3 TGA analysis of PR.	90
Figure 3. 4 DSC analysis of PR.	90
Figure 3. 5 Percentage weight loss over 1440 min for 1 % PR in PG, DMI, glycerol, OSaI, IPM, TC and PEG 400 ($n=3$, mean \pm SD).	91
Figure 3. 6 The permeation profiles of PR in porcine skin from DMI, OSaI, IPM, PG, glycerol, TC and PEG 400 following the application of 50 $\mu\text{L}/\text{cm}^2$ of solution (mean	

± SD, 4 ≤ n ≤ 5).....	92
Figure 3. 7 The percentage permeation of PR in porcine skin from DMI, OSaI, IPM, PG, glycerol, TC and PEG 400 following the application of 50 μL/cm ² of solution (mean ± SD, 4 ≤ n ≤ 5).....	93
Figure 3. 8 The permeation profiles of PR in porcine skin from OSaI, IPM, DMI, PG, glycerol, TC and PEG 400 following the application of 5 μL/cm ² of solution (mean ± SD, 3 ≤ n ≤ 5).....	95
Figure 3. 9 The percentage permeation of PR in porcine skin from DMI, OSaI, IPM, PG, glycerol, TC and PEG 400 following the application of 5 μL/cm ² of solution (mean ± SD, 3 ≤ n ≤ 5).....	96
Figure 3. 10 The permeation profiles of PR in human epidermis from PG, IPM, OSaI, DMI, TC and glycerol following the application of 5 μL/cm ² of solution (mean ± SD, 3 ≤ n ≤ 5).....	98
Figure 3. 11 The percentage permeation of PR in human epidermis from PG, IPM, OSaI, DMI, TC and glycerol following the application of 5 μL/cm ² of solution (mean ± SD, 3 ≤ n ≤ 5).....	99
Figure 3. 12 The permeation profiles of PR from OSaI, DMI, IPM, glycerol, PG, TC and PEG 400 in the Skin PAMPA model following application of 30 μL of formulation per well, corresponding to 90 μL/cm ² (mean ± SD, n=5).	102
Figure 3. 13 The percentage permeation of PR from OSaI, DMI, IPM, glycerol, PG, TC and PEG 400 in the Skin PAMPA model following application of 30 μL of formulation per well, corresponding to 90 μL/cm ² (mean ± SD, n=5).	103
Figure 3. 14 The permeation profiles of PR from OSaI, DMI, IPM, glycerol, PG, TC and PEG 400 in the Skin PAMPA model following application of 17 μL of formulation per well, corresponding to 51 μL/cm ² (mean ± SD, n=5).	104
Figure 3. 15 The percentage permeation of PR from OSaI, DMI, IPM, glycerol, PG, TC and PEG 400 in the Skin PAMPA model following application of 17 μL of formulation per well, corresponding to 51 μL/cm ² (mean ± SD, n=5).	105
Figure 3. 16 The permeation profiles of PR from OSaI, DMI, IPM, glycerol, PG, TC and PEG 400 in the Skin PAMPA model following application of 1 μL of formulation per well, corresponding to 3 μL/cm ² (mean ± SD, n=5).	106
Figure 3. 17 The percentage permeation of PR from OSaI, DMI, IPM, glycerol, PG, TC and PEG 400 through the Skin PAMPA model following application of 1 μL of formulation per well, corresponding to 3 μL/cm ² (mean ± SD, n=5).	107
Figure 3. 18 Correlations between the cumulative amounts of PR that permeated in human skin and the Skin PAMPA model under finite dose conditions.....	108
 Figure 4. 1 Permeation profiles of NIA from seven binary vehicles containing PG as the primary solvent in the Skin PAMPA model (mean ± SD, n=5).	116
Figure 4. 2 Percentage permeation of NIA from seven binary PG vehicles in the Skin PAMPA model (mean ± SD, n=5).	117
Figure 4. 3 Permeation profiles of NIA from six binary vehicles containing TC as the primary solvent in the Skin PAMPA model (mean ± SD, n=5).	118
Figure 4. 4 Percentage permeation of NIA from six TC binary vehicles in the Skin PAMPA	

model (mean \pm SD, n=5).....	118
Figure 4. 5 The permeation profiles of NIA from nine binary vehicles containing T-BA in the Skin PAMPA model (mean \pm SD, n=5).	120
Figure 4. 6 Percentage permeation of NIA from nine T-BA binary vehicle formulations in the Skin PAMPA model (mean \pm SD, n=5).	120
Figure 4. 7 Permeation profiles of NIA from ternary vehicles in the Skin PAMPA model (mean \pm SD, n=5).	121
Figure 4. 8 Percentage permeation of NIA from ternary vehicles in the Skin PAMPA model (mean \pm SD, n=5).....	122
Figure 4. 9 Permeation profiles of NIA in porcine skin from binary systems composed of PG with other solvents or PG alone (mean \pm SD, n=4).	123
Figure 4. 10 Percentage permeation of NIA in porcine skin from binary systems composed of PG with other solvents and PG alone (mean \pm SD, n=4).....	123
Figure 4. 11 Permeation profiles of NIA in porcine skin for binary vehicles composed of TC with other solvents or TC alone (mean \pm SD, n=4).	125
Figure 4. 12 Percentage permeation of NIA in porcine skin from binary systems composed of TC with other solvents or TC alone (mean \pm SD, n=4).	126
Figure 4. 13 Permeation profiles of NIA in porcine skin for binary vehicles composed of T-BA and other solvents or neat T-BA (mean \pm SD, $4 \leq n \leq 5$).....	127
Figure 4. 14 Percentage permeation of NIA in porcine skin from binary systems composed of T-BA and other solvents or neat T-BA (mean \pm SD, $4 \leq n \leq 5$).....	127
Figure 4. 15 Permeation profiles of NIA from ternary systems in porcine skin (mean \pm SD, n=4).	129
Figure 4. 16 Percentage permeation of NIA from ternary systems in porcine skin (mean \pm SD, n=4).	129
Figure 4. 17 Correlations between the cumulative amounts of NIA that permeated in porcine skin and the Skin PAMPA model from binary and ternary solvent systems.	132
Figure 4. 18 Permeation profiles of NIA in human skin for the binary vehicles composed of PG with other solvents or neat PG (mean \pm SD, n=4).	133
Figure 4. 19 Percentage permeation of NIA from the binary vehicles composed of PG with other solvents or neat PG (mean \pm SD, n=4).....	133
Figure 4. 20 Permeation profiles of NIA in human skin for binary vehicles composed of TC or T-BA with other solvents or neat TC or T-BA (mean \pm SD, n=4).....	136
Figure 4. 21 Percentage permeation of NIA in human skin for binary vehicles composed of TC/T-BA with other solvents or neat TC/T-BA (mean \pm SD, n=4).	137
Figure 4. 22 Permeation profiles of NIA from ternary solvent systems in human skin (mean \pm SD, n=4).	138
Figure 4. 23 Percentage permeation of NIA from ternary solvent systems in human skin (mean \pm SD, n=4).	138
Figure 4. 24 Correlations between the cumulative amounts of NIA that permeated through human skin and the Skin PAMPA model from binary and ternary solvent systems (mean \pm SD, $4 \leq n \leq 5$).	141

Figure 5. 1 The permeation profiles of PR from binary systems composed of PG and other solvents in the Skin PAMPA model (mean \pm SD, n=5).....	147
Figure 5. 2 Percentage permeation of PR from binary systems composed of PG and other solvents in the Skin PAMPA model (mean \pm SD, n=5).....	147
Figure 5. 3 The permeation profiles of PR from the binary systems composed of TC or DMI with other solvents in the Skin PAMPA model (mean \pm SD, n=5).....	148
Figure 5. 4 Percentage permeation of PR from the binary systems composed of TC or DMI with other solvents in the Skin PAMPA model (mean \pm SD, n=5).....	149
Figure 5. 5 Permeation profiles of PR from ternary systems composed of TC, PG and IPM in the Skin PAMPA model (mean \pm SD, n=5).....	150
Figure 5. 6 Percentage permeation of PR from ternary vehicle systems composed of TC, PG and IPM in the Skin PAMPA model (mean \pm SD, n=5).....	150
Figure 5. 7 The permeation profiles of PR from binary systems composed of PG and other solvents in porcine skin (mean \pm SD, n=4).....	151
Figure 5. 8 Percentage permeation of PR from binary systems composed of PG and other solvents in porcine skin (mean \pm SD, n=4).....	152
Figure 5. 9 The permeation profiles of PR from binary systems composed of TC or DMI and other solvents in porcine skin (mean \pm SD, n=4).....	153
Figure 5. 10 Percentage permeation of PR from binary systems composed of TC or DMI and other solvents in porcine skin (mean \pm SD, n=4).....	154
Figure 5. 11 Permeation profiles of PR from ternary systems in porcine skin (mean \pm SD, n=4).....	155
Figure 5. 12 Percentage permeation of PR from ternary systems in porcine skin (mean \pm SD, n=4).....	155
Figure 5. 13 The permeation profiles of PR from binary systems in human skin (mean \pm SD, n=4).....	158
Figure 5. 14 Percentage permeation of PR from binary systems in human skin (mean \pm SD, n=4).....	158
Figure 5. 15 Permeation profiles of PR from ternary systems in human skin (mean \pm SD, n=4).....	160
Figure 5. 16 Percentage permeation of PR from ternary systems in human skin (mean \pm SD, n=4).....	161
Figure 6. 1 Schematic representation of <i>in vivo</i> confocal Raman spectroscopy measurements on the skin. Laser light (NIR) is focused on a small spot at the selected depth below the skin surface. The location of the laser focus in the skin can be varied to investigate the local chemical composition at various depths in the stratum corneum. The figure was adapted and modified from Caspers et al. (2000).	168
Figure 6. 2 Raman spectrum of 5 % w/v NIA in water (spectrum A); Raman spectrum of water (spectrum B); created difference spectrum of NIA (spectrum C), this reference spectrum was used as an additional model spectrum.	173
Figure 6. 3 Raman spectrum of 5 % w/v PR in EtOH: water (50:50) (spectrum A); Raman	

spectrum of EtOH: water (50:50) (spectrum B); created difference spectrum of PR (spectrum C), this reference spectrum was used as an additional model spectrum.	175
Figure 6. 4 Raman spectra of PG, TC, LA, OA, DMI, CCT, OSal and IPM using an exposure time of 60 s. The spectra were averaged by 3 frames.	176
Figure 6. 5 NIA depth profiles in the stratum corneum after application of five tested solutions, namely PG, TC, PG:OA, PG:LA and TC:CCT:DMI. (mean \pm SD, n=6).	177
Figure 6. 6 Averaged AUC for NIA depth profiles for six volunteers after application of five tested solutions, namely PG, TC, PG:OA (oleic acid), PG:LA (linolenic acid) and TC:CCT:DMI. (mean \pm SD, 18 \leq n \leq 26).	178
Figure 6. 7 The depth profile of NIA (A) and PG (B) in the SC after application of NIA in neat PG.	179
Figure 6. 8 Correlation between the signal intensity of NIA and signal intensity of PG in the SC with depth (x/h=1, 0.9, 0.8, 0.7, 0.6, 0.5, 0.4, 0.3, 0.2, 0.1 and 0).	179
Figure 6. 9 The depth profiles of NIA (A), PG (B) and LA (C) in the SC after the application of binary PG:LA (50:50) systems.	180
Figure 6. 10 The depth profiles of NIA (A), PG (B) and OA (C) in the SC after the application of binary PG:OA (10:90) systems.	181
Figure 6. 11 The depth profiles of NIA (A) and TC (B) in the SC after the application of neat TC; The depth profiles of NIA (C) and TC (D) in the SC 1 h after the application of ternary TC:CCT:DMI (50:25:25) solution.	182
Figure 6. 12 PR depth profiles in the skin 1 h post application of five systems, namely PG, TC, OSal, TC:IPM (50:50) and PG:TC:IPM (50:25:25). (mean \pm SD, n=6).	183
Figure 6. 13 Averaged AUC for PR depth profiles measured for each volunteer after application of five systems containing 5 % (w/v) of PR, namely neat PG, TC, OSal, TC:IPM (50:50) and PG:TC:IPM (50:25:25) (mean \pm SD, 18 \leq n \leq 24).	184
Figure 6. 14 The depth profile of PR (A) and PG (B) in the SC after application of PR in neat PG solutions.	185
Figure 6. 15 Correlation between the signal intensity of PR and signal intensity of PG in the SC with depth (x/h=1, 0.9, 0.8, 0.7, 0.6, 0.5, 0.4, 0.3, 0.2, 0.1 and 0).	185
Figure 6. 16 The depth profiles of PR (A) and TC (B) in SC after the application of PR in neat TC solutions.	186
Figure 6. 17 The depth profile of PR (A) and OSal (B) in the SC after the application of neat OSal formulations (mean \pm SD, n=6).	187
Figure 6. 18 The depth profiles of PR (A), IPM (B) and TC (C) in the SC after the application of the TC-IPM system. Figure 6.17 (D) shows the correlation between the signal intensity of PR and signal intensity of IPM in the SC with depth (x/h=1, 0.9, 0.8, 0.7, 0.6, 0.5, 0.4, 0.3, 0.2, 0.1 and 0).	188
Figure 6. 19 The depth profiles of PR (A), PG (B), TC (C) and IPM (D) in the SC after application of the PG-TC-IPM system.	189
Figure 6. 20 Determination of the theoretical SC thickness. The total amount of SC protein content can be determined at the x-intercept. The estimated SC protein content was 790.5 $\mu\text{g cm}^{-2}$ (mean \pm SD, n=12).	190
Figure 6. 21 Depth profiles of NIA in the SC after application of PG, TC, PG:OA (10:90),	

PG:LA (50:50) and TC:CCT:DMI (50:25:25) evaluated using tape stripping.....	191
Figure 6. 22 Averaged AUC values for NIA depth profiles measured in tape stripping studies (mean \pm SD, n=6)	192
Figure 6. 23 Depth profiles of PR in the SC after application in PG, TC, OSaI, TC:IPM (50:50) and PG:TC:IPM (50:25:25) evaluated using tape stripping.....	193
Figure 6. 24 Averaged AUC values for PR depth profiles measured in tape stripping studies (mean \pm SD, n=6)	194
Figure 6. 25 (A) Correlation of the <i>in vivo</i> area under curve (AUC) of the depth profiles determined in CRS studies and <i>in vitro</i> cumulative permeation of NIA at 24 h in human skin ($R^2=0.84$). (B) Correlation of the <i>in vivo</i> AUC values of the depth profiles determined in tape stripping studies and <i>in vitro</i> cumulative permeation of NIA at 24 h in human skin ($R^2=0.86$). (mean \pm SD, $4 \leq n \leq 24$).....	195
Figure 6. 26 The <i>in vitro</i> permeation data of PR plotted against the AUC values of the depth profiles determined in CRS studies (A) and in tape stripping studies (B) <i>in vivo</i> . (mean \pm SD, $4 \leq n \leq 24$)	196
Figure 6. 27 The AUC values of PR determined in <i>in vivo</i> CRS studies plotted against the data determined in <i>in vivo</i> tape stripping studies ($R^2=0.68$) (mean \pm SD, $6 \leq n \leq 24$).	197

List of tables

Table 1. 1 Physicochemical properties of NIA.....	38
Table 2. 1 HPLC conditions for analysis of NIA.....	53
Table 2. 2 HPLC method validation parameters for quantitative analysis of NIA, data presented as mean \pm SD, (% RSD).....	54
Table 2. 3 Solubility of NIA in different solvents (mean \pm SD, n=3).	56
Table 2. 4 The results of mass balance studies following the permeation studies using porcine skin under following application of 50 $\mu\text{L}/\text{cm}^2$ ($3 \leq n \leq 5$, mean \pm SD).	61
Table 2. 5 The results of mass balance studies following the permeation studies using porcine skin following application of 5 $\mu\text{L}/\text{cm}^2$ of formulations ($3 \leq n \leq 5$, mean \pm SD).....	63
Table 2. 6 The results of the mass balance studies following the permeation studies using human skin following application of 50 $\mu\text{L}/\text{cm}^2$ of formulations ($3 \leq n \leq 5$, mean \pm SD).....	65
Table 2. 7 The results of mass balance studies following the permeation studies in human skin following application of 5 $\mu\text{L}/\text{cm}^2$ of formulations ($3 \leq n \leq 5$, mean \pm SD).....	68
Table 3. 1 HPLC conditions for analysis of PR.....	85
Table 3. 2 HPLC method validation characteristics for quantitative analysis of PR, data presented as mean \pm SD, (% RSD).	87
Table 3. 3 Solubility of PR in various solvents (mean \pm SD, n=3).	88
Table 3. 4 The results of mass balance studies following the permeation studies of PR using porcine skin following application of 50 $\mu\text{L}/\text{cm}^2$ of solution($4 \leq n \leq 5$, mean \pm SD).....	94
Table 3. 5 The results of mass balance studies following the permeation studies of PR using porcine skin following application of 5 $\mu\text{L}/\text{cm}^2$ of solution ($3 \leq n \leq 5$, mean \pm SD).....	97
Table 3. 6 The results of mass balance studies following the permeation studies of PR in human epidermis following application of 5 $\mu\text{L}/\text{cm}^2$ of solution ($3 \leq n \leq 5$, mean \pm SD).....	101
Table 4. 1 The composition of the PG binary solvent systems of NIA screened using the Skin PAMPA model.....	113
Table 4. 2 The composition of the TC binary solvent systems of NIA screened using the Skin PAMPA model.....	113
Table 4. 3 The binary systems of NIA containing varying ratios of volatile alcohol and chemical penetration enhancers.....	114
Table 4. 4 NIA binary vehicle formulations evaluated using porcine skin.	114
Table 4. 5 NIA binary vehicle formulations evaluated using human skin.	115

Table 4. 6 Results of the mass balance studies following permeation studies in porcine skin of NIA binary vehicle systems composed of PG and other solvents (n=4, mean \pm SD).	124
Table 4. 7 Results of the mass balance studies for permeation of NIA in porcine skin from binary systems composed of TC and other solvents (n=4, mean \pm SD).	126
Table 4. 8 Mass balance studies for the binary systems composed of T-BA and other solvents evaluated in porcine skin (mean \pm SD, $4 \leq n \leq 5$).	128
Table 4. 9 Results of the mass balance studies following the permeation of NIA in porcine skin permeation for ternary systems (n=4, mean \pm SD).	130
Table 4. 10 Cumulative amounts of NIA permeation in porcine skin and the Skin PAMPA model from binary and ternary solvent systems (mean \pm SD, $4 \leq n \leq 5$).	131
Table 4. 11 Mass balance results following NIA permeation in human skin for binary vehicle systems composed of PG and other solvents (n=4, mean \pm SD).	134
Table 4. 12 Mass balance results following the permeation studies for NIA binary systems composed of volatile alcohol/TC or neat solvents. (n=4, mean \pm SD).	137
Table 4. 13 Mass balance results following the permeation studies for NIA ternary solvent systems (n=4, mean \pm SD).	139
Table 4. 14 Cumulative permeation of NIA in human skin and the Skin PAMPA model from binary and ternary solvent systems (mean \pm SD, $4 \leq n \leq 5$).	140
 Table 5. 1 PR binary solvent systems assessed in the Skin PAMPA model	145
Table 5. 2 Mass balance results following the permeation studies of PR in binary systems composed of PG and other solvents in porcine skin. (n=4, mean \pm SD).	152
Table 5. 3 Mass balance results following the permeation studies of PR in binary systems composed of TC and other solvents in porcine skin. (n=4, mean \pm SD).	154
Table 5. 4 Mass balance results following the permeation studies of ternary systems of PR in porcine skin. (n=4, mean \pm SD).	156
Table 5. 5 Cumulative permeation of PR in porcine skin and the Skin PAMPA model from binary and ternary systems (mean \pm SD, $4 \leq n \leq 5$).	157
Table 5. 6 Mass balance results of PR for permeation studies of binary systems in human skin, (n=4, mean \pm SD).	159
Table 5. 7 Mass balance results for PR following permeation from ternary systems in human skin, (n=4, mean \pm SD).	161
Table 5. 8 Cumulative permeation of PR in human skin, porcine skin and the Skin PAMPA model from binary and ternary solvent systems (mean \pm SD, n=4).	162

List of symbols and abbreviations

ANOVA	Analysis of variance
BG	Butylene glycol
CRS	Confocal Raman spectroscopy
CCD	Charge-coupled device
CCT	Caprylic/capric triglyceride
DCS	Differential scanning calorimetry
DVS	Dynamic vapour sorption
DL	Detection limit
DMI	Dimethyl isosorbide
EMA	European Medicine Agency
HPLC	High performance liquid chromatography
IPM	Isopropyl myristate
ICH	International Conference on Harmonisation
LA	Linolenic acid
LogP _(octanol/water)	Partition coefficient
NIA	Niacinamide
NMF	Natural moisturising factor
OECD	Organization for Economic Co-operation and Development
OA	Oleic acid
OSal	Octyl salicylate
PAMPA	Parallel artificial membrane permeability assay
PEG6CCG	PEG-6-caprylic/capric glycerides
PBS	Phosphate buffered saline
PR	Phenylethyl resorcinol
PEG	Polyethylene glycol
PG	Propylene glycol
QL	Quantitation limit
RH	Relative humidity
SCCS	Scientific Committee on Consumer Safety
T-BA	T-butyl alcohol
TC	Transcutol [®] P
TEWL	Transepidermal water loss
TGA	Thermogravimetric analysis

Chapter 1.

Introduction

1.1 Structure of human skin

Skin is the largest human organ with an average total surface of 2 m² (Hadgraft, 2001). It serves as a unique interface between the human body and the outside environment, preventing the egress of water and the ingress of toxins, ultraviolet (UV) radiation or foreign organisms (Lane et al., 2012b). As well as its physical barrier role, human skin plays a role in homeostasis, maintaining body temperature and blood pressure (Benson, 2012). Human skin is also a major sensory organ, transmitting information regarding temperature, pressure, pain and itch to the central nervous system (Zimmerman et al., 2014).

While human skin is a formidable membrane barrier for most compounds, it provides an accessible site for administration of some therapeutic compounds. This heterogeneous membrane has been of interest to scientists since the 19th century, and new paradigms on skin structure have been elucidated over the past decades (Menon et al., 2012). Human skin may be divided into four main regions: the stratum corneum (non-viable epidermis), the viable epidermis, dermis and the subcutaneous tissue (hypodermis) (Katz and Poulsen, 1971). Appendages such as hair follicles and apocrine sweat glands are also associated with the skin (Fig 1.1).

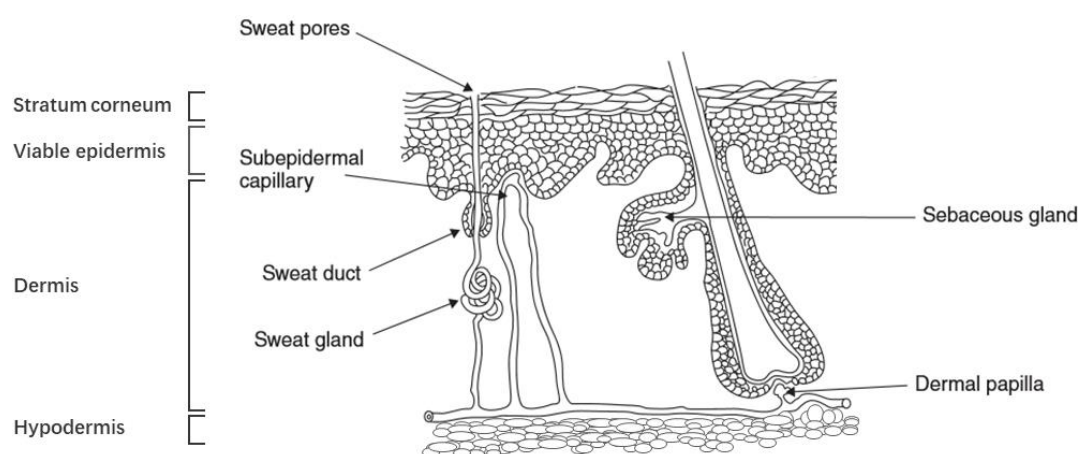


Figure 1. 1 Cross-section of human skin adapted from Benson (2005).

1.1.1 Hypodermis

The subcutaneous tissue (subcutis, also known as hypodermis) is the innermost layer of the skin and is responsible for attachment of the overlying dermis to underlying muscle, fascia or periosteum (Diegel et al., 2013). The subcutis consists of fat cells and is divided by fibrous septae into separate anatomical units, arranged as lobules. The lobules are connected by veins and arteries (Stecco et al., 2015). The subcutis also contains nerve bundles and it primarily serves to provide heat insulation, energy storage and protection against physical shock (Benson, 2012).

1.1.2 Dermis

The dermis is the 2-5 mm thick connective layer sandwiched between the epidermis and subcutaneous tissue. The dermis is subdivided into the papillary dermis and reticular dermis. The papillary dermis is a thin layer in contact with the epidermis basement zone and is rich in blood vessels and sensory nerve endings; the reticular dermis is a thick layer in contact with the subcutis (Lai-Cheong and McGrath, 2009). The dermis is paucicellular compared to the dense cellular structure of the epidermis. It consists mainly of the extracellular matrix made up of collagen, elastin and ground substance. Collagen accounts for 70 % of the dry weight of the dermis, providing support and strength, and elastic fibers make up 5 % of the dry weight of the dermis, providing elasticity and flexibility (Lai-Cheong and McGrath, 2009). The basic cellular components found in the dermis are the fibroblast that produces the three extracellular components (collagen, elastin and ground substance) (Haskell, 2010), mast cells responsible for immune responses, and melanocytes involved in pigment production (Benson, 2012). Various appendages including sweat glands, hair follicles, and sebaceous glands originate within the dermis. Blood and lymph vessels and nerves course through the layer supplying both nutrition and sensation (Fenner and Clark, 2016).

Because of its structure, the dermis provides little barrier function to the percutaneous absorption of most substances. However, the permeation of very lipophilic compounds may

be reduced by the dermis (Benson, 2012). Furthermore, the blood vessels contained in the dermis ensure the rapid clearance of permeants through the epidermis from the dermo-epidermal junction to the systemic blood supply. This function also establishes the concentration gradient between the permeants on the skin surface and the dermis (Benson, 2012).

1.1.3 Epidermis

The epidermis is a stratified squamous epithelium and varies in thickness from 0.06 mm on the eyelid to 0.8 mm found on the palms and soles. There are no blood vessels in the epidermis and epidermal cells source nutrients and clear waste by diffusion through the epidermal-dermal layer (Benson, 2012). As shown in Fig 1.2, the epidermis consists of multilayers, and the multilayers from the outmost layer are: stratum corneum, stratum granulosum, stratum spinosum and stratum basale (also known as stratum germinativum) (Katz and Poulsen, 1971). Furthermore, a layer known as stratum lucidum can be found only in glabrous skin between the stratum corneum and stratum granulosum layers (Gould, 2018).

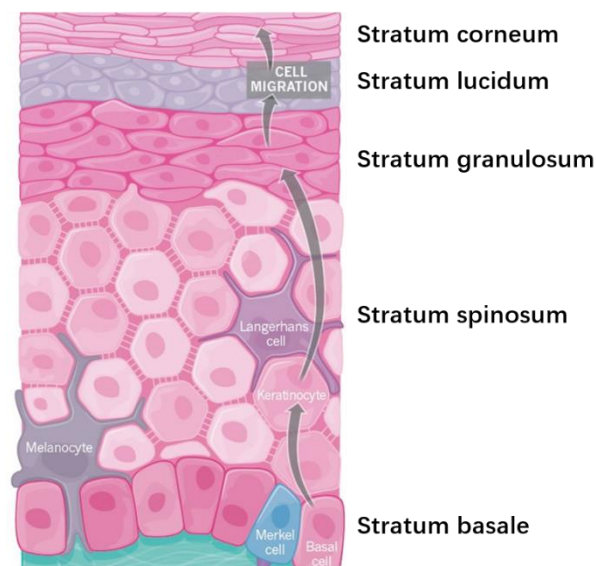


Figure 1. 2 Schematic representation of the structure of human epidermis. Adapted from Gould (2018)

The epidermis is in a constant state of renewal and these layers contain cells at varying levels of differentiation. The formation of the proliferative layer happens in the basal cell

layer: keratinocytes are generated in the stratum basale, then ascending, through the stratum spinosum and granulosum, the cells form altered and dead corneocytes on their journey towards desquamation (Walters, 2002). The other cell types contained in the stratum basale are melanocytes, Langerhans cells and Merkel cells. Each basal layer melanocyte is associated with approximately 30-40 keratinocytes and one Langerhans cells, proposed as a melanin unit (Fitzpatrick and Breathnach, 1963). Melanocytes produce melanin, which is a high molecular weight polymer responsible for skin pigmentation, for absorbing harmful ultraviolet (UV) radiation and minimizing the liberation of free-radicals in the stratum basale (Benson, 2012).

1.1.4 Stratum corneum

The stratum corneum (SC) is the outmost layer of the skin with an average thickness of 10-20 μm . The SC is also known as the non-viable epidermis. It serves as the major barrier of the skin, preventing the loss of water and the permeation of potentially harmful substances. This barrier consists of eight to sixteen layers of overlapped fully keratinized dead cells, corneocytes (Katz and Poulsen, 1971). The corneocytes are pentagonal or hexagonal in shape with high density and low hydration compared to other cells (Hadgraft and Lane, 2011). The corneocytes are renewed and replaced approximately every 14 days as the outcome of epidermal proliferation and progressive differentiation (Hadgraft and Lane, 2011; Menon et al., 2012). Corneocytes are connected by corneodesmosomes and embedded in a continuous intercellular lipid matrix (Hadgraft and Lane, 2011). Unlike most biological lipid membranes there are no phospholipids in the SC and the molecules found in the SC lipid matrix contain small hydrophilic groups and show a large variability in their structures (Das and Olmsted, 2016). As the continuous domain in the SC, the lipid composition and the structural arrangement of lipids as multiple lamellar patterns in the intercellular lipid matrix are critical to the barrier functions of SC (Benson, 2012). Ceramides, cholesterol and free fatty acids are the main lipid components and are present in approximately equimolar proportions in the extracellular domain. Ceramides are a group of structurally heterogeneous sphingolipids composed of sphingosine and long chain fatty acid. It was

reported that ceramides make up half of the lipid by mass (Ng and Lau, 2015). Cholesterol and free fatty acids amount to 25 and 10 % by weight of the SC lipid matrix, respectively (Menon et al., 2012). Scientists have reported that the structure of the extracellular lipid matrix consists of stacked bilayers of fully extended ceramides with cholesterol molecules associated with the ceramide sphingoid moiety (Iwai et al., 2012).

The SC has been described as a “brick and mortar” model by Michaels et al. (1975), where the corneocytes are the “bricks” in a “mortar” composed of the intercellular lipids. Corneodesmosomes act as the molecular rivets holding the “bricks” together. The structure of the SC is crucial for its barrier function and is considered to be the major challenge to transdermal/dermal drug delivery (Menon et al., 2012).

1.2 Skin permeation

As the main barrier protecting the human body from the outside world, the stratum corneum (SC) is well recognized to be the rate-limiting step in the percutaneous penetration process (Hadgraft, 2001; Trommer and Neubert, 2006; Donnelly et al., 2010; Coulman et al., 2011). As introduced previously, the structure of the SC has been investigated and likened to a “brick-and-mortar” model (Michaels et al., 1975). Theoretically, there are a number of possible pathways by which substances can penetrate through the SC, namely transappendageal, transcellular and intercellular diffusion routes (Fig 1.3) (Hadgraft, 1983; Barry, 1991). The appendages traversing the SC may serve as a route for skin absorption of high molecular weight non-charged substances (Wiechers, 2008). The surface area of sweat glands and hair follicles accounts for less than 0.1 % of the skin surface. Therefore, the transappendageal pathway is not considered as the predominant route followed by the majority of molecules (Lane, 2013). Additionally, there appears to be a valve mechanism at the opening of the sweat gland only activated with perspiration (Hadgraft, 1983). Experimental evidence has confirmed that the intercellular space is the preferential transport pathway for skin penetration (Nemanic and Elias, 1980) and the pathlength for diffusion was reported as 500 μm for water (Potts and Francoeur, 1991). As shown in Fig 1.3, the intercellular lipids are organized as multiple lamellar layers forming a continuous lipid

domain. The intercellular route involves partition and diffusion into the lipid matrix, and it has been well established that most substances preferentially overcome the SC barrier via the intercellular lipid channels (Albery and Hadgraft, 1979; Hadgraft, 2004; Hadgraft and Lane, 2005; Lane et al., 2012b).

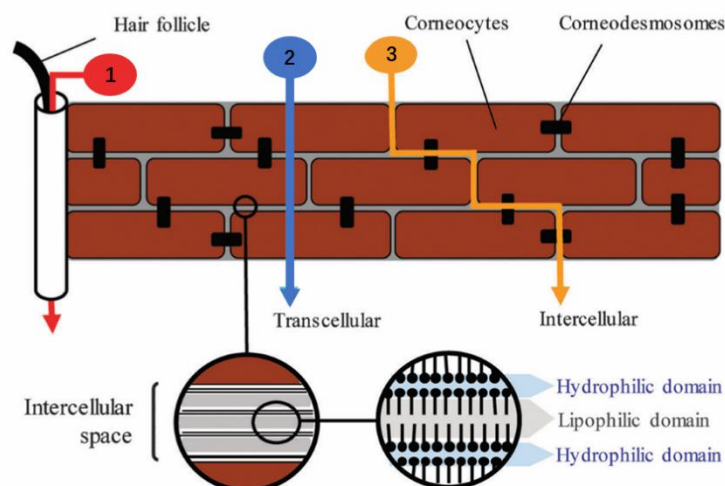


Figure 1. 3 Schematic representation of the possible penetration pathways through the stratum corneum (Hadgraft and Lane, 2011). Route 1 (highlighted in red) represents the possible transappendageal pathway; route 2 (highlighted in blue) shows the transcellular pathway and route 3 (highlight in orange) illustrates the intercellular pathway

1.3 Fick's diffusion law (physicochemical determinants of topical delivery)

Percutaneous permeation involves a series of steps beginning with the release of the substance from applied formulations, followed by diffusion into the SC, then partitioning to the more aqueous epidermal layers and deeper tissues (Benson, 2012). Despite the heterogeneous nature of the SC, the transport via intercellular lipid domains may be treated as a passive kinetic process (Godin and Touitou, 2007). The diffusion process can be viewed simplistically based on Fick's first law of diffusion. The permeation of an applied substance under infinite dose conditions in an *in vitro* permeation assessment can be measured over time. The cumulative permeated amounts of active that cross a unit skin area in a time interval is referred to as the steady-state flux (J_{ss}) (Benson, 2012; Finnin et al., 2012; Wiechers et al., 2012).

$$J_{ss} = \frac{dQ}{dt} = \frac{K \times D \times (C_{app} - C_{rec})}{h}$$

Equation 1.1

This equation describes the steady state flux (J_{ss}) in terms of the partition of the diffusing substance between the SC and the applied formulation (K), the diffusion coefficient (D) of the molecule in the SC, the pathlength of the diffusion process (h), the concentration of the substance in the donor phase applied on the skin surface (C_{app}) and the concentration in the receptor phase (C_{rec}). Under infinite dose conditions, as occurs in most circumstances $C_{rec} \ll C_{app}$, thus Equation 1.1 can be written as Equation 1.2.

$$J_{ss} = \frac{K \times D \times C_{app}}{h} \quad \text{Equation 1.2}$$

Theoretically, the maximum flux could be achieved when the concentration of substance in the formulation is equal to its solubility. The important physicochemical properties deciding the efficacy of a substance in dermal delivery are partition coefficient, diffusion coefficient and solubility. It has been reported that the ideal permeant has good solubility in both oils and water, with a log $K_{(o/w)}$ \sim 1-3 being optimal (Hadgraft, 2004). The molecular size of the permeant will influence the diffusivity in the SC (Pugh et al., 2000) and good skin permeants tend to have a molecular weight less than 500 Da (Benson, 2012). Permeants with a suitable size and log $K_{(o/w)}$ value tend to be molecules with low melting points. Therefore, the melting point value is considered as an important indicator for dermal delivery of actives (Hadgraft, 2004).

1.4 Skin penetration enhancement

1.4.1 Passive enhancement strategies

It is deduced from Equation 1.2 that the factors affecting the permeation rate through the SC are K , C_{app} , D and h . With these parameters in mind, for passive skin permeation enhancement, the flux of a substance across the skin can be enhanced by increasing the diffusion coefficient, partition coefficient and/or the concentration of the substance in the formulation (Williams and Barry, 2004).

1.4.1.1 Chemical penetration enhancers

Skin penetration enhancers are chemicals which can change the solubility/partition

behavior of a substance in the SC and/or affect the diffusion properties of the substance (Lane, 2013). The applications of chemical penetration enhancers on dermal/transdermal delivery of various substances have been widely reported in the literature. There are a variety of mechanisms underlying enhancement actions and so far the mechanism has not been fully explored for some enhancers (Trommer and Neubert, 2006). Penetration enhancers can be classified according to their chemical structure. In the literature, the main chemical classes which have been applied as penetration enhancers are: alcohols, glycols, amides, fatty acids, esters, ether alcohols, pyrrolidones, sulphoxides, surfactants and terpenes (Williams and Barry, 2004; Lane, 2013). Alcohols applied as penetration enhancers can be classified into the short alkyl chain (ethanol and isopropyl alcohol) and the long alkyl chain group (fatty alcohols) (Trommer and Neubert, 2006). The mechanism of alcohol's enhancement ability has been reported to include extraction and fluidization of lipids (Lane, 2013) as well as effects on the thermodynamic activity of the substances in the formulations. Glycols have also been used in topical and transdermal products with propylene glycol (PG) being one of the most widely used. The mechanism of PG as a skin penetration enhancer is not fully understood and several theories have been proposed. The potential mechanisms of action include reducing skin hydration, possible "carrier-solvent" effects and incorporation within the head group regions of the lipids (Lane, 2013). Research shows that PG has a short residence time in the skin. Once PG is cleared from the tissue, the possibility of stranding the substance in the SC must be considered (Santos et al., 2011). Transcutol®P is also reported to enhance skin permeation for some substances, including lidocaine (Cázares-Delgadillo et al., 2005) and clonazepam (Mura et al., 2000). Fatty acids have been used in some commercially available products because of their GRAS status (Dragicevic et al., 2015). Furthermore, the synergistic effect of combining fatty acids with other solvents was reported by researchers (Ben-Shabat et al., 2007; van Zyl et al., 2016). Some surfactants were also reported to serve as skin penetration enhancers, however there are concerns regarding their skin irritancy and toxicity (Lane, 2013).

1.4.1.2 Supersaturated systems

A further strategy of skin permeation enhancement is via manipulation of the thermodynamic activity of a substance in the formulation. This can be achieved by building supersaturated systems. The first application of supersaturated systems in transdermal delivery systems was proposed by Higuchi and Higuchi (1960). In a supersaturated system, the substance reaches a higher concentration or chemical potential than its solubility limit. The flux from supersaturated systems increases proportionally as the flux through the membrane is driven by the chemical potential gradient (Lane et al., 2012b). Pellett et al. (1997) investigated *in vitro* permeation of supersaturated solutions of piroxicam across human skin using the tape stripping technique. Various degrees of saturation were evaluated in the study, up to a degree of 4. The authors reported a linear relationship between the degree of saturation and the amount of piroxicam that permeated in the SC ($R^2=0.97$). Raghavan et al. (2001) reported the permeation of hydrocortisone acetate (HA) from supersaturated solutions across a model silicone membrane. The supersaturated solutions were prepared with cosolvent systems composed of propylene glycol, water and were mixed with polymers. Flux enhancement was observed as a result of supersaturation. The infrared spectroscopic and differential scanning calorimetry results indicated that the polymer formed interactions with HA and acted as anti-nucleant agents.

1.4.2 Physical enhancement strategies

1.4.2.1 Microneedle technology

With the application of chemical penetration enhancers and/or supersaturated systems, human skin penetration will still be restricted to substances with relatively small molecular weights and appropriate $\log K_{(o/w)}$ values. Therefore, many therapeutic agents are limited due to their inability to overcome the SC barrier. Microneedles (MN) were developed to address this problem. MN arrays offer the potential to bypass the SC barrier and deliver a wide range of drug into/or cross the skin with minimally invasive devices (Donnelly et al., 2010; Thakur et al., 2010). The mechanism of MN is to puncture the superficial layer of the skin surface and

then achieve the ingress of the therapeutic agents from the device. The design and the materials of MN arrays vary considerably. MN were initially introduced as a drug delivery system in the 1970s and applications continue to expand rapidly with the technological advances over the past decades (Quinn et al., 2015). The earlier microneedle systems were composed of solid needles. MN were removed once the needles pierced the skin surface; followed by the application of formulations on the pre-treated skin site (Moss, 2015). Microfabricated silicon MN arrays were manufactured by Coulman et al. (2006) for cutaneous delivery of charged macromolecules and plasmid DNA. The microconduits created were visualized using scanning electron microscopy. The outcomes from the study confirmed the capacity of the silicon MN to create microchannels through the SC of *in vitro* human skin and to facilitate delivery. Coulman et al. (2011) performed the first *in vivo* study employing optical coherence tomography (OCT) to determine the architectural changes in skin induced by MN treatment. The authors investigated a range of MN devices with different materials and morphologies. From *in situ* transverse images it was observed that the microchannels created by MN collapse following the removal of the device. Hydrogel-forming microarrays were designed by Donnelly et al. (2012) using crosslinked polymers. The MN demonstrated their potential to rapidly take up skin interstitial fluid upon skin insertion creating continuous hydrogel conduits from adhesive patch-like MN drug reservoirs to the dermal tissue.

1.4.2.2 Other physical methods

The other physical techniques involved in penetration enhancement include ultrasound, iontophoresis, electroporation magnetophoresis and photomechanical waves (Barry, 2001; Alkilani et al., 2015). Polat et al. (2011) reviewed and compared the application of ultrasound for transdermal drug delivery, for both low-frequency ultrasound (LFS) and therapeutic and high-frequency ultrasound (HFS). The authors reported that HFS is more effective in dermal delivery of small molecules while LFS is capable of driving high molecular weight compounds into the skin. The application of physical enhancement strategies leads to a wider range of substances which can be delivered through skin. However, there are safety concerns

regarding the possibility of electrically mediated delivery systems causing irreversible damage to the area of application. In addition, the convenience of these delivery systems is limited by their electrically driven power. More work is necessary to address these potential concerns relating to electrically mediated delivery systems (Maurya et al., 2015).

1.5 *In vitro* skin permeation assessment

1.5.1 Diffusion cells

The regulatory acceptance of *in vitro* assessment of dermal and transdermal formulations efficacy was established in the final international acceptance of the Organization for Economic Cooperation and Development (OECD) 428 “Guideline for the Testing of Chemicals: Skin Absorption *in vitro* Method” and the associated Guidance 28 in 2004 (OECD, 2004b, a), the guideline published by the European Medicines Agency (EMA, 2018), and the US Food and Drug Administration (FDA).

Most permeability studies are performed using a diffusion cell method (Flaten et al., 2015). The diffusion cells can be classified into horizontal and vertical types. Employed by most of researchers, the state-of-the-art diffusion cells are the vertical Franz diffusion cells which were first reported in the mid-70s by Franz (1975). A number of modifications have been introduced to the original design and Fig 1.4 illustrates the vertical Franz diffusion cell employed in the present work. The cell consists of a donor chamber and a receptor chamber between which the skin/membrane is positioned. The receptor chamber is filled with receptor medium which is constantly mixed by a Teflon-coated magnetic stir bar. The cells are incubated in a thermostatically controlled water bath during the course of the study.

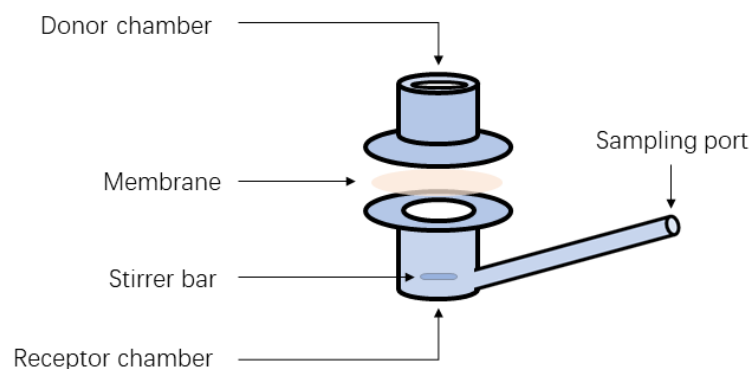


Figure 1. 4 Vertical Franz diffusion cell used in the present work.

1.5.2 Skin model membranes

The nature of the skin membrane is one of the major potential variants in the design of *in vitro* permeation studies. Human skin has been recognized as the most relevant model to obtain data relevant to man (Flaten et al., 2015) since the earliest systematic work conducted by Franz (1975). The author performed *in vitro* permeation studies using excised human skin for 12 organic compounds. The permeation data of the 12 compounds was compared with the corresponding data obtained in living subjects by Feldmann and Maibach (1970) and a good correlation was observed for the systematic comparison of *in vitro* - *in vivo* data. Human skin sourced from plastic surgery procedures and amputations has been used for *in vitro* assessment (Godin and Touitou, 2007). The skin tissue is usually taken from the abdomen, back, leg and breast (Abd et al., 2016). Appropriate ethical approvals and laboratory facilities are required for studies with human skin, which restricts access to *ex vivo* human tissue. Furthermore, the permeability of human skin varies greatly. The barrier function of the membrane is affected by age, anatomical site, ethnicity, gender, skin disorders and environmental factors (Sandby-Moller et al., 2003; Barbero and Frasch, 2009; Benson, 2012). In an assessment of the transdermal delivery of fentanyl in cancer pain patients of different age groups, the drug absorption for patients > 75 years was significantly lower compared with the group of patients < 65 years (Solassol et al., 2005). Furthermore, the skin permeability is also influenced by storage conditions and the preparation procedures (Finnin et al., 2012).

Tissues from various mammals, rodents and reptiles have been used as possible

substitutes for human skin, (Godin and Touitou, 2007; Praça et al., 2018). However, these animal models vary greatly in their biological and physical characteristics and permeability compared with human skin. Of all the investigated animal models, the histological and biochemical properties of porcine skin most closely resemble the properties of human skin (Godin and Touitou, 2007; Jung and Maibach, 2014). Jacobi et al. (2007) investigated and reported similarity in the thickness of different skin layers and the follicular characteristics between human skin and porcine skin. The similarity in lipid composition between human skin and porcine skin was reported by Gray and Yardley (1975).

Jung and Maibach (2014) reviewed *in vitro* skin permeation studies using different animal tissues published after 1993. The authors concluded that the permeability of monkey, pig and hairless guinea pig are more predictive of human skin than rat, rabbit and guinea pig. The authors also reviewed 46 permeation studies using both pig and human skin involving 77 substances. The Factor of Difference (FOD) was calculated from permeability studies and 65 chemicals of 77 fell within the range of $0.3 < \text{FOD} < 3.0$. Similar results were also published by Barbero and Frisch (2009) who reviewed 18 *in vitro* penetration studies involving 41 chemicals. The correlation coefficient between the permeation data obtained in human skin and porcine skin was determined to be 0.88.

Simplified non-lipid based model membranes, including poly(dimethylsiloxane) (PDMS) and silicone membranes have been employed to screen various solvents and to assess their impact on the mechanisms of the percutaneous absorption process (Oliveira et al., 2010; Santos et al., 2011; Oliveira et al., 2012; Flaten et al., 2015). Dias et al. (2007b) investigated the diffusion of caffeine, benzoic acid and salicylic acid in silicone membrane from different solvents. The authors also assessed solvent uptake in the silicone membrane using DSC. It was reported that the vehicles that were highly absorbed by the membrane altered the properties of the membrane and enhanced the permeation of compounds. PDMS and silicone membranes offer advantages when employed in permeation studies, including low cost, ease of storage and reproducible results. However, the limitations of the silicone membrane are that it is non-lipid based, of non-biological origin and has low resemblance to the SC. The more permeable nature of these model membranes has also been confirmed

by other researchers (Luo et al., 2016; Haque et al., 2017a).

1.5.3 The Skin Parallel Artificial Membrane Permeability Assay (PAMPA) model

The PAMPA model was initially developed in the 1990s as a rapid screening tool to evaluate passive membrane permeability of drugs (Kansy et al., 1998). The PAMPA model has subsequently been used in assessment of drug permeation through the blood-brain barrier (Müller et al., 2015; Grumetto et al., 2016) and for gastrointestinal absorption (Avdeef and Tsinman, 2006). The first application of the PAMPA model in the study of percutaneous absorption was reported by Ottaviani et al. (2006). In this study, the authors used filter paper immobilized with either isopropyl myristate and/or silicone oil as the experimental membrane mounted between the two 96-well plates. The state-of-the-art “Skin PAMPA” model was developed by Sinko and colleagues in 2012 (Fig 1.5). The current Skin PAMPA model is a 96-well plate with an artificial lipid membrane (Sinkó et al., 2012). The lipid membrane consists of a mixture of free fatty acids, cholesterol and synthetic ceramide analogues (ceramides). Luo et al. (2016) performed *in vitro* permeation assessments of a lipophilic molecule, ibuprofen, using the Skin PAMPA model, silicone membrane, human and pig skin. It was reported that the most efficient formulation observed in human skin also delivered significantly higher amounts of ibuprofen in the Skin PAMPA model. Vizserálek et al. (2015) also investigated the transdermal delivery of nicotine, fentanyl and rivastigmine using the Skin PAMPA model.

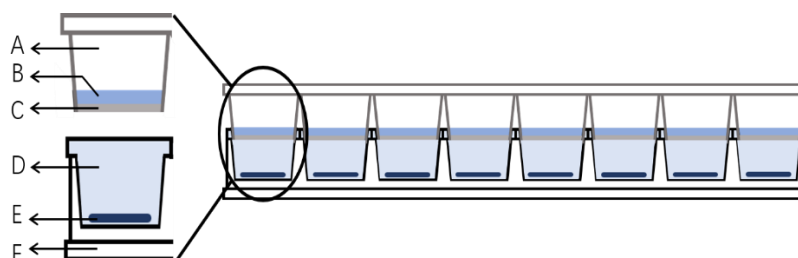


Figure 1. 5 Schematic diagram of the Skin PAMPA system. The donor compartment (A), applied formulations (B), pre-coated lipid membrane (C), receptor phase (D), individual stirrer (E) and the receptor plate (F) are indicated in the figure.

1.5.4 Human skin equivalents (HSEs)

In the past decades, a number of human skin equivalents (HSEs) have been developed and investigated to determine their suitability to be used as human skin models (Francesco et al., 2015). HSEs are typically based on cultured human cells, such as keratinocytes (Godin and Touitou, 2007). These human reconstructed models are useful models for assessment of skin irritation, phototoxicity and corrosivity assessments. However, HSEs have not been proved to be suitable skin permeation models because of their comparatively low barrier function (Mathes et al., 2014).

1.6 *In vivo* skin permeation assessment

1.6.1 Tape stripping and the measurement of transepidermal water loss (TEWL)

Tape stripping is a procedure used for SC sampling that requires multiple application to, and removal of adhesive tapes, from the skin surface (Wiedersberg and Nicoli, 2012). This technique is considered to be minimally invasive because only dead corneocytes in the SC layer are collected and homeostatic repair mechanisms should repair the skin barrier relatively quickly (Menon et al., 1992). Tape stripping as a sampling technique has been used for the assessment of skin barrier function (Breternitz et al., 2007), to examine the effects of photodamage (Gureri et al., 2018) and to collect samples for gene expression studies (Jones et al., 2002). SC tape stripping experiments have also been used as a tool to determine formulation efficacy both *in vitro* and *in vivo* (Pellett et al., 1997; Herkenne et al., 2006; Klang et al., 2012; Binder et al., 2018). Herkenne et al. (2006) investigated the skin uptake of ibuprofen using tape stripping on isolated pig ears (*in vitro*) and living human volunteers (*in vivo*). Herkenne and colleagues reported that the permeation data of ibuprofen obtained *in vitro* were in line with those observed *in vivo* following a 30-min application period. A similar correlation between skin uptake data for *in vitro* pig skin and *in vivo* human volunteers was also reported by Klang et al. (2012). These authors performed comparative tape stripping experiments evaluating the percutaneous absorption of curcumin and fluorescein sodium from microemulsions and hydrogels.

TEWL is the amount of water that passively evaporates through skin to the external environment and is driven by the water vapor pressure gradient internally and externally (Honari and Maibach, 2014). TEWL measurements were first conducted in the 1960s (Spruit and Malten, 1965) and have been used to characterise skin barrier function (Sotoodian and Maibach, 2012). Machado et al. (2010) applied this technique to investigate permeation routes in the SC. The authors investigated the relationship between *in vivo* TEWL and the diffusional permeation pathlength through the SC for different anatomic sites. It was reported that the skin sites with smaller corneocytes have higher TEWL values. The authors also observed a direct reciprocal relationship between TEWL and the skin permeation pathlength. However, the accuracy of TEWL measurement is affected by environmental factors including temperature and humidity. Therefore, it is essential to perform TEWL measurements under standardised and controlled conditions (Sotoodian and Maibach, 2012).

1.6.2 Confocal Raman spectroscopy (CRS)

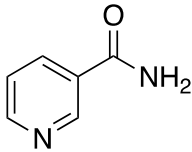
Skin is a complex heterogeneous membrane and various spectroscopic techniques have been used to understand the nature of this barrier. CRS is a novel approach which permits the successive collection of Raman spectra at various skin depths (Caspers et al., 2000). CRS was originally used to determine skin profiles of water concentration and endogenous skin components (Caspers et al., 2001). More recently, CRS has been used to probe the effects of excipients on the distribution of actives in the SC *in vivo* (Hadgraft and Lane, 2016). Mateus et al. (2013) performed the first study of CRS for dermatopharmacokinetic assessment of a drug. The researchers investigated *in vivo* permeation of ibuprofen after application from a neat propylene glycol (PG) solution and PG/water solutions on human volunteers using CRS. The results were then compared with previously published data from tape stripping studies conducted by Herkenne et al. (2006). A similar trend in skin distribution of the active was observed between the two methods. Furthermore, CRS allows the direct measurement of SC thickness as well as collection of drug profiles in the skin.

1.7 Model actives

1.7.1 Niacinamide

Niacinamide (NIA), also known as nicotinamide, is the amide form of vitamin B3. Table 1.1 summarizes the physicochemical properties of NIA. This hydrophilic compound with a low molecular weight has suitable physicochemical properties for dermal delivery. The benefits of its dermal application have long been described in the literature. NIA was initially discovered as a preventative agent against pellagra (Matts et al., 2002). Topical application of NIA was associated with a series of skin condition improvements including anti-inflammatory, antipruritic, antimicrobial, and photo-protective effects (Rolfe, 2014; Wohlrab and Kreft, 2014; Forbat et al., 2017). Suzuki et al. (2010) investigated the action of NIA in poly(ADP-ribose) polymerase-1 (PARP-1)-mediated astrocyte death. The authors assessed the uptake characteristics of [14 C]NIA using cultured mouse astrocytes while monitoring the cell viability and PARP-1 activity. It was reported that NIA had a protective effect against PARP-1-triggered astrocyte cell death. Mohammed et al. (2013) investigated the effects of NIA-containing formulations on the biophysical properties of the SC at the molecular level. NIA formulations were repeatedly applied to the forearms of 20 human subjects for 28 days. The barrier function of the SC was improved after the treatment. Most recently, Snaidr et al. (2019) reviewed the role of NIA in dermatology and its actions in preventing photodamage in human skin. It was reported that NIA enhanced DNA repair and decreased the UV-induced suppression of immunity.

Table 1. 1 Physicochemical properties of NIA

Chemical structure	
	
Molecular weight	122.1 Da
Melting point ^a	128 – 131 °C
Log P _(octanol/water) ^b	-0.4
pK _a ^a	3.3 (20 °C)

a (O'Neil et al., 2013)

b (Moffat et al., 2010)

Haque et al. (2017a) assessed the *in vitro* permeation of NIA in silicone membrane and porcine skin from two NIA containing oil-in-water formulations and a commercial control formulation for three dosing conditions (5, 20 and 50 $\mu\text{L}/\text{cm}^2$). The permeation of NIA from the two oil-in-water formulations was lower than for the control formulation in porcine skin for the 5 and 50 $\mu\text{L}/\text{cm}^2$ doses. NIA also exhibits a suitable Raman signal and CRS has been successfully used to investigate *in vivo* distribution of NIA over a total depth of 40 μm (Mohammed et al., 2014b). The CRS measurement was performed 30 min after the application of formulations *in vivo* and compared with data from *in vitro* permeation studies using heat separated human epidermis. The signal intensity of NIA at 4 μm *in vivo* correlated well with the *in vitro* flux of NIA permeation.

1.7.2 Phenylethyl resorcinol

Phenylethyl resorcinol (PR, 4-(1-phenylethyl)1,3-benzenediol) is a phenolic compound developed and optimized as a tyrosinase inhibitor by Symrise in 2007 (Vielhaber et al., 2007). Tyrosinase inhibition is an established strategy for modulation of melanin synthesis and to reduce the progress of melanogenesis (Mishima et al., 1988; Mishima and Kondoh, 2000; Ando et al., 2007; Pillaiyar et al., 2017). This is because melanogenesis is a complex biosynthetic pathway and initial melanin synthesis is catalyzed by tyrosinase. Moreover, at physiological pH, the remainder of the melanogenesis reaction sequence can spontaneously proceed (Pillaiyar et al., 2017). PR showed more than 20-fold efficiency in inhibition of mushroom tyrosinase compared with kojic acid; a concentration of 0.1 % of PR resulted in almost complete suppression of melanin synthesis after a 14-day treatment to pigmented 3D epidermis models (Vielhaber et al., 2007). The efficacy of a formulation containing PR and other actives as an alternative to hydroquinone and kojic acid was also examined *in vivo* with 20 female patients with mild-to-moderate melasma (Gold and Biron, 2011). After a 4-week washout period with a sunscreen, the recruited volunteers were treated with an oil-in-water emulsion cream containing disodium glycerophosphate, L-leucine, PR and undecylenoyl phenylalanine for a 12-week period. The same sunscreen was consistently used during the whole study period. The facial skin of the patients was evaluated before and after the

washout period and after the 12-week treatment. There was no significant change in the facial skin during the 4-week washout; signs for uneven skin tone including appearance of lentigines and melasma area and severity index (MASI) reduced up to 43 % after the treatment period. In a later study, this formulation was evaluated again with 80 human volunteers using the same procedure and improvements in signs of facial skin discoloration were also evident (Dreher et al., 2013). Most recently, Kang et al. (2019) probed the mechanisms of the tyrosinase inhibition by PR. The authors assessed the melanin content with cellular tyrosinase activity, real-time PCR analysis, a luciferase-reporter assay, Western blot analysis and an ELISA assay of cyclic AMP (cAMP), measurement of protein kinase A (PKA), and the levels of the cAMP response element binding (CREB) protein and mitogen-activated protein kinases (MAPKs). It was reported that PR could attenuate melanogenesis by activating p44/42 MAPK kinase which regulates the signaling pathways mediating melanogenesis in melanocytes. Fig 1.6 shows the 2D structure of this compound. However, information regarding experimental physicochemical values of PR has not appeared previously in the literature.

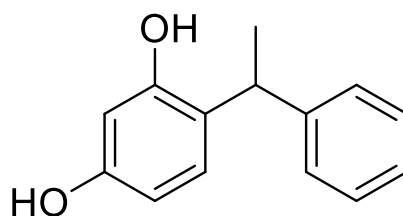


Figure 1. 6 The structure of PR

There are a number of publications reporting the development of advanced carriers containing PR (Fan et al., 2014; Limsuwan et al., 2017; Amnuaikit et al., 2018; Köpke et al., 2019). Fan et al. (2014) developed PR loaded nanostructured lipid carriers (PR-NLC) with an average particle size of 218.1 ± 9.2 nm using a hot melt high-pressure homogenization method. Limsuwan et al. (2017) developed ethosome formulations containing 0.5 % (w/v) PR, 0.5 % (w/v) cholesterol, 3 % (w/v) L-a-phosphatidylcholine, 30% (v/v) absolute ethanol and water up to 100% (v/v). Permeation studies were conducted using newborn pig skin with an application of 1 mL of 0.5 mg/mL PR-ethosome formulation over a diffusion area of 1.77 cm^2 .

At 24 h, the cumulative amount of PR that permeated through skin was recorded as 58.7 $\mu\text{g}/\text{cm}^2$. Amnuaikit et al. (2018) prepared elastic carrier loaded PR vesicles and the permeation study was performed using the same procedure as Limsuwan et al. (2017). However, the experiments were conducted under infinite dose conditions and do not simulate typical doses of a topical formulation that consumers and patients apply to skin (Haque et al., 2017a).

1.8 Aims and objectives

The overall aim of this project is to improve skin delivery of NIA and PR by a rational selection of excipients tested on varied skin permeability assays, both *in vitro* and *in vivo*. The objectives are main aims of the thesis are to:

- Perform a comprehensive characterization of the model active, PR.
- Investigate dermal delivery of the two model actives (NIA and PR) in mammalian skin under various dosing conditions from single solvents.
- Identify solvents for development of complex vehicles to be tested in mammalian skin *in vitro*.
- Investigate the suitability of the Skin PAMPA model for prediction of human skin penetration
- Identify optimum dosing and experimental conditions for the two model actives in the Skin PAMPA model.
- Determine any correlations between the PAMPA model and experiments conducted in mammalian tissue.
- Conduct *in vivo* measurement of various formulations containing NIA and PR using confocal Raman spectroscopy (CRS) and tape stripping.

Chapter 2.

**Development and evaluation of
simple formulations of NIA using
mammalian skin and
the Skin PAMPA model**

2.1 Introduction

The aim of this chapter are to develop and validate an appropriate analytical method for the model active NIA, and to investigate the effects of different vehicles on the permeation behavior of NIA *in vitro* using different skin models. The models included in the present works are full-thickness porcine skin, heat-separated human epidermis, and an artificial lipid membrane, the Skin PAMPA model.

Skin penetration studies play a crucial role in optimizing skin delivery of an active ingredient/drug. The final international acceptance of the Organization for Economic Cooperation and Development (OECD) 428 “Guideline for the Testing of Chemicals: Skin Absorption *In Vitro* Method” and the associated Guidance 28 in 2004 (OECD, 2004b), and Scientific Committee on Consumer Safety (SCCS) adopted “Basic Criteria for the In Vitro Assessment of Dermal Absorption of Cosmetic Ingredients” opinion 2010 (SCCS, 2010), marked an important point in the regulatory acceptance of *in vitro* methods for examination of skin percutaneous absorption and distribution. As introduced in the previous chapter, the outermost layer of human skin, the stratum corneum (SC) is the major barrier in percutaneous absorption. Franz (1975) reported a quantitative agreement between the permeation results obtained from excised skin and living man and confirmed that *in vitro* absorption studies reflect the corresponding living state. The use of *ex vivo* human skin to investigate percutaneous absorption has been widespread (Hadgraft and Lane, 2005). However, there are ethical and practical difficulties associated with sourcing human tissue. Thus, as mentioned earlier, many *in vitro* permeation studies have been performed using a range of animal skin models including porcine skin (Dick and Scott, 1992; Godin and Touitou, 2007; Barbero and Frasc, 2009), rodent skin (Schaefer, 2008) and guinea pig skin (Barbero and Frasc, 2009). The feasibility of these models in evaluation of human skin permeation varies considerably and full-thickness pig ear skin is recognized as the most appropriate animal model (Flaten et al., 2015). In comparison, the simplified artificial model membranes serve as simple and reproducible alternatives to human skin to understand the basic physicochemical mechanisms of permeation (Oliveira et al., 2012). In recent years efforts have also been made to develop lipid-based models to predict human skin percutaneous

absorption. The Skin Parallel Membrane Permeability Assay (PAMPA) model is one of these models. The components of the Skin PAMPA membrane are ceramides, free fatty acid, and cholesterol. Synthetic ceramides are analogs of the ceramides present in human stratum corneum, which were developed and presented in the Skin PAMPA membrane to match the permeability of human skin (Sinkó et al., 2012).

Vehicle manipulation is an important strategy to overcome the complex SC barrier and improve the delivery of actives. Various solvents were selected in the present studies because of their GRAS status and widespread use in skin preparations, including propylene glycol (PG) (Andersen, 1994), Transcutol[®] P (TC) (SCCP, 2006; Sullivan et al., 2014), dimethyl isosorbide (DMI) (Elshafeey et al., 2012), t-Butyl alcohol (T-BA) (Chen, 2005), PEG 400 and PEG 600 (Frujtier-Pölloth, 2005). Since 1932 PG has been used in topical and transdermal products as a co-solvent and/or permeation enhancer. It is the most commonly used glycol in skin preparations (Lane, 2013). TC is a monoethyl ether of diethylene glycol. TC is a potent solubilizer and has been shown to improve dermal delivery of different actives including clonazepam (Mura et al., 2000), lidocaine (Cázares-Delgadillo et al., 2005) and climbazole (Paz-Alvarez et al., 2018). DMI has been used as a solubilizer and penetration enhancer of many topical actives. DMI demonstrated synergistic effects with TC on transdermal delivery of fenoterol hydrobromide (Elshafeey et al., 2012). PEGs are widely used in cosmetics. These polymers are hygroscopic. After application on the skin surface, PEGs absorb water increasing their molecular weight. This steric effect limits the skin penetration of most PEGs. They serve as solubilizers in skin preparations, and PEG blends are preferred bases of topical and transdermal products (D'souza and Shegokar, 2016). A complex commercially available product (Olay[®]) contains the same concentration level of NIA was selected as the control for the permeation studies.

The primary objectives of this chapter are to perform analytical method validation, solubility and stability studies of NIA. The secondary objective was to evaluate the permeation behavior of NIA using porcine skin and human epidermis using various simple solutions. The suitability of the Skin PAMPA model for prediction of NIA skin permeation and optimal experimental conditions for permeant NIA in the PAMPA model were also

investigated.

2.2 Materials and methods

NIA (NIA), 2-ethylhexyl salicylate (OSal), glycerol and oleic acid were purchased from Sigma Aldrich, UK. Analytically pure propylene glycol (PG), glycerol, t-butyl alcohol (T-BA), Poly(ethylene glycol) 200 (PEG 200), PEG 400 and PEG 600 were purchased from Fisher Scientific, UK. Phosphate buffer saline (PBS) tablets ($\text{pH } 7.3 \pm 0.2$ at 25°C) were purchased from Oxoid Limited, England. Dimethyl isosorbide (DMI) was a gift from Croda Limited, UK. Caprylic/capric triglyceride (CCT), and Transcutol[®] P (TC) were received as gifts from Gattefossé, St. Priest, France. HPLC grade water and methanol were purchased from Fisher Scientific, UK. The commercial control NIA product was Olay[®] Total Effects 7 (Procter & Gamble, UK) and was purchased from a local pharmacy. Pre-coated PAMPA Plates (Pion Inc. PN120657), hydration solution, stirring disks and a Gut-Box[™] device were supplied by pION Inc. Billerica, USA.

2.2.1 Development and validation of HPLC method of NIA

To identify the wavelength number at which the absorption of UV light was selected for analysis of active, a spectronic BioMate[™] 3 UV/vis spectrophotometer (Thermo Scientific, U.S.A.) was used to conduct UV scans (200 to 300 nm, step=1 nm) of solutions of NIA. NIA quantification was performed using a HPLC (Agilent 1100, Agilent technologies, U.S.A.), operated with ChemStation[®] Rev.A.09.03. Both HPLC methods were validated according to the International Conference on Harmonisation (ICH) guidelines Q2 (R1) (ICH, 2005). Validation was conducted with the following criteria: linearity, specificity, accuracy, precision, detection limit (DL), quantitation limit (QL), system suitability and robustness.

A linearity study was conducted by preparing a series of concentrations of sample solutions within a given range. Linearity was calculated by the regression line of the response versus analyte concentration. The accuracy of a measurement is defined as the closeness of the tested value to the true value. The accuracy was assessed by analyzing three concentration levels of analytes in triplicate and reported as percent recovery using Eq 2.1.

$$\% Recovery = 100\% \left(\frac{C_{measured}}{C_{actual}} \right) \quad \text{Equation. 2.1}$$

Precision should be determined by analyzing a homogeneous sample for multiple times. It was assessed by analyzing sample solutions with three different concentrations within one day (intraday precision) and over three days (interday precision). The precision was expressed as the percent relative standard deviation (RSD).

The sensitivity of the analytical method in terms of the DL and QL were validated based on the standard deviation of the response (σ) and the slope (S). The slope was estimated from the calibration curve of the analyte; the standard deviation of the response was estimated from the standard deviation of y-intercepts of regression lines.

System suitability studies were carried out by analyzing six sample solutions with the same concentration. Parameters such as RSD of retention time, symmetry, and peak area for the six samples were determined.

Robustness was validated by introducing small and typical changes for the analytical methods, including detection wavelength, flow rate, temperature, injection volume, and the composition of mobile phases.

2.2.2 Solubility and stability studies of NIA

The Hildebrand and van Krevelen solubility parameters of NIA and solvents were calculated using Molecular Modelling Pro[®] (Version 6.3.3 ChemSW, Fairfield, CA, USA). The solubility study of NIA was conducted by adding an excess amount of the model active to a known volume of solvent. The mixtures were continuously stirred with a Teflon coated magnetic bar for 48 h in a water bath maintained at 32 ± 1 °C. The glass tubes were capped and sealed with Parafilm[®]. After 48 h of stirring, samples containing saturated active were transferred into 2.5 mL Eppendorf[®] tubes and centrifuged (13,200 rpm at 32 ± 1 °C) for 15 min. The supernatant was then diluted with methanol:water (50:50) in order to lie within the detection limit of the HPLC method.

The stability of NIA in selected solvents was examined over 72 h at 32 ± 1 °C. The

studies were conducted by preparing solutions of known concentrations of NIA in the solvent. The solution was placed in glass tubes with screw caps and sealed with Parafilm[®]. The solutions were incubated in an oven maintained at 32 ± 1 °C. Samples were withdrawn at 0, 24, 48 and 72 h. All the samples were analyzed using the validated HPLC methods. All measurements were conducted in triplicate. The solvents evaluated for solubility of NIA were dimethyl isosorbide (DMI), oleic acid (OA), caprylic/capric triglyceride (CCT), propylene glycol (PG), PEG 200, PEG 400, PEG 600, Transcutol[®] P (TC), t-butyl alcohol (t-BA), glycerol, phosphate buffered saline (PBS, pH 7.30 ± 0.10).

2.2.3 Preparation of NIA solutions

A concentration of 5 % (w/v) was selected as the level of NIA solution tested in this study. The concentration level was selected as it is typically used in personal care products. Donor solutions were prepared by adding 150 mg of NIA to a glass vial containing 3 mL of solvent (PG, TC, DMI, T-BA, PEG400 and PEG600). The glass vial was sealed with Parafilm[®] and was allowed to stir overnight or until the active dissolved at room temperature. The commercial product also contains 5 % (w/v) of NIA.

2.2.4 Dynamic vapour sorption (DVS) studies of single solvent formulations

A series of vehicles were evaluated in dynamic vapour sorption studies. To study the evaporation or hydration of tested vehicles, a Q5000 SA sorption analyzer (TA Instruments, U.S.A.) was used to examine the mass differences over 24 h (1,440 min). Nitrogen was used as the carrier gas (200 mL/min). Temperature and relative humidity (RH) were maintained throughout the experiment at 32 ± 1 °C and 50 ± 2 % RH, respectively. Tested solutions were 5 % (w/v) NIA solutions in PG, DMI, T-BA, TC, PEG400, and PEG600.

2.2.5 Permeation studies of NIA from single solvent formulations using porcine skin

Porcine tissue was obtained from healthy animals from a local abattoir and it was prepared on the same day. After washing the ear with running cold water, hairs were gently cut using scissors. A continuous cut was made around the perimeter using a scalpel on the

back of the ear, followed by a cut on the subcutaneous tissue to surgically remove the full-thickness skin from cartilage. After preparation, porcine tissue was mounted on aluminum foil, covered with polyethylene bags and stored at -20 °C until required. Flaten et al. (2015) suggested that pig skin should be used within 6 months after preparation. When required, frozen porcine skin was cut into discs using a 16 mm cork-borer and allowed to thaw at room temperature prior to permeation studies.

Vertical glass Franz diffusion cells were used to conduct the permeation studies as reported previously (Oliveira et al., 2012). As shown in Fig 2.1, Franz diffusion cells contain donor and receptor compartments. The skin membrane was mounted in the cell with the stratum corneum uppermost. The diameters of donor and receptor compartments were measured, and the available diffusion area was calculated accordingly. To ensure a good seal around the skin, the contact surface of both compartments was coated with a thin layer of silicone based high vacuum grease (Dow Corning, USA). According to the test guideline OECD 428, the confirmation of skin membrane integrity is an essential component of the *in vitro* method. (OECD, 2004b). After setting up the Franz diffusion cells, the skin integrity was examined by assessment of electrical resistance (Davies et al., 2004). The donor and receptor chambers were filled with PBS, and two stainless steel electrodes were inserted into the fluid in the receptor and donor compartments, respectively. The impedance reading (k Ω) was recorded at 50 Hz. There is no guideline suggesting the acceptable range of impedance reading. Lawrence (1997) reported that a skin membrane with an initial electrical resistance of 45.4 k Ω cm² demonstrated an intact barrier function. Previous experiments in our group confirmed that skin with impedance readings lower than 20 k Ω allows over-permeation of the active. Therefore, any impedance reading greater than 20 k Ω was considered as a compulsory criterion in the study, and skin membranes with electrical resistance lower than this value were discarded.

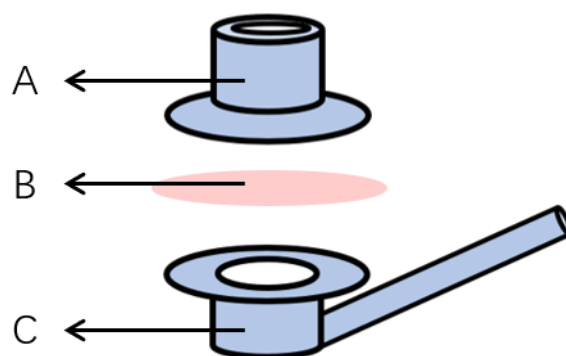


Figure 2. 1 Schematic view of vertical Franz diffusion cell. The donor compartment (A), skin membrane (B), and the receptor compartment (C) are indicated in the figure.

2.5 mL degassed freshly prepared PBS solution ($\text{pH } 7.30 \pm 0.10$) was used as the receptor medium. At each sampling interval, 200 μL of receptor phase was withdrawn, and an equal volume of fresh PBS solution was added. Homogeneous temperature distribution in the receptor phase was maintained using a Teflon-covered magnetic stirring bar. Franz cells were placed in a thermostatically controlled water bath (JB Nova, Grant, UK) set at $36 \pm 1^\circ\text{C}$. The skin surface was maintained at $32 \pm 1^\circ\text{C}$ (TM-22 Digitron digital thermometer, RS Components, Corby, UK). The permeation study was conducted up to 24 h at two dose levels. With the higher dose (infinite), 50 $\mu\text{L}/\text{cm}^2$ of NIA solution was added into each donor compartment; whereas for finite dosing the formulation was applied at a dose of 5 $\mu\text{L}/\text{cm}^2$ to mimic real-life application amounts.

At the end of the permeation studies, the receptor phase was removed completely, and the mass balance study was conducted following a procedure validated previously (Haque et al., 2017a). The skin surface was washed three times with 1 mL of methanol-water (50:50) mixture for finite dose studies and five times for infinite dose studies, followed by swabbing with a cotton bud. The washing solutions and cotton buds were collected and placed in 2 mL Eppendorf[®] tubes (Eppendorf[®], UK) with 1 mL of methanol-water (50:50) solution. To extract the quantity of NIA in the skin, the skin membrane was removed and cut into small pieces and placed in 2 mL Eppendorf[®] tubes with 1 mL of methanol-water (50:50) solution. All the tubes were placed in an incubating orbital shaker at $32 \pm 1^\circ\text{C}$, at a speed of 800 rpm (VWR International, LLC, USA) overnight. After extraction was completed, the tube was centrifuged at 13,200 rpm (5415 R centrifuge Eppendorf[®], UK). The supernatant was collected for analysis.

NIA quantification was performed using the validated HPLC method. Samples were diluted where necessary. `

2.2.6 Permeation studies of NIA from single solvent formulations using human skin

Human female abdominal tissue was obtained from surgery. After removing excess subcutaneous fat using a scalpel, human epidermis was prepared by heat separation (Kligman and Christophers, 1963). The tissue was immersed in deionized water maintained at 60 °C for 45 s, and then the epidermal membrane was carefully peeled away from the dermis. Separated human epidermis was mounted on filter paper (Grade no. 1, Whatman, U.K.) as a support, covered with aluminum foil and stored at -20 °C until required. On the day of the *in vitro* skin permeation study, human epidermis was defrosted at room temperature. The skin membrane was cut into appropriate sizes and mounted on the Franz cells with the filter paper as support. It has previously been confirmed that the filter paper has no interaction with the permeant and has no rate-limiting interference (Oliveira et al., 2012). Before use, the integrity of the skin was examined by assessment of electrical resistance. Skin membranes with electrical resistance values lower than 20 kΩ were discarded.

This study was carried out in the same way as for the permeation study using porcine skin. Vertical glass Franz diffusion cells were used to conduct the studies in human skin. Degassed freshly prepared PBS solutions were used as the receptor medium; the study was performed up to 24 h at 32 ± 1 °C. The same dosing conditions as for the porcine skin studies were used (5 and 50 µL/cm²). 200 µL of receptor medium was withdrawn and an equal volume of PBS solution was added at each sampling time. Mass balance studies were performed after the permeation studies. All the samples were analyzed using HPLC.

2.2.7 The development of the Skin PAMPA method

The Skin Parallel Artificial Membrane Permeability Assay (PAMPA) is a high-throughput screening tool recently developed for human skin permeation prediction and evaluation (Sinkó et al., 2012). This method has been used for *in vitro* screening of ibuprofen preparations (Balazs et al., 2016; Luo et al., 2016). The permeation studies were conducted

up to 6 h for PAMPA, and a dose of 1 μL was determined as the appropriate dose for finite dose studies of ibuprofen. To investigate the suitability of the Skin PAMPA method for *in vitro* permeation studies of NIA, various doses were investigated, and the same permeation time was used.

As stated previously (Session C.1.5.3), the Skin PAMPA is a 96-well plate-based model. An artificial lipid membrane pre-coated plate is used as the donor compartment and a 96-well plate is used as the receptor compartment. This artificial membrane was developed based on the structure of the intercellular lipid matrix in human stratum corneum. As shown in Fig 2.2, this whole Skin PAMPA kit is commonly referred to as a “PAMPA sandwich”. The pre-coated Skin PAMPA membrane was hydrated overnight prior to use. 200 μL of hydration solution was filled in each well of the bottom plate of the Skin PAMPA sandwiches. The Skin PAMPA top plate was submerged in a hydration solution. The top plate was covered and sealed with Parafilm® to ensure good contact between the membrane and the hydration solution. The top plate was removed from the bottom plate once hydration was completed.

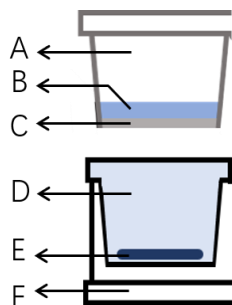


Figure 2. 2 Schematic view of the Skin PAMPA system. The donor compartment (A), formulations (B), pre-coated lipid membrane (C), receptor phase (D), individual stirrer (E) and the receptor plate (F) are indicated in the figure.

Five NIA formulations were tested in this study, namely 5 % (w/v) NIA in PG, DMI, PEG 400 and PEG 600, and one commercial product containing the same amount of active (Olay®). Two different doses were applied, 1 and 17 μL per well, corresponding to 3 and 51 $\mu\text{L}/\text{cm}^2$, respectively. Degassed freshly prepared PBS was used as the receptor medium and a volume of 180 μL was added to each receptor compartment. A stirring disk was placed in each well. After dosing with the chosen formulations, the donor plate was placed on the

receptor plate. To maintain the temperature of the membrane at 32 ± 1 °C, the Skin PAMPA kit was incubated in the stirring unit of the "Gut-Box™" during the course of the permeation studies. At 0.3, 0.5, 1, 2, 3, 4, 5 and 6 h, the receptor plate was replaced with a new 96-well plate prefilled with fresh temperature equilibrated PBS solution. 150 µL of sample solution was withdrawn and subsequently analyzed by HPLC. The sample solutions were diluted with the same fresh receptor medium when needed.

2.2.8 Permeation studies using the Skin PAMPA model

After determining the optimum parameters for assessment of NIA formulations in the Skin PAMPA model NIA formulations were then further examined. The Skin PAMPA model was hydrated and prepared following the procedure described in 2.2.7. The permeation studies were conducted using a modified protocol. Two doses of the NIA formulation were assessed, 1 and 30 µL per donor well, corresponding to 3 and 90 µL/cm². The NIA solutions were prepared in PG, DMI, T-BA, TC, PEG 400 and PEG 600. The same commercial product (Olay®) was also included. The studies were performed at 32 ± 1 °C up to 2.5 h, the sampling time points were 0.1 0.2, 0.3, 0.7, 1, 1.5, 2 and 2.5 h. Degassed freshly prepared PBS served as the receptor medium. 150 µL samples were collected and analyzed using HPLC.

2.2.9 Statistical analysis

All the results are presented as the mean \pm standard deviation (SD). The statistical analysis was conducted using SPSS® Statistics Version 24 (IBM, USA). The data were examined for normality using the Shapiro-Wilk Test, and the homogeneity of variance was assessed using Levene's test. For data that met the assumptions of normality and homogeneity of variance, one-way ANOVA was performed. Tukey's HSD post hoc test was used after ANOVA analysis to perform pairwise analysis. For non-parametric data or where the assumption of homogeneity of variance between groups was violated in the ANOVA analysis, the Kruskal-Wallis H test was used. A p-value lower than 0.05 ($p < 0.05$) was considered a statistically significant difference. The correlation between cumulative amounts of NIA that penetrated through PAMPA and skin membranes was determined using the

Pearson Product-moment correlation coefficient (r^2) with MS Excel (Microsoft Corp., USA).

2.3 Results and discussion

2.3.1 Development and validation of HPLC assay method of NIA

A wavelength scan of a NIA solution with a concentration of 1 mg/mL was carried out using methanol as the blank and 263 nm was selected as the optimum UV absorbance. Table 2.1 presents the chromatographic conditions developed for the HPLC method for NIA.

Table 2. 1 HPLC conditions for analysis of NIA

HPLC Conditions	
Column	Phenyl-Hexyl 250x4.6mm
Mobile phase (v/v)	20% methanol 80% water
Temperature (°C)	25
Flow rate (mL/min)	1.0
Run time (min)	5.5
Wavelength (nm)	263
Injection volume (μL)	10

Table 2.2 summarises the results for the HPLC analytical method validation. A calibration curve ranging from 0.25 to 50 μg/mL was constructed. The correlation coefficient (r^2) was determined as >0.99 which confirms the linearity of this method (Fig 2.1). The accuracy was validated by spiking NIA at three concentration levels (1, 20, 50 μg/mL). The recovery was determined within the range of 99 to 102 %. This indicated that this analytical method is accurate for NIA quantification. The % RSD values of intra-day precision studies were < 1 %; the % RSD values of inter-day precision studies were < 2 %. The detection limit and quantitation limit were 0.13 and 0.39 μg/mL, respectively. For the system suitability study, the % RSD values of the retention time of NIA, peak area of the absorbance, and symmetry were 2.35 %, 0.60 %, and 0.54 %, respectively. Chromatographic conditions were changed to

investigate the robustness of this analytical method; the values of the correlation coefficient (r^2) were > 0.99 under all tested conditions. This method is therefore suitable and robust for NIA quantitation.

Table 2. 2 HPLC method validation parameters for quantitative analysis of NIA, data presented as mean \pm SD, (% RSD).

Linearity		> 0.99		
Detection limit ($\mu\text{g mL}^{-1}$)		0.13		
Quantitation limit ($\mu\text{g mL}^{-1}$)		0.39		
System suitability n=6	Peak area	279.12 \pm 1.68 (0.60)		
	Retention time (min)	3.62 \pm 0.08 (2.35)		
	Symmetry	0.72 \pm 0.01 (0.54)		
Accuracy	Concentration ($\mu\text{g mL}^{-1}$)	1	20	50
	Recovery	101.96 \pm 0.82	99.98 \pm 0.09	100.14 \pm 0.24
Precision	Concentration ($\mu\text{g mL}^{-1}$)	1	20	50
	Intraday	(0.66)	(0.07)	(0.19)
	Intermediate	(1.67)	(0.40)	(0.52)

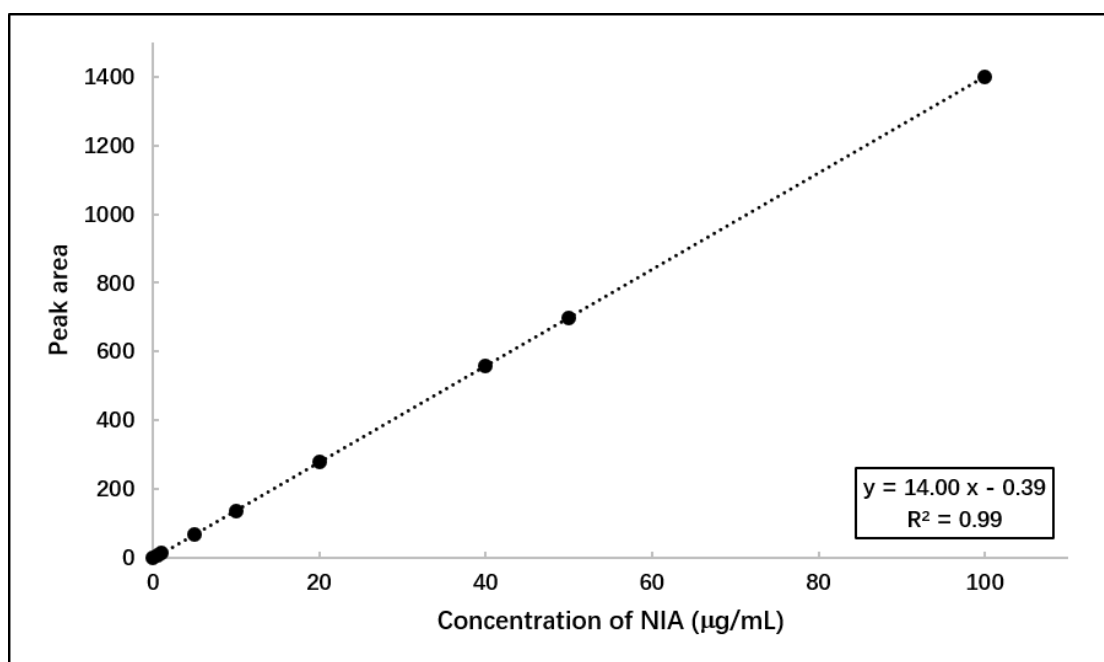


Figure 2. 3 The calibration curve for NIA

2.3.2 Solubility and stability studies of NIA

The solubility parameter offers a numerical estimate of the compatibility and the degree of interaction between solute and solvent (Welker, 2012), and may facilitate the assessment of the solubility of a model active in solvents. A series of solvents with a range of solubility parameters were selected to investigate the solubility of NIA. The measurement was performed in triplicate and the solubility parameter was calculated by the Van Krevelen and Hoftyzer type 3-D method using Molecular Modelling Pro software[®]. The results are shown in Table 2.4.

Table 2. 3 Solubility of NIA in different solvents (mean \pm SD, n=3).

Solvent	Abbreviation	Solubility parameter (cal/cm ³) ^{1/2}	Solubility of NIA (% w/v)
Isopropyl myristate	IPM	8.21	0.10 \pm 0.01
Oleic acid	OA	8.67	3.40 \pm 0.15
Caprylic/capric triglyceride	CCT	7.82	0.16 \pm 0.03
Dimethyl isosorbide	DMI	9.97	8.01 \pm 0.57
Polyethylene glycol 600	PEG 600	10.59	12.12 \pm 0.22
Transcutol® P	TC	10.62	13.71 \pm 0.35
t-Butyl alcohol	T-BA	10.75	10.96 \pm 0.20
Polyethylene glycol 400	PEG 400	11.67	18.70 \pm 0.88
Polyethylene glycol 200	PEG 200	12.06	22.76 \pm 0.25
Propylene glycol	PG	14.07	28.41 \pm 0.85
Glycerol	GLY	17.14	2.75 \pm 0.01

The solubility parameter of NIA was calculated as 13.85 (cal/cm³)^{1/2}. This molecule is expected to be more soluble in vehicles that are also hydrophilic. The solubility of NIA ranged from 0.1 to 29 % (w/v) in the tested solvents, and NIA is more soluble in those vehicles with solubility parameter values closest to that of NIA itself. The solubility of NIA in DMI, PEG 600, TC, T-BA, PEG 400, PEG 200 and PG was determined as > 5 %; the solubility of NIA in IPM, CCT and OA was < 5 %. The solubility values for NIA in DMI and PG were also consistent with the results reported by Mohammed et al. (2014a). Since the level of NIA in the tested solution was selected as 5 % (w/v), IPM, CCT and OA were not taken forward for the preparation of single solvent systems. The solubility of NIA in PBS was also determined as 61.22 \pm 2.19 % (w/v). The result confirmed that PBS is an appropriate receptor solution as the

solubility of NIA is sufficient to maintain sink conditions and minimize back diffusion during the course of the permeation study (Finnin et al., 2012).

The stability of NIA in a series of solvents and PBS was also assessed at a concentration of 5 % (w/v) over a 72 h period at 32 ± 1 °C (Fig 2.4). With the exception of TC, after 72 h, the recovery values of NIA were greater than 90 % in all tested solvents. The corresponding value for TC was 88.5 % and the stability of NIA in PBS was also confirmed.

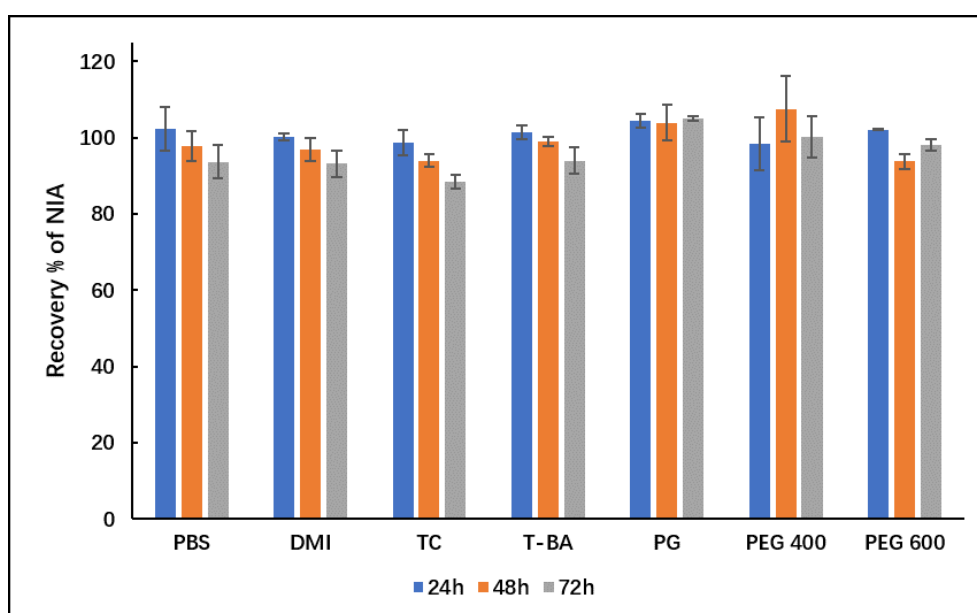


Figure 2. 4 The stability of NIA in a series of tested solvents (mean \pm SD, n=3).

2.3.3 DVS

The hydration and evaporation of NIA solutions were investigated using DVS over the same time period of the permeation studies. Fig 2.5 shows the DVS results for all NIA solutions over the time course of the permeation studies (24 h) at 32 ± 1 °C and 50 % RH. Rapid evaporation was evident for the T-BA solution. Approximately 90 % of the applied T-BA solution evaporated in the first 10 min, and only 5.1 ± 3.0 % of the initial applied weight was recovered at 24 h. Although the PG, TC and DMI solutions showed an initial increase in weight because of their hygroscopic nature, these solvents evaporated with time. 44.6 ± 0.02 %, 17.6 ± 0.5 % and 76.3 ± 0.1 % of the applied PG, TC and DMI solutions were recovered at 24 h, respectively. The rapid evaporation of TC and PG is consistent with previous studies reported by Paz-Alvarez et al. (2018) and Haque et al. (2017b). For the two polyethylene

glycols, the weight increased because of their hygroscopic nature; $110.7 \pm 0.02 \%$ and $105.1 \pm 1.2 \%$ were recovered for PEG 400 and PEG 600 at 24 h, respectively.

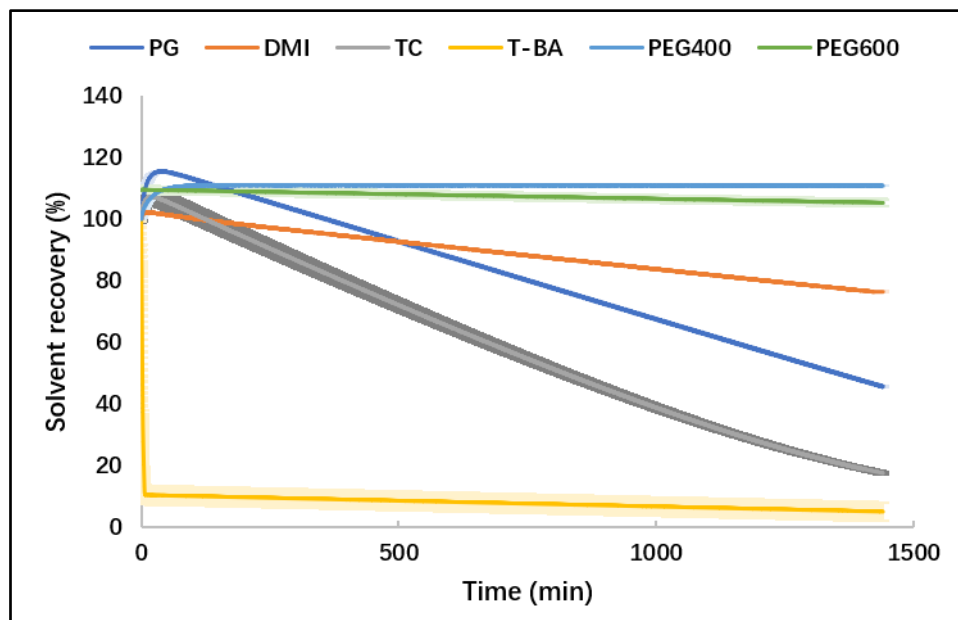


Figure 2. 5 Percentage weight loss over 1440 min for 5 % (w/v) NIA in PG, DMI, TC, T-BA, PEG 400 and PEG 600 (n=3, mean \pm SD).

2.3.4 Permeation studies of NIA using porcine skin under infinite dose conditions

The permeation behavior of NIA was first investigated using porcine skin. Porcine skin is recognized as the most appropriate surrogate for human skin because of its anatomical, histological and physiological similarities to human skin (Barbero and Frasch, 2009). Two doses (5 and $50 \mu\text{L}/\text{cm}^2$) of the various NIA solutions were examined for NIA *in vitro* permeation studies using porcine skin. Fig 2.6 presents the permeation profiles of NIA from single solvent solutions and the commercial product in porcine skin under infinite dose conditions. The percent of NIA permeated is also shown (Fig 2.7). No permeation of NIA was observed for PEG 400 and PEG 600. For the remaining formulations, the cumulative permeated amount of NIA at 24 h ranged from 39 to $475 \mu\text{g}/\text{cm}^2$. A higher permeation was observed for the T-BA solution compared to other formulations at 24 h, corresponding to $\sim 18 \%$ of the applied amount. T-BA is a tertiary aliphatic alcohol and is used as a solvent and alcohol denaturant in cosmetics (Chen, 2005). There is only limited information regarding the

effect of this tertiary alcohol on skin permeation of actives. However, various mechanisms have been proposed to explain the penetration enhancer action of short chain alcohols (Lane, 2013). It has been reported that ethanol acts as a permeation enhancer by modifying the barrier function of the skin, including lipid fluidization and lipid extraction (Goates and Knutson, 1994). Watkinson et al. (2009) investigated the influence of ethanol on the permeation characteristics of ibuprofen in silicone and human skin. The authors suggested that ethanol enhanced permeation by increasing ibuprofen solubility in the skin. Later, Oliveira et al. (2012) investigated the effect of ethanol in combination with TC, DMI, and IPM on the enhancement of percutaneous absorption using methyl paraben as a model active. The authors reported that TC and DMI incorporated with ethanol showed higher efficiency compared with TC and DMI prepared as single solvent solutions. The authors suggested that rapid evaporation of ethanol occurred from the preparations leaving a saturated residue of the active in the formulations on the skin surface. The evaporation of T-BA solution was evident in DVS studies (2.3.3). In the permeation studies, following application of the formulation in the donor compartment, the evaporation of T-BA may lead to an increased level of NIA in the formulation, and potentially enhance permeation of NIA in skin. The effects of this solvent on the skin barrier function were probed further by measuring trans-epidermis water loss (TEWL). Results are shown in Appendix 1.

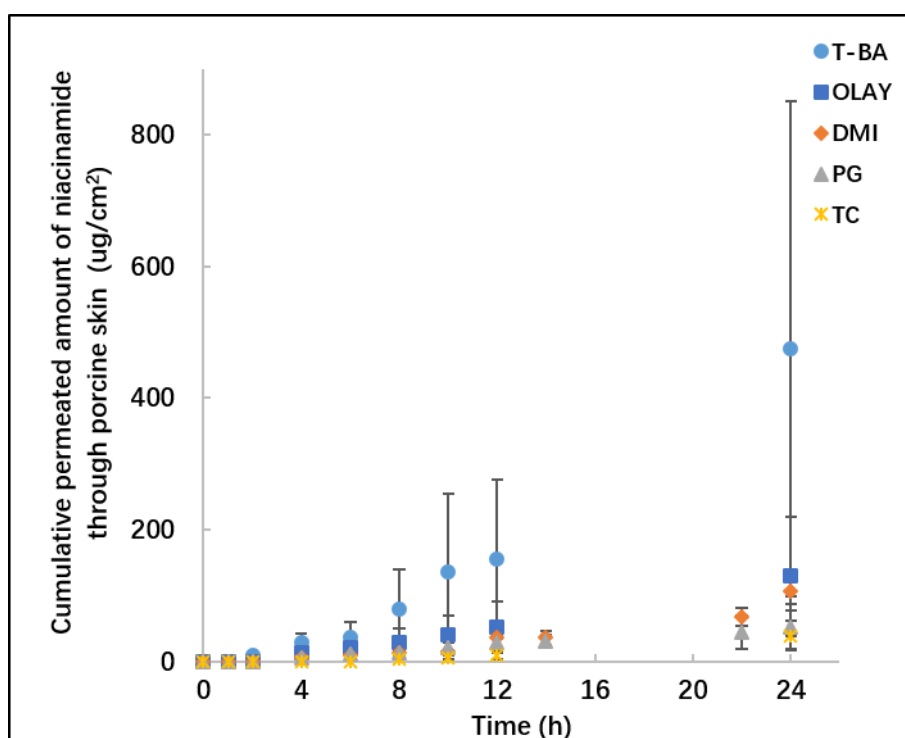


Figure 2. 6 Permeation profiles of NIA from Olay®, T-BA, PG, TC and DMI in porcine skin following the application of 50 $\mu\text{L}/\text{cm}^2$. Each data point represents the mean \pm SD, $3 \leq n \leq 5$.

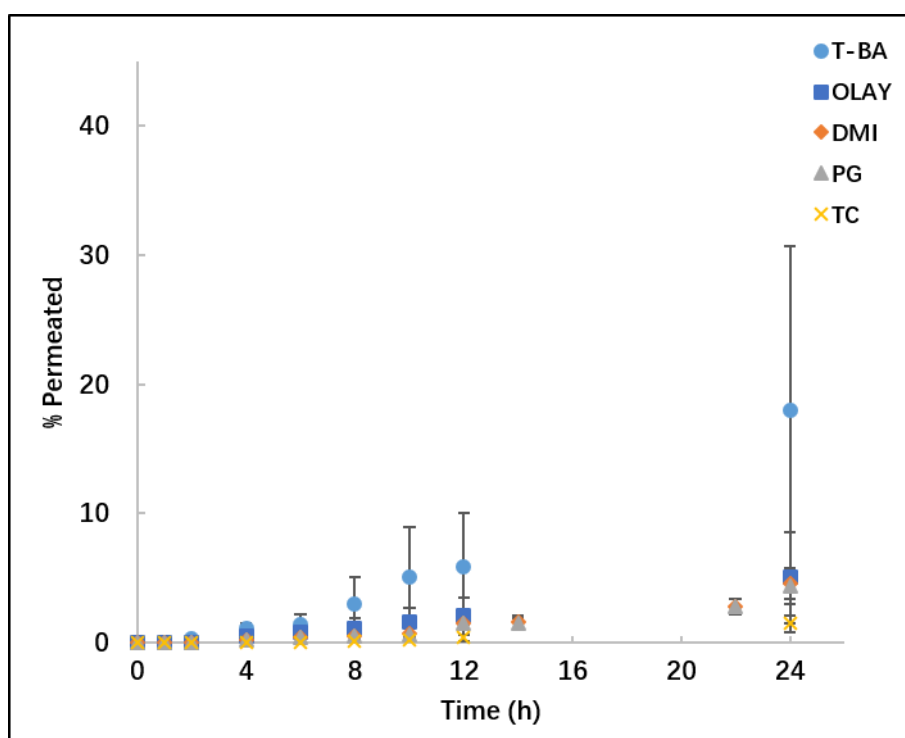


Figure 2. 7 Percent of NIA permeated from Olay®, T-BA, PG, TC and DMI in porcine skin following the application of 50 $\mu\text{L}/\text{cm}^2$. Each data point represents the mean \pm SD, $3 \leq n \leq 5$.

There was no difference in the percentage of NIA that permeated from T-BA, Olay®, PG,

TC and DMI, with the values observed being 18.0 ± 12.7 , 5.1 ± 3.5 , 4.6 ± 1.2 , 4.4 ± 1.4 , and 1.5 ± 0.7 % of applied amounts, respectively ($p > 0.05$).

Mass balance studies were conducted after the permeation studies. Table 2.4 shows the percentage of applied NIA recovered from the skin surface and inside the skin. With the exception of T-BA, for most formulations, more than 70 % of the applied amounts of NIA were recovered from the skin surface by washing; the corresponding value for T-BA was 45 %. Among all the tested formulations, a higher skin retention was observed for T-BA (at 20.8 %, $p < 0.05$) compared to PG, Olay®, TC, PEGs. There was no difference for the skin extraction values between T-BA and DMI (at 7.6 %, $p > 0.05$). For PEG 400 and PEG 600 solutions, no permeation was observed; the percentages of NIA extracted from the skin were 0.4 and 0.1 %, respectively ($p > 0.05$).

Table 2. 4 The results of mass balance studies following the permeation studies using porcine skin under following application of $50 \mu\text{L}/\text{cm}^2$ ($3 \leq n \leq 5$, mean \pm SD).

	Formulation						
	Olay® %	T-BA %	PG %	TC %	DMI %	PEG 400 %	PEG 600 %
Washing %	75.2 ± 11.1	45.4 ± 21.4	96.1 ± 8.9	81.3 ± 0.3	90.7 ± 3.5	87.1 ± 12.0	87.5 ± 11.3
Extraction %	3.4 ± 1.3	20.8 ± 9.4	3.3 ± 1.1	0.8 ± 0.2	7.6 ± 3.2	0.4 ± 0.3	0.1 ± 0.1
Permeation %	5.1 ± 3.0	18.0 ± 12.7	2.3 ± 1.4	1.5 ± 0.7	4.4 ± 1.4	0	0
Total recovery %	84.2 ± 11.8	84.1 ± 7.0	101.7 ± 8.2	83.6 ± 0.4	102.7 ± 4.7	87.5 ± 12.1	87.6 ± 11.4

2.3.5 Permeation studies of NIA using porcine skin under finite dose conditions

The permeation profiles of NIA in porcine skin following the application of a $5 \mu\text{L}$ dose are illustrated in Fig 2.8; the corresponding percentages permeated are shown in Fig 2.9. In this finite dose study, the permeation profiles of NIA exhibited plateaus as a result of donor depletion. The cumulative amount of NIA that permeated ranged from 43 to $116 \mu\text{g}/\text{cm}^2$ ($p > 0.05$); the percentages of the applied doses that permeated for the corresponding formulations ranged from 18 to 55 % ($p > 0.05$). At 24 h, the permeation from TC and PG were determined as 95.1 and $46.0 \mu\text{g}/\text{cm}^2$, respectively.

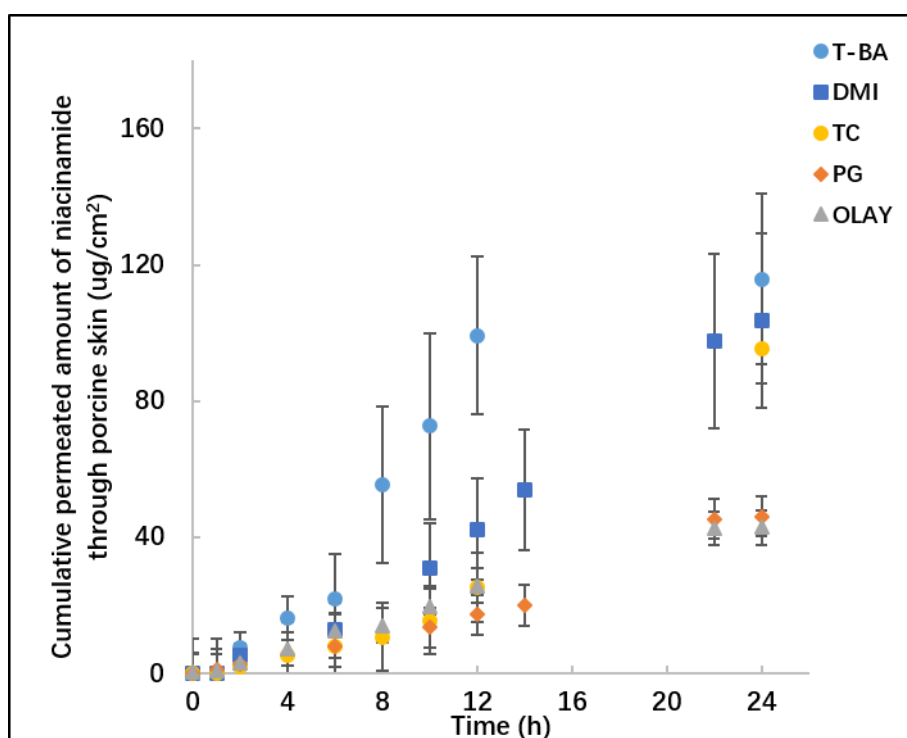


Figure 2. 8 Permeation profiles of NIA that permeated from Olay®, T-BA, PG, TC and DMI in porcine skin following the application of 5 $\mu\text{L}/\text{cm}^2$. Each data point represents the mean \pm SD, $3 \leq n \leq 5$.

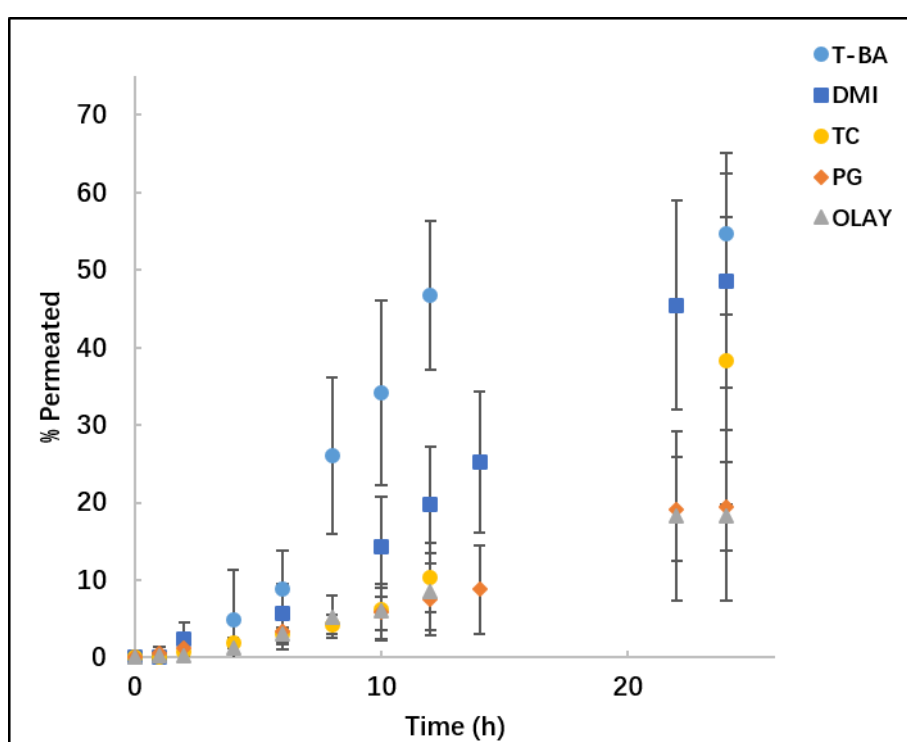


Figure 2. 9 Percentages of NIA that permeated from Olay®, T-BA, PG, TC and DMI in porcine skin following the application of 5 $\mu\text{L}/\text{cm}^2$. Each data point represents the mean \pm SD, $3 \leq n \leq 5$.

Table 2.5 shows the results of the mass balance study. Higher skin extraction was

evident for Olay[®], namely 25 % of the applied dose ($p>0.05$), followed by DMI (17 %), TC (16 %), T-BA (5 %), and PG (3 %). The total amount of NIA recovered in the mass balance studies for Olay[®], TC, PEG 400 and PEG 600 solutions fell in the range required by the Scientist Committee on Consumer Safety (SCCS) for dermal absorption studies (85-115 %) (SCCS, 2010). Sil et al. (2018) reported chemical reduction of NIA following permeation studies in full-thickness porcine skin. The authors utilized LC-MS to elucidate various by-products of NIA following skin penetration and identified a number of different by-products. The comparatively low recovery of NIA from the T-BA, PG, and DMI formulations in this work might be attributed to a similar chemical derivatization of NIA following dermal absorption. However, further studies with these solvents would need to be conducted to confirm this.

Table 2. 5 The results of mass balance studies following the permeation studies using porcine skin following application of 5 $\mu\text{L}/\text{cm}^2$ of formulations ($3 \leq n \leq 5$, mean \pm SD).

	Olay [®]	T-BA	PG	TC	DMI	PEG 400	PEG 600
Washing %	42.1 \pm 12.1	20.5 \pm 2.4	55.6 \pm 7.0	33.3 \pm 15.8	8.4 \pm 2.5	89.0 \pm 17.5	100.5 \pm 1.3
Extraction %	24.5 \pm 5.1	4.9 \pm 1.8	2.7 \pm 1.2	16.4 \pm 5.8	16.7 \pm 6.3	0	0.7 \pm 0.1
Permeation %	18.3 \pm 11.0	54.7 \pm 11.7	19.5 \pm 5.7	38.3 \pm 18.5	48.6 \pm 13.8	0	0
Total recovery %	84.9 \pm 10.0	80.0 \pm 7.5	77.8 \pm 3.9	88.0 \pm 10.0	73.7 \pm 11.1	89.0 \pm 17.5	101.3 \pm 1.3

2.3.6 Permeation studies of NIA using human skin under infinite dose conditions

The permeation behavior of NIA was subsequently determined using human skin following an application of 50 μL of formulations. The same formulations studied in porcine skin were examined. No permeation of NIA was observed for PEG 400 and PEG 600 for human tissue. At 24 h, the cumulative amount of NIA that permeated through human skin ranged from 2 to 169 $\mu\text{g}/\text{cm}^2$. Significantly higher permeation of NIA was observed for T-BA (169.2 \pm 37.9 $\mu\text{g}/\text{cm}^2$) compared with other formulations ($p<0.05$), corresponding to 8 % of the applied amount. The amounts of NIA that permeated from Olay[®], TC, DMI, and PG were 10.3, 7.5, 5.6, and 1.5 $\mu\text{g}/\text{cm}^2$ ($p>0.05$).

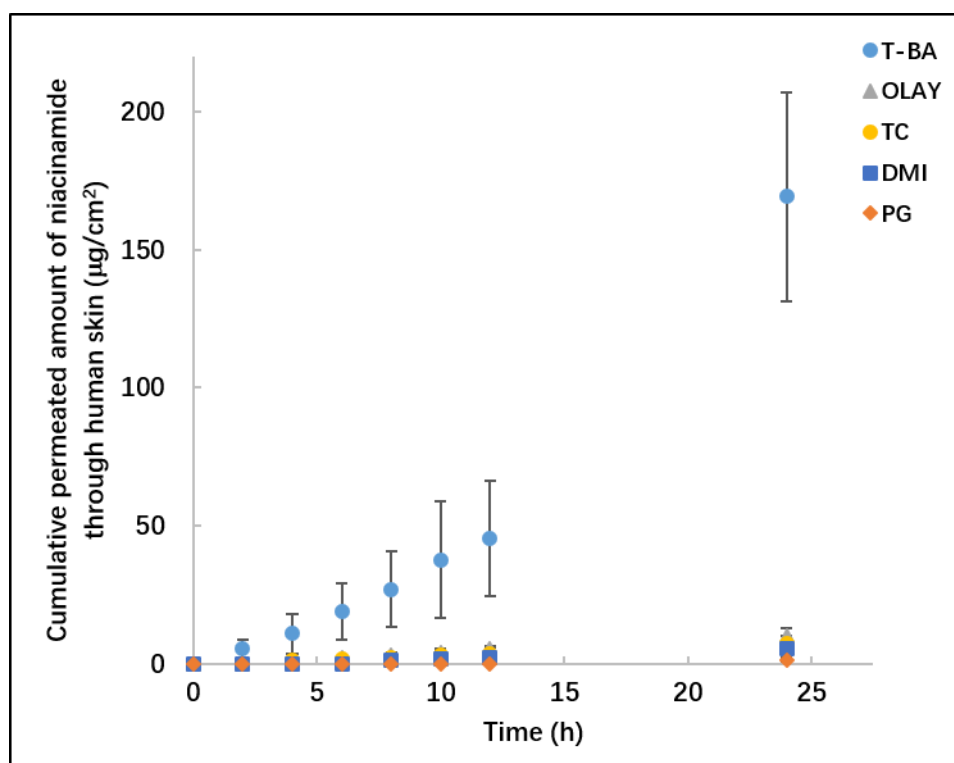


Figure 2. 10 Permeation profiles of NIA that permeated from Olay®, T-BA, PG, TC and DMI in human skin following the application of 50 $\mu\text{L}/\text{cm}^2$ of formulations. Each data point represents the mean \pm SD, $3 \leq n \leq 5$.

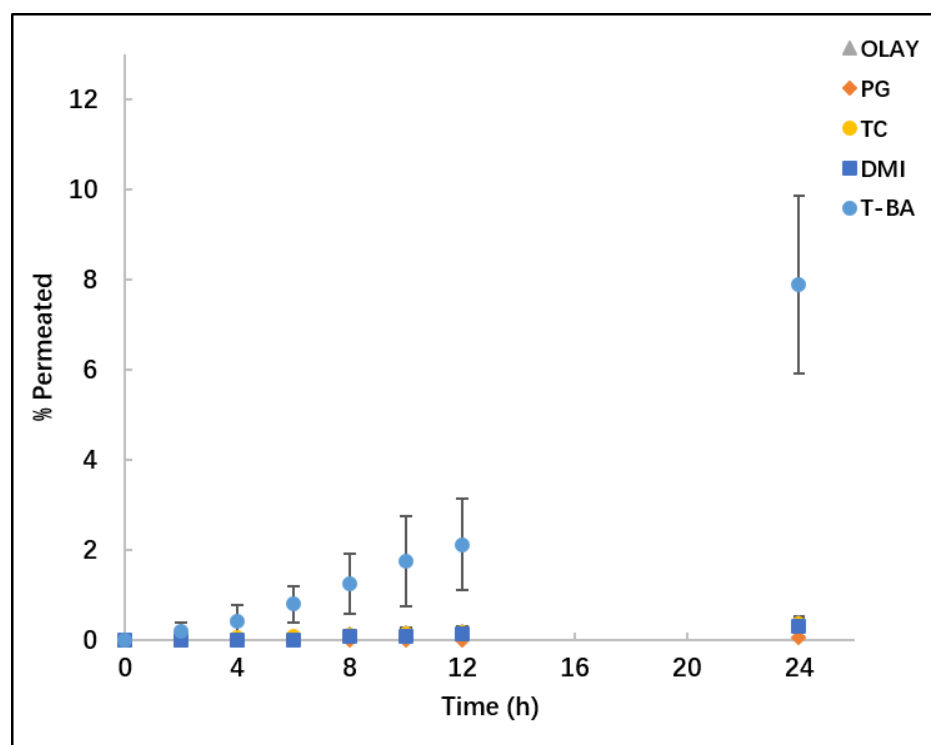


Figure 2. 11 Percentages of NIA that permeated from Olay®, T-BA, PG, TC and DMI in human skin following the application of 50 $\mu\text{L}/\text{cm}^2$ of formulations. Each data point represents the mean \pm SD, $3 \leq n \leq 5$.

The results from the mass balance studies are summarized in Table 2.7. The overall recovery for all tested formulations ranged from 85 to 101 %, which fell below the SCCS limits (SCCS, 2010). The results from the mass balance study confirmed that more than 80% of the dosed NIA remained on the skin surface after 24 h, and less than 2 % of the applied NIA was retained in the epidermal membrane. A significantly higher amount of NIA was retained in the skin for the PG solution compared with the other formulations ($p < 0.05$).

Table 2. 6 The results of the mass balance studies following the permeation studies using human skin following application of 50 $\mu\text{L}/\text{cm}^2$ of formulations ($3 \leq n \leq 5$, mean \pm SD).

	Olay [®]	T-BA	PG	TC	DMI	PEG 400	PEG 600
Washing %	97.3 \pm 3.8	86.8 \pm 0.2	94.6 \pm 9.1	91.9 \pm 10.5	100.3 \pm 9.0	85.1 \pm 3.8	86.3 \pm 2.2
Extraction %	0.9 \pm 0.1	0.9 \pm 0.1	1.9 \pm 0.5	0.5 \pm 0.2	0.5 \pm 0.1	0.2 \pm 0.1	0.5 \pm 0.3
Permeation %	0.4 \pm 0.1	7.9 \pm 2.0	0.1 \pm 0.0	0.4 \pm 0.2	0.3 \pm 0.1	0	0
Total recovery %	98.5 \pm 3.8	95.6 \pm 1.7	96.6 \pm 9.5	92.7 \pm 10.7	101.1 \pm 9.2	85.0 \pm 4.3	86.8 \pm 2.1

2.3.7 Permeation studies of NIA in human skin under finite dose conditions

The permeation studies through human skin were also assessed under finite dose conditions. Fig 2.12 shows the permeation profiles of NIA in human skin following the application of 5 $\mu\text{L}/\text{cm}^2$ of formulations. There was no permeation of NIA from PEG 400 and PEG 600. For the remaining formulations, the permeation profiles demonstrated plateaus, reflecting the depletion of the formulation in the donor compartment. The highest cumulative amount of NIA permeated from T-BA, 50.8 \pm 11.0 $\mu\text{g}/\text{cm}^2$ ($p < 0.05$), corresponding to 24 % of the applied amount. Corresponding amounts that permeated from TC, DMI, Olay[®] and PG were 16.5 \pm 4.6, 15.0 \pm 3.4, 5.3 \pm 1.5 and 1.8 \pm 0.4 $\mu\text{g}/\text{cm}^2$. There was no difference in permeation values between TC, DMI, the commercial product and PG ($p > 0.05$).

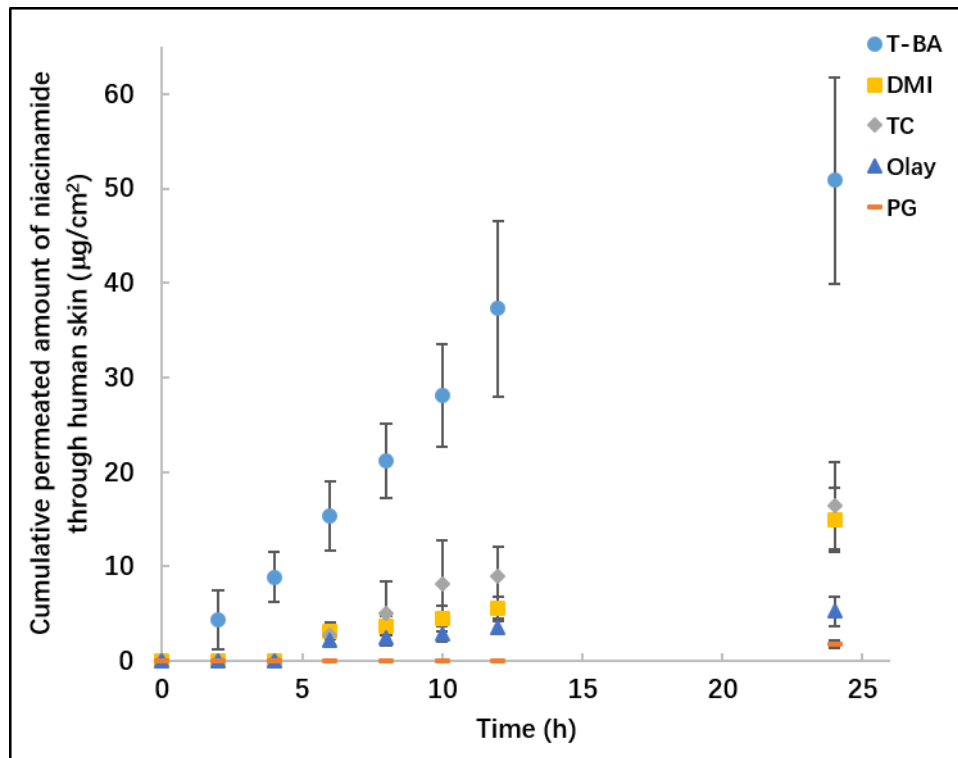


Figure 2. 12 Permeation profiles of NIA from Olay®, T-BA, PG, TC and DMI in human skin following the application of 5 $\mu\text{L}/\text{cm}^2$ of formulations. Each data point represents the mean \pm SD, $3 \leq n \leq 5$.

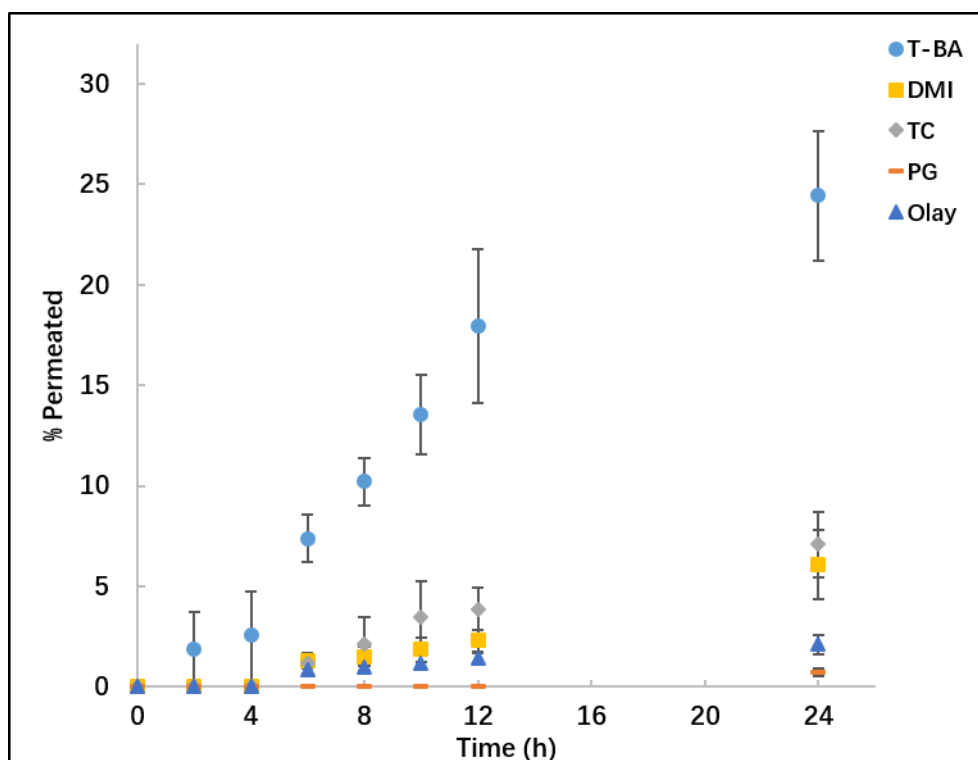


Figure 2. 13 Percentages of NIA that permeated from Olay®, T-BA, PG, TC and DMI in human skin following the application of 5 $\mu\text{L}/\text{cm}^2$ of formulations. Each data point represents the mean \pm SD, $3 \leq n \leq 5$.

Table 2.7 shows the mass balance results following the permeation studies in human skin under finite dose conditions. Interestingly, the results of the skin retention observed in finite dose studies were different from the results observed in previous infinite dose studies. The skin retention for all vehicles ranged from 2 to 33 %. These values are comparatively higher than the skin extraction obtained in infinite dose studies ($p < 0.05$). A higher percentage of NIA was retained in human epidermis for TC, (33 %), compared with PEG 400 and PEG 600 ($p < 0.05$). The values for percentage skin retention of NIA observed for DMI, PG, and Olay® were 18, 12, and 5 % ($p > 0.05$), respectively. In contrast, as reported in section 2.3.6, the highest human skin retention of NIA under infinite dose conditions was observed for PG ($p < 0.05$). PG is widely used as penetration enhancer in topical preparations (Lane, 2013). The mechanism of action of PG has not been fully elucidated. A number of studies have investigated the influence of PG on dermal delivery of actives (Trottet et al., 2004; Brinkmann and Müller-Goymann, 2005; Santos et al., 2011). It has been suggested that PG partitions into the stratum corneum and changes the environment, thus improving the solubility of the permeant. Trottet et al. (2004) investigated the effect of PG on penetration enhancement at clinically relevant doses. The authors reported that PG enhancement was limited by the depletion of PG from the formulation compared with studies conducted under infinite dose conditions. This may explain the differences in skin retention in the present work for infinite and finite dose conditions.

The total recoveries of NIA from all the tested formulations ranged from 81 to 105 %. As discussed earlier, low recovery may reflect the chemical derivatization of NIA during skin penetration. A comparatively low recovery of NIA was also reported by other researchers. Haque et al. (2017a) investigated the permeation behavior of NIA from three commercial products following three doses, namely 5, 20 and 50 $\mu\text{L}/\text{cm}^2$. For the two lower dosages, the overall recovery from mass balance studies lay outside the range of 85-115 %.

Under finite dose conditions, the cumulative permeated amounts of NIA through human skin were significantly lower than corresponding values in porcine skin ($p < 0.05$). This is consistent with the results observed by other researchers (Dick and Scott, 1992; Singh et al., 2002; Barbero and Frasch, 2009).

Table 2. 7 The results of mass balance studies following the permeation studies in human skin following application of 5 $\mu\text{L}/\text{cm}^2$ of formulations ($3 \leq n \leq 5$, mean \pm SD).

	Olay [®]	T-BA	PG	TC	DMI	PEG 400	PEG 600
Washing %	95.3 \pm 10.0	30.4 \pm 3.7	92.3 \pm 7.4	42.8 \pm 2.2	58.9 \pm 11.0	79.4 \pm 4.5	100.3 \pm 27.8
Extraction %	5.0 \pm 0.5	25.8 \pm 4.3	12.1 \pm 8.3	32.9 \pm 11.2	18.0 \pm 0.1	1.5 \pm 0.7	1.6 \pm 0.9
Permeation %	2.1 \pm 0.5	24.4 \pm 3.2	0.7 \pm 0.2	7.1 \pm 1.6	6.1 \pm 1.7	0	0
Total recovery %	102.4 \pm 10.1	80.6 \pm 5.7	105.1 \pm 7.6	82.8 \pm 12.2	83.0 \pm 9.9	81.0 \pm 4.9	101.9 \pm 28.0

2.3.8 The development of the Skin PAMPA method for NIA

To assess the suitability of the initial Skin PAMPA procedure for evaluation of NIA formulations, the permeation behavior of NIA was investigated using four simple solutions and one commercial product (Olay[®]). Fig 2.14 shows the permeation profiles of NIA following the application of 1 μL per well, corresponding to 3 $\mu\text{L}/\text{cm}^2$. The percentage NIA that permeated is shown in Fig 2.15. For all tested formulations, the permeation was detectable from the first sampling time point. At 0.5 h, 28 to 65 % of dosed NIA permeated through the lipid membrane. At 2 h, for all tested formulations, more than 56 % of the applied NIA permeated and the profiles started to plateau. At 6 h, the cumulative permeated amounts ranged from 95 to 182 $\mu\text{g}/\text{cm}^2$. Higher permeation was observed for DMI and PG solutions, with values of 181.6 ± 20.8 and 163.06 ± 27.7 $\mu\text{g}/\text{cm}^2$, respectively ($p > 0.05$). A lower amount was evident for PEG 600, at 95.3 ± 17.7 $\mu\text{g}/\text{cm}^2$. This value was significantly different from the corresponding values from DMI and PG solutions ($p < 0.05$).

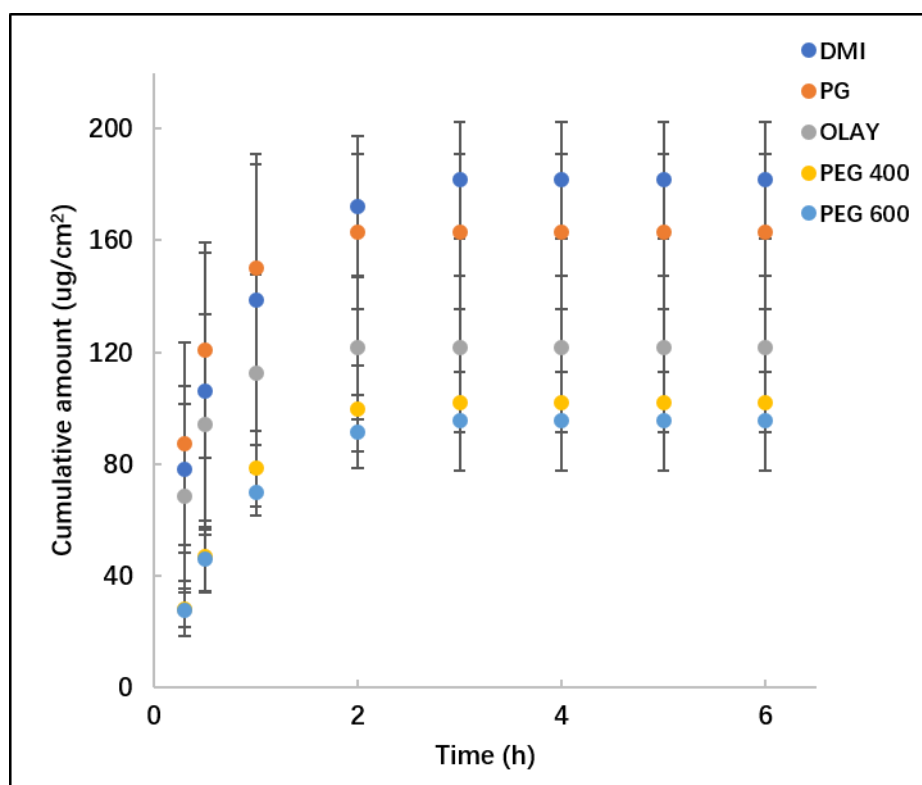


Figure 2. 14 The PAMPA permeation profiles of NIA from DMI, PG, Olay®, PEG 400 and PEG 600 following the application of 1 μ L of formulation. Each data point represents the mean \pm SD, n=6

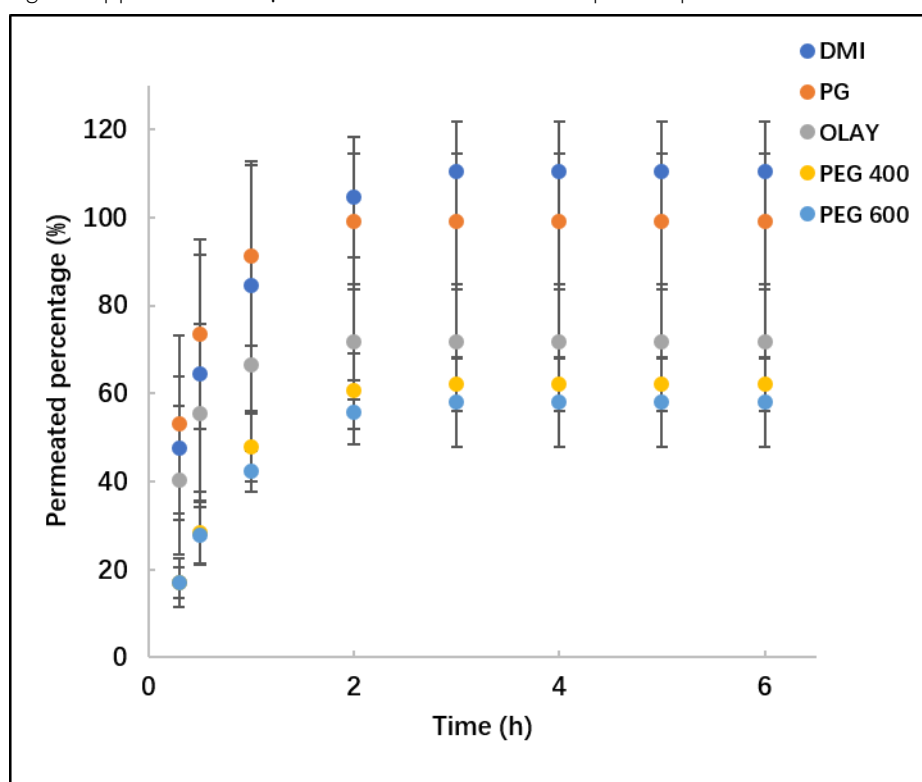


Figure 2. 15 The percentage permeation of NIA from DMI, PG Olay, PEG 400 and PEG 600 following the application of 1 μ L of formulation. Each data point represents the mean \pm SD, n=6.

Fig 2.16 and 2.17 illustrate the permeation profiles of NIA following the application of 17 μL per well, corresponding to 51 $\mu\text{L}/\text{cm}^2$ and the percentages permeated, respectively. At 6 h, more than 64 % of the applied NIA had been delivered to the receptor phase. The cumulative amounts of NIA that permeated ranged from 2984 to 1786 $\mu\text{g}/\text{cm}^2$. High permeation was evident for DMI, Olay[®] and PG, with values of 2834.0 ± 128.6 , 2984 ± 126.9 , and 2477.9 ± 171.9 $\mu\text{g}/\text{cm}^2$, respectively. The cumulative amounts of NIA that permeated from DMI, Olay[®] and PG were significantly higher than for PEG 400 and PEG 600 ($p < 0.05$).

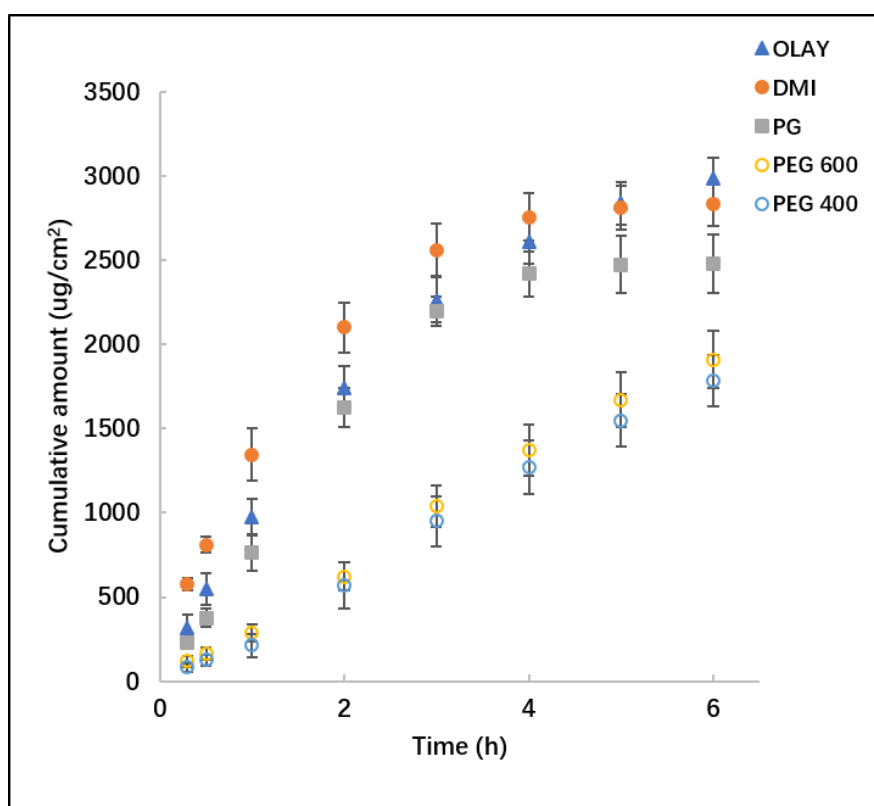


Figure 2. 16 PAMPA permeation profiles of NIA from DMI, PG, Olay[®], PEG 400 and PEG 600 following the application of 17 μL of formulation. Each data point represents the mean \pm SD, $n=6$.

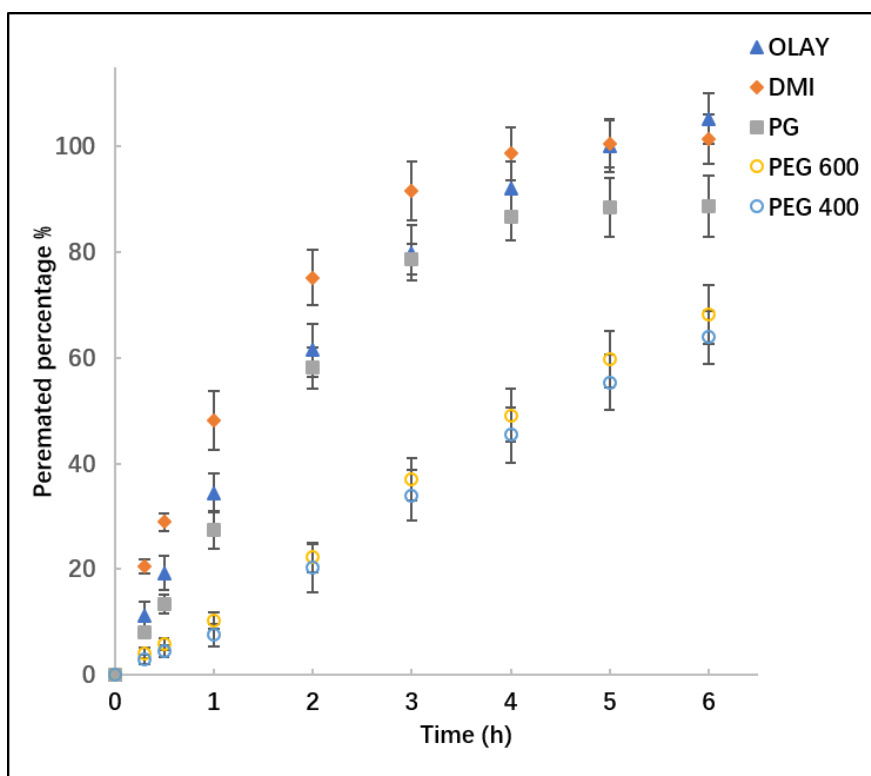


Figure 2. 17 Percentage NIA permeation from DMI, PG Olay, PEG 400 and PEG 600 following the application of 17 μL of formulation. Each data point represents the mean \pm SD, $n=6$.

Overall, a greater permeation of each formulation in the Skin PAMPA for the application of 17 μL compared to 1 μL was evident ($p<0.05$), while there was no difference in the percentages of NIA that permeated at 6 h for the two tested doses ($p>0.05$). For the dose of 1 μL , the permeation started to level off at 0.5 h, and the profile reflects the depletion of the NIA formulations. The dose of 1 μL per well is therefore an appropriate dose representing finite dose conditions for NIA testing. A shorter permeation time period with more sampling points should provide the necessary information for the study of the permeation behavior of the permeant.

2.3.9 Permeation studies of NIA using the Skin PAMPA model

Two doses of the various formulations of NIA were assessed in the Skin PAMPA model, namely 1 and 30 μL per well, corresponding to 3 and 90 $\mu\text{L}/\text{cm}^2$. For the finite dose conditions, the permeation profiles are shown in Fig 2.18. The cumulative amounts of NIA that permeated ranged from 146 to 196 $\mu\text{g}/\text{cm}^2$. The rank order for the cumulative amounts

of NIA that permeated at 2.5 h was: T-BA > TC > DMI > Olay > PG > PEG 400 > PEG 600. Higher permeation was evident for the T-BA formulation, with a value of $196.5 \pm 4.3 \mu\text{g}/\text{cm}^2$. This value was significantly higher than PEG 400 and PEG 600 ($p < 0.05$). At 2.5 h, the cumulative amounts of NIA that permeated from PEG 400 and PEG 600 were 146.3 and $156.2 \mu\text{g}/\text{cm}^2$, respectively.

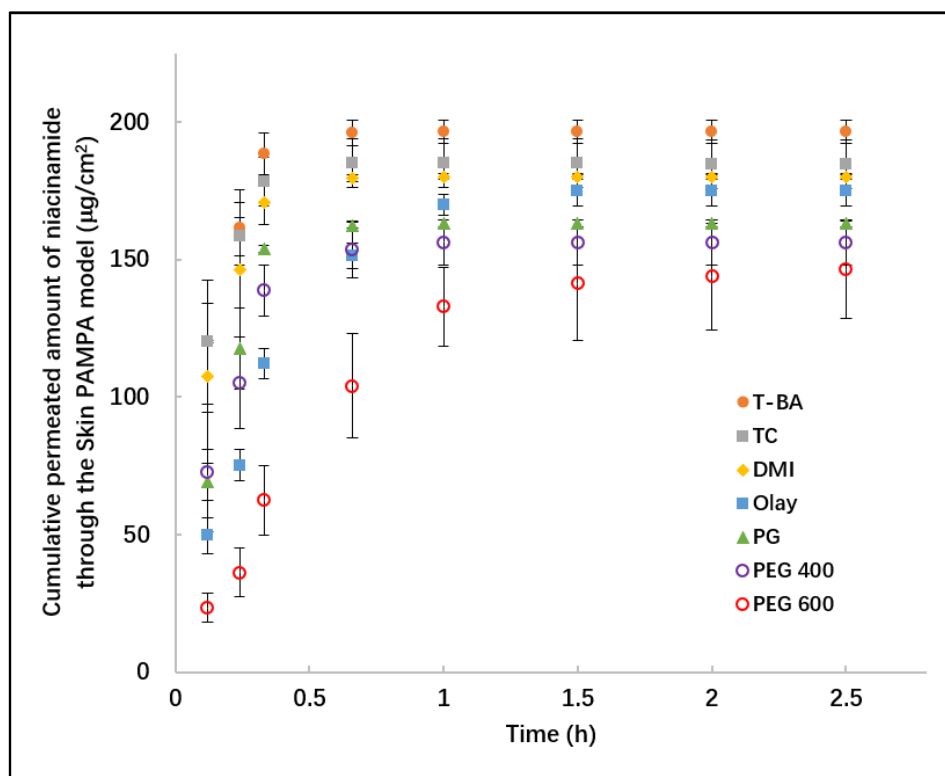


Figure 2. 18 PAMPA permeation profiles of NIA from T-BA, TC, DMI, PG, Olay®, PEG 400 and PEG 600 following the application of 1 μL of formulation. Each data point represents the mean \pm SD, $n=4$.

The corresponding percentages of NIA that permeated are shown in Fig 2.19. At 2.5 h, for all tested formulations, 93 – 95 % of the dosed NIA was delivered through the Skin PAMPA membrane, while there was no significant difference among the permeated percentages($p > 0.05$).

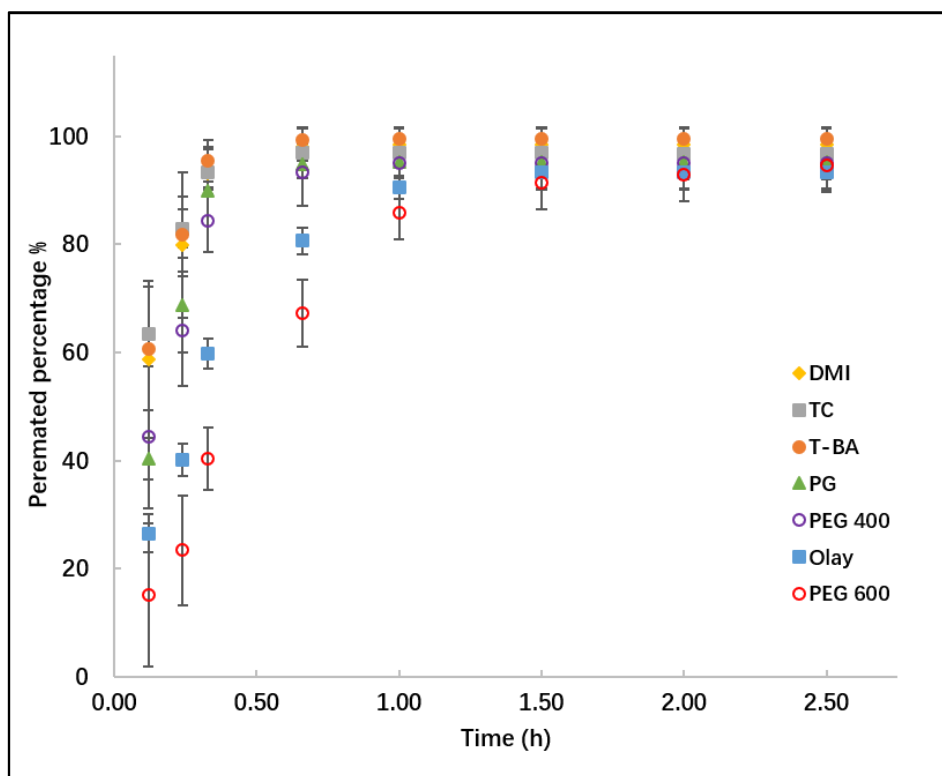


Figure 2. 19 The percentage permeation of NIA from TC, T-BA, DMI, PG, Olay, PEG 400 and PEG 600 following the application of 1 μL of formulation. Each data point represents the mean \pm SD, $n=4$.

The permeation profiles and the percentages permeated of NIA following the applications of 30 μL are shown in Fig 2.20 and 2.21. Significantly higher permeation was evident for the T-BA formulation at 2.5 h compared with all other formulations ($p<0.05$). The cumulative amount of NIA that permeated from T-BA was $2318.5 \pm 197.1 \mu\text{g}/\text{cm}^2$, followed by the permeation values from DMI and PG, namely 1603.6 ± 141.2 and $1522.6 \pm 127.1 \mu\text{g}/\text{cm}^2$, respectively. Permeation of NIA from DMI and PG was significantly higher than the cumulative amounts that permeated from Olay[®], TC, PEG 400 and PEG 600 ($p<0.05$). Although no permeation of NIA was observed for PEG 400 and PEG 600 in porcine skin and human skin, in the Skin PAMPA model NIA permeation was observed for both vehicles under both dose conditions. Following the application of 30 μL of formulation, for PEG 400 and PEG 600, significantly lower cumulative amounts of NIA permeation were evident (397.7 and $425.7 \mu\text{g}/\text{cm}^2$) compared with all other formulations ($p<0.05$). The corresponding values for the 1 μL application were 146.3 and $156.2 \mu\text{g}/\text{cm}^2$. However, at the lower doses these values were not statistically different from the other formulations ($p>0.05$).

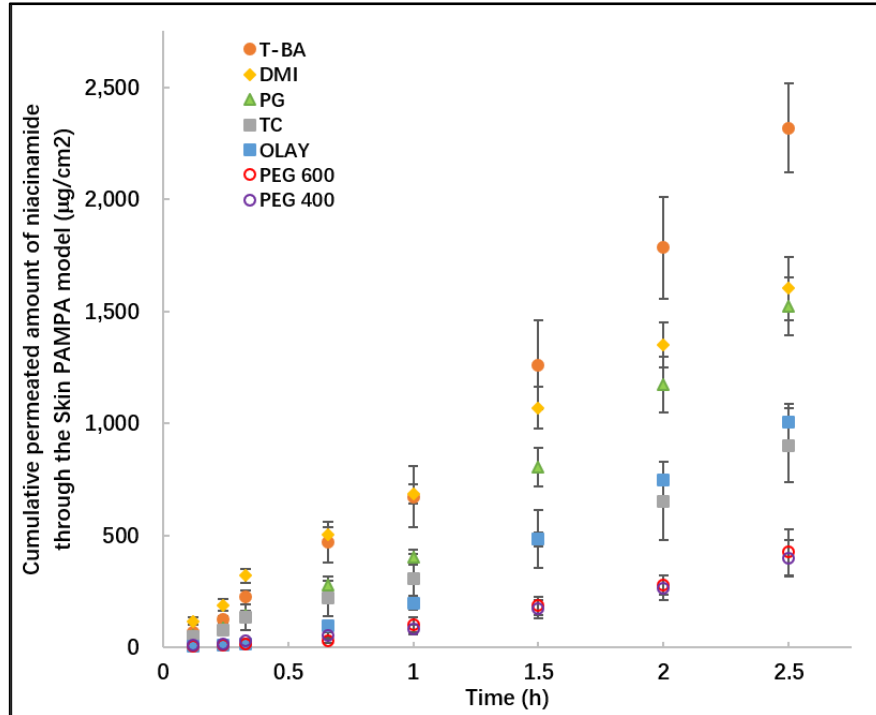


Figure 2. 20 PAMPA permeation profiles of NIA from T-BA, TC, DMI, PG, Olay®, PEG 400 and PEG 600 following the application of 30 µL. Each data point represents the mean \pm SD, n=4.

Curvilinear permeation profiles of NIA following the application volume of 1 µL were evident for all tested formulations (Fig 2.18), presumably reflecting donor depletion. In contrast, permeation profiles were generally linear for the 30 µL dose, exhibiting steady-state flux regions consistent with infinite dosing conditions. For the 1 µL application, in the Skin PAMPA model, all formulations delivered more than 90 % of the applied amounts of NIA through the membrane at 2.5 h; lower values were observed for the 30 µL application, ranging from 7 % to 52 %.

For the three tested models, higher permeation of NIA was evident in the Skin PAMPA model under both infinite and finite dose conditions ($p < 0.05$). This is consistent with the results of a previous investigation of ibuprofen permeation in human and porcine skin and the Skin PAMPA model by Luo et al. (2016). The NIA permeation in the various models may be ranked as follows: Skin PAMPA model > Porcine skin > Human skin ($p < 0.05$).

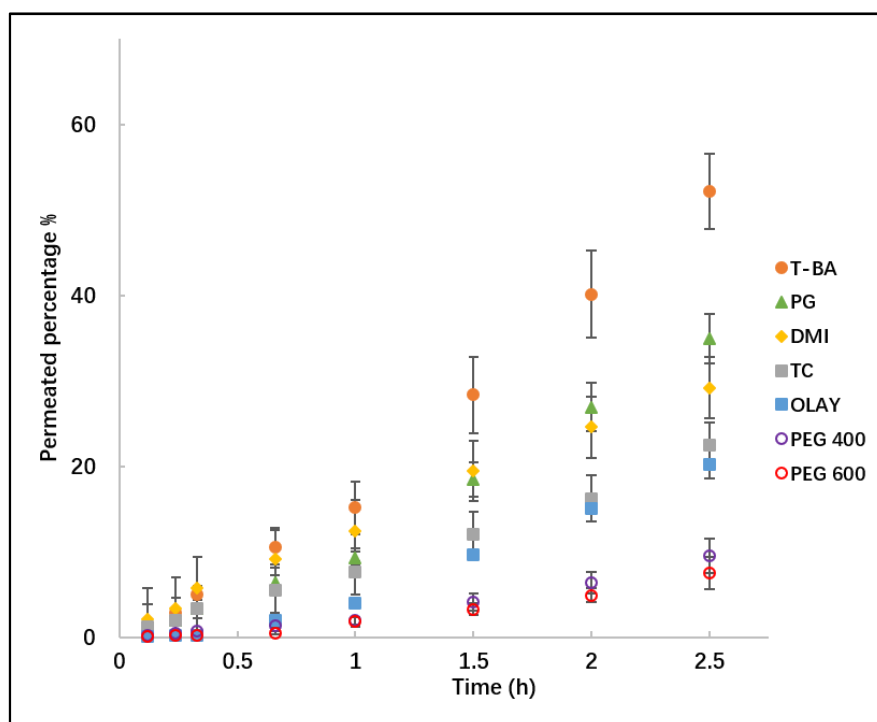


Figure 2. 21 The percentage of NIA permeation from TC, T-BA, DMI, PG, Olay, PEG 400 and PEG 600 following the application of 30 μ L of formulation. Each data point represents the mean \pm SD, n=4.

The results for the finite dose skin permeation studies using the Skin PAMPA model are plotted against corresponding values obtained in the porcine and human skin studies in Fig 2.22. A correlation coefficient (r^2) of 0.88 was observed for the linear regression of porcine skin and PAMPA model (Fig 2.22 A) with a value of 0.71 obtained for human skin and PAMPA results (Fig 2.22 B). Although attempts were made to fit the data to an exponential model and to compare the results of different models under infinite dose conditions, no meaningful correlations were obtained.

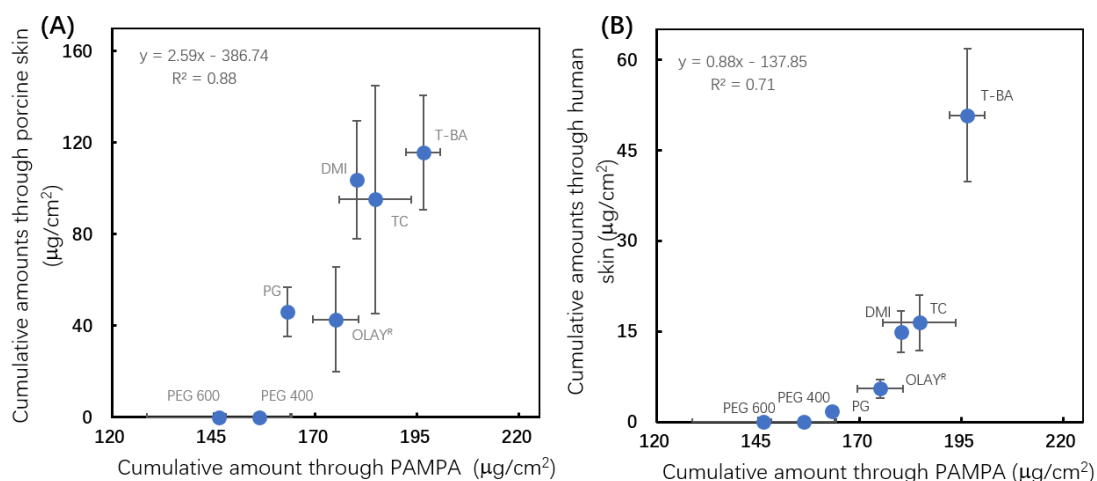


Figure 2. 22 Correlations between the cumulative amounts of NIA that permeated through (A) porcine skin and the Skin PAMPA model and (B) human skin and the Skin PAMPA model under finite dose conditions.

2.4 Conclusion

The permeation behavior of NIA was evaluated in three different models with varied doses. A significantly higher permeation was observed for T-BA in human skin under finite and infinite dose conditions ($p < 0.05$). As there is only limited information about this tertiary alcohol in skin permeation enhancement, further investigation regarding the effects of this solvent on skin integrity should be considered to probe the hypothesis. The permeation of NIA in porcine tissue, human skin and the Skin PAMPA model confirms the lower barrier function of PAMPA compared with biological tissues. The permeation of NIA from PEGs in the Skin PAMPA model but not in porcine or human skin indicates that this model may not be suitable for examining formulations containing these materials. However, correlations between permeation in the Skin PAMPA model and porcine or human skin under finite dose conditions were observed. This suggests that a wider range of actives and/or excipients should be included and evaluated to explore fully the potential of PAMPA as a high throughput model in skin permeation prediction. With respect to the permeability of human and porcine skin, the results confirm a higher permeation of NIA observed in porcine skin compared with human epidermis. This is line with the work of other researchers. Additionally, the importance of conducting finite versus infinite dose studies is underlined once more. Finite dose studies simulate the application of topical formulations to the skin in the real

world, while permeation studies conducted with infinite doses may overestimate the effects of the investigated excipients.

Chapter 3.

**Development and evaluation of
simple formulations of PR using
mammalian skin and
the Skin PAMPA model**

3.1 Introduction

The characterization of the physicochemical properties of a new active ingredient provides valuable information for development of a topical preparation (Parisi et al., 2015). As described in the previous section, characteristics such as molecular weight, partition coefficient and melting point are important in determining the active ingredient's suitability for dermal delivery. More than half a century ago the importance of a balanced aqueous and lipid solubility for good skin permeants was observed (Hadgraft and Somers, 1956; Hadgraft, 2004). At various stages during the development of a new topical product, the active molecule must be formulated as a preparation that is appropriate for its potential application (Jones, 2018). Understanding the interaction between a model active and other formulation excipient can minimize attrition during the formulation development process. Therefore, an assessment of solubility characteristics is of fundamental importance. Furthermore, stability studies are also an indispensable step as the drug and excipient stability will impact on manufacture, transport and storage of formulations. On the other hand, providing reproducible, reliable data is the core role of the analytical chemist and is the key factor in the success of development of formulations (Green, 1996). The validation of an analytical procedure can demonstrate its suitability for the intended application, minimize potential method problems and control the data quality. Guidelines for conducting such validation include those issued by the International Conference on Harmonisation (ICH) (ICH, 2005) and the Food and Drug Administration (FDA) (FDA, 2015). In general, a thorough validation should detail investigations of the method's specificity, linearity, accuracy, precision, range, detection limit, quantitation limit, and robustness.

Phenylethyl resorcinol (PR), is a phenolic compound that was developed as a tyrosinase inhibitor (Vielhaber et al., 2007; Sorg et al., 2013). This active has been used widely in the personal care industry as a novel anti-hyperpigmentation ingredient. Surprisingly, there is only limited information describing the physicochemical properties of this active. Therefore, this active has been selected as the focus for the current work. The vehicles examined in these studies were isopropyl myristate (IPM), 2-ethylhexyl salicylate (also known as octyl salicylate, OSal), glycerol, propylene glycol (PG), dimethyl isosorbide (DMI), Transcutol® P (TC)

and poly(ethylene glycol) (PEG) with varying molecular weights. As described previously, PG, DMI, TC and PEGs were included as they are widely used in skin preparations. IPM is the most common ester which has been investigated as a chemical penetration enhancer in topical and transdermal formulations (Lane, 2013). In the literature, it was reported that IPM increased human skin delivery of hydrocortisone (Brinkmann and Müller-Goymann, 2003), fentanyl (Santos et al., 2012) and testosterone (Zidan et al., 2017) OSal is another fatty acid ester and it has also been reported to enhance the permeation of testosterone (Morgan et al., 1998) and fentanyl (Santos et al., 2011, 2012). Glycerol is a component of the natural moisturizing factors present in skin which protects skin from severe drying and the molecule has been reported to increase porcine skin percutaneous absorption of metronidazole (Bjorklund et al., 2013).

The primary objectives of this chapter are to perform a comprehensive characterization of PR and to assess the delivery of this molecule to mammalian skin. A secondary objective was to investigate the permeation behavior of this model active using the synthetic stratum corneum model, the Skin PAMPA model. A suitable Skin PAMPA method was developed for PR and appropriate dosing conditions to reflect real life applications were also identified.

3.2 Materials and methods

3.2.1 Materials

PR (Symrise, Holzminden, Germany) was a gift from pION Inc. Billerica, USA. OSal and glycerol were purchased from Sigma Aldrich, UK. Analytically pure PG, IPM, glycerol, PEG 200, PEG 400 and PEG 600 were purchased from Fisher Scientific, UK. Phosphate buffer saline (PBS) tablets (pH 7.3 ± 0.2 at 25°C) were purchased from Oxoid Limited, England. DMI was a gift from Croda Limited, UK. TC was a kind donation from Gattefossé, St. Priest, France. HPLC grade water, acetonitrile and methanol were purchased from Fisher Scientific, UK. Pre-coated PAMPA Plates, hydration solution, stirring disks and a Gut-Box™ device were supplied by pION Inc. Billerica, USA.

3.2.2 Methods

3.2.2.1 Development and validation of the HPLC method for PR

The analytical method of PR was developed using HPLC as described in Chapter 2. A concentration of 1 mg/mL was measured using a spectronic BioMate™ 3 UV/vis spectrophotometer (Thermo Scientific, U.S.A.). The analysis was conducted using HPLC (Agilent 1100, Agilent technologies, U.S.A., operated with ChemStation® Rev.A.09.03). The method was subsequently validated following the International Conference on Harmonisation (ICH) guidelines (ICH, 2005), and the validation characteristics were linearity, specificity, accuracy, precision, detection limit (DL), quantitation limit (QL), system suitability and robustness.

3.2.2.2 Solubility and stability studies of PR

The solubility and stability studies of PR were performed as described in Chapter 2. An excess amount of PR was added to tested solvents and stirred with a Teflon coated magnetic bar for 48 h in at 32 ± 1 °C. After 48 h, the sample solution containing the saturated PR suspension was collected and centrifuged at consistent temperature conditions (13,200 rpm at 32 ± 1 °C) for 15 min. The supernatant was subsequently diluted using neat methanol in order to lie within the detection limit for the HPLC method. The solubility parameters of the solvents were calculated using the Hoftyzer and van Krevelen approach using Molecular Modelling Pro®. The solvents evaluated for solubility of PR were IPM, OSaI, PG, PEG 200, PEG 400, PEG 600, TC, glycerol and PBS. The stability of PR was examined over 72 h at 32 ± 1 °C.

3.2.2.3 LogP_(octanol/water) measurement

The logP_(octanol/water) of PR was experimentally determined using the shake flask method following the guidelines published by the OECD (1995). Octanol pre-saturated with water and water pre-saturated with octanol were prepared by mixing water and octanol in two stock bottles, one containing 100 mL octanol and a sufficient quantity of water, and the other containing 100 mL of water and a sufficient quantity of octanol. After stirring the

mixtures of two phases for 24 h at room temperature (21°C), and equilibration for 48 h, the phases were separated. A PR stock solution (100 mg/mL) was prepared in octanol, pre-saturated with water. The stock solution was subsequently diluted to 1 mg/mL and then mixed with water, pre-saturated with octanol (1:1, 1:2, 2:1 v/v). Mixtures were agitated for 5 min, and the aqueous and octanol phases were separated after 48 h. A sample from each phase was collected and analysed by HPLC to calculate the $\log P_{(\text{octanol/water})}$ as shown in Equation 3.1, where C_{octanol} is the concentration of PR in the organic phase and C_{aqueous} is the concentration in the aqueous phase. All measurements were conducted in triplicate.

$$\text{Log } P_{(\text{octanol/water})} = \log \left(\frac{C_{\text{octanol}}}{C_{\text{aqueous}}} \right) \quad \text{Equation 3.1}$$

3.2.2.4 Thermal analysis

The degradation temperature of PR was investigated using thermogravimetric analysis (TGA, TA Instruments, U.S.A.) and the melting point was examined using differential scanning calorimetry (DSC, TA instruments, USA). A suitable amount of PR was placed in an open, tared aluminum pan (TA Instruments, U.S.A.) and then heated inside the TGA furnace. PR was equilibrated at 40 °C and heated up with a ramp of 20 °C /min to a terminal temperature of 400 °C. Nitrogen (25 mL/min) was purged throughout the experiment to maintain an inert environment around the sample. The mass change of PR as a function of temperature change was recorded. To perform DSC analysis, PR was weighed in a Tzero™ pan (TA Instruments, U.S.A.) and then subsequently sealed with a Tzero™ lid (TA Instruments, U.S.A.) using a Tzero™ press (TA Instruments, U.S.A.). The PR sample was heated from 0 to 150 °C at 10 °C/min under nitrogen (50 mL/min) throughout the measurement. TA Universal software was used for data analysis.

3.2.2.5 Preparation of PR solutions

PR solutions were prepared at a concentration of 1 % (w/v) as this is within the range of concentrations found in commercial products (Gohara et al., 2013). PR solutions were

prepared by dissolving 30 mg of PR in 3 mL of solvents (PG, DMI, OSaI, IPM, TC, glycerol and PEG 400) in a glass vial. The glass vial was sealed with Parafilm[®] and stirring was continued overnight to allow dissolution at room temperature.

3.2.2.6 Dynamic vapour sorption (DVS) studies

A series of vehicles were evaluated in dynamic vapour sorption studies. The methods were the same as those described for the DVS studies described in Chapter 2. The tested solutions were composed of PR 1 % (w/v) in PG, glycerol, DMI, OSaI, IPM, TC and PEG 400.

3.2.2.7 Permeation and mass balance studies of PR using porcine skin

The *in vitro* permeation studies of PR were performed using Franz diffusion cells and full-thickness porcine skin as described in Chapter 2.2.5. 1 % (w/v) solutions of PR were prepared in PG, DMI, OSaI, IPM, TC, glycerol and PEG 400. The permeation studies were initially performed under infinite dose conditions ($50 \mu\text{L}/\text{cm}^2$) and followed by finite dose studies ($5 \mu\text{L}/\text{cm}^2$) up to 24 h. Degassed freshly prepared PBS solution was used as the receptor medium. All samples were analyzed using HPLC.

Mass balance studies were carried out to examine the distribution of PR and to estimate the total recovery (OECD, 2004b). The receptor fluid was removed once the permeation studies were completed. The skin was washed by adding 1 mL of water:methanol (10:90) three times for the $5 \mu\text{L}/\text{cm}^2$ application; and five times for the $50 \mu\text{L}/\text{cm}^2$ application. A cotton bud was used to swab the skin surface and the cotton bud was placed in Eppendorf[®] tubes with 1 mL of water: methanol (10:90). The sample solutions were subsequently extracted overnight. Skin retention was determined by cutting the skin membrane into small pieces and extracting the tissue in 1 mL of water:methanol (10:90) in an orbital shaker overnight at room temperature. Samples for skin extraction measurement were centrifuged at 13,200 rpm at room temperature for 20 min and all other samples were centrifuged at 12,000 rpm for 13 min. The supernatant solution was analyzed by HPLC. The results were calculated using Equation 3.2, where T represents total recovery, W is the recovery from the skin surface by washing and swabbing using a cotton bud, E is the value for skin extraction

and P is the recovery from the receptor medium.

$$T = W + E + P$$

Equation 3.2

3.2.2.8 Permeation and mass balance studies of PR using human skin

The *in vitro* permeation studies of PR were conducted using Franz cells and human epidermis following the procedure described previously (Session C.2.2.6). 1 % (w/v) solutions of PR were prepared in PG, DMI, OSaI, IPM, TC and glycerol. The studies were conducted under finite dose conditions ($5 \mu\text{L}/\text{cm}^2$) up to 24 h at $32 \pm 1^\circ\text{C}$. Prior to use, the integrity of the epidermis was examined by assessment of electrical resistance at 50 Hz. Skin membranes with electrical resistance values greater than $20 \text{ k}\Omega$ were included. Approximately 2 mL of freshly prepared PBS solution ($\text{pH } 7.3 \pm 0.1$) was filled in the receptor compartment serving as the receptor phase. The solubility determination confirmed that sink conditions were maintained throughout the experiments. 200 μL of receptor medium was withdrawn at each sampling interval and replaced with the same volume of fresh PBS solution. Mass balance studies were performed following the procedure described previously to assess the distribution of the PR and to examine the total recovery. All samples were analyzed by HPLC.

3.2.3.9 Permeation studies of PR using the Skin PAMPA model

The permeation behavior of PR from selected vehicles were subsequently examined using the Skin PAMPA model. The Skin PAMPA model was prepared as described previously (Session C.2.2.7). The permeation studies were conducted using the same protocol as described in Session C.2.2.8. Three doses of the PR solutions were investigated, 1, 17 and 30 μL per donor well, corresponding to 3, 51 and $90 \mu\text{L}/\text{cm}^2$ of preparations, respectively. The PR solutions were prepared in PG, DMI, OSaI, IPM, TC, glycerol and PEG 400. The studies were conducted at $32 \pm 1^\circ\text{C}$ up to 2.5 h and the sampling time points were 0.1, 0.2, 0.3, 0.7, 1, 1.5, 2 and 2.5 h.

3.2.3.10 Statistical analysis

All the results were presented as the mean \pm standard deviation (SD). The statistical analysis was performed as described in Session C.2.2.8.

3.3 Results and discussion

3.3.1 Development and validation of HPLC method for PR

Prior to HPLC method development, a standard solution of PR in methanol (1 mg/mL) was scanned using a UV spectrophotometer (200 to 300 nm, 1 nm/step), and 280 nm was determined as the optimal detection UV wavelength. Table 3.1 illustrates the chromatographic conditions developed for PR quantitation.

Table 3. 1 HPLC conditions for analysis of PR

HPLC Conditions	
Column	C18 150x4.6mm
Mobile phase (v/v)	60% methanol 40% water
Temperature (°C)	30
Flow rate (ml/min)	1.0
Run time (min)	5
Wavelength (nm)	280
Injection volume (μ L)	20

The validation parameters for PR are shown in Table 3.2. HPLC analysis calibration curves (ranging from 0.25 to 50 μ g/mL) were constructed. Linearity was determined as $r^2 > 0.99$ (Fig. 3.1). The accuracy of this analytical method was confirmed by the recovery within the range of 99–106 %. Precision was assessed by determination of intermediate variability and intraday repeatability. The % RSD values for intermediate variability and intraday repeatability were below 2 and 1 %, respectively. LD was determined as 0.26 μ g/mL, while LQ

was determined as 0.79 µg/mL. The % RSD values of the suitability studies were calculated as 0.13, 0.08 and 1.39 % for PR retention time, peak area and symmetry. Chromatographic conditions including injection volume, mobile phase flow rate, composition, temperature and detection number were changed for robustness studies, and the values of r^2 were > 0.99 . This analytical method was confirmed to be suitable and sufficiently robust for PR quantitative analysis.

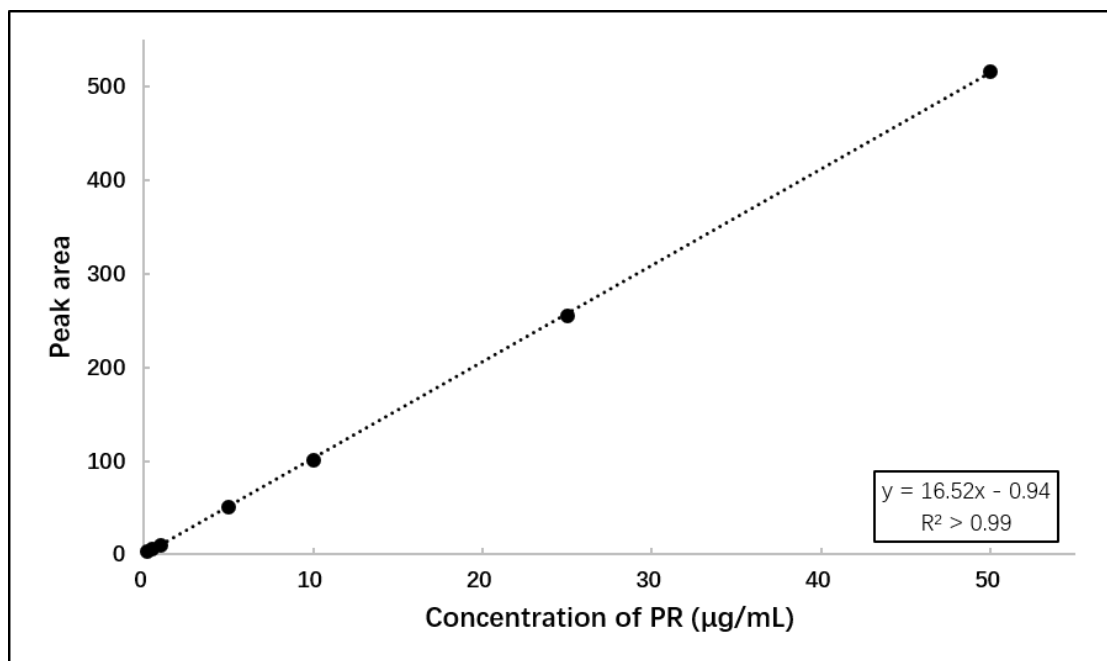


Figure 3. 1 The calibration curve for PR

Table 3. 2 HPLC method validation characteristics for quantitative analysis of PR, data presented as mean \pm SD, (% RSD).

Linearity		> 0.99		
Detection limit ($\mu\text{g mL}^{-1}$)		0.19		
Quantitation limit ($\mu\text{g mL}^{-1}$)		0.57		
System suitability n=6	Peak area	408.37 \pm 0.31 (0.08)		
	Retention time (min)	2.50 \pm 0.003 (0.13)		
	Symmetry	0.68 \pm 0.01 (1.39)		
Accuracy	Concentration ($\mu\text{g mL}^{-1}$)	1	25	50
	Recovery	105.77 \pm 1.59	99.16 \pm 0.03	100.25 \pm 0.04
Precision	Concentration ($\mu\text{g mL}^{-1}$)	1	25	50
	Intraday	(0.27)	(0.08)	(0.76)
	Intermediate	(1.15)	(0.23)	(0.07)

3.3.2 Solubility and stability studies of PR

Measurements were conducted in triplicate and quantified by HPLC. Table 3.3 summarizes the solubility of PR in various solvents. The solubility of the active in the tested vehicles ranged from 0.34 to 88 % (w/v, g/100mL) with the lowest observed in TC (8.95 \pm 0.53 %) among all tested vehicles ($p>0.05$). The solubility parameter components may be predicted from group contributions (Krevelent and Nijenhuis, 2009) and the determined value of PR was calculated as 14.27 (cal/cm³)^{1/2}. For PG, PEG 200, PEG 400, PEG 600, glycerol, OSal and TC, the smaller the difference between the solubility parameter of the solvent and the solute, the higher the solubility of PR obtained. However, an increased solubility of PR

was observed in DMI, as 87.57 ± 1.45 %, while the difference between the calculated solubility parameter of DMI ($9.97 \text{ (cal/cm}^3)^{1/2}$) and the corresponding value of PR ($14.27 \text{ (cal/cm}^3)^{1/2}$) was not the smallest. Zia et al. (1991) reported that the solubilization behavior of DMI could be explained by its complexation with water and PG through hydrogen bonding interactions. Therefore, the increase in solubility of PR in DMI regardless of the solubility parameter may possibly reflect hydrogen bond formation.

The solubility values of PR in PBS and water were determined as 0.34 and 0.37 %, respectively. According to the OECD Guidance Document for skin absorption studies, it is imperative that solubility of the test substance in the receptor fluid should not be a rate-limiting step in dermal absorption (OECD, 2004a). The likely maximum achieved concentration of test substance in the receptor medium should be estimated, and about 10 times this concentration should be achievable in the receptor phases under the experimental conditions (OECD, 2004a). For PR *in vitro* permeation studies, the maximum achievable concentration was determined to be 0.025 % (w/v), which is 10 times lower than the solubility of the molecule in PBS. This confirmed that sink conditions would be maintained over the course of the permeation studies.

Table 3. 3 Solubility of PR in various solvents (mean \pm SD, n=3).

Solvent		Solubility parameter ($\text{cal/cm}^3)^{1/2}$	Solubility of PR (% w/v)
Isopropyl myristate	IPM	8.21	31.7 ± 2.1
Dimethyl isosorbide	DMI	9.97	87.6 ± 1.5
PEG600	PEG 600	10.59	13.0 ± 1.3
Transcutol® P	TC	10.62	9.0 ± 0.5
2-ethylhexyl salicylate/ Octyl salicylate	OSal	10.87	9.7 ± 0.6
PEG400	PEG 400	11.67	11.4 ± 2.5
PEG200	PEG 200	12.06	39.6 ± 3.5
Propylene glycol	PG	14.07	56.8 ± 0.4
Glycerol	GLY	17.14	36.8 ± 1.3

The stability of the tested active in varied solvents was examined over a period of 72 h at a concentration of 1 % (w/v), at 32 ± 1 °C. Fig. 3.2 illustrates the results from the stability studies. After 72 h, the recovery values of PR in all tested solvents and PBS were > 90%.

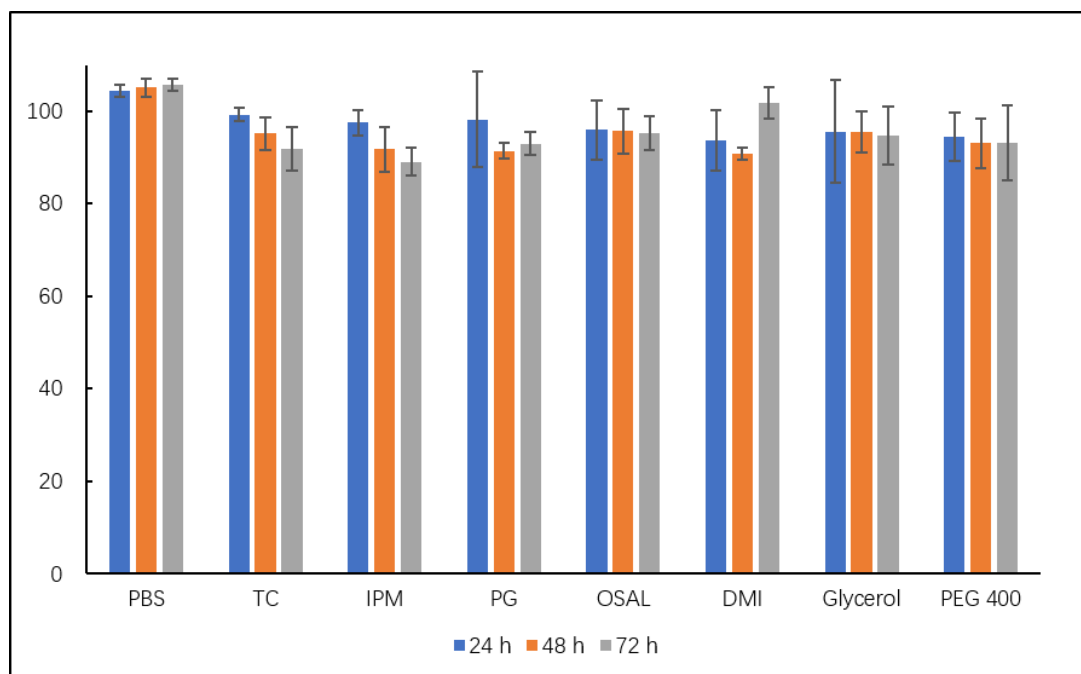


Figure 3. 2 The stability of PR in various solvents at 32 ± 1 °C (mean \pm SD, n=3).

3.3.3 $\log P_{(\text{octanol/water})}$ measurement

The mean value of the $\log P_{(\text{octanol/water})}$ for the three octanol:water ratios evaluated was determined to be 3.35 ± 0.03 at room temperature (21 °C). This experimental value is in line with the predicted $\log P_{(\text{octanol/water})}$ values. Calculated $\log P_{(\text{octanol/water})}$ values for PR have been reported as 3.74 and 3.02 using ChemAxon and ALOGPS, respectively (DrugBank, 2018).

3.3.4 Thermal analysis

TGA measurements were conducted prior to DSC investigations. There was no weight loss of PR up to 213.3 °C, which indicated that degradation of PR occurs at 213.3 °C (Fig. 3.3). As shown in Fig. 3.4, the onset temperature of the melting point and the enthalpy of fusion were measured as 79.1 °C and 113.6 J/g, respectively. Furthermore, the purity of the PR

sample was confirmed by the single endothermic event in the DSC curve in Fig. 3.4.

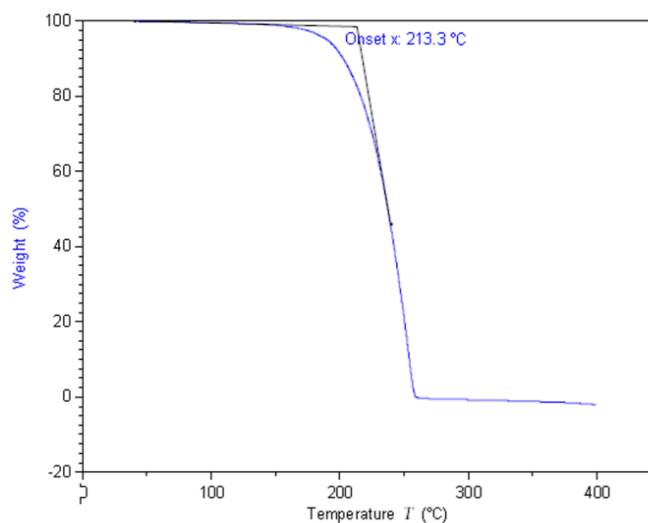


Figure 3. 3 TGA analysis of PR.

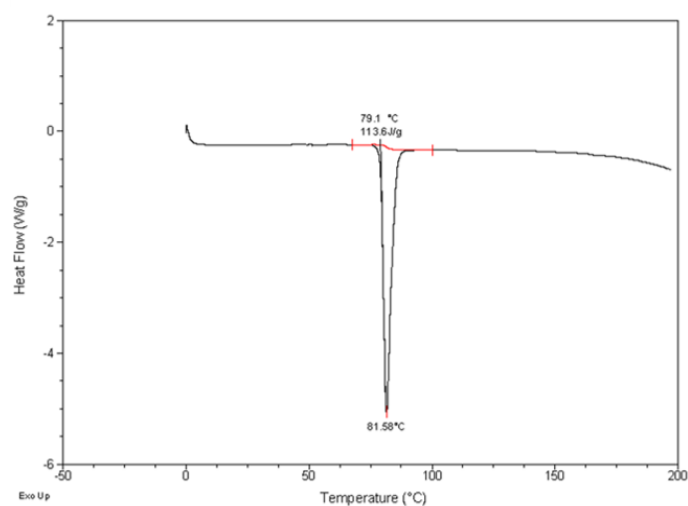


Figure 3. 4 DSC analysis of PR.

3.3.5 DVS studies

The hydration and evaporation of vehicles were examined using DVS at normal skin temperature (32 ± 1 °C) and average room humidity (relative humidity 50 %) for 24 h (1,440 min). The results for the 1 % PR solutions in PG, glycerol, DMI, OSaI, IPM, TC and PEG 400 are shown in Fig 3.5. For PG, glycerol, TC, and PEG 400 solutions all demonstrated an initial increase in weight related to their hygroscopic nature. DMI, PG and TC solutions evaporated with time. 69.5 ± 2.4 , 48.4 ± 3.0 and 2.9 ± 0.0 % of the applied DMI, PG and TC solutions were

recovered at 24 h, respectively. The rapid evaporation of TC and PG is consistent with previous studies (Haque et al., 2017b; Paz-Alvarez et al., 2018). The weight of glycerol and PEG 400 solutions increased to 124.0 ± 1.6 and 110.4 ± 0.1 % of the initial applied weight at the end of the studies. Glycerol contains hydrophilic alcoholic hydroxyl groups which are responsible for its hygroscopic nature (Pagliaro and Rossi, 2010) and the polymer chains in PEG 400 are able to form extensive hydrogen bonds with water molecules (Thijs et al., 2007). No mass changes were evident for IPM and OSal solutions, 99.0 ± 0.1 and 98.4 ± 0.8 % were recovered at 24 h, respectively. The behaviour of OSal was consistent with results reported in previous studies (Paz-Alvarez et al., 2018) and the results for IPM agree with those reported by Haque et al. (2017b).

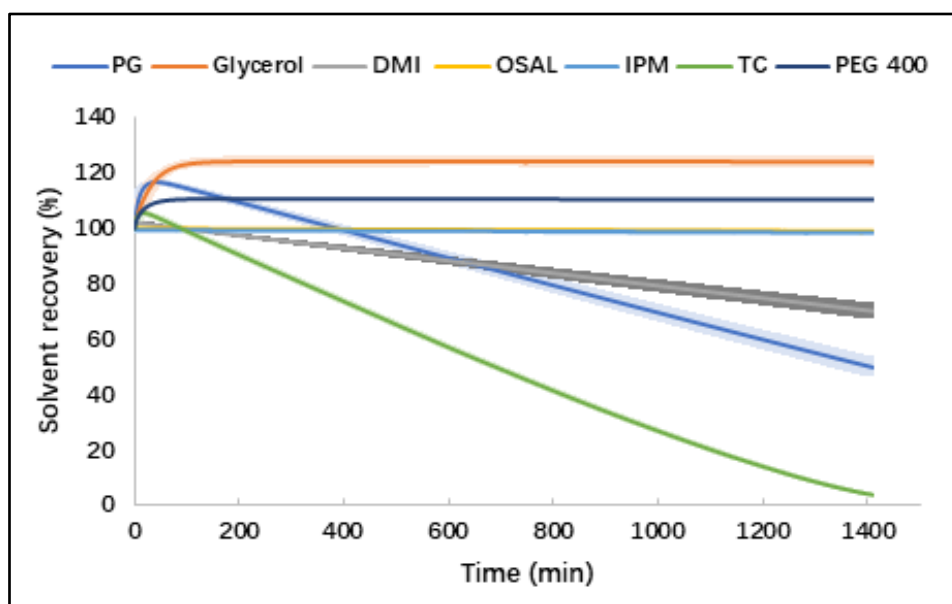


Figure 3.5 Percentage weight loss over 1440 min for 1 % PR in PG, DMI, glycerol, OSal, IPM, TC and PEG 400 (n=3, mean \pm SD).

3.3.6 Permeation and mass balance studies of PR in porcine skin under infinite dose conditions

The permeation behaviour of PR through full-thickness porcine skin under infinite dose conditions is illustrated in Fig 3.6. The permeation of PR was evident from 8 h for IPM and OSal, however the permeation was not detected for DMI and TC until 10 h. The permeation of PR was only observed at 22 h for PG, glycerol, and PEG 400. At 24 h, the cumulative

amounts of PR permeated through porcine skin from all tested solutions ranged from 3 to 37 $\mu\text{g}/\text{cm}^2$. A higher cumulative permeation was evident for DMI ($36.8 \pm 21.3 \mu\text{g}/\text{cm}^2$), significantly higher than the corresponding values for TC ($3.7 \pm 1.9 \mu\text{g}/\text{cm}^2$) and PEG 400 ($3.1 \pm 1.6 \mu\text{g}/\text{cm}^2$, $p < 0.05$). The cumulative permeation values of PR from OSal, IPM, PG and glycerol were 22.1 ± 3.4 , 15.9 ± 10.2 , 5.3 ± 0.7 , and $4.5 \pm 0.6 \mu\text{g}/\text{cm}^2$, respectively ($p > 0.05$).

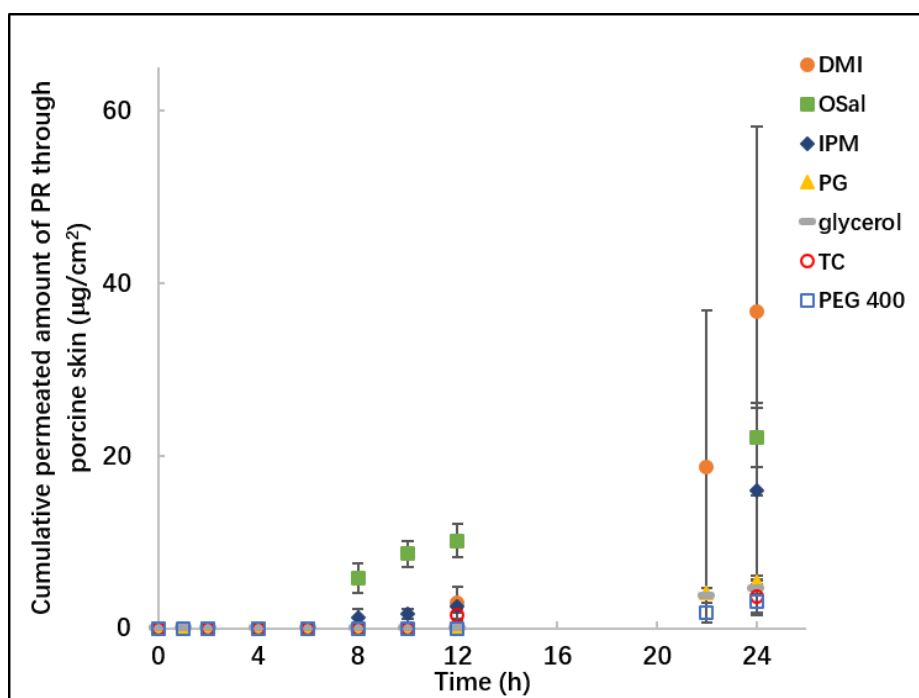


Figure 3.6 The permeation profiles of PR in porcine skin from DMI, OSal, IPM, PG, glycerol, TC and PEG 400 following the application of $50 \mu\text{L}/\text{cm}^2$ of solution (mean \pm SD, $4 \leq n \leq 5$).

The permeation percentage of PR from the tested solutions is presented in Fig 3.7. At 24 h, less than 8 % of applied PR was delivered through porcine skin. The percentage permeation of PR from DMI was significantly higher than for glycerol, TC and PEG 400, determined as $7.6 \pm 4.7 \%$ ($p < 0.05$).

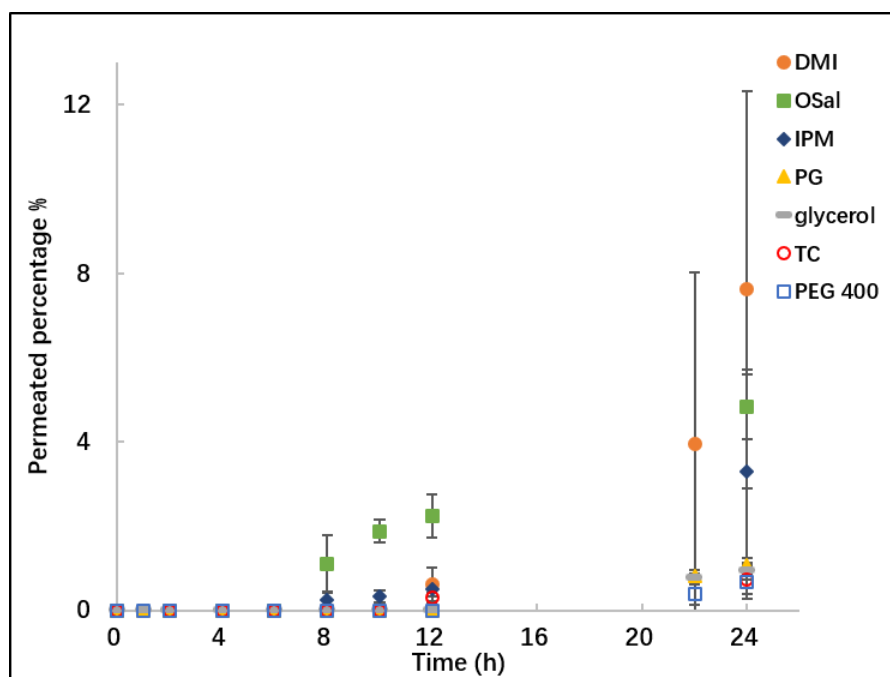


Figure 3. 7 The percentage permeation of PR in porcine skin from DMI, OSal, IPM, PG, glycerol, TC and PEG 400 following the application of 50 $\mu\text{L}/\text{cm}^2$ of solution (mean \pm SD, $4 \leq n \leq 5$).

The results from the mass balance studies are summarized in Table 3.4. For all tested solutions, more than 66 % of the applied PR was recovered from the skin surface. For all formulations, a higher percent of the PR dose was extracted from the skin membrane compared to the percentage permeated ($p < 0.05$). The high skin retention is consistent with the lipophilic nature of PR. The skin extraction from neat OSal solution was determined as 24.9 ± 5.8 %, and this value was significantly different from PEG 400 ($p < 0.05$). The overall recoveries of PR from the mass balance studies for all solutions ranged from 91-106 % which fell within the limits required by the SCCS for dermal absorption studies (85-115 %) (SCCS, 2010) and the Organization for Economic Co-operation and Development (OECD) for skin absorption: *in vitro* studies (90-110 %) (OECD, 2004b).

Table 3. 4 The results of mass balance studies following the permeation studies of PR using porcine skin following application of 50 $\mu\text{L}/\text{cm}^2$ of solution ($4 \leq n \leq 5$, mean \pm SD).

	DMI	IPM	OSal	PG	Glycerol	TC	PEG 400
Washing %	69.9 \pm 14.7	84.8 \pm 7.6	66.3 \pm 8.5	100.9 \pm 3.5	86.4 \pm 12.3	91.5 \pm 8.1	101.3 \pm 6.4
Extraction %	16.7 \pm 14.3	11.8 \pm 7.7	24.9 \pm 5.8	3.9 \pm 1.9	3.9 \pm 2.3	2.4 \pm 0.2	1.4 \pm 1.0
Permeation %	9.1 \pm 3.2	3.3 \pm 2.4	4.8 \pm 0.8	1.2 \pm 0.2	0.9 \pm 0.2	0.7 \pm 0.3	0.6 \pm 0.4
Total recovery %	95.7 \pm 16.4	99.9 \pm 6.0	96.0 \pm 6.8	105.9 \pm 2.0	91.3 \pm 13.6	94.6 \pm 8.2	103.2 \pm 7.7

3.3.7 Permeation and mass balance studies of PR in porcine skin under finite dose conditions

The permeation behaviour of PR was investigated using full thickness porcine skin under finite dose conditions. Permeation profiles are illustrated in Fig 3.8. For the OSal solution, as for infinite dose studies, the permeation of PR was observed at 8 h. For IPM and DMI solutions, the permeation was not detected until 10 h. For PG and glycerol solutions, the permeation was observed at 12 h, and the permeation from PEG 400 and TC was not detected until 22 h. At 24 h, the permeation of PR from all tested solutions ranged from 3 to 26 $\mu\text{g}/\text{cm}^2$. 25.7 \pm 5.1 and 22.0 \pm 0.9 $\mu\text{g}/\text{cm}^2$ of PR permeated through porcine skin from the OSal and IPM solutions, respectively. These values were significantly higher than those observed for PEG 400 and glycerol ($p < 0.05$). The cumulative permeated amounts of PR from DMI, PG, and TC were 12.9 \pm 1.7, 11.0 \pm 6.3, 7.5 \pm 4.5 $\mu\text{g}/\text{cm}^2$, ($p > 0.05$).

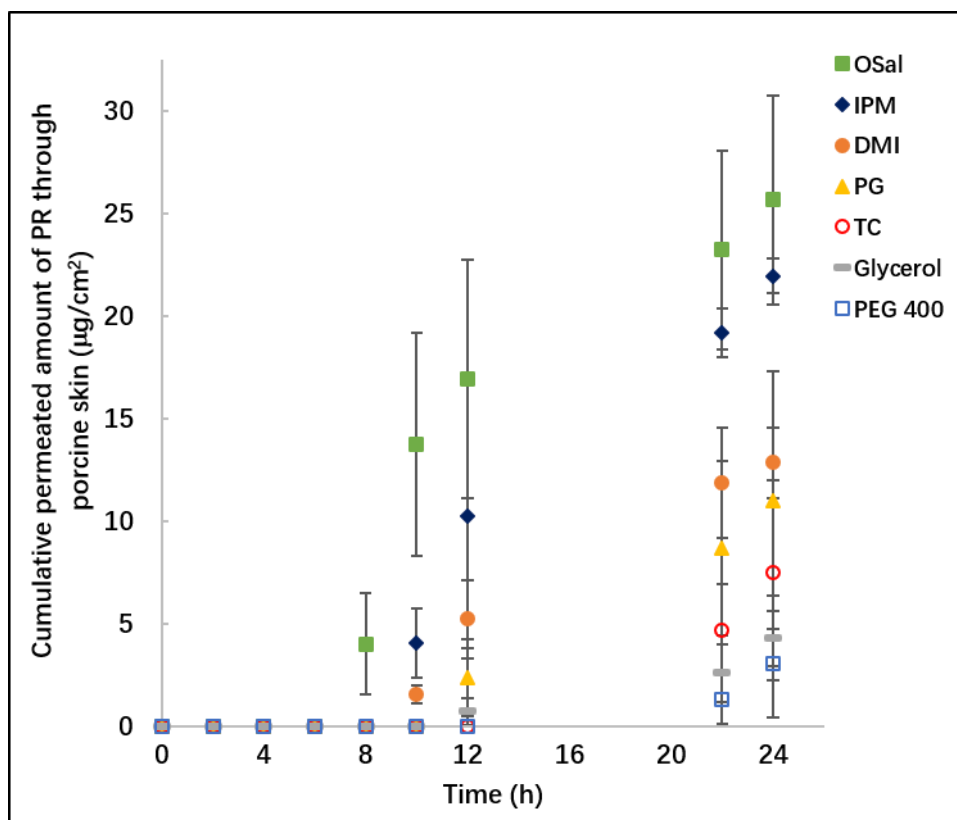


Figure 3. 8 The permeation profiles of PR in porcine skin from OSal, IPM, DMI, PG, glycerol, TC and PEG 400 following the application of 5 $\mu\text{L}/\text{cm}^2$ of solution (mean \pm SD, $3 \leq n \leq 5$).

The percentage permeation of PR from the various vehicles is shown in Fig 3.9. At 24 h, the percentage permeated varied from 4 to 50 % for the tested vehicles. A significantly higher percentage permeated was evident for OSal compared to the other vehicles ($p < 0.05$). 50.2 ± 3.8 % of the applied active permeated through porcine skin from OSal. The next highest value was observed for IPM with a value of 40.9 ± 3.6 %.

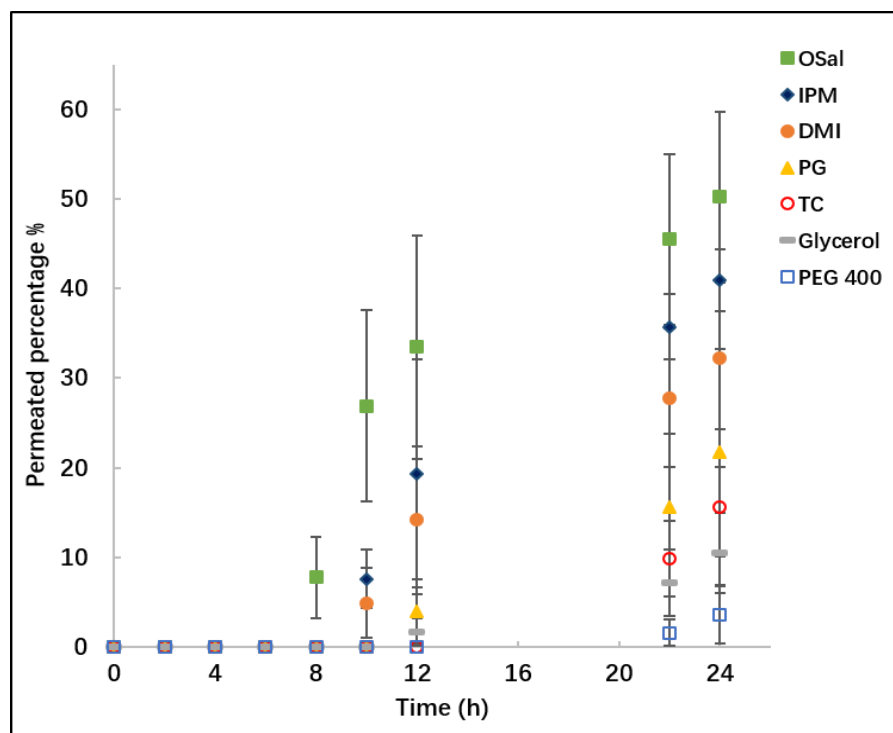


Figure 3. 9 The percentage permeation of PR in porcine skin from DMI, OSal, IPM, PG, glycerol, TC and PEG 400 following the application of 5 $\mu\text{L}/\text{cm}^2$ of solution (mean \pm SD, $3 \leq n \leq 5$).

Mass balance studies were conducted after the permeation studies to determine the distribution of the active and the overall recovery (Table 3.5). For PEG 400, 79 % of the applied active was recovered from the skin surface, which was significantly different compared to the other solutions ($p < 0.05$). For the other solvents, less than 18 % of the applied PR was recovered from the skin surface. The skin retention values determined for PG, TC, DMI and glycerol were 57.7 ± 7.9 , 55.3 ± 11.8 , 53.8 ± 9.1 and 48.9 ± 8.1 %, respectively ($p > 0.05$). For OSal and IPM, all the applied active was delivered into or through the skin membrane. There was no PR recovered from the skin surface following washing for these two vehicles. The skin retention values for OSal and IPM were determined as 48.5 ± 7.2 and 48.9 ± 3.6 %, respectively. OSal and IPM are two types of esters widely used as permeation enhancers in transdermal and topical drug delivery systems (Lane, 2013). OSal was initially used as a UV filter and sunscreen as it absorbs UVB radiation (Jiang et al., 1997; DrugBank, 2015); it was also reported to enhance the skin permeation of sex hormones (testosterone, estradiol, progesterone and norethindrone acetate) (Morgan et al., 1998) and fentanyl (Epstein, 2015). Various mechanisms have been suggested for the permeation enhancement

observed for OSal. Maghraby et al. (2005) reported that OSal enhances skin penetration by disrupting intercellular lipid domains. Santos et al. (2012) investigated the roles of OSal, IPM and PG in *in vitro* human skin delivery of fentanyl using volatile formulations. The results from ATR-FTIR studies suggested that OSal does not induce molecular changes in the lipid organization. The authors hypothesised that OSal may increase drug diffusivity by creating “pools” of solvent within the skin lipid phase. IPM is the most commonly used fatty acid ester penetration enhancer in topical and transdermal formulations (Lane, 2013). Again, there are various theories regarding the enhancement mechanism of this fatty acid ester. DSC studies indicated that IPM integrates within the lipid bilayers and induces the fluidisation of the lipid bilayers (Leopold and Lippold, 1995b), while Brinkmann and Müller-Goymann (2003) reported that IPM incorporation into the SC resulted in more densely packed bilayer lipids. Santos et al. (2012) suggested that IPM increases drug penetration by increasing the active's solubility in the SC.

Table 3. 5 The results of mass balance studies following the permeation studies of PR using porcine skin following application of 5 $\mu\text{L}/\text{cm}^2$ of solution ($3 \leq n \leq 5$, mean \pm SD).

	OSal	IPM	DM	PG	Glycerol	TC	PEG 400
Washing %	0.0 \pm 0.0	0.0 \pm 0.0	4.0 \pm 0.7	17.8 \pm 7.3	17.3 \pm 5.4	15.0 \pm 3.4	78.8 \pm 15.1
Extraction %	48.5 \pm 7.2	48.9 \pm 3.6	53.8 \pm 9.1	57.7 \pm 7.9	48.9 \pm 8.1	55.3 \pm 11.8	8.0 \pm 7.4
Permeation %	50.2 \pm 3.8	40.9 \pm 3.7	27.4 \pm 3.4	21.7 \pm 11.6	18.8 \pm 8.0	15.6 \pm 8.7	3.6 \pm 3.2
Total recovery %	98.7 \pm 10.3	89.7 \pm 7.2	85.2 \pm 9.3	96.7 \pm 9.2	85.0 \pm 18.3	86.0 \pm 13.9	93.2 \pm 0.5

3.3.8 Permeation and mass balance studies of PR in human skin under finite dose conditions

Following on from the porcine skin studies, the permeation behaviour of PR was investigated using heat separated human epidermis under finite dose conditions (5 $\mu\text{L}/\text{cm}^2$). To our knowledge, this is the first study that has investigated human skin percutaneous absorption of PR. The permeation profiles of PR from varying vehicles are shown in Fig 3.10, The permeation of PR was observed at 4 h for the OSal vehicle. At 24 h, the cumulative permeated amount of PR from OSal was the highest compared to all other tested solutions, $18.60 \pm 1.07 \mu\text{g}/\text{cm}^2$ ($p < 0.05$). This was followed by the cumulative permeation from PG, TC and DMI, with values of 10.18 ± 3.12 , 10.15 ± 1.50 and $9.08 \pm 2.30 \mu\text{g}/\text{cm}^2$, respectively. The

cumulative permeation values of PR from TC and glycerol were 4.34 ± 0.93 and 2.52 ± 0.22 $\mu\text{g}/\text{cm}^2$, respectively. The permeation of PR from TC and glycerol was significantly lower than for the other vehicles ($p < 0.05$).

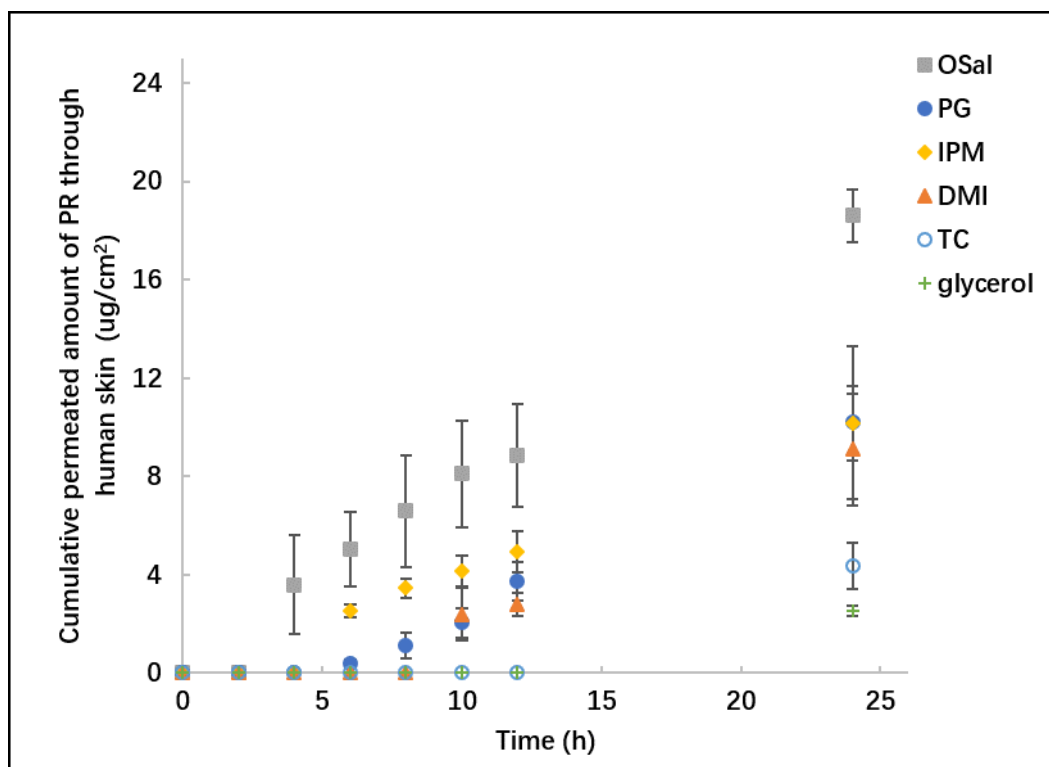


Figure 3. 10 The permeation profiles of PR in human epidermis from PG, IPM, OSal, DMI, TC and glycerol following the application of $5 \mu\text{L}/\text{cm}^2$ of solution (mean \pm SD, $3 \leq n \leq 5$).

The percentage permeation of PR from the various vehicles is shown in Fig 3. 11. At 24 h, the amount of active that permeated from the tested solutions accounted for 5 to 37 % of applied amounts. The percentage of PR that permeated from OSal (36.7 %) was significantly higher than for the TC (8.4 %) and glycerol (5.2 %) solutions ($p < 0.05$).

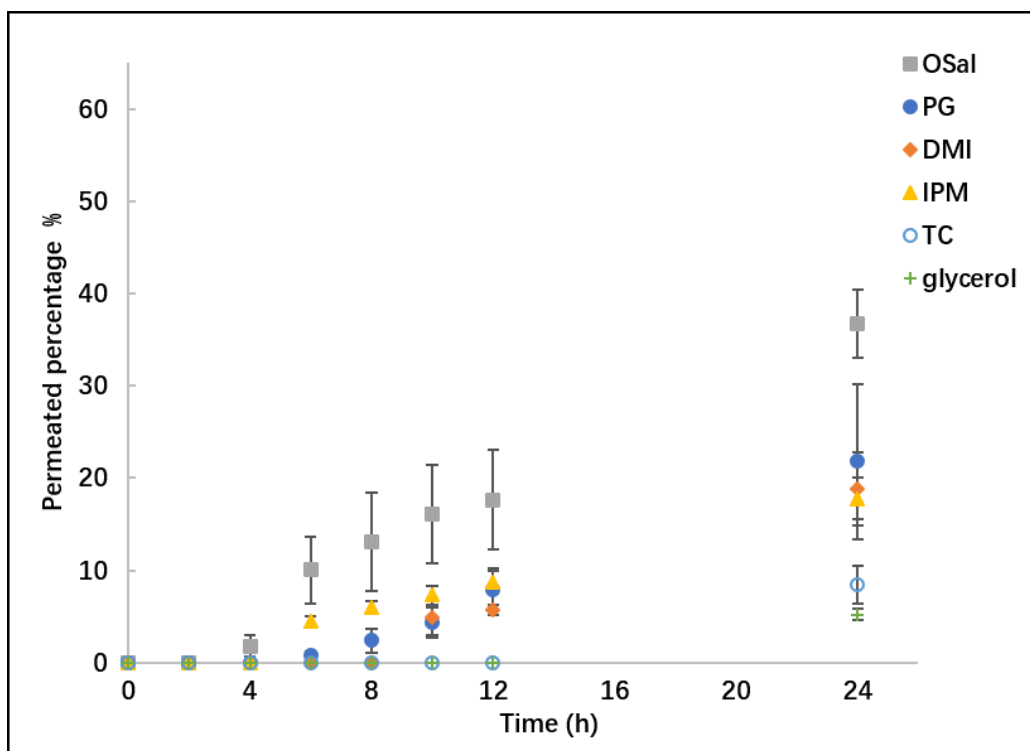


Figure 3. 11 The percentage permeation of PR in human epidermis from PG, IPM, OSal, DMI, TC and glycerol following the application of $5 \mu\text{L}/\text{cm}^2$ of solution (mean \pm SD, $3 \leq n \leq 5$).

Mass balance studies were performed at the end of the permeation studies to investigate the distribution and recovery of PR (Table 3.6). The glycerol solution deposited a higher percentage of PR on the skin surface, at $78.2 \pm 16.5 \%$, compared to OSal and DMI ($p < 0.05$). The percentage of PR extracted from the membrane was significantly higher for TC (36 %) and DMI (34 %) than glycerol (9 %) ($p < 0.05$). The overall recoveries of the active fell within the limits required by the SCCS guidelines ($100 \pm 15 \%$) (SCCS, 2010).

The OSal solutions were the most effective formulations in human skin ($p < 0.05$) but not in porcine skin ($p > 0.05$), under finite dose conditions. OSal delivered more than half of the dosed PR into human skin. At 24 h, $\sim 56 \%$ of the applied active was either retained in the epidermal tissue or had permeated through the skin membrane. Santos et al. (2012) investigated solvent uptake gravimetrically by immersing pre-treated human SC sheets in neat OSal, PG and IPM. The authors reported that the solvent uptake reached a maximum after 3 h and the solvent uptake appeared to be highest for OSal, followed by IPM and lowest for PG. The authors also reported that the skin residence time of the active was longer for OSal than for the other solvents. The higher skin retention of OSal and IPM is in line with

the lipophilic nature of these molecules. In addition, the solubility parameter for OSaI is similar to the value proposed for human SC, as $10 \text{ cal}^{1/2} \text{ cm}^{3/2}$ (Roberts et al., 2002), and this may contribute to the higher skin uptake and permeation of the active for these vehicles. In this human skin study, for OSaI, 20 % of PR was extracted from the skin, while 37 % was recovered from the receptor medium. As discussed previously, OSaI has been used as a penetration enhancer in skin formulations but has been reported to have different mechanisms of action (Lane, 2013). One of the possible mechanisms proposed is that the molecule enhances diffusion of actives by forming separate solvent phases in the lipid bilayers. As described previously, PR shows good solubility in OSaI, 9.7 % (w/v) (Section 3.3.2). The ability of this solvent to be retained in the skin membrane and solubilize PR could explain the efficient delivery and high skin retention of the active.

With reference to permeation from TC solutions, the amount of PR extracted from human skin was four times higher than the amount that permeated through human epidermis ($p < 0.05$). Under the same dosing conditions, similar results were observed for TC in porcine skin. A higher percent of active was extracted from porcine skin than observed in the receptor medium ($p < 0.05$). The evaporation of TC during permeation studies is likely, based on the DVS studies (Session C.3.3.2). At 24 h, the mass recovered for the 1 % PR TC solution following an application of 5 μL was about 3 % of the initial applied amount. This study suggests that the lack of permeation enhancement with the TC solutions could be caused by the depletion of the donor. However, for porcine skin studies, similar results were observed for an infinite dose. The amount of PR extracted from porcine skin following the application of 50 $\mu\text{L}/\text{cm}^2$ was three times higher than the percentage that permeated through the skin ($p < 0.05$). To further understand the solvent behavior under infinite dose conditions, the DVS studies were conducted for the same active in TC solution following the infinite dose. The results are shown in Appendix 2. At 24 h, for TC solutions, the mass recovered for the 50 μL application was greater than 80 % of the initial applied amount. Therefore, solvent evaporation only partly explains the lack of permeation enhancement. TC, is known to permeate through human epidermis and is also retained in human epidermis (Haque et al., 2017b). This molecule is reported to enhance percutaneous permeation by

changing the solubility of the active in the skin rather than increasing the diffusion of the active in skin (Harrison et al., 1996; Lane, 2013). Considering the lipophilicity of PR, the high skin retention could reflect its physicochemical properties. Higher skin retention than permeation were observed in studies of clotrimazole solutions in TC, a lipophilic antifungal agent (Paz-Alvarez et al., 2018).

Interestingly, PR permeation from glycerol was observed both in porcine skin and human skin. There was no difference in human skin retention of PR between glycerol and PG ($p>0.05$). Glycerol serves as an emollient, humectant and solvent in personal care products (Pagliaro and Rossi, 2010). It was reported that glycerol could integrate into orthorhombically ordered lipids in human SC (Brinkmann and Müller-Goymann, 2005). Good solubility of PR is evident in glycerol, determined as 36.78 % (w/v) (Session C.3.3.2), which may contribute to enhanced skin permeation and retention of the molecule.

Table 3. 6 The results of mass balance studies following the permeation studies of PR in human epidermis following application of 5 $\mu\text{L}/\text{cm}^2$ of solution ($3 \leq n \leq 5$, mean \pm SD).

	OSal	IPM	PG	DMI	TC	Glycerol
Washing %	35.4 \pm 3.1	62.0 \pm 6.7	69.3 \pm 16.7	45.1 \pm 12.3	58.9 \pm 10.9	78.2 \pm 16.5
Extraction %	19.7 \pm 4.3	14.5 \pm 2.5	11.6 \pm 5.0	34.1 \pm 9.2	36.4 \pm 7.9	8.8 \pm 0.7
Permeation %	36.7 \pm 3.7	18.5 \pm 2.0	21.8 \pm 8.4	18.8 \pm 4.0	8.4 \pm 2.1	5.2 \pm 0.6
Total recovery %	91.8 \pm 6.7	94.9 \pm 4.9	102.6 \pm 6.4	97.9 \pm 9.0	103.7 \pm 8.5	92.2 \pm 16.5

Under finite dose conditions, lower permeability in human skin compared to porcine skin was evident for OSal, IPM and DMI ($p<0.05$). This is in line with findings reported by other researchers (Dick and Scott, 1992; Singh et al., 2002). However, the differences in cumulative amounts of PR that permeated in human epidermis and pig skin were not statistically significant for PG, TC and glycerol solutions ($p>0.05$). Heat separation of porcine skin was not carried out as it has been shown to compromise the membrane integrity. Full thickness pig skin including epidermal and dermal layers was used in this study and heat separated epidermis was used for human skin studies. It has been suggested that the hydrated dermal layer in full thickness porcine skin could act as an additional aqueous barrier for lipophilic permeants (Dick and Scott, 1992). This theory could also explain the greater skin retention of PR observed in porcine skin compared to human skin ($p<0.001$).

The higher retention in porcine skin was also consistent with the results observed for topical delivery of climbazole. Paz-Alvarez et al. (2018) reported that statistically higher amounts of climbazole were extracted from pig skin compared to human epidermis.

3.3.9 Permeation studies of PR using the Skin PAMPA model

The permeation behaviour of PR was investigated using the Skin PAMPA model with varying dose conditions. Fig 3.12 shows the permeation profiles of PR following an application of 30 μL per well. At 2.5 h, the amounts of PR delivered through the Skin PAMPA membrane ranged from 68 to 469 $\mu\text{g}/\text{cm}^2$. Highest permeation was evident for OSal (468.7 \pm 23.9 $\mu\text{g}/\text{cm}^2$) ($p < 0.05$). The next highest value was observed for the DMI solution ($p < 0.05$), 340.1 \pm 38.9 $\mu\text{g}/\text{cm}^2$. A significantly lower amount of PR was delivered by TC and PEG 400 ($p < 0.05$), with values of 99.2 \pm 13.1 and 68.2 \pm 14.4 $\mu\text{g}/\text{cm}^2$, respectively.

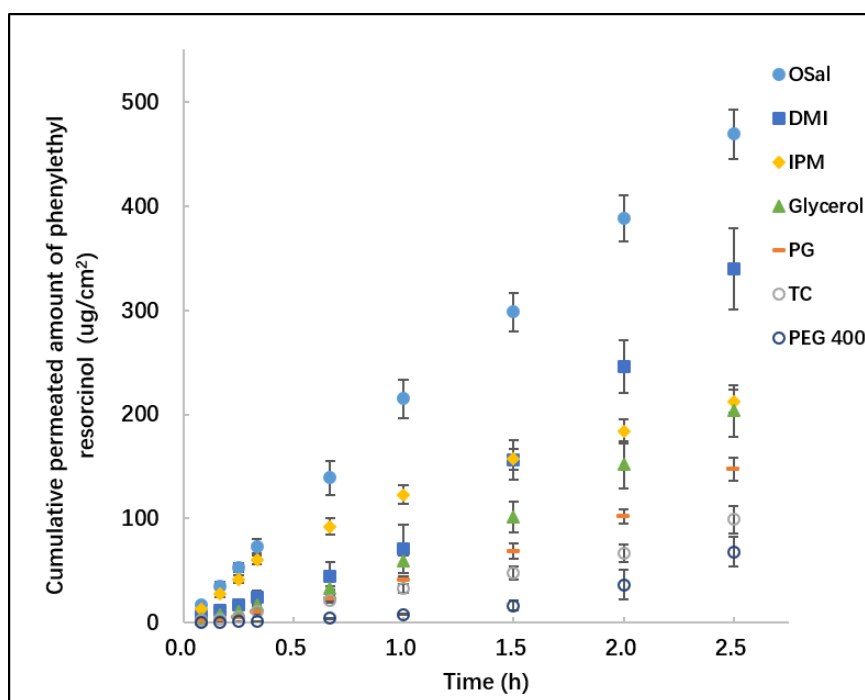


Figure 3. 12 The permeation profiles of PR from OSal, DMI, IPM, glycerol, PG, TC and PEG 400 in the Skin PAMPA model following application of 30 μL of formulation per well, corresponding to 90 $\mu\text{L}/\text{cm}^2$ (mean \pm SD, $n=5$).

Fig 3. 13 illustrates the corresponding percentages of PR that permeated for each solution. At 2.5 h, the two most efficient vehicles in this study ($p < 0.05$), were OSal and DMI

with 29 and 25 % of dosed amounts permeating, respectively. The linearity of the permeation profiles was also evident ($r^2 > 0.99$). This indicated the permeation of PR reached a steady-state flux. This result confirmed that the depletion of the donor does not occur. Consequently, a dose of 30 μL /well was considered to be constant and infinite. The corresponding values for glycerol, PG, IPM, TC and PEG 400 were 17.4 ± 2.1 , 14.8 ± 1.2 , 14.2 ± 0.7 , 7.8 ± 1.0 and 6.2 ± 1.3 %, respectively.

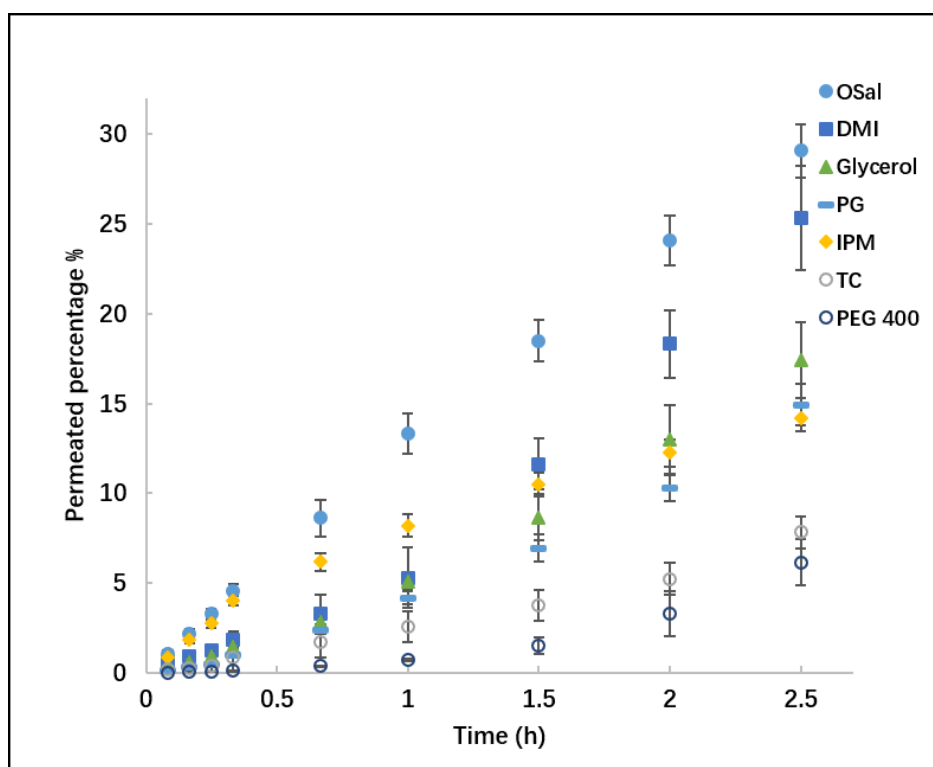


Figure 3.13 The percentage permeation of PR from OSal, DMI, IPM, glycerol, PG, TC and PEG 400 in the Skin PAMPA model following application of 30 μL of formulation per well, corresponding to 90 $\mu\text{L}/\text{cm}^2$ (mean \pm SD, $n=5$).

Fig 3.14 illustrates the results from the Skin PAMPA model following an application of 17 μL per well, corresponding to 51 $\mu\text{L}/\text{cm}^2$. The corresponding percentages permeated are shown in Fig 3.15. As for the results obtained under infinite dose conditions, higher permeation of PR was observed for OSal compared with other solvents, $362 \pm 9 \mu\text{g}/\text{cm}^2$ ($p<0.05$). Again, as for the infinite dose studies there were no differences in the amounts of PR delivered by DMI, glycerol, PG, IPM and TC ($p>0.05$). Lower permeation was evident for PEG 400 ($p<0.05$). The corresponding percentages of PR that permeated ranged from 12 to

31 %.

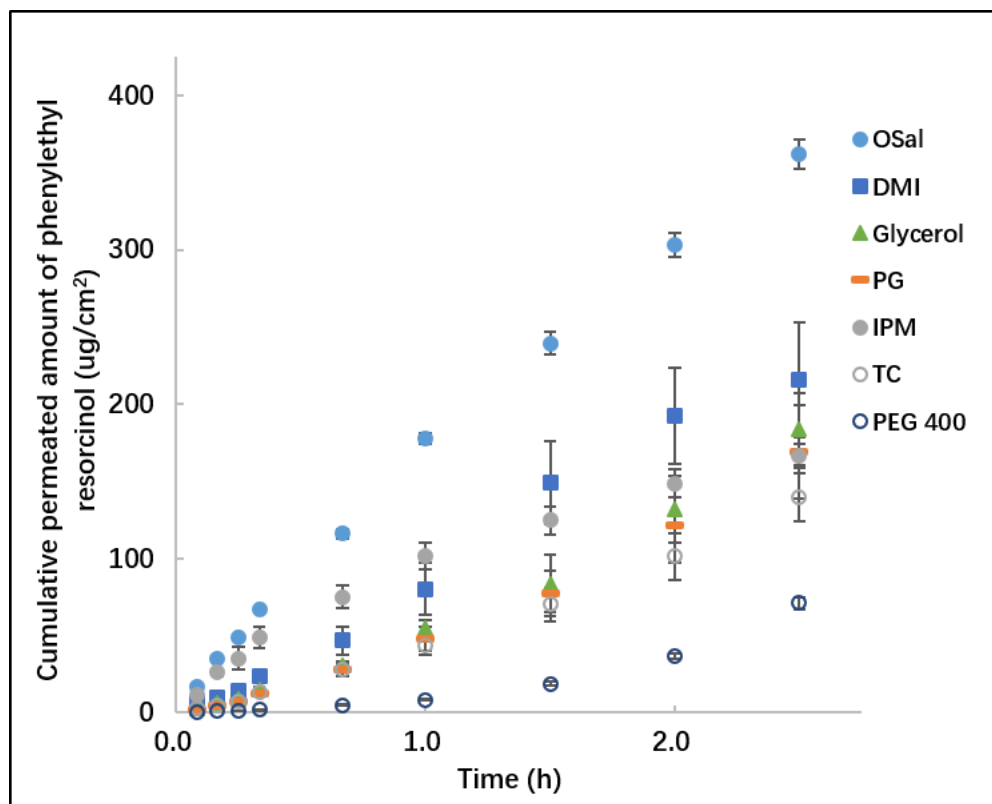


Figure 3. 14 The permeation profiles of PR from OSal, DMI, IPM, glycerol, PG, TC and PEG 400 in the Skin PAMPA model following application of 17 μL of formulation per well, corresponding to 51 $\mu\text{L}/\text{cm}^2$ (mean \pm SD, n=5).

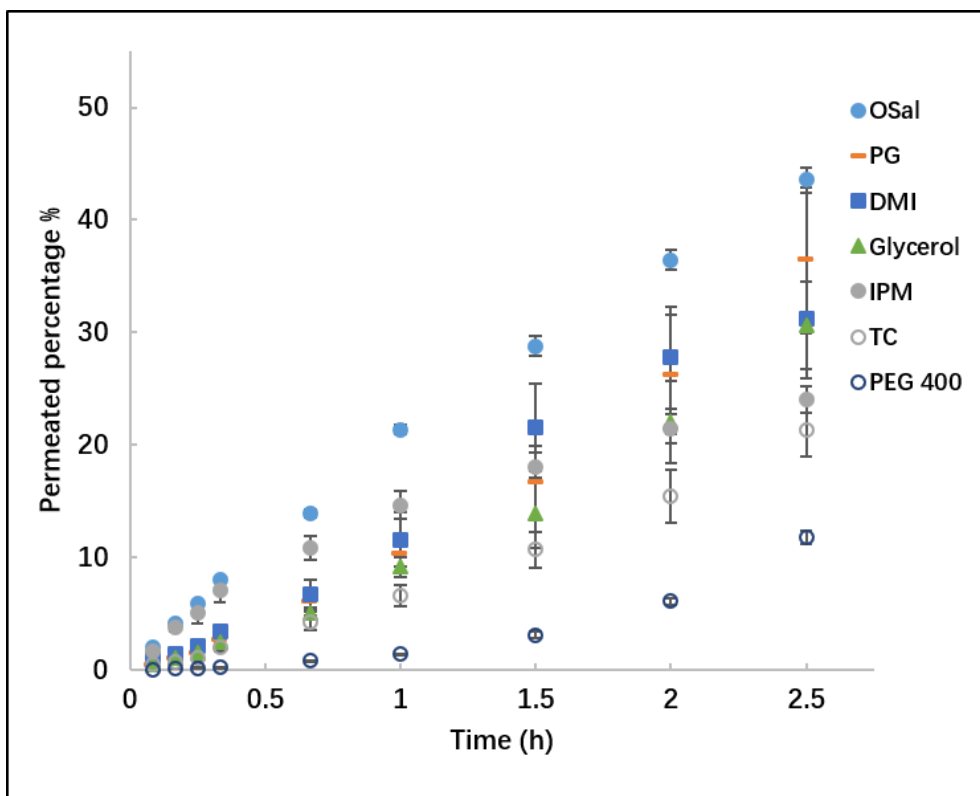


Figure 3. 15 The percentage permeation of PR from OSal, DMI, IPM, glycerol, PG, TC and PEG 400 in the Skin PAMPA model following application of 17 μL of formulation per well, corresponding to 51 $\mu\text{L}/\text{cm}^2$ (mean \pm SD, n=5).

The permeation profiles of PR following the dose of 1 μL per well are presented in Fig 3.16. At 2.5 h, the permeation from all tested solutions was within the range of 30–39 $\mu\text{g}/\text{cm}^2$. 38.6 \pm 3.2 $\mu\text{g}/\text{cm}^2$ of active was delivered through the Skin PAMPA membrane from OSal. This value was greater than the amount permeated from PEG 400, 30.0 \pm 2.5 $\mu\text{g}/\text{cm}^2$ ($p < 0.05$).

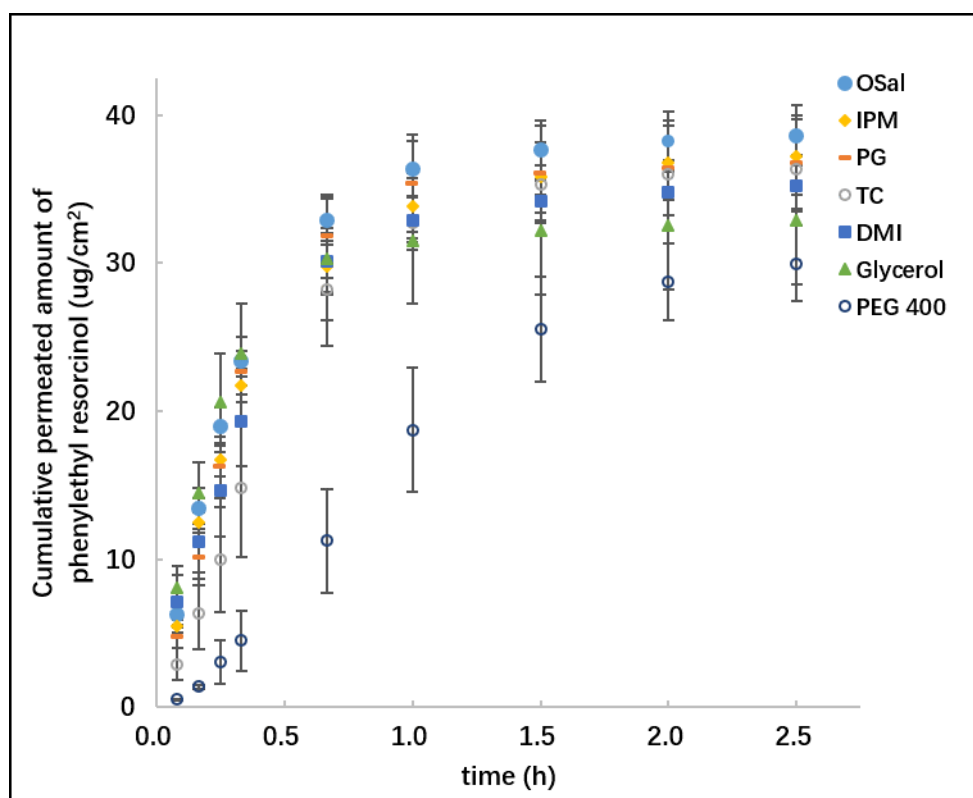


Figure 3. 16 The permeation profiles of PR from OSal, DMI, IPM, glycerol, PG, TC and PEG 400 in the Skin PAMPA model following application of 1 μL of formulation per well, corresponding to 3 $\mu\text{L}/\text{cm}^2$ (mean \pm SD, n=5).

Fig 3. 17 shows the percentage permeation of PR from the tested solutions. For all the vehicles, at 2.5 h, a lower percentage of PR permeated for PEG 400 ($p > 0.05$). The amount of PR delivered from PEG 400 solutions through the Skin PAMPA membrane accounted for $86.6 \pm 7.3 \%$ of dosed amount. Overall, a greater percentage of each formulation permeated in the Skin PAMPA at 1 μL compared to 30 and 17 ml per well ($p < 0.001$). The percentage of PR that permeated following the application of 17 μL was generally higher than results obtained for the 30 μL application ($p < 0.05$).

It is evident from the permeation profiles in Fig 3.17 for all the tested solutions, the permeation profiles exhibit plateaus with the corresponding percentages permeated exceeding 85 % (Fig 3.17). The permeation appears to be significantly reduced as a result of donor depletion which confirmed the application of 1 μL per well is suitable to represent clinically relevant, finite dose conditions.

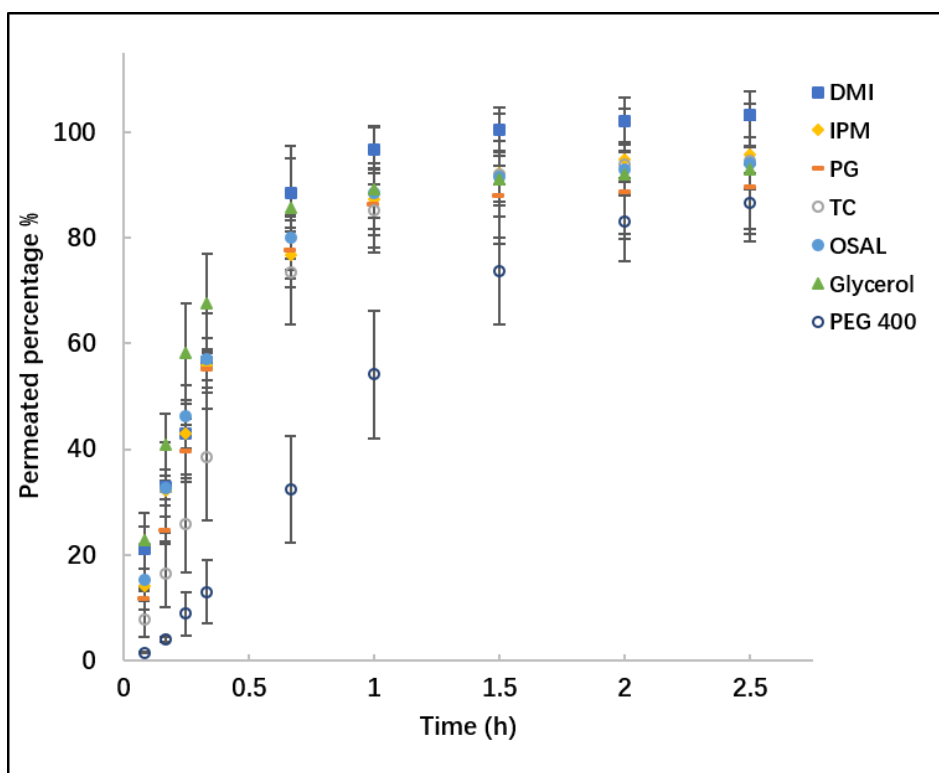


Figure 3. 17 The percentage permeation of PR from OSal, DMI, IPM, glycerol, PG, TC and PEG 400 through the Skin PAMPA model following application of 1 μ L of formulation per well, corresponding to 3 μ L/cm² (mean \pm SD, n=5).

Under finite dose conditions, for all tested PR solutions, the Skin PAMPA model is more permeable than both porcine skin and human skin ($p < 0.001$). To further investigate the feasibility of the permeation of PR from the Skin PAMPA model in predicting human skin percutaneous absorption, the cumulative permeated amounts of PR in this artificial membrane were plotted against corresponding results obtained from human skin studies. Interestingly, a linear correlation was observed between the permeation data from the Skin PAMPA model at 2.5 h and human skin at 24 h under finite dose conditions. The coefficient (R^2) for the linear regression of the correlation is 0.70 (Fig 3.18). Considering the variability in biological skin, the correlations observed here warrant further development of PAMPA as a screening model for human skin permeability of PR.

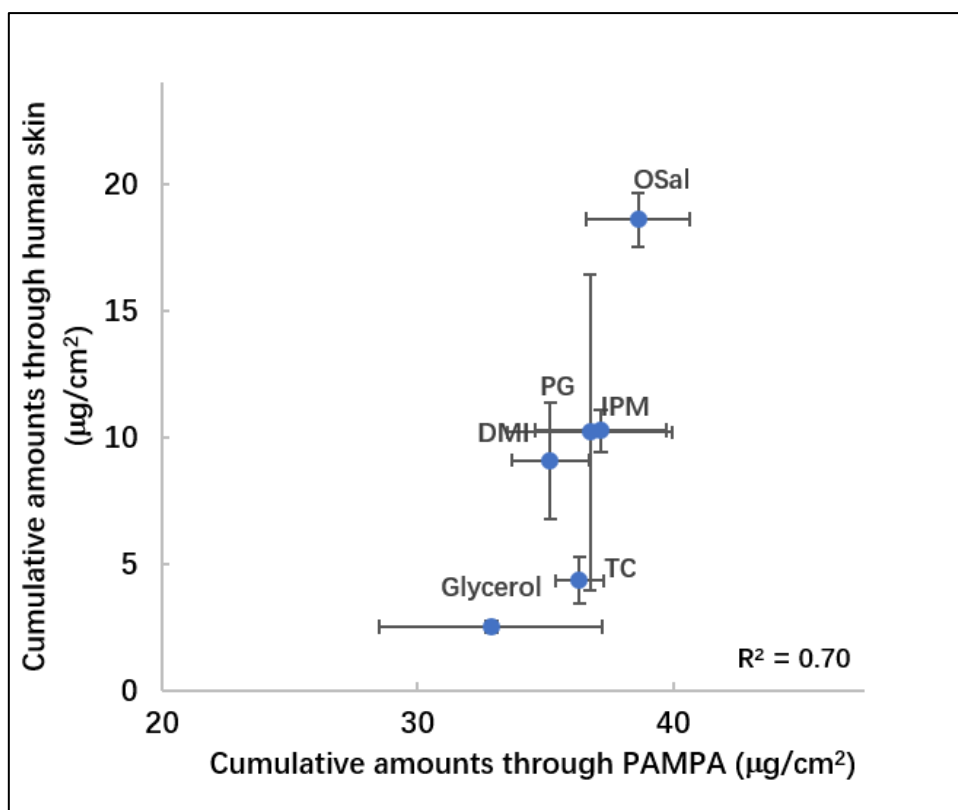


Figure 3. 18 Correlations between the cumulative amounts of PR that permeated in human skin and the Skin PAMPA model under finite dose conditions.

3.4 Conclusion

In this work, a systematic characterization of PR was performed. A new analytical method for PR was developed and validated using HPLC. The thermal analysis confirmed the melting point of PR as 79.1 °C. PR has a molecular weight less than 300 Da, a melting point less than 100 °C, and a favorable partition coefficient for skin permeation. These results confirmed that this active has suitable physicochemical properties for dermal delivery. This was evident in the *in vitro* permeation studies using porcine skin and human skin under varying dose conditions. Several neat solvents were identified to be potential components for optimum skin delivery of PR. From the results obtained from this work, clearly, the permeation behavior in human and porcine skin is dependent on the molecule of interest. Human skin is recognized as the “gold-standard” to obtain data pertaining to man (Franz, 1975). However, porcine skin, whilst not a perfect model to mimic *in vivo* absorption, is regarded as a suitable alternative to assess mammalian skin delivery of actives before progressing to studies in human skin (Barbero and Frasc, 2009; Yoshimatsu et al., 2017).

Furthermore, the skin permeation of PR was also evaluated using the Skin PAMPA model. In general, the Skin PAMPA model was confirmed to be more permeable than biological membranes. A linear correlation of the *in vitro* permeability of PR between human epidermis and the Skin PAMPA model was observed. A wider range of excipients and actives should be tested in the Skin PAMPA model to fully explore its potential to predict human skin delivery of molecules.

Chapter 4.

In vitro evaluation of NIA from binary and ternary systems

4.1 Introduction

One of the main criteria for a successful pharmaceutical formulation is to deliver the therapeutic molecule to the target sites at therapeutically relevant concentrations with the least harm to patients (Kreilgaard 2002). The same principle may be applied to cosmetic products: An appropriate cosmetic product should achieve the effective delivery of an active to the skin (Wiechers, 2008). Aside from the intrinsic activity of the functional ingredient, the design of skin formulations plays a crucial role in the delivery of the active ingredient (Lane et al., 2012a). A typical formulation will contain components with volatile and non-volatile properties. Following application, the volatile components will evaporate from the surface leaving a residual phase on the skin. Lane et al. (2012a) have proposed several concepts for ingredient selection: (i) The vehicles should modify the skin lipid to promote uptake of the functional molecule, (ii) The vehicle should demonstrate sufficient residence time in and on the skin, (iii) The residual phase should promote the lateral diffusion of the skin active, (iv) Last but not least, the vehicle selected should be capable of solubilizing a sufficient amount of active and providing a high thermodynamic activity of the active. A high solubility of the active in the formulation is required while a comparatively low solubility in the formulation relative to the stratum corneum is preferred (Otto et al., 2009). This may be achieved practically by incorporating the primary solvent with high solubility of active along with a secondary solvent in which the active is far less soluble (Wiechers et al., 2004). Furthermore, multicomponent mixtures of chemicals have been shown to promote superior skin permeation enhancement compared to individual chemicals, in a synergistic manner (Karande and Mitragotri, 2009; Ng et al., 2015). Theoretically, synergistic action can be seen when formulation components are present that aid both solubility of the active and alter the stratum corneum lipid spacing (Hadgraft and Walters, 1994).

The use of PG and TC as skin penetration enhancers has been reported extensively in the literature (Kasting et al., 1993; Harrison et al., 1996; Mura et al., 2000; Trotter et al., 2004; Lane, 2013; Osborne and Musakhanian, 2018). These two vehicles are promising components of binary systems and synergistic skin enhancement effects of PG or TC with other penetration enhancers have been reported (Williams and Barry, 2012; Erdal et al., 2014;

Osborne and Musakhanian, 2018).

In Chapter 2, the delivery of NIA (NIA) has been investigated from a range of single vehicle solutions in the Skin PAMPA model, porcine skin and human skin. A significantly higher permeation of NIA was observed for T-BA in heat-separated human epidermis. Accordingly, the main objective of this chapter is to investigate the effect of the selected vehicles on the percutaneous absorption of tested actives. This work is the preliminary step in the development of optimized topical preparations of NIA. A secondary objective of the work is to explore further the feasibility of the Skin PAMPA model for screening of topical formulations screening. Finally, the third objective is to identify the most promising formulations for *in vivo* evaluation.

4.2 Materials and methods

4.2.1 Materials

NIA (NIA) and analytically pure standards of 1,2-butylene glycol (BG), propylene glycol, t-butyl alcohol (T-BA), oleic acid (OA), 2-ethylhexyl salicylate (also known as octyl salicylate, OSal) and linolenic acid (LA) were purchased from Sigma-Aldrich (UK). Isopropyl myristate (IPM) and dimethyl isosorbide (DMI) were gifts from Croda Ltd (UK). Polyethylene glycol (PEG) 400 was obtained from Fisher Scientific (UK). PEG-6-caprylic/capric glycerides (PEG-6-CCG) was a gift from Avon, USA. Transcutol® P (TC) and caprylic/capric triglyceride (CCT) were received from Gattefossé (France).

4.2.2 Methods

4.2.2.1 Evaluation of binary vehicle formulations of NIA using the Skin PAMPA model

The influence of varied neat vehicles on the permeation of NIA was initially assessed using the Skin PAMPA model (Session C.2.2.2.8). The binary systems for formulating the active were selected according to the miscibility data (Appendix 3), solubility data and stability data. For the binary system, the primary solvent in which NIA shows high solubility

was first identified. A second vehicle which is miscible with the first solvent was then considered. In the solubility studies, NIA demonstrated the highest solubility in PG and TC (Session C.2.3.2). Therefore, these two vehicles were identified as the starting point to develop optimum formulations for dermal delivery of NIA. Tables 4.1 summarizes the first category of NIA binary systems, which are composed of PG and other solvents, screened using the Skin PAMPA model. The studies were conducted following the application of 1 μL of formulation per well (3 $\mu\text{L}/\text{cm}^2$).

Table 4. 1 The composition of the PG binary solvent systems of NIA screened using the Skin PAMPA model

Binary solvent systems	Abbreviation
Propylene glycol: Dimethyl isosorbide (70:30 v/v)	PG:DMI (70:30)
Propylene glycol: Dimethyl isosorbide (50:50 v/v)	PG:DMI (50:50)
Propylene glycol: Dimethyl isosorbide (30:70 v/v)	PG:DMI (30:70)
Propylene glycol: Transcutol® P (50:50 v/v)	PG:TC (50:50)
Propylene glycol: PEG-6-caprylic/capric glycerides (50:50 v/v)	PG: PEG6CCG (50:50)
Propylene glycol: Oleic acid (10:90 v/v)	PG:OA (10:90)
Propylene glycol: Linolenic acid (50:50 v/v)	PG:LA (50:50)

Following the Skin PAMPA study of binary systems composed of PG and other solvents, six binary systems composed of TC and other solvents were tested. Table 4.2 shows the compositions of the binary systems.

Table 4. 2 The composition of the TC binary solvent systems of NIA screened using the Skin PAMPA model

Binary solvent systems	Abbreviation
Transcutol® P: Dimethyl isosorbide (50:50 v/v)	TC: DMI (50:50)
Transcutol® P: Caprylic/capric triglyceride (70:30 v/v)	TC: CCT (70:30)
Transcutol® P: Caprylic/capric triglyceride (50:50 v/v)	TC: CCT (50:50)
Transcutol® P: Butyl glycol (50:50 v/v)	TC: BG (50:50)
Transcutol® P: Octyl salicylate (70:30 v/v)	TC: OSal (70:30)

The selectivity and sensitivity of the Skin PAMPA model for discrimination of permeation of similar formulations was further investigated. T-BA was confirmed as the most efficient vehicle in human skin delivery of NIA (Session C.2.3.7). As shown in Table 4.3, nine binary

systems were prepared by combining T-BA with PG, TC or DMI in three different ratios and tested in the Skin PAMPA model.

Table 4. 3 The binary systems of NIA containing varying ratios of volatile alcohol and chemical penetration enhancers.

Volatile binary solvent systems	Abbreviation
Propylene glycol: t-Butyl alcohol (90:10 v/v)	PG:T-BA (90:10)
Propylene glycol: t-Butyl alcohol (70:30 v/v)	PG:T-BA (70:30)
Propylene glycol: t-Butyl alcohol (50:50 v/v)	PG:T-BA (50:50)
Transcutol [®] P: t-Butyl alcohol (90:10 v/v)	TC:T-BA (90:10)
Transcutol [®] P: t-Butyl alcohol (70:30 v/v)	TC:T-BA (70:30)
Transcutol [®] P: t-Butyl alcohol (50:50 v/v)	TC:T-BA (50:50)
Dimethyl isosorbide: t-Butyl alcohol (90:10 v/v)	DMI:T-BA (90:10)
Dimethyl isosorbide: t-Butyl alcohol (70:30 v/v)	DMI:T-BA (70:30)
Dimethyl isosorbide: t-Butyl alcohol (50:50 v/v)	DMI:T-BA (50:50)

4.2.2.2 Evaluation of binary vehicle formulations of NIA in porcine skin

In this work, a range of binary vehicle systems with a content of 5 % w/v of NIA were evaluated in porcine skin following the procedure described in Session C.2.2.2.5. The selected binary solutions may be categorized into two groups according to the selected primary solvents: PG and TC (Table 4.4). To examine the correlation between permeation in porcine skin and the Skin PAMPA model, six binary vehicle formulations containing t-butyl alcohol (T-BA) and other solvents were assessed in porcine skin.

Table 4. 4 NIA binary vehicle formulations evaluated using porcine skin.

PG binary vehicle systems	TC binary vehicle systems	Volatile alcohol binary systems
PG:PEG6CCG (50:50)	TC:PEG400 (50:50)	PG:TBA (50:50)
PG:DMI (30:70)	TC:CCT (70:30)	TC:TBA (50:50)
PG:DMI (50:50)	TC:CCT (50:50)	DMI:TBA (50:50)
PG:DMI (70:30)	TC:DMI (50:50)	PG:TBA (70:30)
PG:OA (10:90)	TC:BG (50:50)	PG:TBA (90:10)
PG:TC (50:50)	TC:OSal (70:30)	TC:TBA (90:10)
PG:PEG 400 (50:50)		
PG:LA (50:50)		

4.2.2.3 Evaluation of binary vehicle formulations of NIA in human skin

Based on the results obtained from porcine skin and the Skin PAMPA studies eight binary solvent systems were taken forward for evaluation in human skin under finite dose conditions (Session C.2.2.2.6). Table 4.5 describes the components of the tested systems.

Table 4. 5 NIA binary vehicle formulations evaluated using human skin.

PG binary vehicle systems	TC binary vehicle systems	Volatile alcohol binary systems
PG:TC (50:50)	TC:PEG400 (50:50)	PG:TBA (90:10)
PG:DMI (50:50)	TC:DMI (50:50)	TC:TBA (90:10)
PG:OA (10:90)		
PG:LA (50:50)		

4.2.2.4 Evaluation of ternary vehicle formulations of NIA in the Skin PAMPA model and mammalian skin

Three ternary vehicles containing 5 % (w/v) of NIA were prepared and examined, namely TC:CCT:DMI (50:25:25) (v/v), TC:PG:DMI (50:25:25) (v/v) and PG:TC:DMI (50:25:25) (v/v). The permeation studies were conducted following the application of 1 μL doses of formulations in the Skin PAMPA model and 5 $\mu\text{L}/\text{cm}^2$ applications in human skin and porcine skin.

4.3 Results and discussion

4.3.1 Evaluation of binary and ternary vehicle systems of NIA in the Skin PAMPA model

4.3.1.1 Binary vehicles of NIA composed of PG and other solvents in the Skin PAMPA model

Seven NIA (5 % w/v) binary vehicle formulations containing PG were evaluated using the Skin PAMPA model under finite dose conditions (Fig 4.1). At 2.5 h, the cumulative amounts of NIA that permeated through the membrane ranged from 44.2 to 140.2 $\mu\text{g}/\text{cm}^2$. High permeation was observed for the systems containing PG:OA (10:90), 140.2 \pm 18.9 $\mu\text{g}/\text{cm}^2$. This value was significantly higher than the permeation from PG:DMI (30:70), PG:PEG6CCG (50:50), PG:TC (50:50), PG:DMI (50:50) and PG:LA (50:50) ($P < 0.05$). There was no difference in the amounts of NIA that permeated from the binary systems of PG and DMI with varying

ratios ($p>0.05$). Significantly lower permeation of NIA was observed for PG:LA compared with all other vehicles ($p<0.05$), with a value of $44.2 \pm 9.4 \mu\text{g}/\text{cm}^2$ at 2.5 h.

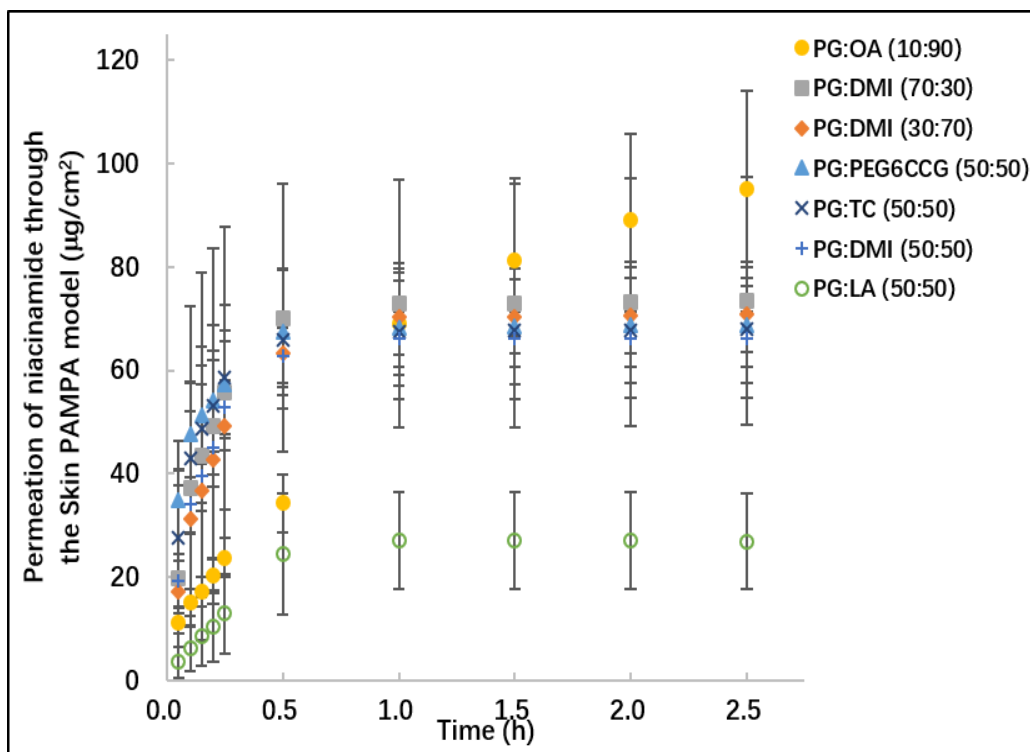


Figure 4. 1 Permeation profiles of NIA from seven binary vehicles containing PG as the primary solvent in the Skin PAMPA model (mean \pm SD, $n=5$).

Fig 4.2 shows the corresponding percentage permeation of NIA from the seven vehicles. The permeation from PG:OA (10:90) started to plateau after 1 h of application, while the profiles for the other vehicles showed a similar levelling off in permeation from 0.5 h. At 2.5 h, 95.2 % of the dosed amounts of active were delivered through the membrane from PG:OA (10:90), while only 26.9 % of the applied NIA had permeated from PG:LA (50:50).

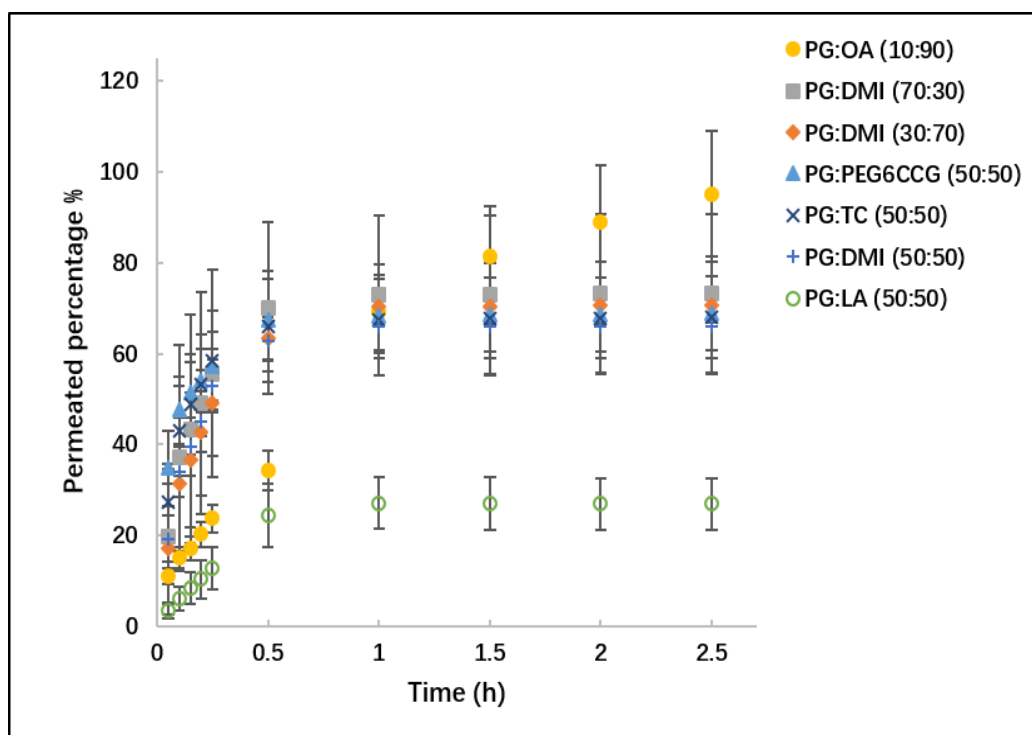


Figure 4. 2 Percentage permeation of NIA from seven binary PG vehicles in the Skin PAMPA model (mean \pm SD, n=5).

4.3.1.2 Binary vehicles of NIA composed of TC and other solvents in the Skin PAMPA model

Six TC binary vehicles containing 5 % (w/v) of NIA were prepared and assessed using the Skin PAMPA model. Fig 4.3 shows the permeation profiles of all tested solutions. At 2.5 h, $159.9 \pm 5.4 \mu\text{g}/\text{cm}^2$ of NIA permeated from DMI:TC (50:50). This value was significantly higher compared with results for TC:CCT (70:30), TC: CCT (50:50), TC: OSal (70:30) and PEG 400: TC (50:50) ($P < 0.05$). For the TC:BG (50:50) binary vehicle, the cumulative amount of NIA that permeated was $138.5 \pm 3.8 \mu\text{g}/\text{cm}^2$, while there was no difference between the permeation of NIA from the DMI:TC (50:50) and TC:BG (50:50) vehicles ($p > 0.05$).

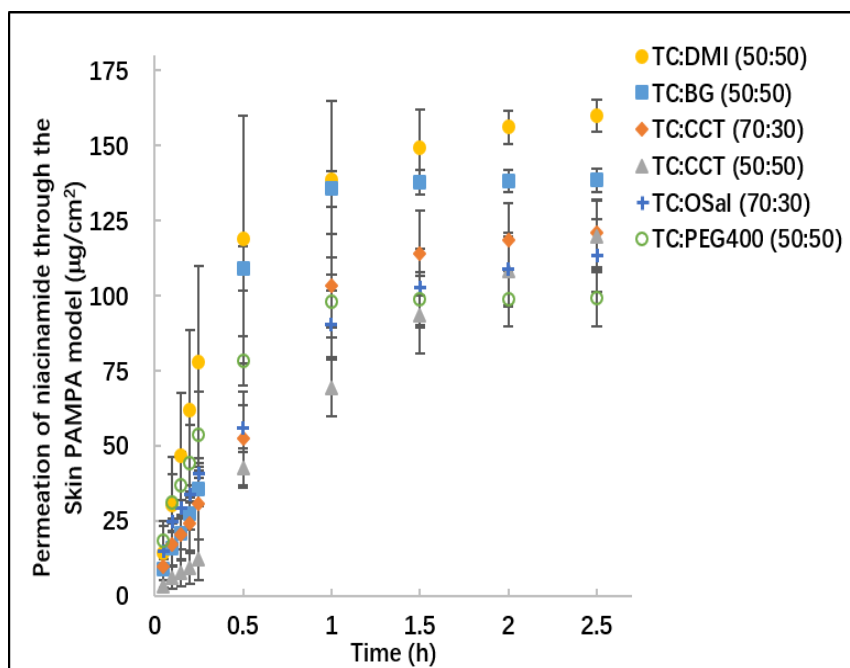


Figure 4. 3 Permeation profiles of NIA from six binary vehicles containing TC as the primary solvent in the Skin PAMPA model (mean \pm SD, n=5).

The corresponding percentages of NIA that permeated are shown in Fig 4.4. For the six tested solutions, the percentage permeation of NIA at 2.5 h ranged from 83.8 %, observed for PEG 400: TC (50:50) to 97.2 % for DMI: TC (50:50) ($p < 0.05$).

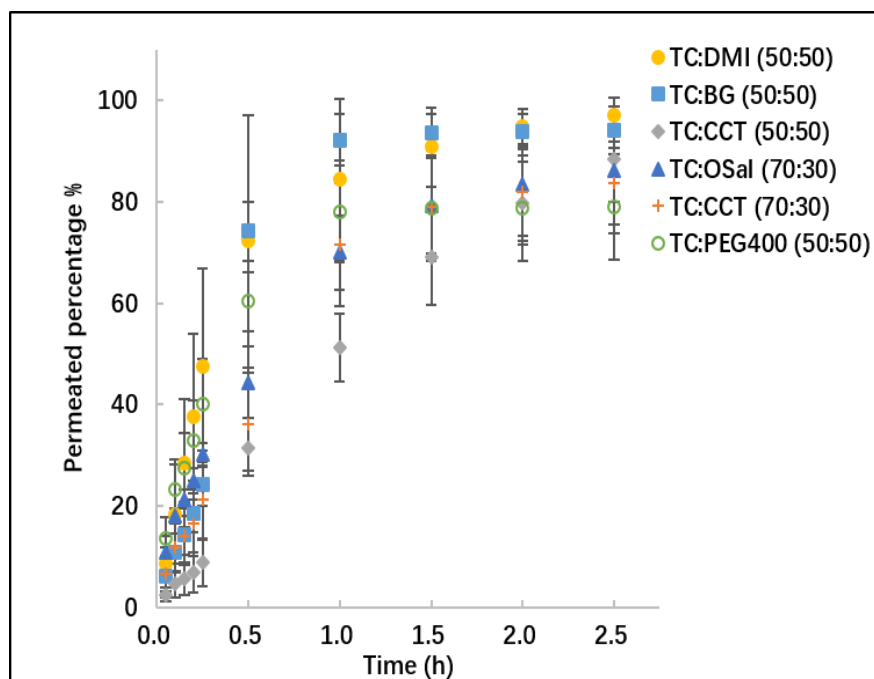


Figure 4. 4 Percentage permeation of NIA from six TC binary vehicles in the Skin PAMPA model (mean \pm SD, n=5).

4.3.1.3 Binary vehicles composed of T-BA and other solvents in the Skin PAMPA model

The permeation behavior of NIA from a series of single solvents was assessed previously. Of all the vehicles, and for all models examined, high permeation was observed for T-BA (Chapter 2). The volatility of T-BA was evident in the DVS studies. In this study, T-BA was combined with PG, TC and DMI in three ratios (50:50, 30:70, 10:90 v/v) to prepare nine binary vehicles containing 5 % w/v of NIA. The permeation behavior was tested using the Skin PAMPA model and results are presented in Fig 4.5 and 4.6. At 2.5 h, the permeation from these binary systems ranged from 160.0 to 181.5 $\mu\text{g}/\text{cm}^2$. As illustrated in Fig 4.6, more than 97 % of dosed NIA permeated through the Skin PAMPA membrane. For all tested ratios, a higher value of skin permeation was observed for T-BA combined with PG, but no significant improvement was evident compared with other binary systems. ($p>0.05$). Similar results were reported by Luo et al. (2016). The authors performed a comparative study investigating the permeation of ibuprofen using the Skin PAMPA, silicone membrane and mammalian skin. The authors reported the more permeable nature of the Skin PAMPA model and silicone membrane compared to human skin.

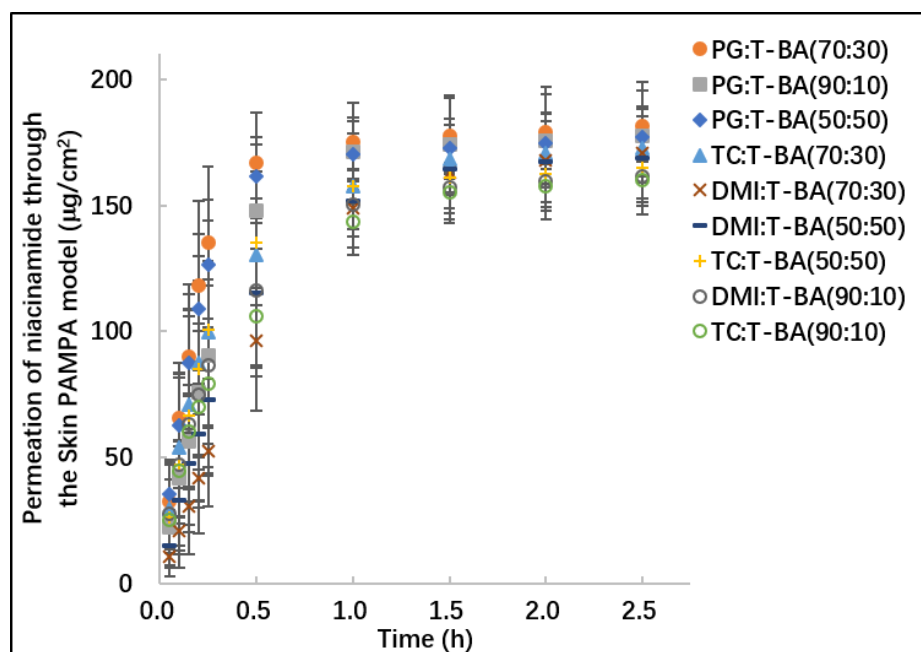


Figure 4. 5 The permeation profiles of NIA from nine binary vehicles containing T-BA in the Skin PAMPA model (mean \pm SD, n=5).

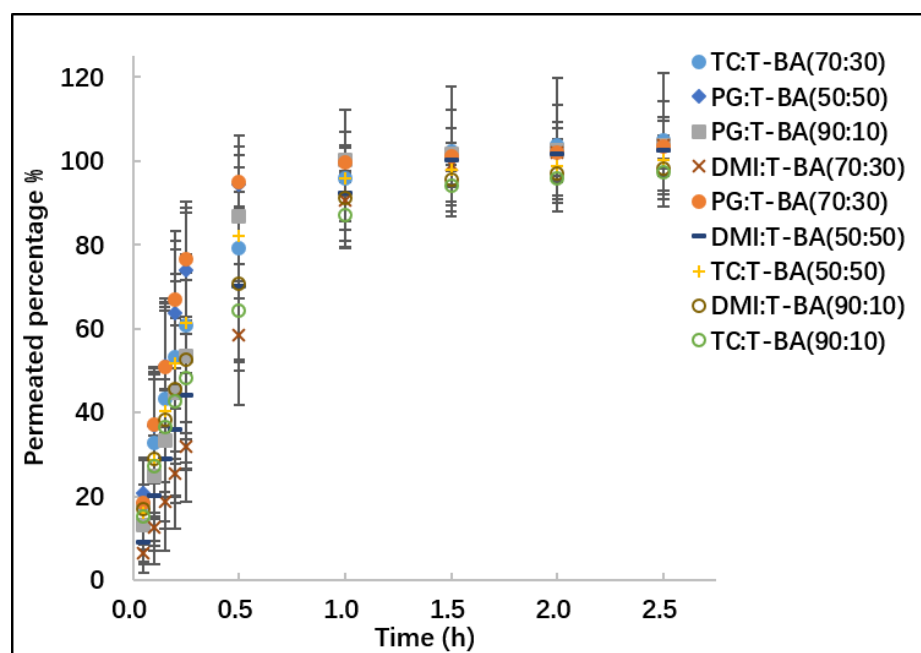


Figure 4. 6 Percentage permeation of NIA from nine T-BA binary vehicle formulations in the Skin PAMPA model (mean \pm SD, n=5).

4.3.1.4 Ternary formulations of NIA in the Skin PAMPA model

PG:TC:DMI (50:25:25), TC:PG:DMI (50:25:25) and TC:CCT:DMI (50:25:25) were selected as the ternary vehicles for NIA dermal delivery. Fig 4.7 shows the permeation profiles

obtained in the Skin PAMPA model following the application of 1 μL of formulation per well. At 2.5 h, 120 to 125 $\mu\text{g}/\text{cm}^2$ of NIA was delivered by the solvent mixtures, with no significant differences evident ($p>0.05$). The amounts accounted for 75 to 81 % of applied doses (Fig 4.8). The Skin PAMPA model did not show differences in the permeation between the formulations. The Skin PAMPA model did not discriminate the permeation behavior of the three tested ternary systems. The formulations were further investigated using porcine skin and human skin.

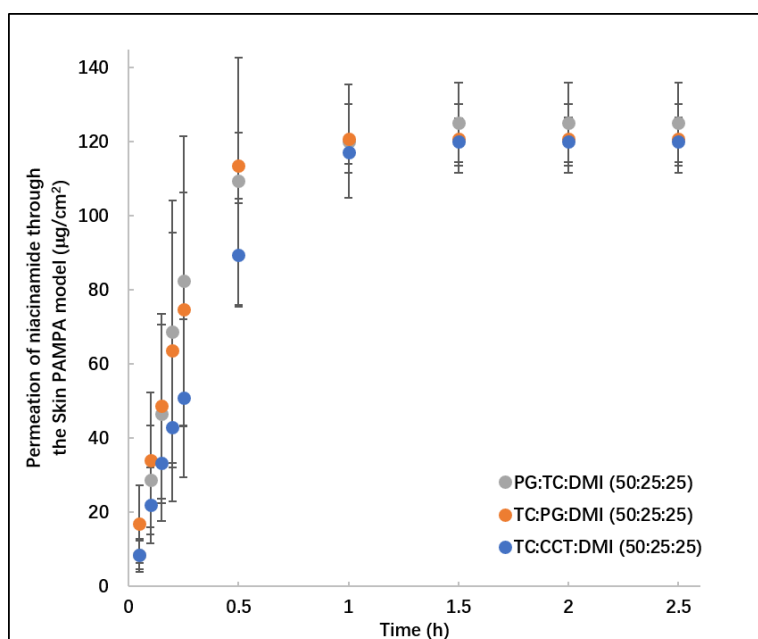


Figure 4. 7 Permeation profiles of NIA from ternary vehicles in the Skin PAMPA model (mean \pm SD, n=5).

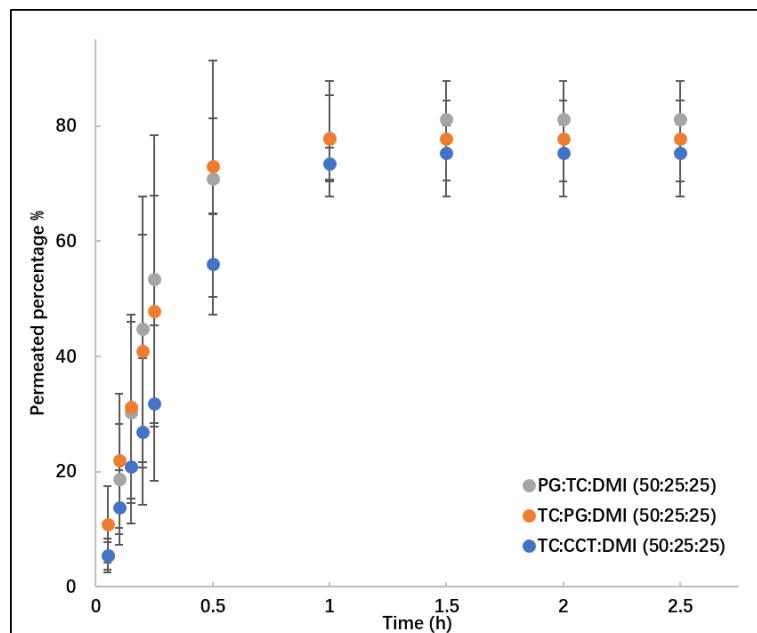


Figure 4. 8 Percentage permeation of NIA from ternary vehicles in the Skin PAMPA model (mean \pm SD, n=5).

4.3.2 Evaluation of binary and ternary vehicle systems of NIA in porcine skin

4.3.2.1 Binary systems composed of PG and other solvents in porcine skin

The permeation profiles of NIA are presented in Fig 4.9. The permeation from PG:OA (10:90) was detected 2 h after application, while permeation was not observed until 6 h for the other formulations. At 24 h, the amounts of permeation in skin ranged from 1.9 to 70.2 $\mu\text{g}/\text{cm}^2$, corresponding to 0.8 to 30.2 % of dosed amounts (Fig 4.10). The PG:OA (10:90) and PG:TC (50:50) mixtures delivered 70.2 ± 18.1 and 28.2 ± 13.7 $\mu\text{g}/\text{cm}^2$ of active into the receptor medium, respectively, significantly higher values than observed for the permeation from PG: PEG 400 (50:50) ($p < 0.05$). On the contrary, the permeation from PG at 24 h was 46.0 ± 10.9 $\mu\text{g}/\text{cm}^2$, corresponding to around 19.5 % of the dosed amounts. High values were observed for the binary systems that combined PG with the fatty acid, oleic acid (OA), but statistical analysis confirmed that no significant difference was evident compared with PG alone ($p > 0.05$).

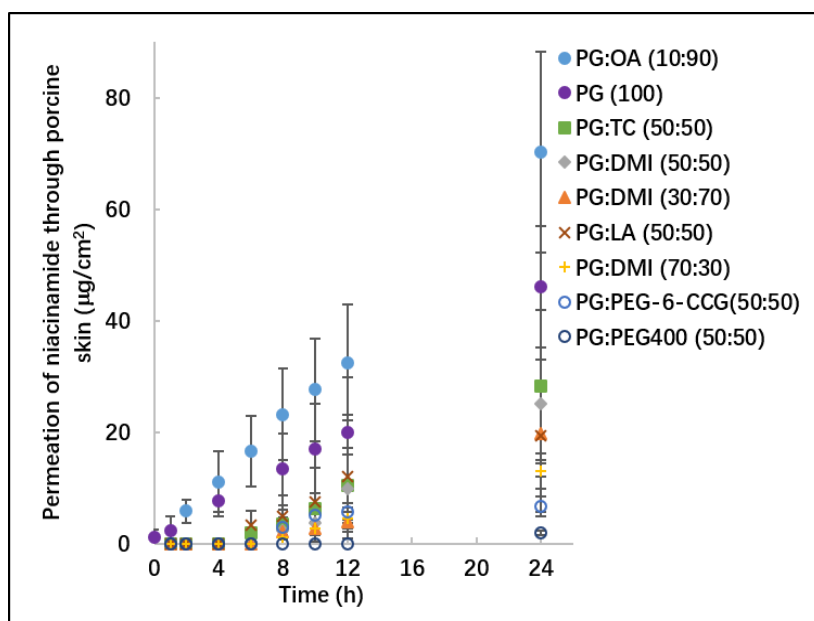


Figure 4. 9 Permeation profiles of NIA in porcine skin from binary systems composed of PG with other solvents or PG alone (mean \pm SD, n=4).

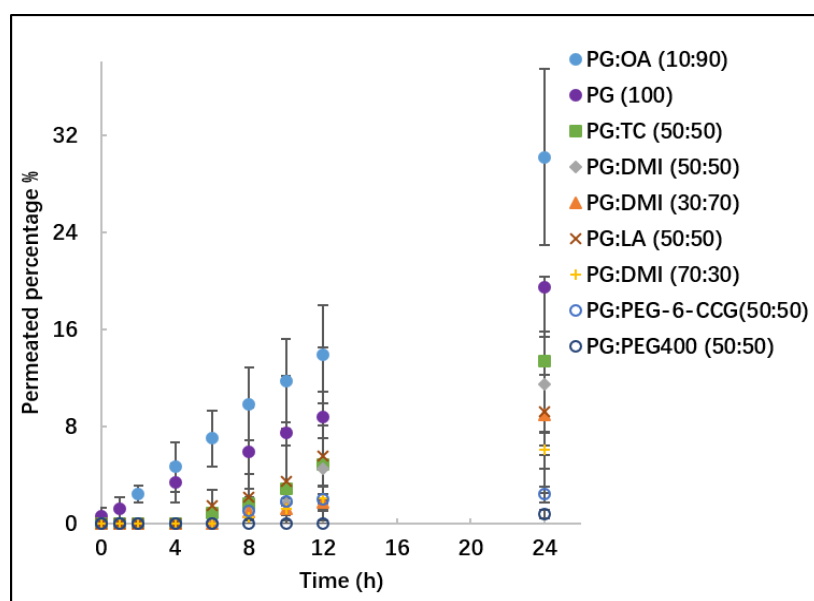


Figure 4. 10 Percentage permeation of NIA in porcine skin from binary systems composed of PG with other solvents and PG alone (mean \pm SD, n=4).

Mass balance results are summarized in Table 4.6. The recovery values of NIA from the skin surface for PG: PEG 400 (50:50) and PG:OA (10:90) were 88 and 37 %, respectively ($p < 0.05$). For the remaining systems, approximately half of the applied doses remained on the skin surface. Low overall recovery of NIA was observed for some formulations (Table 4.6) which was consistent with results reported by Haque et al. (2017a), This might be attributed

to chemical derivatization of this molecule during the permeation process (Sil et al., 2018). After 24 h, the skin uptake ranged from 2.1 to 27.4 %. Significantly higher skin extraction was obtained for PG: PEG6CCG (50:50) compared with PG: PEG 400 (50:50) ($p<0.05$). The percentage skin extraction values for binary systems of PG: PEG6CCG (50:50), PG:DMI (50:50) and PG:LA (50:50) solutions were significantly higher compared to simple PG solutions ($p<0.001$). PEG-6 caprylic/capric glycerides (PEG6CCG) is a polyethylene glycol derived from a mixture of mono-, di-, and triglycerides of caprylic and capric acids (Fiume, 2014). It is used in personal care products as an emollient and emulsifying agent (J and Breslawec, 2014). The solubility of NIA in PEG6CCG was determined as 5.6 %, which is four times lower than the solubility of NIA in PG ($P<0.05$). Therefore, the presence of PEG6CCG leads to a decreased solubility of NIA in the binary system and an increased thermodynamic activity. The increased thermodynamic activity may have provided increased driving force for active penetration and enhanced the permeation of the active in porcine skin (Wiechers et al., 2004; Otto et al., 2009; Lane et al., 2012b).

Table 4. 6 Results of the mass balance studies following permeation studies in porcine skin of NIA binary vehicle systems composed of PG and other solvents ($n=4$, mean \pm SD).

	PG: PEG6CCG (50:50)	PG:DMI (30:70)	PG:DMI (50:50)	PG:DMI (70:30)	PG:OA (10:90)
Washing %	53.1 \pm 4.7	46.3 \pm 4.7	47.1 \pm 5.4	53.5 \pm 2.4	37.1 \pm 5.4
Extraction %	27.4 \pm 4.6	26.8 \pm 6.7	22.9 \pm 13.2	24.3 \pm 10.6	9.6 \pm 1.0
Permeation %	2.4 \pm 0.3	9.0 \pm 3.3	11.5 \pm 3.9	6.1 \pm 1.5	30.2 \pm 7.2
Total recovery %	83.0 \pm 0.3	82.1 \pm 5.9	81.5 \pm 5.6	83.8 \pm 10.8	76.8 \pm 5.9
	PG:TC (50:50)	PG:PEG400 (50:50)	PG:LA (50:50)	PG (100)	
Washing %	43.4 \pm 3.9	87.7 \pm 14.0	55.6 \pm 12.3	55.6 \pm 7.0	
Extraction %	23.4 \pm 5.6	2.1 \pm 0.8	20.6 \pm 4.4	2.7 \pm 1.2	
Permeation %	13.4 \pm 6.9	0.8 \pm 0.3	9.2 \pm 6.6	19.5 \pm 5.7	
Total recovery %	80.2 \pm 6.7	90.6 \pm 14.7	85.4 \pm 7.9	77.8 \pm 3.9	

4.3.2.2 Binary systems composed of TC and other solvents

Fig 4.11 shows the permeation profiles of NIA from binary solvent systems composed of TC and other vehicles. For all tested solutions, permeation was not evident until 6 h. The amount of NIA that permeated from TC:DMI (50:50), $82.6 \pm 41.6 \mu\text{g}/\text{cm}^2$, was significantly higher than the amounts that permeated from TC:PEG 400 (50:50), at $5.8 \pm 3.4 \mu\text{g}/\text{cm}^2$ ($p < 0.05$). No difference was evident comparing the permeation of NIA from TC:DMI (50:50) and neat TC ($p > 0.05$). The percentage permeation of NIA from neat TC and binary systems composed of TC and other vehicles is shown in Fig 4.12. The permeated amounts of NIA from the six tested solutions range from 0.6 to 35.2 % of dosed amounts, with the highest value observed for TC:DMI (50:50) and the lowest valued observed for TC:PEG400 (50:50) ($p < 0.05$). There was no improvement of skin permeation using the binary vehicle systems compromised of TC and other vehicles compared to TC alone ($p > 0.05$).

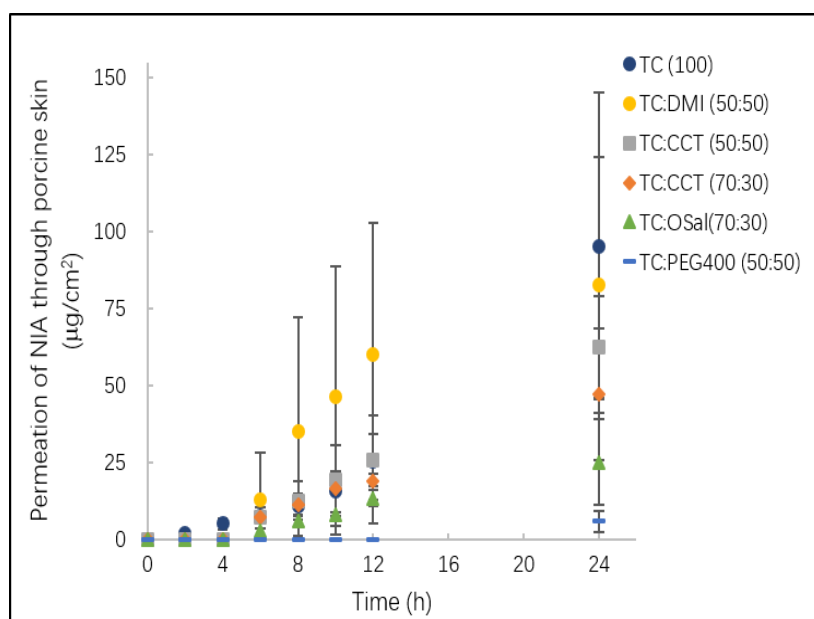


Figure 4. 11 Permeation profiles of NIA in porcine skin for binary vehicles composed of TC with other solvents or TC alone (mean \pm SD, $n=4$).

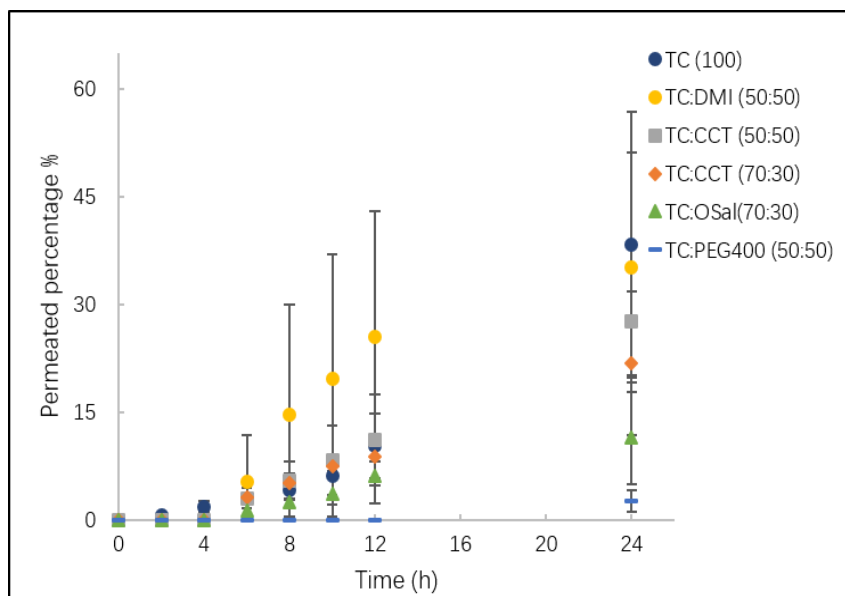


Figure 4. 12 Percentage permeation of NIA in porcine skin from binary systems composed of TC with other solvents or TC alone (mean \pm SD, n=4).

Table 4.7 summarizes the mass balance results following the permeation studies. For NIA binary systems of TC:PEG400 (50:50), TC:CCT (70:30), TC:CCT (50:50), TC:OSal (70:30), ~ 50 % was recovered from the skin surface in the mass balance studies ($p>0.05$). The skin retention for the tested systems ranged from 4 to 32.6 %, and there was no significant increase in skin extraction percentage values compared to neat TC solutions ($p>0.05$).

Table 4. 7 Results of the mass balance studies for permeation of NIA in porcine skin from binary systems composed of TC and other solvents (n=4, mean \pm SD).

	TC:PEG400 (50:50)	TC:CCT (70:30)	TC:CCT (50:50)	TC:DMI (50:50)	TC:OSal (70:30)	TC (100)
Washing %	53.7 \pm 23.2	57.6 \pm 13.7	47.8 \pm 1.8	35.3 \pm 13.6	54.3 \pm 3.5	33.3 \pm 15.8
Extraction %	32.6 \pm 16.9	2.4 \pm 0.8	3.2 \pm 2.2	10.7 \pm 3.5	11.7 \pm 5.6	16.4 \pm 5.8
Permeation %	2.7 \pm 1.5	21.9 \pm 10.0	27.7 \pm 7.5	35.2 \pm 16.0	11.5 \pm 6.4	38.3 \pm 18.5
Total recovery %	89.1 \pm 10.7	81.9 \pm 7.3	78.6 \pm 6.0	81.2 \pm 1.8	77.5 \pm 6.7	88.0 \pm 10.0

4.3.2.3 Binary systems composed of T-BA and other solvents

Fig 4.13 shows the permeation of NIA in porcine skin for the six binary systems composed of the volatile alcohol, T-BA, and other solvents at varying ratios. The corresponding percentages of NIA permeation are illustrated in Fig 4. 14. At 24 h The

cumulative amounts permeated ranged from 119.2 to 222.9 $\mu\text{g}/\text{cm}^2$, with no significant difference between the values ($p>0.05$). The permeation for PG:T-BA (50:50), TC:T-BA (90:10), DMI:T-BA (50:50) and PG:T-BA (70:30) started to level off after 12 h as a result of donor depletion. At 24 h, the percentage permeation of NIA ranged from 79.9 % observed for PG:T-BA (50:50) to 54.7 % for neat T-BA. Statistical analysis indicated that there was no difference among the permeation percentage values observed for all tested systems here ($p>0.05$).

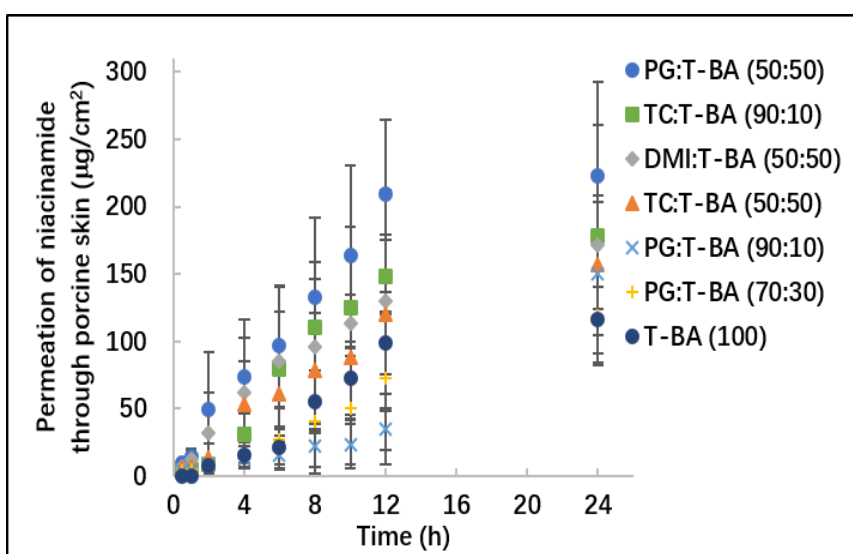


Figure 4. 13 Permeation profiles of NIA in porcine skin for binary vehicles composed of T-BA and other solvents or neat T-BA (mean \pm SD, $4 \leq n \leq 5$).

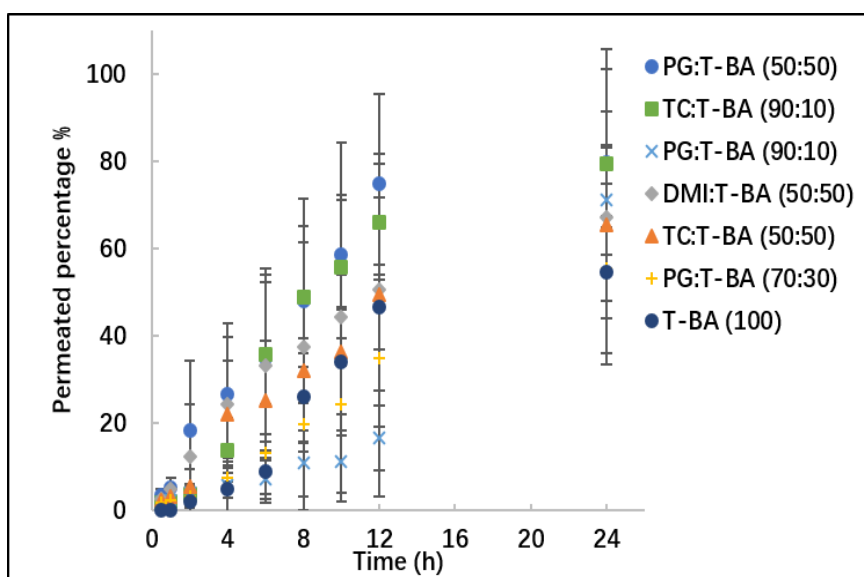


Figure 4. 14 Percentage permeation of NIA in porcine skin from binary systems composed of T-BA

and other solvents or neat T-BA (mean \pm SD, $4 \leq n \leq 5$)

Table 4.8 shows the distribution of NIA following the permeation studies. The skin extraction percentage values for all assessed solutions ranged from 3.1 – 15.3 % ($p > 0.05$). Earlier DVS studies confirmed that T-BA evaporated rapidly after application. On the contrary, DVS confirmed that the residence time application was longer for PG, TC or DMI compared to T-BA ($p < 0.05$). It has been reported that the evaporation of solvent in the skin preparations provided the driving force of permeant partition into the skin at initial stage (Wiechers et al., 2004). For the binary systems composed of T-BA and other solvents, the evaporation of T-BA would increase thermodynamic activity and therefore enhance the permeation. It is also possible that the remaining phase of PG, TC, or DMI in the binary systems contributed to the continuous percutaneous absorption. Similar results were reported by Oliveira et al. (2012). The authors investigated and compared the permeation of saturated solutions of methyl paraben in neat ethanol or binary systems composed of ethanol and TC, DMI and IPM. Oliveira reported that the formulations incorporating the volatile solvent were more efficient compared to the neat IPM, DMI, TC or ethanol.

Table 4. 8 Mass balance studies for the binary systems composed of T-BA and other solvents evaluated in porcine skin (mean \pm SD, $4 \leq n \leq 5$).

	PG:T-BA (50:50)	TC:T-BA (50:50)	T-BA:DMI (50:50)	PG:T-BA (70:30)	PG:T-BA (90:10)	TC:T-BA (90:10)	T-BA (100)
Washing %	2.9 \pm 1.3	11.5 \pm 5.4	14.9 \pm 3.7	27.5 \pm 6.4	3.5 \pm 0.8	6.1 \pm 5.2	20.5 \pm 2.4
Extraction %	3.1 \pm 1.5	3.4 \pm 0.7	8.4 \pm 5.5	13.1 \pm 9.2	10.1 \pm 7.6	15.3 \pm 11.9	4.9 \pm 1.8
Permeation %	79.9 \pm 25.9	65.6 \pm 17.6	67.3 \pm 33.8	55.5 \pm 19.5	71.3 \pm 12.6	79.5 \pm 12.0	54.7 \pm 11.7
Total recovery %	85.8 \pm 26.5	80.5 \pm 11.7	90.5 \pm 25.3	96.2 \pm 14.2	84.9 \pm 7.1	100.9 \pm 13.8	80.0 \pm 7.5

4.3.2.4 Ternary systems of NIA evaluated in porcine skin

The permeation of NIA was determined for three ternary vehicles [PG:TC:DMI (50:25:25), TC:CCT:DMI (50:25:25), TC:PG:DMI (50:25:25)]. Fig 4.15 shows the cumulative amounts of NIA permeation in porcine skin. At 24 h, the permeation values from PG:TC:DMI (50:25:25), TC:CCT:DMI (50:25:25), TC:PG:DMI (50:25:25) were determined as 58.4 ± 7.0 , 47.3 ± 22.4 and $34.1 \pm 6.8 \mu\text{g}/\text{cm}^2$. As shown in Fig 4.16, the permeation accounted for 13 to 25 % of the

applied doses. Comparing the two systems containing varying concentrations of PG, TC and DMI, higher values were observed for PG:TC:DMI (50:25:25), but no significant difference was observed ($p>0.05$). Furthermore, though more complex formulations were evaluated for NIA here, no enhancement was observed for ternary systems compared to neat TC, PG and DMI ($p>0.05$).

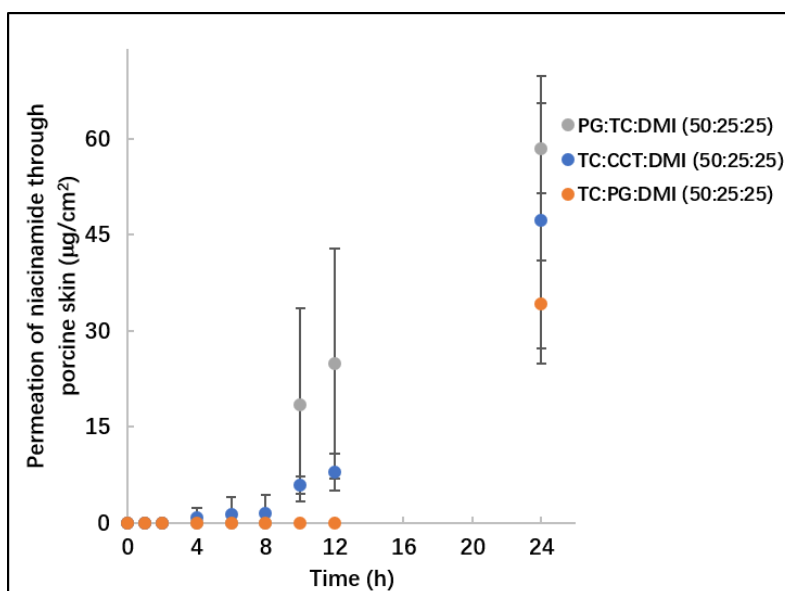


Figure 4. 15 Permeation profiles of NIA from ternary systems in porcine skin (mean \pm SD, $n=4$).

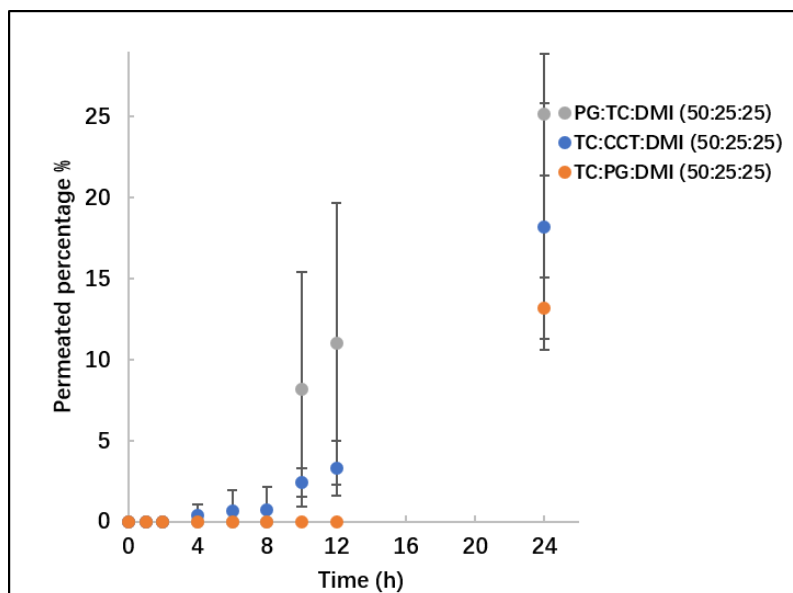


Figure 4. 16 Percentage permeation of NIA from ternary systems in porcine skin (mean \pm SD, $n=4$).

Mass balance studies were conducted to examine the distribution and overall recovery of applied NIA. Table 4.9 summarizes the mass balance results. For TC:CCT:DMI (50:25:25), ~

40 % of the applied dose of NIA was recovered from the skin surface, and 28.0 ± 12.8 % of the applied amount was extracted from the skin tissue. For TC:PG:DMI (50:25:25) and PG:TC:DMI (50:25:25), the skin retention values were 32.9 ± 13.8 and 18.8 ± 8.8 %, respectively ($P > 0.05$).

Interestingly, when comparing distribution of NIA for binary and ternary systems, a higher skin retention was evident for TC:CCT:DMI (50:25:25) than TC:CCT (50:50) and TC:DMI (50:50) ($p < 0.05$). As a mixture of caprylic and capric acid oil, CCT has been widely used in cosmetic products as an emollient (CIRP, 2003). Patel et al. (1985) published the first report regarding its application as a skin penetration enhancer. Leopold and Lippold (1995a) attempted to clarify the mechanism of the penetration enhancing effects of several lipophilic vehicles including CCT via Differential Scanning Calorimetry (DSC) measurements. These authors suggested that the effect of CCT on cutaneous and percutaneous absorption is probably due to dissolution or extraction of the stratum corneum lipids. More recently, in a skin delivery study of kojic acid, CCT was investigated as a component of a kojic acid microemulgel (ME) system. It was reported that the CCT based ME was more efficient compared with an oleic acid (OA) based ME (El Nagar et al., 2016). From this study, the ternary system composed of CCT is promising for dermal delivery of NIA, and the penetration enhancement of this ternary solvent system will be further assessed using human skin.

Table 4. 9 Results of the mass balance studies following the permeation of NIA in porcine skin permeation for ternary systems (n=4, mean \pm SD).

	TC:CCT:DMI (50:25:25)	TC:PG:DMI (50:25:25)	PG:TC:DMI (50:25:25)
Washing %	39.8 ± 15.1	43.2 ± 4.0	36.1 ± 8.5
Extraction %	28.0 ± 12.8	32.9 ± 13.8	18.8 ± 8.8
Permeation %	18.2 ± 7.6	13.2 ± 1.9	25.1 ± 3.8
Total recovery %	86.0 ± 8.9	89.2 ± 16.8	80.1 ± 9.7

4.3.2.5 Comparisons of NIA binary and ternary vehicles in the Skin PAMPA model and porcine skin

Table 4.10 summarizes the cumulative amounts of NIA that permeated in porcine skin

and the Skin PAMPA model for all tested binary and ternary systems. At 24 h, the cumulative permeated amounts of NIA from binary systems composed of T-BA and other solvents were comparable for the values obtained in the Skin PAMPA model ($p>0.05$). In the Skin PAMPA model, TC:DMI (50:50) was more efficient compared with other binary systems composed of TC and other solvents ($P<0.05$). A high value of NIA permeation was also observed for TC:DMI (50:50) in porcine skin, although the value was not significantly higher than other formulations ($p>0.05$).

Table 4. 10 Cumulative amounts of NIA permeation in porcine skin and the Skin PAMPA model from binary and ternary solvent systems (mean \pm SD, $4 \leq n \leq 5$).

Binary and ternary solvent systems	Cumulative permeated amounts of NIA ($\mu\text{g}/\text{cm}^2$)	
	The Skin PAMPA model	Porcine skin
PG:T-BA (70:30)	181.5 \pm 14.1	119.2 \pm 34.8
PG:T-BA (90 10)	177.4 \pm 7.9	150.3 \pm 26.5
PG:T-BA (50 50)	177.1 \pm 12.1	222.9 \pm 69.2
DMI:T-BA (50:50)	168.8 \pm 19.2	171.8 \pm 89.0
TC:T-BA (50:50)	164.8 \pm 5.7	156.6 \pm 52.1
TC:T-BA (90 10)	160.0 \pm 8.5	178.0 \pm 25.5
TC:DMI (50:50)	159.9 \pm 5.4	82.6 \pm 41.6
PG:OA (10:90)	140.2 \pm 19.0	70.2 \pm 18.1
PG:TC:DMI (50:25:25)	125.3 \pm 10.8	58.4 \pm 7.0
TC:PG:DMI (50:25:25)	120.9 \pm 9.2	34.1 \pm 6.8
TC:CCT (70:30)	120.9 \pm 11.2	47.0 \pm 21.5
TC:CCT:DMI (50:25:25)	120.14 \pm 6.6	47.3 \pm 22.4
TC:CCT (50:50)	119.9 \pm 11.9	62.3 \pm 16.6
TC:OSAL (70:30)	113.3 \pm 12.1	25.0 \pm 13.8
PG:DMI (70:30)	106.7 \pm 24.0	13.0 \pm 3.2
PG:DMI (50:50)	101.7 \pm 11.7	25.1 \pm 10.1
TC:PEG400 (50:50)	99.3 \pm 9.3	5.8 \pm 3.4
TC:PG (50:50)	97.5 \pm 13.2	28.2 \pm 13.7
PG:PEG6CCG (50:50)	96.7 \pm 11.2	6.7 \pm 1.8
PG:LA (50:50)	44.2 \pm 9.4	19.3 \pm 13.7

The permeation data for the 22 binary and ternary solvent systems obtained in the Skin PAMPA model were plotted against corresponding values for the porcine skin studies in Fig 4. 17. A correlation coefficient (R^2) of 0.72 was observed for the linear regression of the permeation data in porcine skin and PAMPA model. Considering the variability in porcine

skin, the correlation observed here warrants further development of PAMPA as a screening tool for human skin permeability.

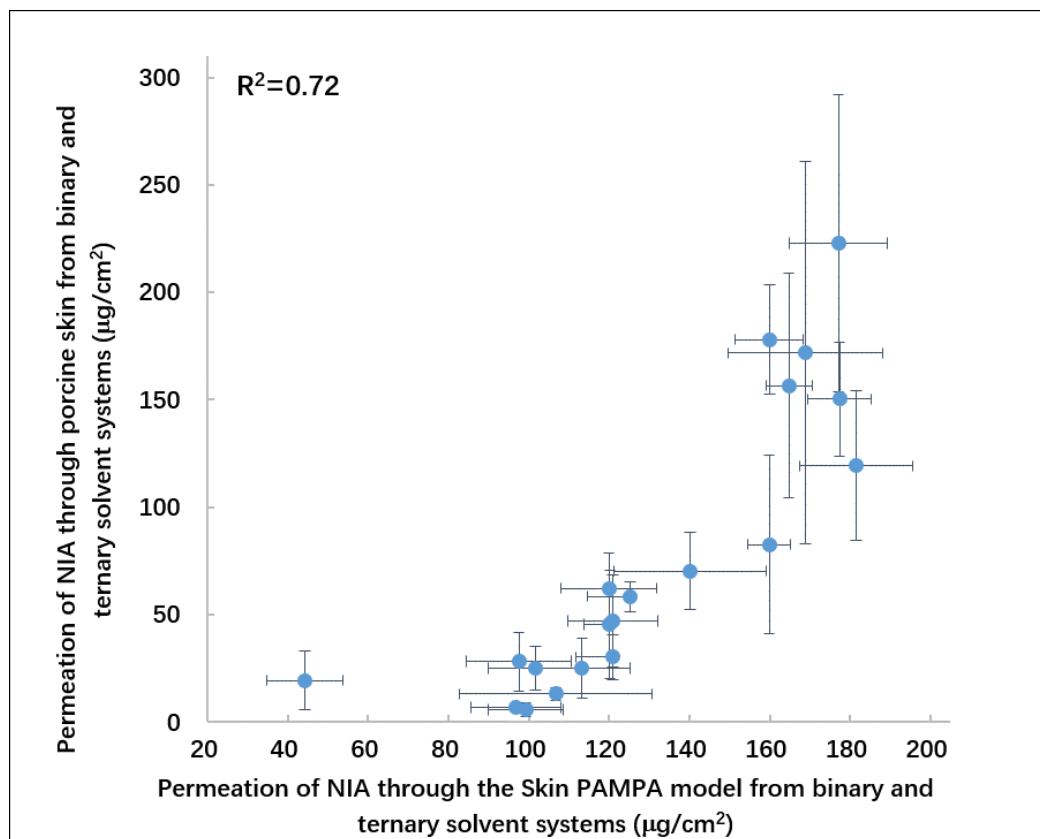


Figure 4. 17 Correlations between the cumulative amounts of NIA that permeated in porcine skin and the Skin PAMPA model from binary and ternary solvent systems.

4.3.3 Evaluations of binary and ternary systems for NIA in human skin

4.3.3.1 Binary vehicle systems composed of PG and other solvents

The permeation profiles of NIA are shown in Fig 4. 18. Higher permeation of NIA was evident from PG:LA and PG:OA compared to other binary formulations or neat PG ($p < 0.05$). At 24 h, the amounts of NIA that permeated from PG:LA (50:50) and PG:OA (10:90) were determined as 100.4 ± 2.4 and $93.3 \pm 7.1 \mu\text{g}/\text{cm}^2$, respectively. Statistical analysis confirmed that there was no significant difference observed between the permeation of NIA from PG:DMI (50:50), PG:TC (50:50) with neat PG ($P > 0.05$). At 24 h, the permeation of NIA

corresponded to 1-46 % of the applied amounts (Fig 4.19).

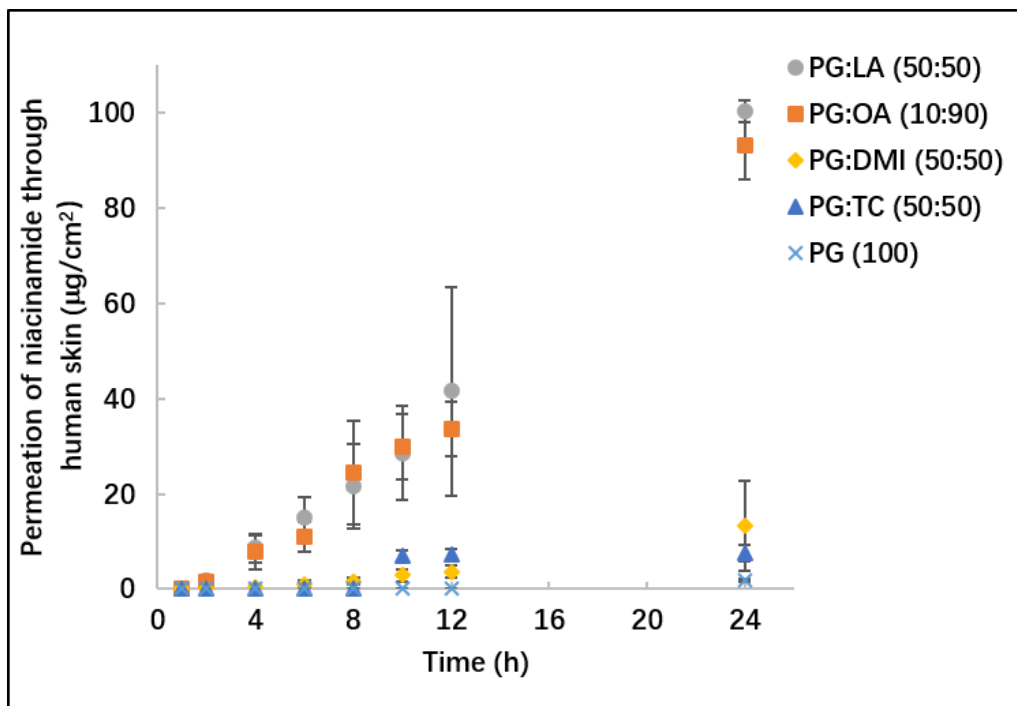


Figure 4. 18 Permeation profiles of NIA in human skin for the binary vehicles composed of PG with other solvents or neat PG (mean \pm SD, n=4).

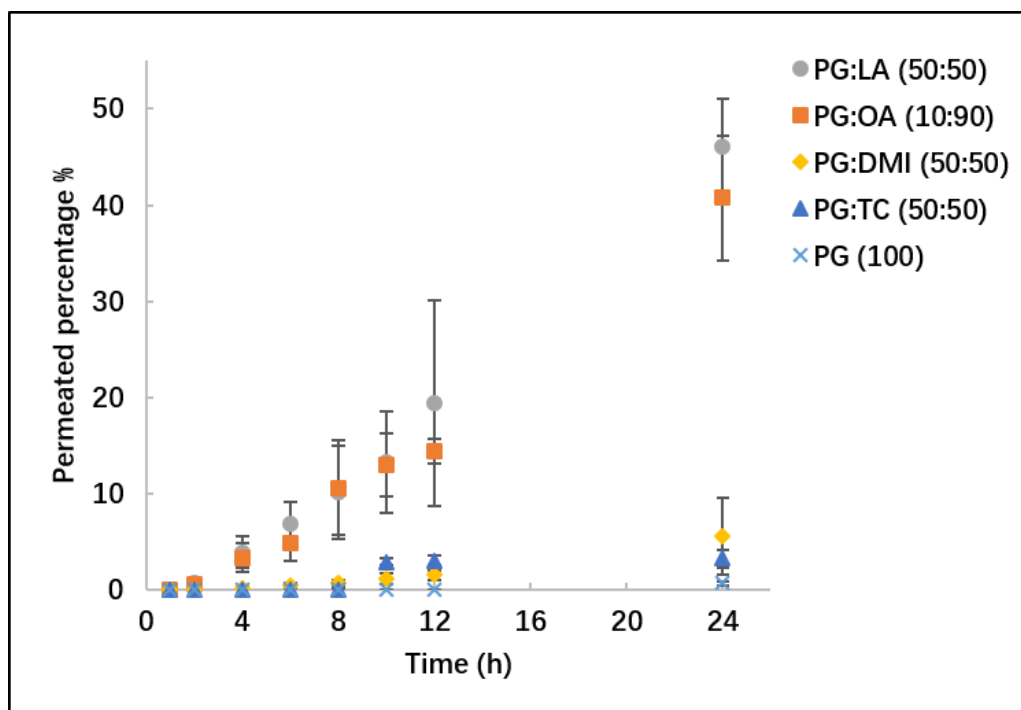


Figure 4. 19 Percentage permeation of NIA from the binary vehicles composed of PG with other solvents or neat PG (mean \pm SD, n=4).

Table 4.11 summarizes the mass balance results. After permeation studies, higher skin retention was evident for PG:TC (50:50) and PG:DMI (50:50) compared with PG:LA (50:50) ($p < 0.05$). The amount of NIA extracted from human epidermis for PG:TC (50:50) and PG:DMI (50:50) accounted for 29 and 17 % of applied NIA, respectively. The skin extraction values of NIA for PG:LA (50:50) and PG:OA (10:90) were 9.2 and 3.4 %, respectively. There was no significant difference between the percentage NIA extracted for single and binary systems ($p > 0.05$). The overall recoveries of NIA for PG:LA (50:50) was determined as 77 %. The low overall recoveries of NIA for those preparations could reflect the possible chemical derivatization of the molecule during skin penetration (Sil et al., 2018).

Table 4. 11 Mass balance results following NIA permeation in human skin for binary vehicle systems composed of PG and other solvents (n=4, mean \pm SD).

	PG:TC (50:50)	PG:OA (10:90)	PG:LA (50:50)	PG:DMI (50:50)	PG (100)
Washing %	69.8 \pm 7.8	37.7 \pm 6.7	27.1 \pm 5.6	59.6 \pm 7.1	92.3 \pm 7.4
Extraction %	29.0 \pm 18.5	9.2 \pm 0.6	3.4 \pm 2.0	17.4 \pm 3.9	12.1 \pm 8.3
Permeation %	4.4 \pm 2.3	40.7 \pm 6.5	46.1 \pm 5.1	5.6 \pm 4.0	0.7 \pm 0.2
Total recovery %	103.1 \pm 13.4	87.6 \pm 0.8	76.5 \pm 5.1	82.6 \pm 7.8	105.1 \pm 7.6

Fatty acids have been reported to enhance the skin penetration of a range of lipophilic and hydrophilic substances (Lane, 2013; Ng et al., 2015; van Zyl et al., 2016). Oleic acid (OA) is one of the most extensively studied penetration enhancers among the fatty acids (Oh et al., 2001; Mittal et al., 2009; van Zyl et al., 2016). Also, linolenic acid (LA), another cis C 18 unsaturated fatty acid has been reported to act as a skin penetration enhancer (Zhou et al., 2019). OA is generally recognized as safe (GRAS) and LA has been reported as safe by the Cosmetic Ingredient Review Expert Panel (CIRP) (CIRP, 2019). Both fatty acids are approved by the FDA as inactive ingredients and have been used extensively in topical and transdermal products worldwide (Carrara, 2001; Deng et al., 2012; Hille et al., 2017). OA is readily absorbed into the stratum corneum after administration. An electron spin resonance study showed that the influence of OA on skin permeability was related to the fluidization of intercellular lipids by the molecule (Gay et al., 1989). Recently, using solid-state nuclear magnetic resonance (NMR), Pham et al. (2016) concluded that OA leads an increased mobility in both stratum corneum protein components and the cholesterol chain segments

in the stratum corneum intercellular lipid domain. Human/porcine skin studies are lacking on explaining the precise mechanisms as penetration enhancers.

The positive synergy between fatty acids and PG was evident in this study. The synergistic effect of fatty acids and alcohols has been reported previously (Cooper, 1984; Ibrahim and Li, 2010). The exact mechanism of synergic mechanism remains unclear. It could be hypothesized that the fatty acid first penetrates into the stratum corneum and contributes to increased lipid fluidity which allows more diffusion of PG with dissolved NIA. The binary solvent systems of PG:OA (10:90) and PG:LA (50:50) resulted in the maximum skin penetration enhancement of NIA compared to other binary systems tested in human skin. Therefore, those two binary solvent systems were chosen for the *in vivo* NIA permeation studies using healthy volunteers.

4.3.3.2 Binary systems composed of TC/T-BA and other solvents

Fig 4.20 shows the permeation profiles of NIA from the binary systems composed of TC and T-BA with other solvents. PG or TC was combined with T-BA, at a ratio of PG: T-BA (90:10, v/v). At 24 h, no enhancement was observed for the permeation for the binary vehicle systems composed of T-BA and PG/TC compared to T-BA applied as a neat solvent ($P>0.05$). There was no increase in NIA percutaneous delivery from the mixture of TC:DMI (50:50) and TC:PEG 400 (50:50) compared to TC alone ($P>0.05$).

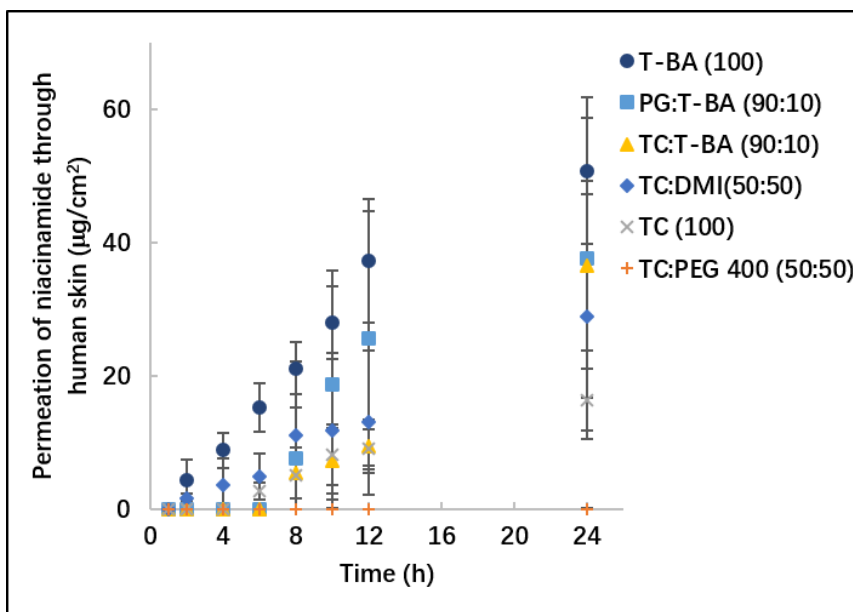


Figure 4. 20 Permeation profiles of NIA in human skin for binary vehicles composed of TC or T-BA with other solvents or neat TC or T-BA (mean \pm SD, n=4).

Fig 4.21 shows the percentage permeation of NIA and Table 4.12 shows the distribution of NIA following the permeation studies. At 24 h, the permeation of NIA from binary systems accounted for 0.02 to 15.6 % of applied amounts. The skin retention percentage values for the four binary formulations accounted for 17 – 35 % of applied amounts. No significant difference was observed comparing the skin extraction percentage values for the four binary systems to the neat T-BA or neat TC ($p > 0.05$).

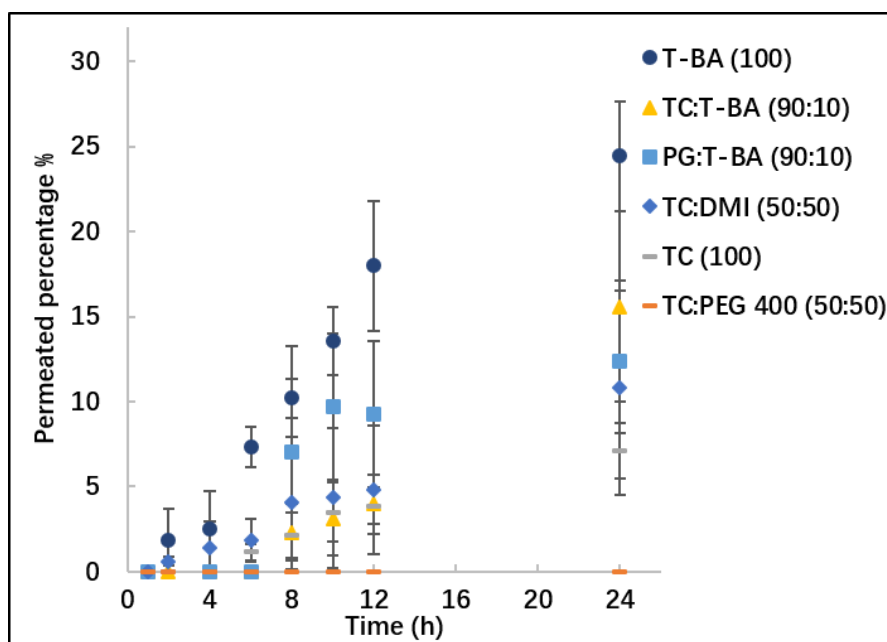


Figure 4. 21 Percentage permeation of NIA in human skin for binary vehicles composed of TC/T-BA with other solvents or neat TC/T-BA (mean \pm SD, n=4).

Table 4. 12 Mass balance results following the permeation studies for NIA binary systems composed of volatile alcohol/TC or neat solvents. (n=4, mean \pm SD).

	TC:T-BA (90:10)	PG:T-BA (90:10)	TC:DMI (50:50)	TC:PEG400 (50:50)	TC (100)	T-BA (100)
Washing %	39.8 \pm 16.5	52.8 \pm 9.0	59.3 \pm 11.7	72.1 \pm 11.9	42.8 \pm 2.2	30.4 \pm 3.7
Extraction %	34.7 \pm 10.5	20.1 \pm 6.0	17.0 \pm 5.3	28.8 \pm 2.9	32.9 \pm 11.2	25.8 \pm 4.3
Permeation %	15.6 \pm 5.6	12.3 \pm 4.2	10.8 \pm 6.3	0.02 \pm 0.01	7.1 \pm 1.6	24.4 \pm 3.2
Total recovery %	90.1 \pm 5.2	85.2 \pm 10.9	87.1 \pm 7.8	100.9 \pm 9.7	82.8 \pm 12.2	80.6 \pm 5.7

4.3.3.3 Ternary vehicle systems of NIA

Three ternary solvent systems of NIA were assessed using human skin. Fig 4.22 shows the permeation profiles. At 24 h, higher permeation was evident for the mixture of TC:CCT:DMI (50:25:25) ($34.1 \pm 7.3 \mu\text{g}/\text{cm}^2$) compared to TC:PG:DMI (50:25:25) and PG:TC:DMI (50:25:25) ($p < 0.05$). The cumulative permeated amounts accounted for 6 – 13 % of dosed NIA (Fig 4.23).

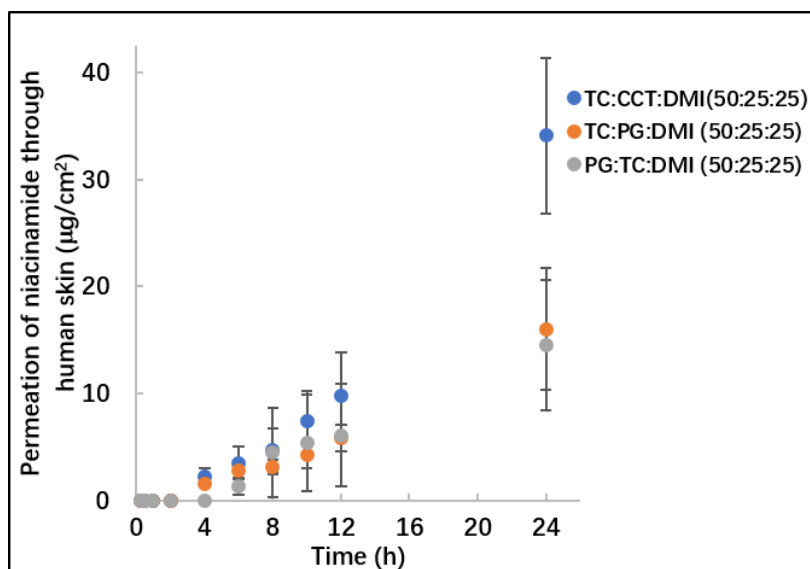


Figure 4. 22 Permeation profiles of NIA from ternary solvent systems in human skin (mean \pm SD, n=4).

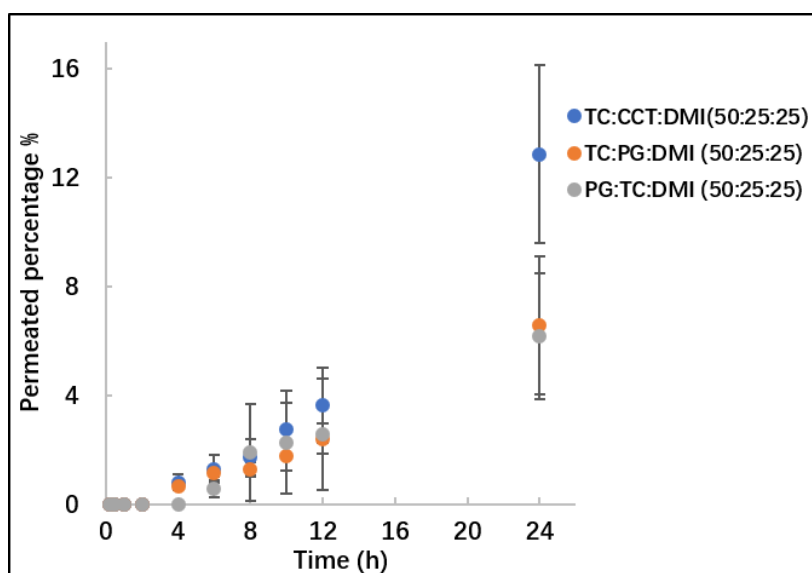


Figure 4. 23 Percentage permeation of NIA from ternary solvent systems in human skin (mean \pm SD, n=4).

As for the mass balance studies, half of the dosed substance was delivered into/through human skin from TC:CCT:DMI (50:25:25) (Table 4.13). The skin retention and percentage permeation were determined as 29.7 ± 4.9 and 12.9 ± 3.3 %, respectively. Comparing the skin extraction percentage values of TC:CCT:DMI (50:25:25) to TC:DMI (50:50), the skin retention was increased with the presence of CCT ($p < 0.05$). This improvement of skin uptake was consistent with the results obtained in porcine skin studies (Session C.4.3.3.4). However, the two ternary solvent systems of TC-PG-DMI did not increase human skin

extraction or permeation compared to the binary systems ($p>0.05$).

Table 4. 13 Mass balance results following the permeation studies for NIA ternary solvent systems ($n=4$, mean \pm SD).

	TC:CCT:DMI (50:25:25)	TC:PG:DMI (50:25:25)	PG:TC:DMI (50:25:25)
Washing %	44.9 \pm 6.0	66.5 \pm 9.1	64.6 \pm 4.5
Extraction %	29.7 \pm 4.9	14.6 \pm 3.4	12.2 \pm 2.0
Permeation %	12.9 \pm 3.3	6.6 \pm 2.5	6.2 \pm 2.3
Total recovery %	87.5 \pm 4.9	87.8 \pm 6.7	83.0 \pm 4.2

4.3.3.4 Comparisons of NIA binary and ternary vehicle formulations in the Skin PAMPA model and human skin

Table 4.14 summarizes the data for binary and ternary vehicle systems obtained in human skin and the Skin PAMPA models. The cumulative permeated amounts of NIA in human skin ranged from 0.1 to 100.4 $\mu\text{g}/\text{cm}^2$; the corresponding values obtained in PAMPA were 44.2 - 177.4 $\mu\text{g}/\text{cm}^2$. For the majority of tested formulations, the artificial membrane is more permeable than human skin. However, there were some exceptions observed. Propylene glycol and linolenic acid, PG:LA (50:50), was determined as the most efficient system in human skin ($p<0.05$). However, the permeation of NIA from PG:LA (50:50) was significantly lower compared with other formulations assessed in the Skin PAMPA studies ($p<0.05$). For PG:LA (50:50), the cumulative amounts permeated in human skin were significantly higher than the Skin PAMPA model ($p<0.05$). Both OA and LA are unsaturated C_{18} fatty acids and they have a double bond in the conformation (Small, 1984; Ibrahim and Li, 2010). It is possible that OA and LA integrated into the PAMPA membrane and modified the lateral chain packing in the lipid matrix. This may lead to changes in the physicochemical properties and influence the permeability of this artificial membrane subsequently. It is hypothesized that the Skin PAMPA model is not suitable for screening formulations containing fatty acids.

Table 4. 14 Cumulative permeation of NIA in human skin and the Skin PAMPA model from binary and ternary solvent systems (mean \pm SD, $4 \leq n \leq 5$).

Binary and ternary solvent systems	Cumulative permeated amounts of NIA ($\mu\text{g}/\text{cm}^2$)	
	The Skin PAMPA model	Human skin
PG:T-BA(90:10)	177.4 \pm 7.9	37.7 \pm 21.1
TC:T-BA (90:10)	160.0 \pm 8.5	36.6 \pm 12.8
TC:DMI (50:50)	159.9 \pm 5.4	28.9 \pm 18.4
PG:OA (10:90)	140.2 \pm 19.0	93.3 \pm 7.1
PG:TC:DMI (50:25:25)	125.3 \pm 10.8	14.5 \pm 6.1
TC:PG:DMI (50:25:25)	120.9 \pm 9.2	16.0 \pm 5.7
TC:CCT:DMI (50:25:20)	120.1 \pm 6.5	34.1 \pm 7.3
PG:DMI(50:50)	101.7 \pm 11.7	13.2 \pm 9.5
TC:PEG400 (50:50)	99.3 \pm 9.3	0.1 \pm 0.02
PG:TC (50:50)	97.5 \pm 13.2	7.7 \pm 1.7
PG:LA (50:50)	44.2 \pm 9.4	100.4 \pm 2.4

Excluding the results of PG:LA (50:50) and PG:OA (10:90), the cumulative permeation of NIA from tested binary and ternary vehicle systems in through human skin was plotted against the corresponding results obtained in the Skin PAMPA studies (Fig 4.24). A correlation coefficient (R^2) of 0.71 was observed for the linear regression of human skin and the Skin PAMPA model. The lower permeation of binary solvent systems composed of propylene glycol and the fatty acid, LA, may reflect interaction of the lipid components with those formulations. Further studies are needed to probe this theory.

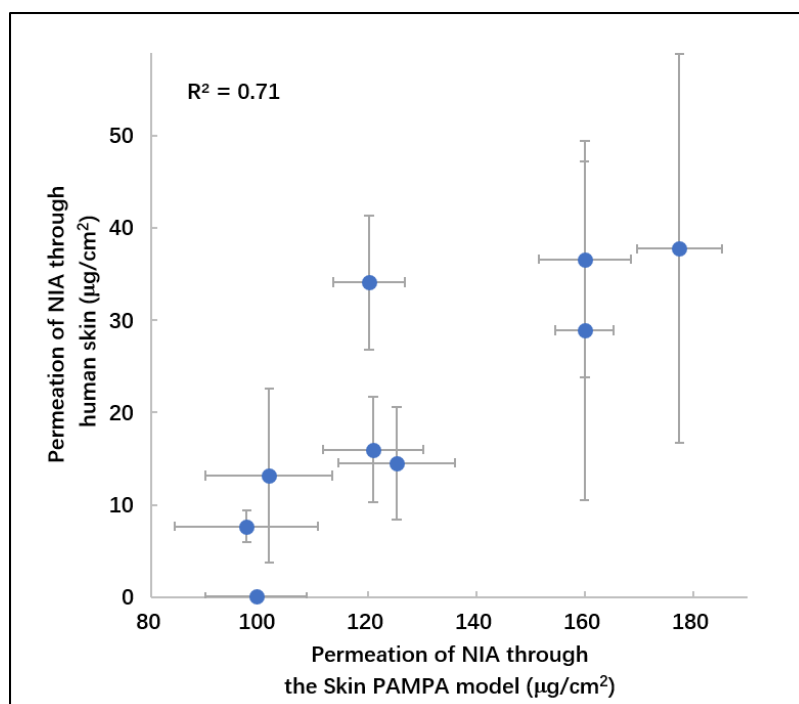


Figure 4. 24 Correlations between the cumulative amounts of NIA that permeated through human skin and the Skin PAMPA model from binary and ternary solvent systems (mean \pm SD, $4 \leq n \leq 5$).

4.4 Conclusions

Previous work investigated the permeation behavior of NIA from a series of neat solvents. In the present work, the influence of a combination of binary or ternary components on *in vitro* permeation of NIA was assessed. Positive synergistic effects were evident for the combinations of PG and fatty acids (OA, LA) on NIA skin delivery. Combining CCT, TC and DMI prepared the most efficient ternary solvent system for NIA dermal delivery.

The permeation data obtained in mammalian skin were compared with the Skin PAMPA studies. It was noticeable that the permeability of this artificial model highly depends on the physicochemical properties of the permeant and the excipients in the formulations. The Skin PAMPA model demonstrated potential for *in vitro* screening of NIA formulations composed of single, binary or ternary solvent substances. However, several excipients (fatty acids, PEGs) were also identified as not suitable for this artificial screening model in the NIA studies. The possible interactions between the lipid composition and the formulations excipients should be explored further.

Based on the results obtained in the studies, two single solvent systems, PG and TC, two binary solvent systems and one ternary solvent systems were selected to be taken forward to

in vivo permeation experiments.

Chapter 5.

In vitro evaluation of PR from binary and ternary solvent systems

5.1 Introduction

It has been suggested that solvent effects play crucial roles in strategies for skin penetration enhancement (Lane, 2013; Hadgraft and Lane, 2016; Pham et al., 2016). Dias et al. (2007a) investigated the effects of vehicles on dermal delivery of caffeine, benzoic acid and salicylic acid. The authors reported that the permeation of the actives from tested saturated solutions was significantly enhanced by the vehicle chosen. More recently, Haque et al. (2017b) investigated the percutaneous absorption of a potent cytotoxic agent, anthramycin (ANT), from a range of single solvents using heat separated human epidermis. The authors monitored the skin penetration of both the active and solvents. A clear dependence of ANT permeation on the amounts of solvents that penetrated was established. A number of publications have also reported the increased dermal delivery of actives by combining different solvents and/or skin penetration enhancers (Oliveira et al., 2012; Santos et al., 2012; Hirata et al., 2013; Mohammed et al., 2014b).

Earlier, the systematic characterization of the physicochemical properties of PR and permeation assessment of PR from a series of neat solvents were reported. The permeation studies of PR were conducted in porcine skin and heat separated human epidermis using a range of vehicles and skin penetration enhancers commonly used for dermal delivery. The permeation and skin extraction of PR were determined for neat OSaI, PG, DMI, IPM, TC and glycerol in human skin. Skin PAMPA studies were also performed and the corresponding correlation coefficient (R^2) was determined as 0.71 for human skin under finite dose conditions. DMI, PG and TC are solvents that have a broad range of physicochemical properties. It was also confirmed that PR has good solubility in these neat vehicles. In this chapter, several binary and ternary systems composed of DMI or PG or TC and other solvents were prepared. Following miscibility studies, the binary and ternary systems were taken forward to permeation studies using the Skin PAMPA model, porcine skin and human skin. Accordingly, the primary objective of this chapter was to investigate the effect of vehicle combinations on the percutaneous permeation of PR and to identify the optimal systems for *in vivo* evaluations. To further understand the potential of the Skin PAMPA model on prediction of human skin permeability, any correlation between the permeation of PR in the

artificial model and mammalian skin was also investigated.

5.2 Materials and methods

5.2.1 Materials

PR (Symrise, Holzminden, Germany) was a gift from pION Inc. Billerica, USA. Analytically pure standards of BG, PG, T-BA, OA, OSal and LA were purchased from Sigma-Aldrich (UK). IPM and DMI were gifts from Croda Ltd (UK). PEG 400 was obtained from Fisher Scientific (UK). PEG-6-CCG was a gift from Avon, USA. TC and CCT were received from Gattefossé (France).

5.2.2 Methods

5.2.2.1 Evaluation of binary vehicle formulations of PR using the Skin PAMPA model

Following miscibility and stability studies, ten binary systems of PR were examined using the Skin PAMPA model following the procedure described previously (Session C.3.2.3.8). For the present work, the binary vehicle formulations containing 1 % w/v of PR and the other components are summarized in Table 5.1.

Table 5. 1 PR binary solvent systems assessed in the Skin PAMPA model

PR binary solvent systems	
PG:DMI (50:50)	TC:OSal (30:70)
PG:TC (50:50)	TC:IPM (50:50)
PG:IPM (50:50)	DMI:TC (50:50)
PG:LA (50:50)	DMI:CCT (50:50)
PG:OA (10:90)	DMI:OSal (10:90)

5.2.2.2 Evaluation of binary formulations of PR in porcine skin

The same ten formulations (Table 5.1) as evaluated in the Skin PMAPA model were taken forward for porcine skin studies. Permeation studies were performed under finite dose conditions (5 $\mu\text{L}/\text{cm}^2$).

5.2.2.3 Evaluation of binary vehicle formulations of PR in human skin

1 % w/v PR in DMI:PG (50:50), DMI:TC (50:50), IPM:TC (50:50), OSaI:TC (50:50) and PG:TC (50:50) systems were prepared and assessed using heat separated human epidermis under finite dose conditions ($5 \mu\text{L}/\text{cm}^2$).

5.2.2.4 Evaluation of ternary vehicle formulations of PR using the Skin PAMPA model and mammalian skin

Three ternary vehicle systems containing 1 % w/v of PR were prepared, namely PG:TC:IPM (50:25:25), TC:PG:IPM (50:25:25) and IPM:TC:PG (50:25:25). Permeation studies were performed using the Skin PAMPA model and mammalian skin following the application of 3 and $5 \mu\text{L}/\text{cm}^2$ amounts of formulation respectively.

5.3 Results and discussion

5.3.1 Evaluation of PR in the Skin PAMPA model

5.3.2.1 Binary systems of PR composed of PG and other solvents

The permeation behavior of PR from five binary systems composed of PG and other solvents was prepared and screened in the Skin PAMPA model. At 2.5 h, the amounts of PR that permeated in the Skin PAMPA model ranged from $13\text{--}39 \mu\text{g}/\text{cm}^2$ (Fig 5.1). Higher amounts of PR were delivered from PG:IPM (50:50) ($39.0 \pm 2.8 \mu\text{g}/\text{cm}^2$) compared to the binary PG-OA and PG-LA systems ($p < 0.05$). The cumulative amounts of PR that permeated from PG:OA (10:90) and PG:LA (50:50) were determined as 15.9 ± 4.2 and $13.3 \pm 2.4 \mu\text{g}/\text{cm}^2$, respectively. The permeation of PR from neat PG was determined as $36.8 \mu\text{g}/\text{cm}^2$ (Session C.3.3.9). PR permeation from PG:LA (50:50) and PG:OA (10:90) was significantly lower than permeation from neat PG ($p < 0.05$). As shown in Fig 5.2, the percentage permeation of PR for PG:OA (10:90) and PG:LA (50:50) accounted for 48 and 40 % of the applied PR, respectively. The percentage permeation values of PR in PG:LA (50:50) and PG:OA (10:90) were significantly lower compared with PG:IPM (50:50), PG:TC (50:50) and PG:DMI (50:50)

($p < 0.05$).

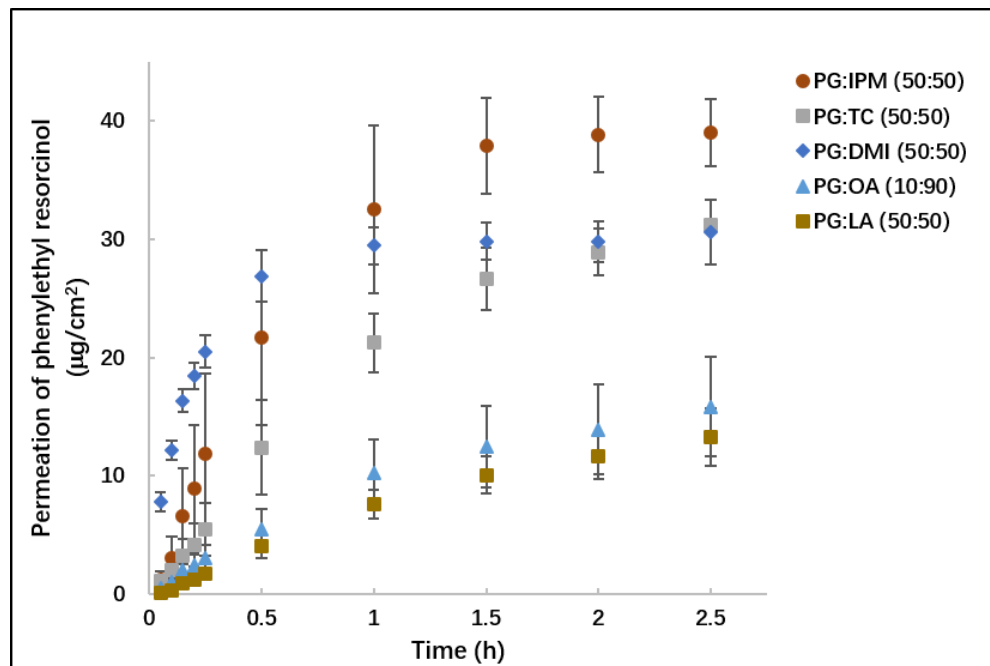


Figure 5. 1 The permeation profiles of PR from binary systems composed of PG and other solvents in the Skin PAMPA model (mean \pm SD, $n=5$).

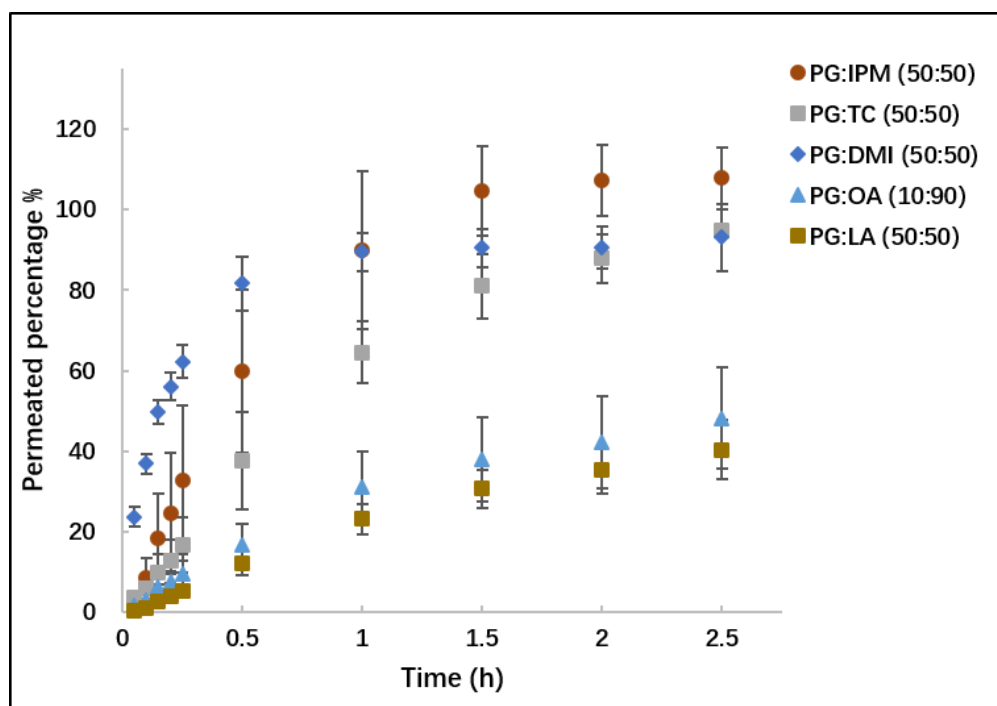


Figure 5. 2 Percentage permeation of PR from binary systems composed of PG and other solvents in the Skin PAMPA model (mean \pm SD, $n=5$).

5.3.3.2 Binary systems of PR composed of TC or DMI and other solvents

Subsequently, the permeation of PR from five binary systems composed of DMI or TC with other solvents was evaluated in the Skin PAMPA model under finite dose conditions. At 2.5 h, the permeation ranged from 22.4 to 36.6 $\mu\text{g}/\text{cm}^2$. The permeation of PR in TC:OSal (30:70) ($36.6 \pm 1.9 \mu\text{g}/\text{cm}^2$) was significantly higher than the amounts observed for PR in TC:IPM (50:50) ($22.4 \pm 3.4 \mu\text{g}/\text{cm}^2$) ($p < 0.05$). Compared with the permeation observed for neat DMI, PR permeation in the Skin PAMPA model did not increase by combining DMI with other solvents ($p > 0.05$). The percentage permeation profiles are shown in Fig 5.4. The amounts of PR delivered through the Skin PAMPA membrane accounted for $> 68 \%$ of applied amounts.

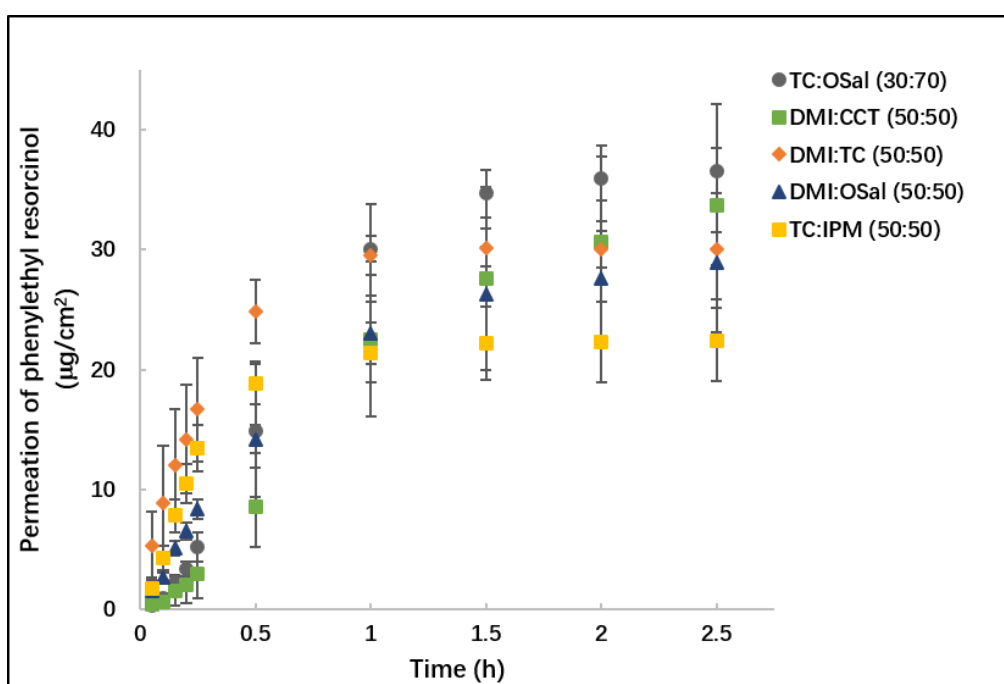


Figure 5. 3 The permeation profiles of PR from the binary systems composed of TC or DMI with other solvents in the Skin PAMPA model (mean \pm SD, $n=5$).

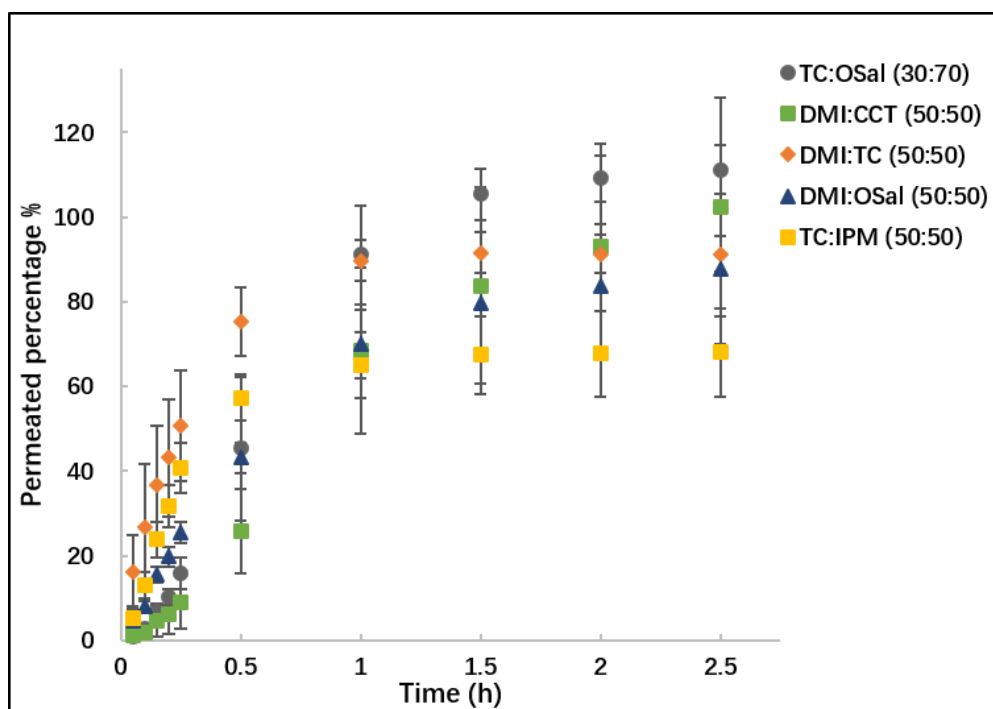


Figure 5. 4 Percentage permeation of PR from the binary systems composed of TC or DMI with other solvents in the Skin PAMPA model (mean \pm SD, n=5).

5.3.3.2 Ternary systems of PR composed of TC, PG and IPM

Fig 5.5 shows the permeation behavior of PR from ternary systems in the Skin PAMPA studies. PG, TC and DMI were combined in varying ratios to prepare the formulations. At 2.5 h, the cumulative amounts of PR that permeated ranged from 27 to 29 $\mu\text{g}/\text{cm}^2$ ($p>0.05$), accounting for 83 to 87 % of applied dose. The ternary solvent systems did not promote permeation enhancement compared with the binary or single system ($p>0.05$). The percentage permeation profiles are shown in Fig 5.6. For the three assessed ternary systems, at 2.5 h, > 82 % of applied PR was delivered through the Skin PAMPA model. The systems were subsequently tested in full thickness porcine skin.

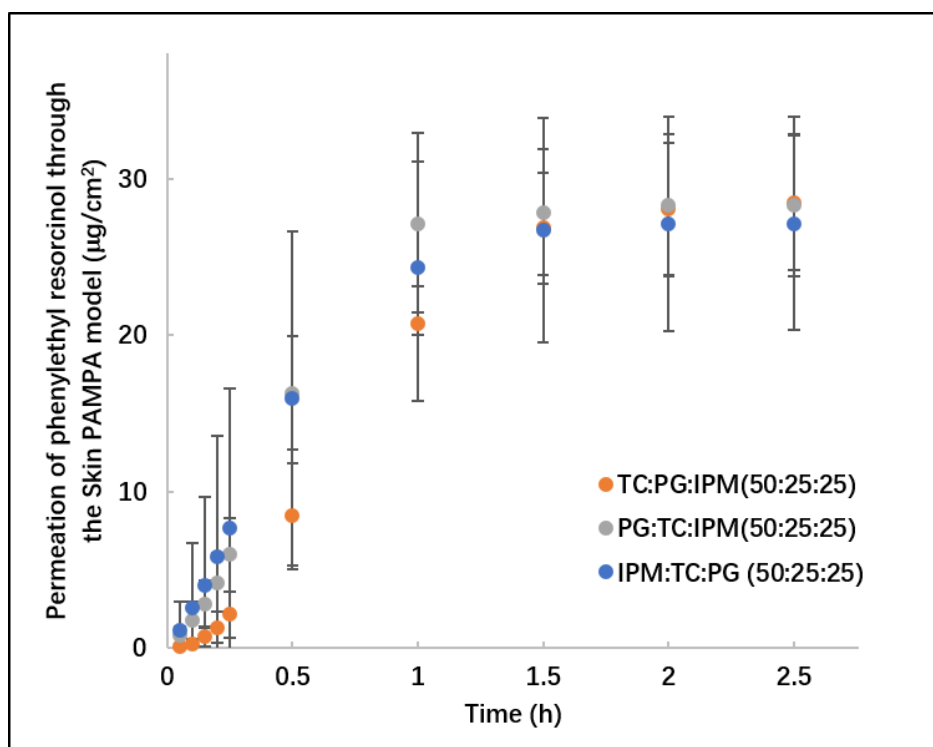


Figure 5. 5 Permeation profiles of PR from ternary systems composed of TC, PG and IPM in the Skin PAMPA model (mean \pm SD, n=5).

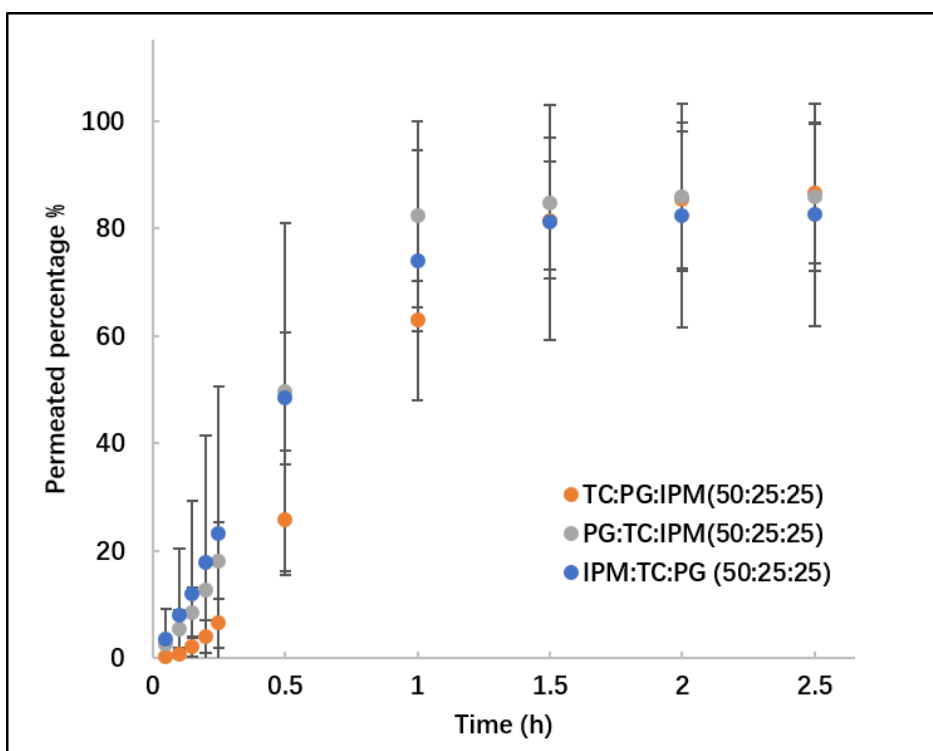


Figure 5. 6 Percentage permeation of PR from ternary vehicle systems composed of TC, PG and IPM in the Skin PAMPA model (mean \pm SD, n=5).

5.3.2 Evaluation of PR in porcine skin

5.3.2.1 Binary systems of PR composed of PG and other solvents

The permeation profiles of PR from binary systems composed of PG and other solvents are shown in Fig 5.7. Higher permeation of PR was observed for PG:IPM (50:50) ($9.8 \pm 3.3 \mu\text{g}/\text{cm}^2$) compared to other systems ($p < 0.05$). The cumulative permeated amount of PR for PG:TC (50:50) was $4.2 \pm 0.3 \mu\text{g}/\text{cm}^2$ and this value was significantly higher than for PG:LA (50:50), PG:OA (10:90) and PG:IPM (50:50) ($p < 0.05$). As illustrated in Fig 5.8, at 2.5 h, the percutaneous absorption ranged from 2.6 to 17.7 % of applied dose. No difference was observed comparing the percentage permeation values of PR for all assessed PG binary systems ($p > 0.05$).

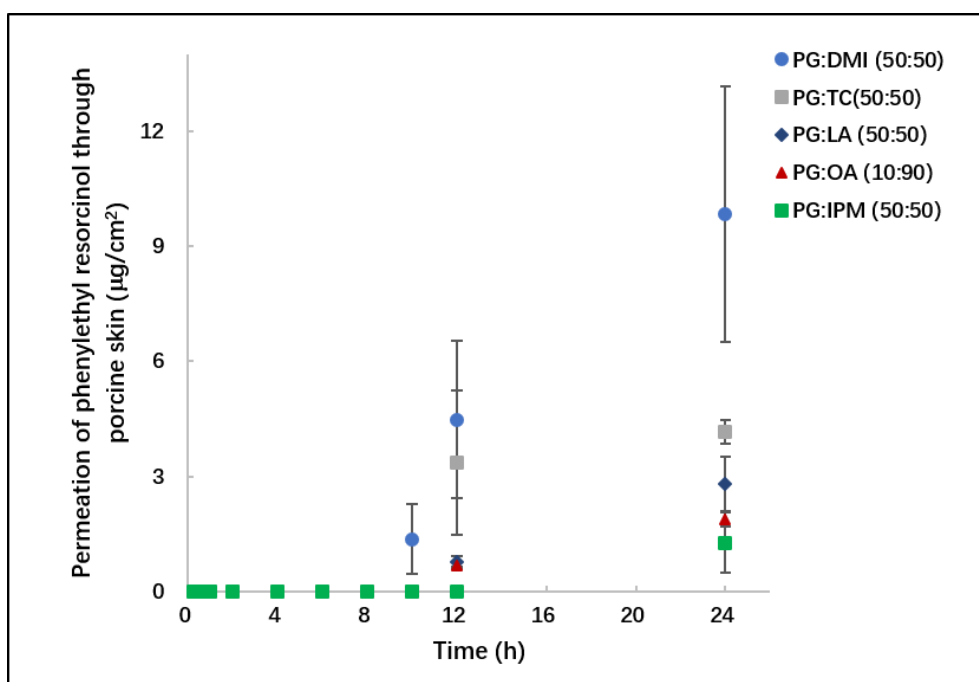


Figure 5. 7 The permeation profiles of PR from binary systems composed of PG and other solvents in porcine skin (mean \pm SD, $n=4$).

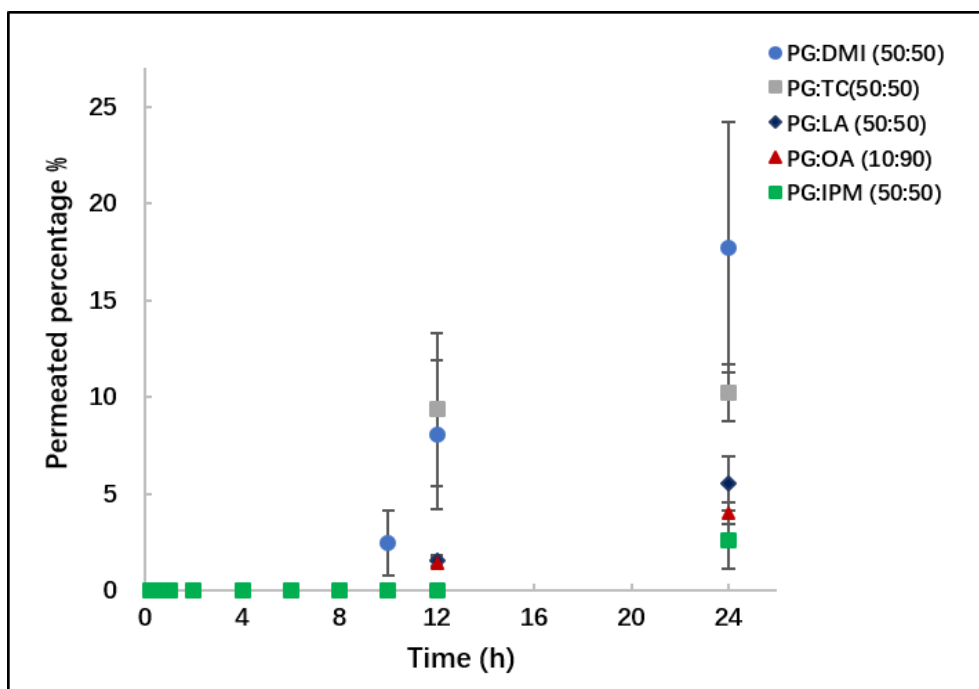


Figure 5. 8 Percentage permeation of PR from binary systems composed of PG and other solvents in porcine skin (mean \pm SD, n=4).

Mass balance studies were performed to examine the distribution of the permeant and results are summarized in Table 5.2. The highest skin extraction of PR was evident for PG:IPM (50:50), 70.1 %, among all tested binary systems ($p < 0.05$). Skin extraction percentage values of PR for PG:IPM (50:50) were comparable with the results observed for neat PG (57.7 %) and neat IPM (48.9 %) ($p > 0.05$).

Table 5. 2 Mass balance results following the permeation studies of PR in binary systems composed of PG and other solvents in porcine skin. (n=4, mean \pm SD).

	PG:IPM (50:50)	PG:TC(50:50)	PG:DMI (50:50)	PG:LA (50:50)	PG:OA (10:90)
Washing %	32.2 \pm 13.2	55.0 \pm 2.4	49.5 \pm 11.9	59.2 \pm 11.5	60.0 \pm 8.1
Extraction %	70.1 \pm 14.9	21.8 \pm 5.4	18.6 \pm 1.6	23.7 \pm 3.8	21.3 \pm 5.1
Permeation %	2.6 \pm 1.5	10.2 \pm 1.5	17.7 \pm 6.5	5.5 \pm 1.4	4.0 \pm 0.6
Total recovery %	104.9 \pm 2.7	87.0 \pm 6.0	85.8 \pm 7.4	88.4 \pm 9.8	85.3 \pm 5.6

5.3.2.2 Binary systems of PR composed of TC or DMI and other solvents

The five PR binary systems combining TC or DMI with other solvents were prepared and evaluated in full-thickness porcine skin. Fig 5.9 shows the permeation profiles. At 24 h, the cumulative permeated amount of PR for TC:IPM (50:50) was determined as 19.5 \pm 6.4

$\mu\text{g}/\text{cm}^2$. This value was higher than the permeation observed for PR in neat TC ($p < 0.05$), but not different from PR in neat IPM ($p > 0.05$). Lower permeation of PR was evident for DMI:CCT (50:50) compared to TC:IPM (50:50), and the cumulative permeation of PR for DMI:CCT (50:50) was $1.0 \pm 0.5 \mu\text{g}/\text{cm}^2$ ($p < 0.05$). The percentage permeation profiles are shown in Figure 5.10. At 24 h, the percentage permeation ranged from 2.4 to 38.3 % of applied amounts. It was evident that TC:IPM (50:50) delivered higher percentages of applied active through porcine skin compared with PR in neat IPM or neat TC ($p < 0.05$).

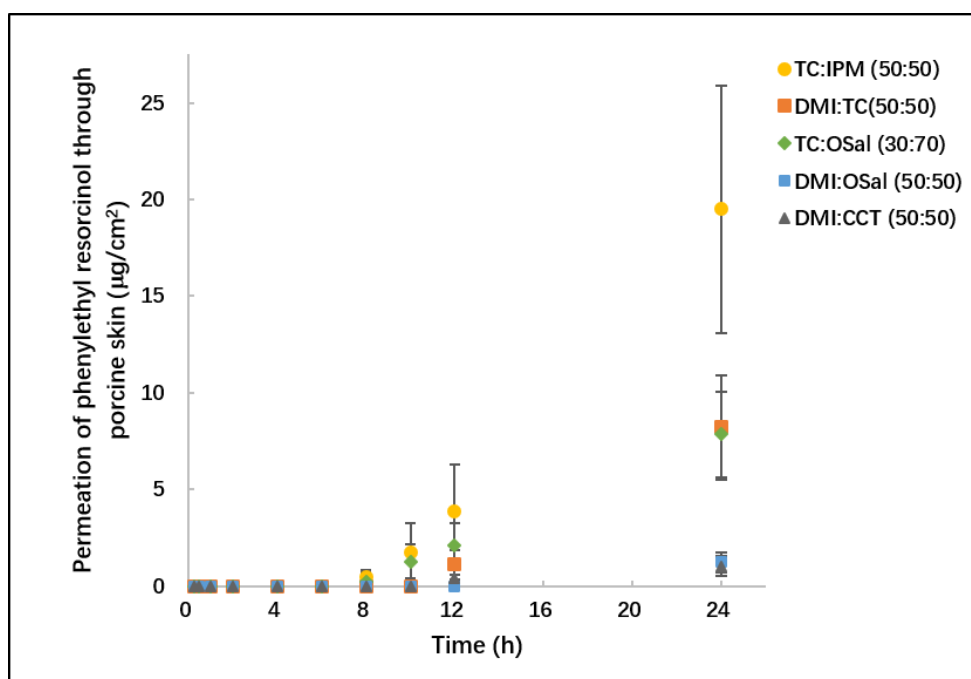


Figure 5. 9 The permeation profiles of PR from binary systems composed of TC or DMI and other solvents in porcine skin (mean \pm SD, $n=4$).

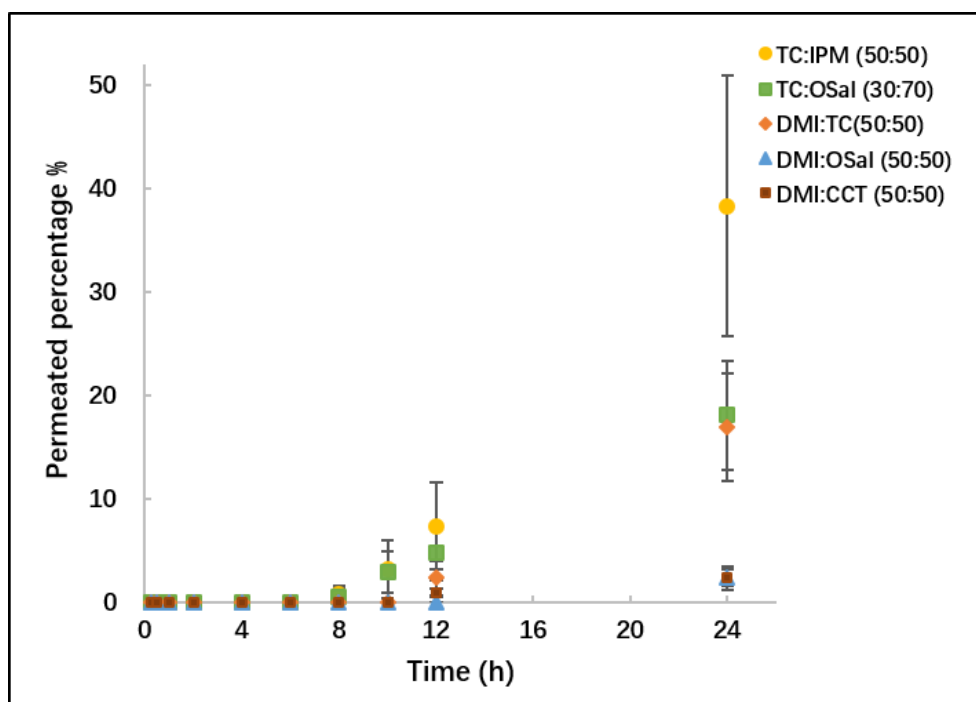


Figure 5. 10 Percentage permeation of PR from binary systems composed of TC or DMI and other solvents in porcine skin (mean \pm SD, n=4)

The results from mass balance studies are summarized in Table 5.3. For TC:IPM (50:50) and TC:OSal (30:70), less than half of the applied doses were recovered from the skin surface. Higher skin extraction percentage values were evident for PR in TC:OSal (30:70), TC:IPM (50:50) and DMI:OSal (50:50) compared with DMI:TC (50:50) and DMI:CCT (50:50) ($p < 0.05$). The skin extraction percentage value of TC:IPM (50:50) was comparable with value observed for neat IPM and neat TC ($p > 0.05$).

Table 5. 3 Mass balance results following the permeation studies of PR in binary systems composed of TC and other solvents in porcine skin. (n=4, mean \pm SD).

	TC:IPM(50:50)	TC:OSal(30:70)	DMI:OSal (50:50)	DMI:CCT (50:50)	DMI:TC(50:50)
Washing %	13.4 \pm 13.0	27.5 \pm 5.9	48.4 \pm 10.5	69.9 \pm 5.1	54.8 \pm 10.0
Extraction %	39.3 \pm 13.6	43.4 \pm 8.1	37.0 \pm 6.1	14.7 \pm 6.8	15.3 \pm 3.8
Permeation %	38.3 \pm 12.6	18.1 \pm 5.2	2.4 \pm 0.8	2.4 \pm 1.1	16.9 \pm 5.2
Total recovery %	91.0 \pm 6.1	89.1 \pm 10.3	87.7 \pm 8.1	86.9 \pm 9.8	87.1 \pm 5.2

5.3.2.3 Ternary systems of PR composed of TC, PG and IPM

The permeation of PR was quantified for three ternary systems in porcine skin. Fig 5.11 shows the profiles of the three ternary systems composed of PG, TC and IPM. At 24 h, the

cumulative amounts of PR delivered through porcine skin ranged from 4.7 to 10.6 $\mu\text{g}/\text{cm}^2$. Higher permeation of PR was evident for PG:TC:IPM (50:25:25) compared with IPM:TC:PG (50:25:25) ($p<0.05$). PG:TC:IPM (50:25:25) significantly increased the percutaneous absorption of PR compared with PG:IPM (50:50) ($p<0.05$). The percentage permeation of PR ranged from 9.5 to 20.5 % (Fig 5.12). No statistical difference was evident comparing the percentage permeation values for the three ternary systems ($p>0.05$).

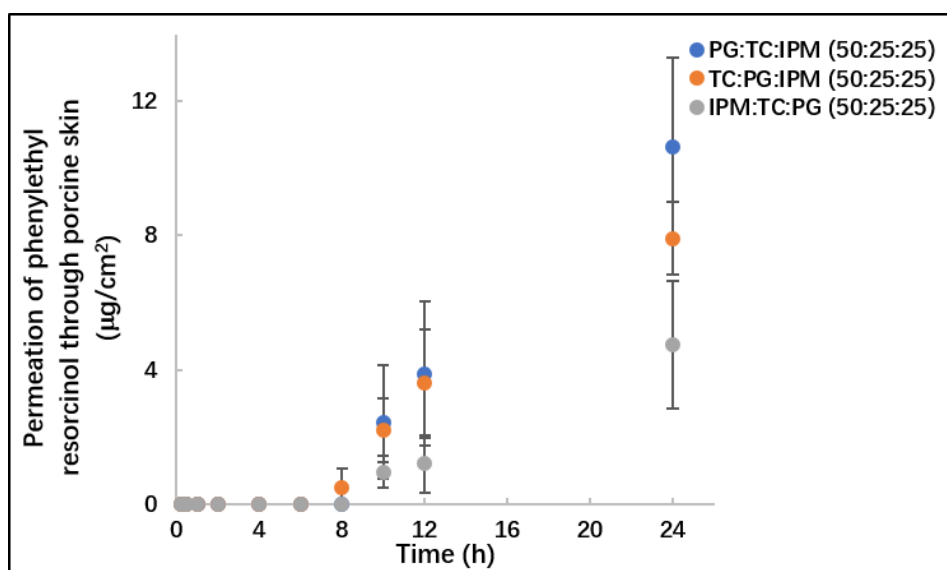


Figure 5. 11 Permeation profiles of PR from ternary systems in porcine skin (mean \pm SD, $n=4$).

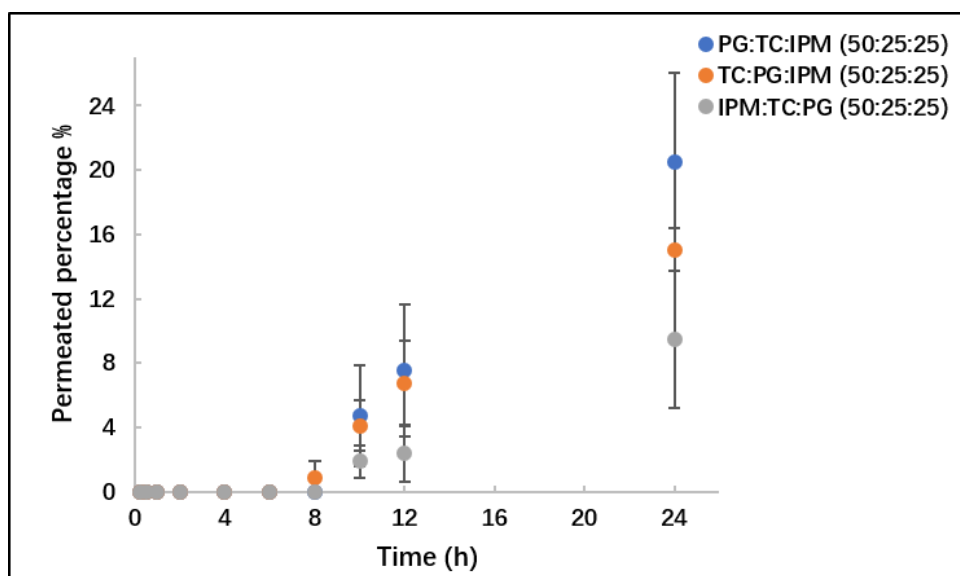


Figure 5. 12 Percentage permeation of PR from ternary systems in porcine skin (mean \pm SD, $n=4$).

Table 5.4 summarizes the distribution of the active determined in mass balance studies.

For the three assessed systems, no difference was evident comparing the percentage values recovered from the skin surface ($p>0.05$). ~ 40 % of the applied PR remained in the skin membrane after the permeation studies. No difference was detected among the three formulations ($p>0.05$). The ternary systems did not increase the skin retention of PR compared to the binary or single systems ($p>0.05$).

Table 5. 4 Mass balance results following the permeation studies of ternary systems of PR in porcine skin. (n=4, mean \pm SD).

	PG:TC:IPM (50:25:25)	TC:PG:IPM (50:25:25)	IPM:TC:PG (50:25:25)
Washing %	29.1 \pm 6.5	36.5 \pm 9.3	38.8 \pm 8.7
Extraction %	38.2 \pm 7.2	41.9 \pm 4.6	39.5 \pm 3.4
Permeation %	20.5 \pm 5.5	15.1 \pm 1.4	9.5 \pm 4.2
Total recovery %	87.8 \pm 7.3	93.5 \pm 5.7	87.8 \pm 5.8

5.3.2.4 Comparison of PR permeation from binary and ternary systems in the Skin PAMPA model and porcine skin

Table 5.5 summarizes the cumulative permeation of PR in the Skin PAMPA model and porcine skin. The permeation of PR obtained in the Skin PAMPA model ranged from 13-39 $\mu\text{g}/\text{cm}^2$, and the corresponding values recorded in porcine skin ranged from 1 to 19.5 $\mu\text{g}/\text{cm}^2$. For TC:IPM (50:50), there was no difference comparing the permeation of PR for the two assessed models ($p>0.05$). The higher permeability of the Skin PAMPA model compared to porcine skin was evident for other tested binary and ternary systems ($p<0.05$). No correlation was observed between the permeation of PR from binary and ternary systems in the Skin PAMPA model and porcine skin.

The binary systems: DMI:PG (50:50), DMI:TC (50:50), IPM:TC (50:50), OSaI:TC (50:50) and PG:TC (50:50) and the three ternary systems: TC:PG:IPM (50:25:25), PG:TC:IPM (50:25:25) and IPM:TC:PG (50:25:25) were taken forward for assessment using heat-separated human epidermis.

Table 5. 5 Cumulative permeation of PR in porcine skin and the Skin PAMPA model from binary and ternary systems (mean \pm SD, $4 \leq n \leq 5$).

Binary and ternary solvent systems	Cumulative permeated amounts of PR ($\mu\text{g}/\text{cm}^2$)	
	The Skin PAMPA model	Porcine skin
PG:IPM (50:50)	39.0 \pm 2.8	1.3 \pm 0.8
OSal:TC (70:30)	36.6 \pm 1.9	7.8 \pm 2.2
DMI:CCT (50:50)	33.7 \pm 8.5	1.0 \pm 0.5
PG:TC(50:50)	31.2 \pm 0.5	4.2 \pm 0.3
DMI:PG(50:50)	30.6 \pm 2.7	9.8 \pm 3.3
DMI:TC(50:50)	30.0 \pm 1.4	8.2 \pm 2.7
DMI:OSal (50:50)	28.9 \pm 5.8	1.2 \pm 0.5
TC:PG:IPM (50:25:25)	28.5 \pm 4.3	7.9 \pm 1.1
PG:TC:IPM (50:25:25)	28.3 \pm 4.5	10.6 \pm 2.7
IPM:TC:PG (50:25:25)	27.1 \pm 6.8	4.7 \pm 1.9
IPM:TC (50:50)	22.4 \pm 3.4	19.5 \pm 6.4
PG:OA (10:90)	15.9 \pm 4.2	1.9 \pm 0.2
PG:LA (50:50)	13.3 \pm 2.4	2.8 \pm 0.7

5.3.3 Evaluation of binary and ternary systems of PR in human skin

5.3.3.1 Binary systems of PR evaluated in human skin

Fig 5.13 shows the permeation profiles of PR in human skin. At 24 h, the permeation for all tested binary formulations ranged from 4 to 19 $\mu\text{g}/\text{cm}^2$. The cumulative permeation of PR from TC:IPM (50:50) was determined as 18.8 \pm 3.8 $\mu\text{g}/\text{cm}^2$. This value was significantly greater compared with other binary systems ($p < 0.05$). The cumulative permeation of PR from TC:IPM (50:50) was significantly higher than for neat TC and neat IPM ($p < 0.05$). The higher permeation of PR for TC:IPM (50:50) in human epidermis skin was consistent with the results obtained in porcine skin studies (Session C.5.3.2.2).

The percentage permeation profiles are illustrated in Fig 5.14. The amounts of PR permeated through human epidermis account for 7 to 38 % of applied amounts. The percent of PR that permeated from IPM:TC (50:50) and PG:IPM (50:50) was 38.1 and 14.8 %, respectively.

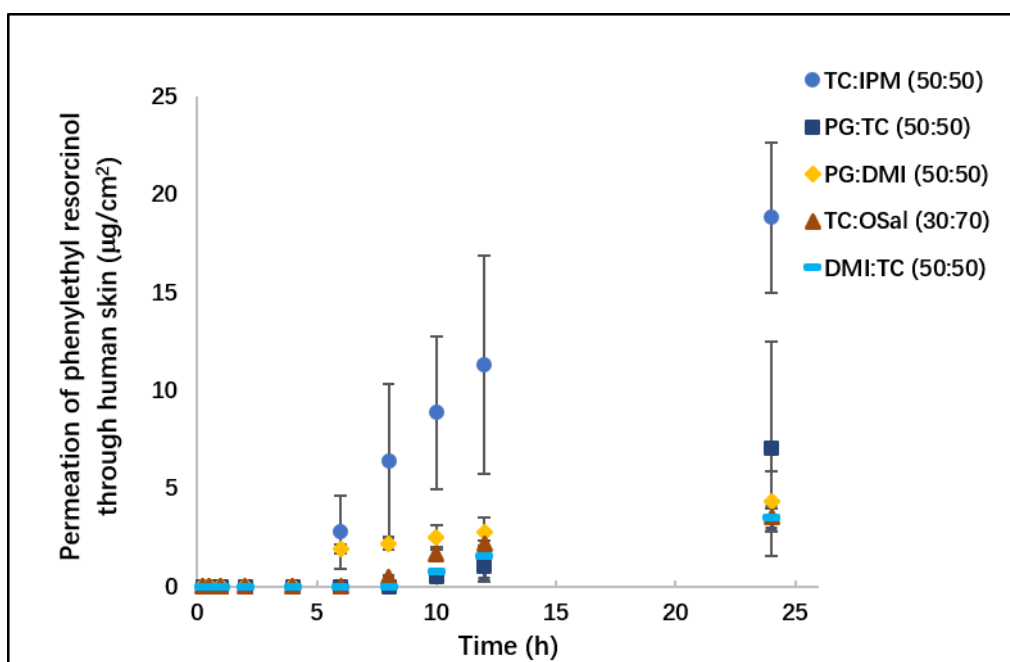


Figure 5. 13 The permeation profiles of PR from binary systems in human skin (mean \pm SD, n=4).

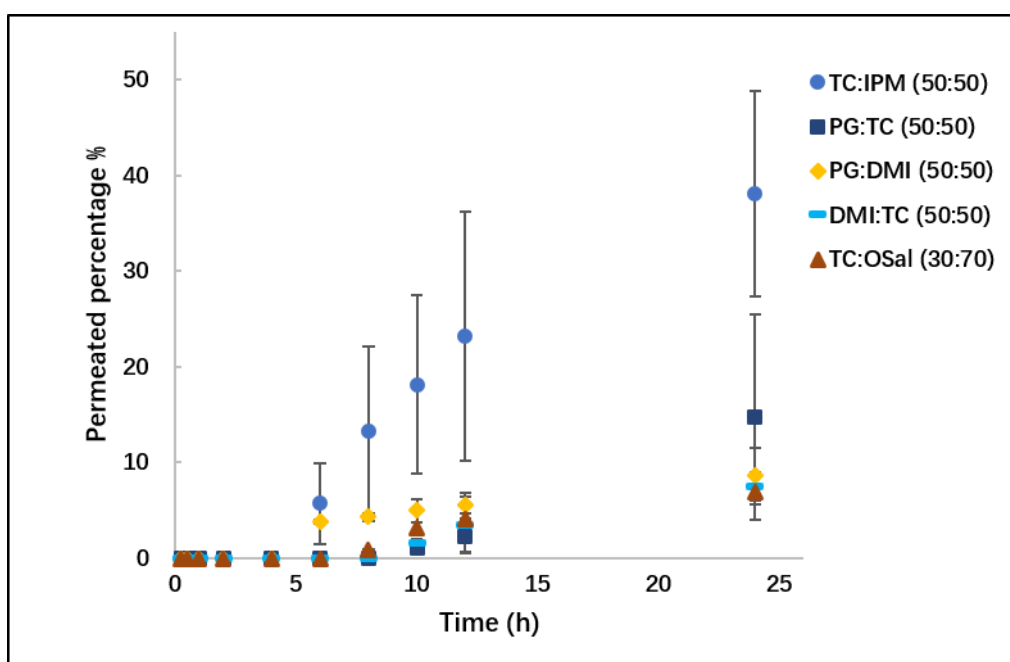


Figure 5. 14 Percentage permeation of PR from binary systems in human skin (mean \pm SD, n=4).

Table 5.6 shows the distribution of PR found on the skin surface, in the epidermis and in the receptor medium. For PG:DMI (50:50), most of the PR was recovered from the skin surface, ~89 %. These values were significantly higher than the skin surface recovery of PR for DMI:TC (50:50) ($p < 0.05$). For DMI:TC (50:50), 24 % of the applied dose remained on the skin surface, 55 % was retained in the epidermal membrane and 8 % permeated into the receptor

phase. The skin extraction value of PR observed for DMI:TC (50:50) was comparatively higher than for PG:DMI (50:50) ($p<0.05$).

For PR in TC:IPM (50:50), the percentages of active found on the skin, in the skin and the receptor were determined as 41, 19 and 38 %, respectively. The human epidermis extraction values of PR in neat IPM and neat TC were determined as 14.5 and 36.4 %, respectively (Session C.3.3.8). Combining IPM and TC significantly increased skin permeation of PR compared to IPM or TC alone ($p<0.05$). The percutaneous absorption was consistent with the results observed by Hirata et al. (2013). These authors investigated combinations of binary and ternary vehicles on dermal delivery of carbenoxolone in human skin. They reported the synergistic enhancement of TC and IPM on carbenoxolone transport across human skin compared with TC alone.

Table 5. 6 Mass balance results of PR for permeation studies of binary systems in human skin, ($n=4$, mean \pm SD).

	TC:IPM (50:50)	PG:TC (50:50)	PG:DMI (50:50)	DMI:TC (50:50)	TC:OSal (30:70)
Washing %	41.2 \pm 4.7	49.9 \pm 6.0	89.0 \pm 5.7	24.4 \pm 10.8	52.7 \pm 13.9
Extraction %	18.8 \pm 3.8	33.7 \pm 13.8	7.5 \pm 4.2	55.3 \pm 17.3	40.5 \pm 18.9
Permeation %	38.1 \pm 10.8	14.8 \pm 10.7	8.6 \pm 2.9	7.5 \pm 1.4	6.9 \pm 0.5
Total recovery %	98.1 \pm 12.3	98.4 \pm 11.3	105.1 \pm 6.8	87.3 \pm 9.3	100.1 \pm 6.4

For PG:IPM (50:50), the percentages of active extracted from human epidermis and recovered from the receptor medium were 37 and 29 %, respectively. The binary system PG:IPM (50:50) did not increase the percutaneous absorption of PR compared to neat PG and neat IPM ($p>0.05$). Higher skin extraction was evident for PG:IPM (50:50) than IPM ($p<0.05$). Brinkmann and Müller-Goymann (2005) investigated the effect of PG and IPM on human SC microstructure by means of differential scanning calorimetry (DSC) and wide and small angle X-ray-diffraction (WAXD and SAXD). The authors noted that in WAXD measurements, the combination of PG/IPM affects the short distances of orthorhombically and hexagonally packed SC lipids in the same way as PG alone. The long distance was affected in a similar way as for IPM treatment. The authors concluded that the binary system of IPM-PG affects the microstructure of human SC lipids in a specific manner compared with neat PG or neat IPM. The authors considered that it is possible the IPM molecules laterally

integrated into SC lipid molecules when PG molecules inserted between the polar headgroups of the lipid molecules in a lateral direction between the bilayers.

5.3.3.2 Ternary systems of PR composed of PG, TC and IPM

Fig 5.15 shows the permeation profiles of PR from the assessed ternary formulations in human skin. At 24 h, an amount of $11.7 \pm 1.3 \mu\text{g}/\text{cm}^2$ was delivered from PG:TC:IPM (50:25:25) which was determined as the most efficient ternary vehicle system ($p < 0.05$). Permeation of PR from IPM:TC:PG (50:25:25) and TC:PG:IPM (50:25:25), was determined as 5.1 ± 0.8 and $4.2 \pm 2.4 \mu\text{g}/\text{cm}^2$, respectively. The ternary systems did not demonstrate higher percutaneous delivery than the binary TC-IPM and PG-TC systems as no difference was evident for the cumulative amounts of PR that permeated ($p > 0.05$). As shown in Fig 5.16, the permeation of PR accounted for 8.4 to 24.4 % of applied amounts. A significantly higher percentage of PR was delivered from PG:TC:IPM (50:25:25) compared with IPM:TC:PG (50:25:25) and TC:PG:IPM (50:25:25) ($p < 0.05$).

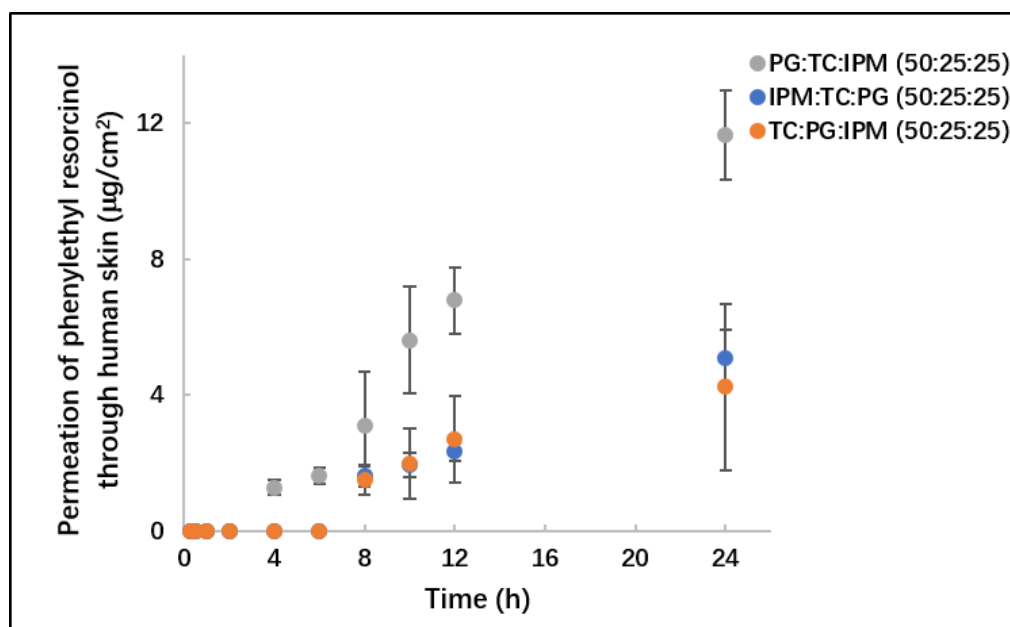


Figure 5. 15 Permeation profiles of PR from ternary systems in human skin (mean \pm SD, $n=4$).

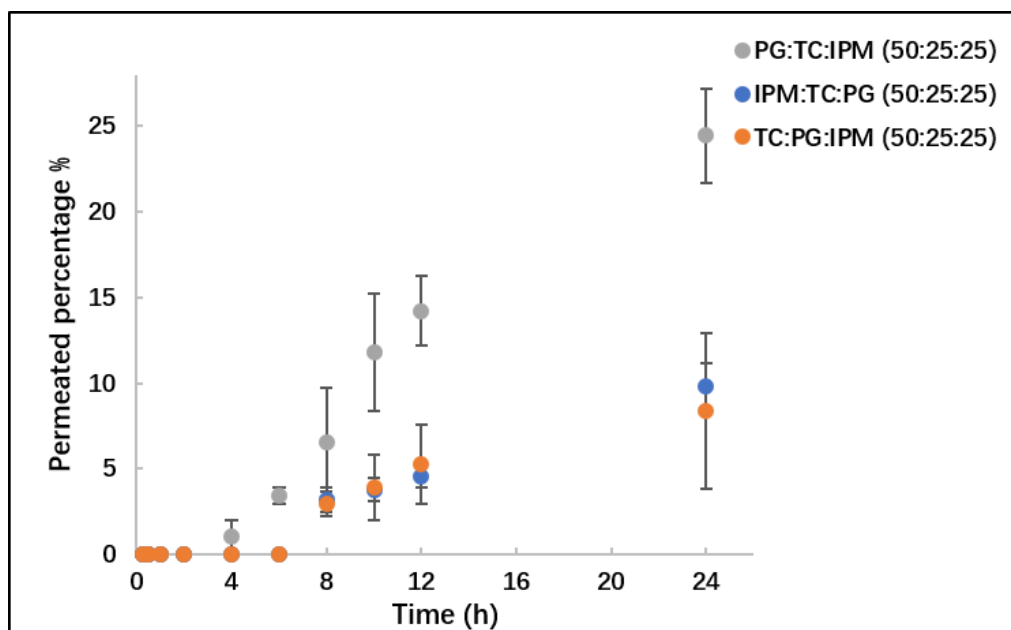


Figure 5. 16 Percentage permeation of PR from ternary systems in human skin (mean \pm SD, n=4).

Table 5.7 illustrates the mass balance results following the permeation studies. The skin retention of PR in human epidermis accounted for 44-68 % of applied amounts. A higher skin extraction of PR was evident for IPM:TC:PG (50:25:25) compared with PG:TC:IPM (50:25:25) and IPM:TC (50:50) ($p < 0.05$). Interestingly, there was no difference between the amounts of PR that permeated through human epidermis and porcine skin ($p > 0.05$).

Table 5. 7 Mass balance results for PR following permeation from ternary systems in human skin, (n=4, mean \pm SD).

	PG:TC:IPM (50:25:25)	TC:PG:IPM (50:25:25)	IPM:TC:PG (50:25:25)
Washing %	23.1 \pm 2.6	35.5 \pm 7.1	27.5 \pm 2.3
Extraction %	43.6 \pm 3.0	45.8 \pm 2.6	67.7 \pm 4.9
Permeation %	24.4 \pm 2.8	8.4 \pm 4.5	9.8 \pm 1.3
Total recovery %	91.1 \pm 3.7	89.6 \pm 12.0	105.0 \pm 2.2

5.3.3.3 Comparison of PR permeation from binary and ternary systems in the Skin PAMPA model and mammalian skin

Table 5.8 summarizes the cumulative permeated amounts of PR in the Skin PAMPA model and human skin. The permeation of PR observed in the Skin PAMPA model ranged from 22 to 39 $\mu\text{g}/\text{cm}^2$, while the corresponding results observed in human skin were 4 to 19 $\mu\text{g}/\text{cm}^2$. For binary and ternary systems of TC:IPM (50:50), PG:TC (50:50), IPM:TC:PG (50:25:25)

and PG:TC:IPM (50:25:25), the permeation of PR obtained in the Skin PAMPA model was comparable to the corresponding values in human skin studies ($p>0.05$). Although attempts were made to fit the PR data obtained in the Skin PAMPA model and human skin to an exponential model, no correlations were evident. It is generally agreed that the intercellular lipid lamellae are the major pathway for percutaneous permeation of small drug molecules across the stratum corneum (Hadgraft and Walters, 1994). To mimic the permeability of human skin, the Skin PAMPA model contains components including cholesterol, free fatty acid and the ceramide-analog compound (certramide) (Sinkó et al., 2015). However, the results observed in this work indicated that the Skin PAMPA model is not a suitable method to predict *in vitro* human skin absorption of PR from binary and ternary solvent systems.

Table 5. 8 Cumulative permeation of PR in human skin, porcine skin and the Skin PAMPA model from binary and ternary solvent systems (mean \pm SD, $n=4$).

Binary and ternary solvent systems of PR	Cumulative permeated amounts of PR ($\mu\text{g}/\text{cm}^2$)		
	The Skin PAMPA model	Human skin	Porcine skin
TC:OSal (30:70)	36.6 \pm 1.9	3.6 \pm 0.4	7.8 \pm 2.2
PG:TC(50:50)	31.2 \pm 0.5	7.0 \pm 5.5	4.2 \pm 0.3
DMI:PG(50:50)	30.6 \pm 2.7	4.3 \pm 5.5	9.8 \pm 3.3
DMI:TC(50:50)	30.0 \pm 1.4	3.5 \pm 1.5	8.2 \pm 2.7
TC:PG:IPM (50:25:25)	28.5 \pm 4.3	4.2 \pm 2.4	7.9 \pm 1.1
PG:TC:IPM (50:25:25)	28.3 \pm 4.5	11.7 \pm 1.3	10.6 \pm 2.7
IPM:TC:PG (50:25:25)	27.1 \pm 6.8	5.1 \pm 0.8	4.7 \pm 1.9
IPM:TC (50:50)	22.4 \pm 3.4	18.8 \pm 3.8	19.5 \pm 6.4
PG:IPM (50:50)	39.0 \pm 2.8	-	1.3 \pm 0.8
DMI:CCT (50:50)	33.7 \pm 8.5	-	1.0 \pm 0.5
DMI:OSal (50:50)	28.9 \pm 5.8	-	1.2 \pm 0.5
PG:OA (10:90)	15.9 \pm 4.2	-	1.9 \pm 0.2
PG:LA (50:50)	13.3 \pm 2.4	-	2.8 \pm 0.7

Note: The binary PG-IPM, DMI-CCT, DMI-OSal, PG-OA and PG-LA systems were only evaluated in Skin PAMPA model and porcine skin under finite dose conditions.

A comparatively higher permeation of PR in TC:IPM (50:50) compared to other formulations was observed in both human and porcine skin. At 24 h, a higher permeation in porcine skin compared to human skin was evident for PR in PG:DMI (50:50), DMI:TC (50:50), TC:OSal (30:70) and TC:PG:IPM (50:25:25) ($p<0.05$). On the other hand, the cumulative

amounts of PR in TC:IPM (50:50), PG:TC (50:50), PG:TC:IPM (50:25:25) and IPM:TC:PG (50:25:25) that permeated in human skin and porcine skin were comparable ($p>0.05$).

5.4 Conclusions

Previous work investigated the skin extraction and permeation of PR from a series of simple solutions in the Skin PAMPA model and mammalian. OSal was identified as the most efficient neat vehicle for dermal delivery of PR in human skin. A correlation was confirmed between the permeation of PR in the Skin PAMPA model and human skin in a series of neat solvents. Several binary and ternary solvent systems were prepared and examined for dermal delivery of PR using the Skin PAMPA model, porcine skin and porcine skin in this chapter. No correlations between the permeation data obtained in the Skin PAMPA model and the data obtained in human skin or porcine skin were observed. A higher amount of permeation was observed for PR in TC:IPM (50:50) compared with other assessed binary systems in human skin. However, no difference was evident between the permeation of PR from TC:IPM (50:50) and the best single solvent, neat OSal ($p>0.05$). PG:TC:IPM (50:25:25) was confirmed as the most efficient ternary system for PR percutaneous absorption in human skin ($p<0.05$). However, this ternary system did not improve PR delivery compared with TC:IPM (50:50) and PG:TC (50:50) in human skin. To conclude, the binary TC:IPM (50:50) and ternary PG:TC:IPM (50:25:25) demonstrated promising potential for the dermal delivery of PR and the two systems were selected for further evaluation *in vivo*.

Chapter 6.

***In vivo* evaluation of NIA and PR formulations**

6.1 Introduction

Robust assessment of percutaneous absorption of drug/actives has always been of interest from both medical and personal care standpoints. The most relevant and desirable data come from *in vivo* human studies. In the past, the sensitivity of radioisotopes was required for percutaneous absorption measurements (Feldmann and Maibach, 1970; Bronaugh and Franz, 1986). Radio-labelled compounds are not always feasible considering their potential toxicity. Later, *in vivo* dermal absorption was determined by measurement of the parent chemical and/or its metabolite level using microdialysis or stratum corneum tape stripping (Kezic, 2008; Raney et al., 2015). Tape stripping is a minimally invasive method which can determine the amount of substance in the outmost layer of the skin. This technique is considered as a suitable permeation kinetic method according to the newest draft guideline on quality and equivalence of topical products released by the European Medicines Agency (EMA) (EMA, 2018).

On the other hand, *in vitro* permeation studies using different model membranes have been investigated extensively as surrogates of *in vivo* human studies (Hadgraft and Lane, 2005). Franz (1975) developed the vertical Franz diffusion cell and conducted some of the early assessments of *in vivo-in vitro* comparisons. Franz and colleagues compared the *in vitro* permeation data of 12 chemicals with the corresponding results obtained *in vivo*. Good agreement between the two sets of data was reported.

Confocal Raman spectroscopy is a novel technique which was developed as a non-invasive approach to monitoring skin penetration. This technique has been applied for measurement of endogenous skin components (Caspers et al., 2001), water content (Caspers et al., 2000) and SC thickness (Egawa et al., 2007). More recently, CRS was used to investigate the *in vivo* permeation of retinol (Pudney et al., 2007), ibuprofen (Mateus et al., 2013) and salicylic acid (Mateus et al., 2014). Previously in our group, we investigated the *in vivo* penetration of NIA using CRS on one human volunteer and good *in vivo-in vitro* correlations were reported (Mohammed et al., 2014b). Considering the variability of human skin, the correlation observed in that study warrants further investigation with a larger sample size. Binder et al. (2018) conducted comparative studies using CRS and combined ATR-FTIR

spectroscopy and tape stripping experiments assessing *in vitro* porcine skin penetration of four model substances. It was reported that the penetration profiles determined using the two techniques were comparable for all chemicals.

Accordingly, the aim of this chapter was to investigate the effects of selected solvent systems on skin penetration of NIA and PR *in vivo*. The secondary purpose was to monitor the permeation for both the active and solvent using the CRS technique. The *in vivo* permeation assessment of the actives was also performed using the tape stripping technique. The *in vivo-in vitro* correlations in skin permeation using two study methods were subsequently investigated.

6.2 Materials and methods

6.2.1 Materials

NIA, propylene glycol, oleic acid (OA), 2-ethylhexyl salicylate (also known as octyl salicylate, OSal) and linolenic acid (LA) were purchased from Sigma-Aldrich (UK). Isopropyl myristate (IPM) and dimethyl isosorbide (DMI) were gifts from Croda Ltd (UK). Transcutol® P (TC) and caprylic/capric triglyceride (CCT) were received from Gattefossé (France). PR (Symrise, Holzminden, Germany) was a gift from pION Inc. Billerica, USA. Standard D-Squame tapes (diameter: 2.2 cm; area: 3.8 cm²) were purchased from CuDerm Corporation (Dallas, TX, USA).

6.2.2 Volunteer recruitment

Data Protection Registration (Z6364106/2018/09/34) and the approval of this *in vivo* study from UCL Research Ethic Committee (REC) (13271/001) were obtained prior to the recruitment of any volunteers. A sample size of 12 volunteers was proposed. The inclusion criteria were that the participants must enjoy good health; be between 18 and 60 years old; should not have experienced allergic reactions to the products or adhesives applied to the skin; should agree to participate in the study and sign a written informed consent.

The participants were recruited from the staff and students of the UCL School of

Pharmacy. An information sheet was provided to the potential participants, with detailed information about the project. A questionnaire was given to the prospective participants to verify that they understood the inclusion and exclusion criteria. Finally, a written and informed consent was sought from the prospective participants before they were included. Participation in this research project was entirely voluntary. On agreeing to participate in this study, a unique ID number was assigned to the participant. All the samples and data obtained in this study were labelled and saved using the ID number.

6.2.3 Confocal Raman spectroscopy (CRS) studies

6.2.3.1 Confocal Raman spectroscopy

In vivo evaluation of penetration was determined from Raman spectra using the confocal Raman spectroscopy skin composition analyzer, Model 3510 SCA (River Diagnostics, Rotterdam, the Netherlands) (Fig 6.1). The instrument enables rapid *in vivo* quantitative and depth-resolved determination of the molecular composition of the stratum corneum. Two near-infrared (NIR) lasers, at 785 and 690 nm, are coupled to the instrument via fiber optic cables. The laser at 785 nm allows for measurements in the fingerprint region ($400\text{--}1800\text{ cm}^{-1}$) and the Raman laser at 690 nm allows measurement in the high wavenumber region ($2060\text{--}4000\text{ cm}^{-1}$) of the Raman spectrum. For *in vivo* human measurements the arm of the volunteer is placed on a fused silica sample window. As shown in Fig 6.1, the laser light is focused into the skin with an inverted microscope objective located behind the window. An internal video camera allows for inspection of the skin surface and evaluation of the measurement spot. Immersion oil in the space between the measurement window and the microscope objective minimized the refractive index mismatch (Mélot et al., 2009). The location of the laser light focus relative to the skin surface can be accurately adjusted for data acquisition (typically in $2\text{ }\mu\text{m}$ steps). In this way, detailed Raman depth profiles can be acquired. Raman scattered light, the light scattered by the skin, is collected by the same microscope objective through a pinhole. The pinhole only allows the passage of Raman photons originating from the focal plane set on the instrument (Giridhar et al., 2017). The

light then passes through the notch filter (NF) which attenuates the excitation line of the laser reflection and returns with the same wavelength as the incident light, elastic light. The light with a change in wavelength is then recorded by the detector. The detector is one of the key components as well as a charge-coupled device (CCD) cooled to $-70\text{ }^{\circ}\text{C}$ throughout the measurement to reduce thermal noise (Hollricher, 2011).

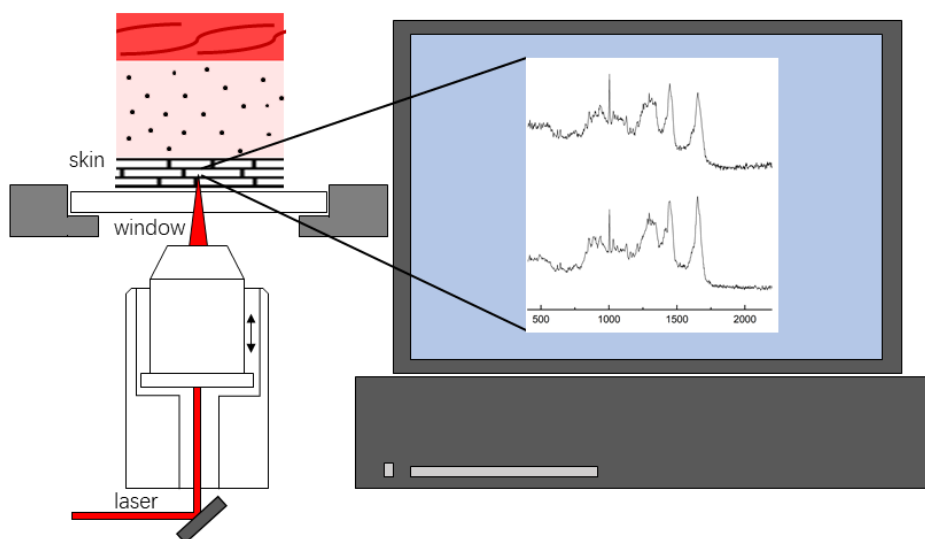


Figure 6. 1 Schematic representation of *in vivo* confocal Raman spectroscopy measurements on the skin. Laser light (NIR) is focused on a small spot at the selected depth below the skin surface. The location of the laser focus in the skin can be varied to investigate the local chemical composition at various depths in the stratum corneum. The figure was adapted and modified from Caspers et al. (2000).

To allow adequate time for the system to stabilize, all the instrument modules were switched on about 2 h prior to use. Data acquisition was conducted using RiverlCon V3.0 software (River Diagnostics, Rotterdam, the Netherlands). A Starlab V2.0 (Ophir Photonics, Israel) device was used to verify that the laser power was within the required range of 25 – 30 mW and 7 – 10 mW for the 785 nm and 690 nm Raman lasers, respectively. The sensitivity of CRS is wavelength dependent (Puppels et al., 1991). Therefore, to verify the spectra generated by this CRS instrument, a calibration was performed after confirming the laser power. The calibration was conducted by measuring the spectrum of a well-defined luminescence spectrum of a relative intensity correction standard green-glass (National Institute of Standards, NIST, USA) when excited with specific wavelength laser radiation. The

built-in template “auto calibration sequence” was used to calculate the wavelength dependent instrument response and match the reference spectrum to the spectrum of an internal Raman standard. The calibration was considered as successful when the signal to noise ratio was above 30 (Mélot et al., 2009). All the CRS experiments were performed at 22 ± 2 °C and 40 ± 15 % RH.

6.2.3.2 Preparation of standards and reference spectra

Water is the ideal vehicle to prepare the active in solution since the Raman spectrum of water is insensitive and weak which provides a comparatively clear background in the spectra (Williams et al., 1992). As NIA has good aqueous solubility (Session C.2.3.2), for NIA Raman reference spectrum measurement, the standard solution was prepared in water. The solubility of PR in water was determined as lower than the formulation concentration (Session C.3.3.2). For PR Raman reference spectrum collection, a standard solution of PR was prepared in ethanol:water (50:50) mixture solutions.

The Raman spectra of the two model actives, NIA and PR, were taken under the same physical conditions in the fingerprint region with the 785 nm laser. The Raman experiment mode was selected. 100 μ L of standard solution was applied on the window, and the measurement location selection was set at a focus of 100 μ m. A 3 s exposure time was selected, avoiding the evaporation of solvent in the solutions. 3 frames were taken for each measurement and the final Raman spectrum was generated by averaging the 3 spectra. The Raman spectra of neat water and ethanol:water (50:50) were collected using the same parameters. To subtract the Raman spectrum for NIA and PR from the standard solutions, a difference spectrum was calculated using the difference spectrum option in SkinTools V2.0 D2O (River Diagnostics, Rotterdam, the Netherlands). The Raman spectrum for each excipient, PG, TC, OSal, IPM, CCT, OA and LA were acquired under consistent physical conditions in the fingerprint region.

6.2.3.3 *In vivo* determination of water profile for human skin

The water content in human skin was determined by the default method analyzing the

high wavenumber Raman spectral data between 2600 – 3800 cm^{-1} using SkinTools V 2.0 R120802 Beta (River Diagnostics, Rotterdam, The Netherlands). The algorithm was based on the ratio of the Raman intensities of the OH-stretching vibrations of water at 3350–3550 cm^{-1} and the CH_3 stretch of protein, at 2910–2965 cm^{-1} (Caspers et al., 2000; Caspers et al., 2001). Scans of 2 μm steps over a total depth of 40 μm into the skin surface were collected. After each measurement, the laser was positioned on different areas of the forearm and the measurement repeated. Overall, six measurements were taken to generate the average water profile for each volunteer. From the water profile across the epidermis the border between the stratum corneum and stratum granulosum can be estimated, and the stratum corneum thickness was calculated using SkinTools V 2.0 R120802 Beta (River Diagnostics, Rotterdam, the Netherlands) (Bielfeldt et al., 2009).

6.2.3.4 Preparation of formulations and *in vivo* evaluation of skin penetration

The application site of 3.8 cm^2 (2.2 cm in diameter, approximately the size of a one-pound coin) was delineated on both left and right volar forearms. There were three well separated investigation sites on each forearm marked using a surgical marker for a total of five application sites and one control site. This allowed the potential application of five formulations with one control site without any treatment during the course of the study. Hair was carefully cut without touching the skin surface using surgical scissors. Water profiles were measured in the high wavenumber laser region, using the laser of 690 nm. An exposure time of 2 s was used with 2 μm steps to a final depth of 30 or 40 μm .

Solutions of NIA (5 %, w/v) were prepared in two single solvents PG, TC, two binary solvent systems PG:OA (10:90), PG:LA (50:50), and one ternary solvent system TC:CCT:DMI (50:25:25). Solutions of PR (5 %, w/v) were prepared in three single solvents PG, TC, OSal, one binary solvent system IPM:TC (50:50), and one ternary solvent system PG:TC:IPM (50:25:25). A volume of 10 μL was applied on each application site using a micropipette without rubbing. The amount of the active remaining in the micropipette was extracted and determined. To assess the depth profiles of actives and excipients, the Raman spectra of the fingerprint region were measured using the 785 nm laser, 1 h post formulation application. A 5 s

exposure time was used with 2 μm steps to a final depth of 30 μm . Because of the biological lateral variation in skin composition, 3 frames were taken at each measurement position and the spectra were averaged. A minimum of 3 measurements were taken for each site.

6.2.3.5 Data analysis

Stratum corneum thickness of each volunteer was determined. As the stratum corneum thickness varies greatly between individuals, the depth of the measurements was normalized as reported previously (Herkenne et al., 2006; Mateus et al., 2013). Eq 6.1 shows the calculation. The measurement depth (x) was divided by the total stratum corneum thickness (h). This allows the excipients' depth profiles to be expressed as a function of the relative position within the stratum corneum (x/h), removing the inter-subject variability. The value of the normalized stratum corneum thickness should fall in the range of $0 \leq x/h \leq 1$. The outermost skin surface is therefore indicated as the normalized thickness of 0 and the whole thickness of the stratum corneum is represented as 1. To analyze the average depth profile in all tested volunteers, the values of normalized stratum corneum thickness were rounded to one decimal place. Normalized skin thickness values were rounded to one decimal place to align data points and for data presentation and statistical analysis.

$$\text{Normalized stratum corneum thickness} = x/h \quad \text{Equation 6.1}$$

The model actives and other excipients were analyzed using SkinTools 2.0 (River Diagnostics, Rotterdam, the Netherlands). The default NMF (natural moisturizing factor) method was used to analyze fingerprint Raman spectra between 400 – 1800 cm^{-1} . The reference spectra of model actives and excipients were loaded as additional model spectra. Reference spectra were fitted to the experimental skin Raman spectra using a non-restricted multiple least-squares algorithm (Caspers et al., 2001). The algorithm thus determined the distribution of added molecules in the SC. The depth profiles of each added component were generated. As the NMF algorithm was built using a library set of spectra based on the endogenous SC composition of human skin, the permeation behavior of model actives was

only investigated and reported within the non-viable epidermis in human subjects. The total area under the curve (AUC) was calculated for NIA and PR profiles using trapezoidal integration.

All the results were presented as the mean \pm standard deviation (SD). The statistical analysis was performed as described in Session C.2.2.8.

6.2.4 Tape stripping

6.2.4.1 Tape stripping studies

In vivo tape stripping experiments were performed on 12 human volunteers. The penetration profiles of NIA or PR were established for the same systems investigated in CRS studies. The method of formulation application was in line with the procedure used in CRS studies (Session C.6.2.3.4). There were three well separated application sites on each forearm for a total of five application sites and one control site. Tape stripping experiments were performed 1 h post formulation application. Consistent factors were used during the course of the whole study: Standard D-Square tape[®] (2.2 cm in diameter, 3.8 cm²) was applied to the application sites. A constant pressure of 225 g/cm² was applied on each tape using a pressure device for 5 s. 15 consecutive tape were collected from each application site with intervals of 20 \pm 5 s between each tape stripping (Breternitz et al., 2007; Mohammed et al., 2013; Guneri et al., 2018).

Each tape collected from every application site was placed into an Eppendorf[®] with 1 mL of methanol. The Eppendorf tubes were left on a shaker maintained at 32 \pm 1 °C and incubated overnight. The amounts of NIA or PR extracted from the layer of the SC adhering to each tape was quantified using HPLC.

6.2.4.2 Trans Epidermal Water Loss (TEWL) and SC protein content measurement

Volunteers were acclimatized for 30 min prior to the tests at ambient conditions of 21 \pm 2 °C and 45 \pm 1 % RH (relative humidity). TEWL was measured (Aquaflux AF102, Biox Systems Ltd. London, UK) at baseline and after the first, third, sixth, ninth, twelfth and fifteenth tape

stripping at the control site. The amount of protein absorbance (%) collected from the adhesive tape was measured using a SquameScan™ A850 infrared meter (Heiland Electronic, Wetzlar, Germany) at 850 nm (Voegeli et al., 2007a; Mohammed et al., 2011) and the protein content calculated using Eq 6.2 (Voegeli et al., 2007b).

$$C_{\text{Protein}} [\mu\text{g cm}^{-2}] = 1.366 \times \text{Absorption} [\%] - 1.557 \quad \text{Equation 6.2}$$

The TEWL values at baseline and with disruption of the barrier using tape stripping and the amount of protein collected give information regarding the SC thickness (Mohammed et al., 2012). The thickness of the SC was calculated for each volunteer following the procedure described previously (Guner et al., 2018).

6.3 Results and discussion

6.3.1 Confocal Raman spectroscopy studies

6.3.1.1 Model actives and vehicle reference spectra

The Raman spectra of NIA are shown in Fig 6.2. The difference spectrum was treated as the reference of NIA. It was subtracted from the spectrum of the mixture of NIA and water.

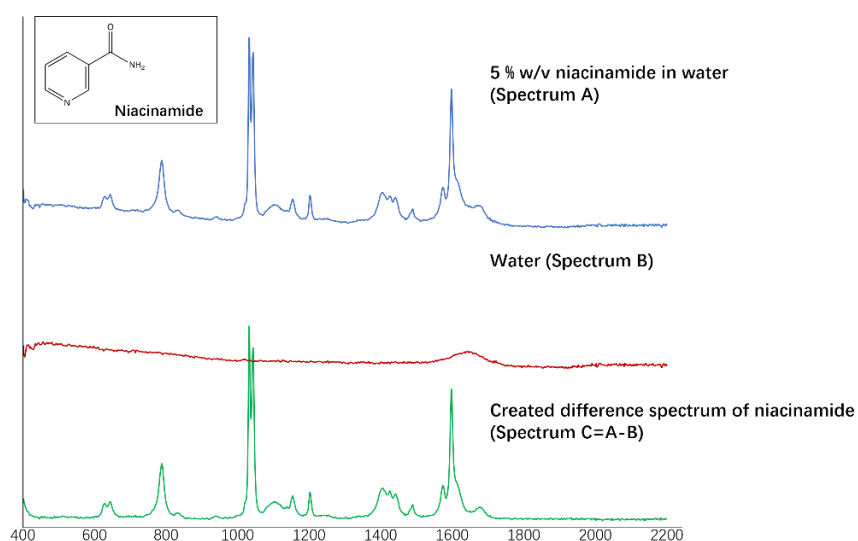


Figure 6. 2 Raman spectrum of 5 % w/v NIA in water (spectrum A); Raman spectrum of water (spectrum B); created difference spectrum of NIA (spectrum C), this reference spectrum was used as

an additional model spectrum.

The Raman spectrum of NIA observed in this study was similar to the results reported by Li et al. (2016). The author applied transmission Raman spectroscopy for determination of NIA content in tablet cores. The Raman spectra of NIA was taken in the region of 1500-600 cm^{-1} when the active was applied in the crystalline state. When comparing the Raman spectra obtained in this study to the results reported by Li, peaks in the region ranges of 878 – 608 cm^{-1} , 1008-1064 cm^{-1} and 1223 - 1130 cm^{-1} were consistent. It was evident that the shapes of the intense peaks in these two spectra were not identical. This is expected considering that the physical forms of NIA measured in these two studies were different. In Fig 6.2, the intense sharp bands in the region of 1064-1008 cm^{-1} are caused by the C-H bending vibrations of the pyridine ring; the peak of 1597 cm^{-1} arises from the C=N stretching vibration. The peak at 788 cm^{-1} may be the C-N stretching vibration. These assignments are supported by the literature (Ramalingam et al., 2010; Socrates, 2012).

The Raman spectra of PR are shown in Fig 6.3. To determine the Raman spectrum of PR, the active was dissolved in ethanol (EtOH): water (50:50). The Raman spectrum of EtOH:water (50:50) was measured using the same parameters, and the difference spectrum of neat PR was subtracted subsequently. To our knowledge, this is the first study reporting the Raman spectrum of PR. According to the peak description from Singh et al. (2016), peaks at 1003 and 978 cm^{-1} correspond to the ring stretching modes of resorcinol and benzene. The C-O stretching occurs as the band at 1655 to 1568 cm^{-1} (Law et al., 2017).

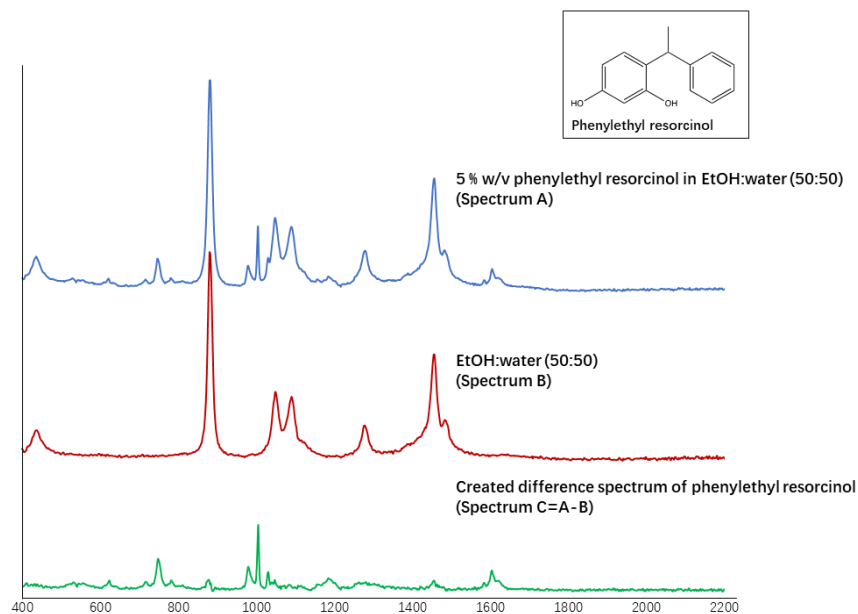


Figure 6. 3 Raman spectrum of 5 % w/v PR in EtOH: water (50:50) (spectrum A); Raman spectrum of EtOH: water (50:50) (spectrum B); created difference spectrum of PR (spectrum C), this reference spectrum was used as an additional model spectrum.

Figure 6.4 shows the reference spectrum of each individual excipient contained in the formulations, namely PG, TC, LA, OA, DMI, CCT, OSaI and IPM. These spectra were used to analysis the depth profile of the corresponding vehicle.

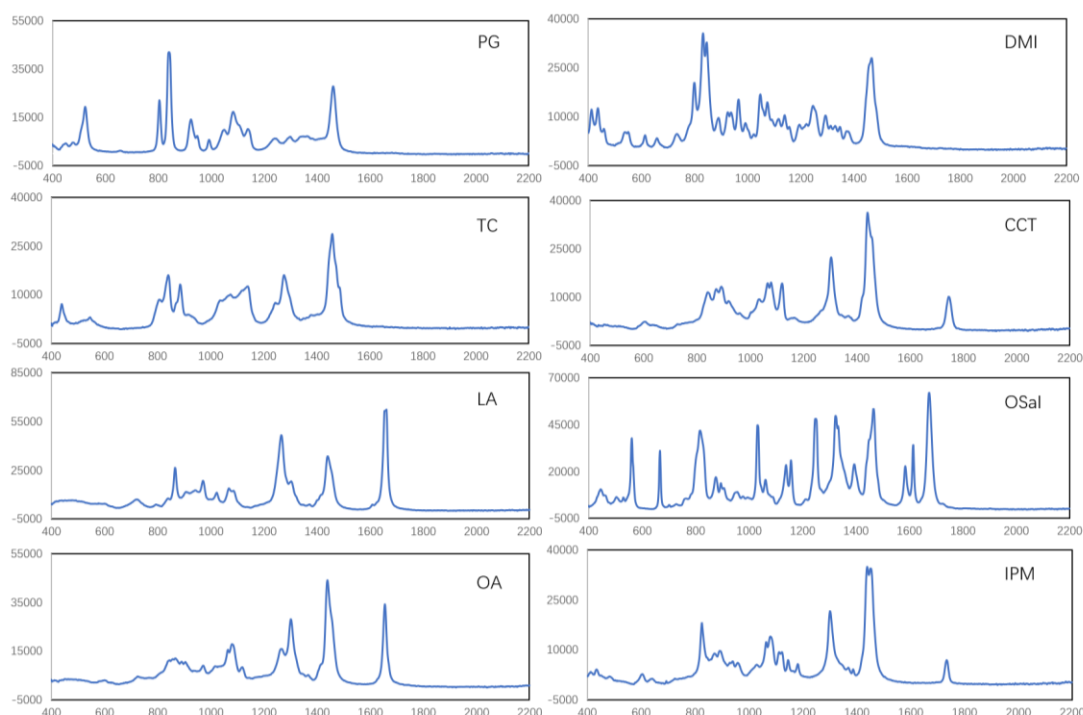


Figure 6. 4 Raman spectra of PG, TC, LA, OA, DMI, CCT, OSaI and IPM using an exposure time of 60 s. The spectra were averaged by 3 frames.

6.3.1.2 Stratum corneum thickness determined using CRS

12 healthy volunteers (7 female, 5 males; 7 Asian, 5 Caucasian; 29.4 ± 6.6 years) were recruited to participate in this study. The SC thickness of their volar forearms was determined using CRS. The SC thickness ranged from 11.6 to 24.6 μm with a 4.2 μm standard deviation values at most for any subject (data not shown). The results were in line with the thickness values of volar forearm SC reported in the literature (Egawa et al., 2007; Crowther et al., 2008; Dąbrowska et al., 2016).

6.3.1.3 *In vivo* evaluation of NIA using CRS

NIA in the SC was measured 1 h after application of the solutions. The depth profiles of the NIA signal intensity in the SC were determined for individuals (data not shown) and the mean results were subsequently calculated. The averaged depth profiles are shown in Fig 6.5. A higher signal intensity of NIA was observed in the upper layers of the SC for neat PG, neat TC and the ternary TC:CCT:DMI (50:25:25) solutions. The profiles of NIA in neat PG and NIA

in neat TC were similar: The signals of NIA decreased exponentially as a function of depth, typical for non-steady state diffusion. However, the depth profiles of NIA in PG:LA (50:50) and PG:OA (10:90) showed that the solvents penetrated into the SC and modified the barrier function. From Fig 6.4, the binary systems delivered greater amounts of NIA compared with other formulations. At normalized depth intervals of $x/h = 0.3$, higher intensity of the NIA signals were evident for PG:LA (50:50) and PG:OA (10:90) compared with other vehicles ($p < 0.05$), and no difference was observed between the two binary systems ($p > 0.05$). For PG:LA (50:50), the lower values at $x/h = 0$ could be indicative of NIA depletion in the applied formulation.

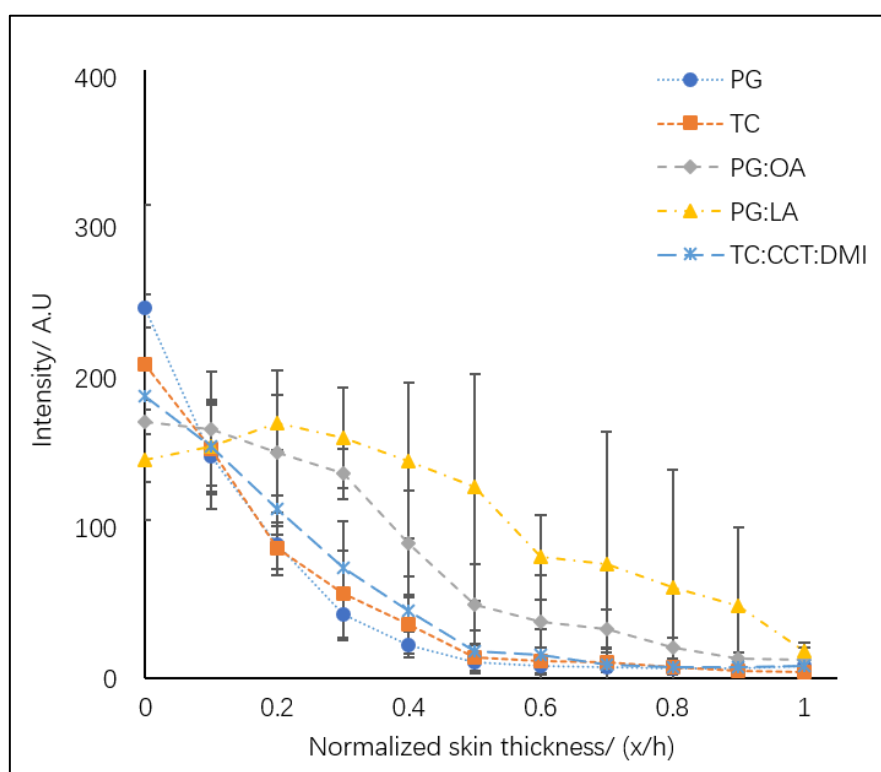


Figure 6. 5 NIA depth profiles in the stratum corneum after application of five tested solutions, namely PG, TC, PG:OA, PG:LA and TC:CCT:DMI. (mean \pm SD, $n=6$).

The AUC for NIA depth profiles was calculated for each volunteer included in the NIA assessment and Figure 6.6 shows the averaged results for five tested formulations. Inter-subject variability is evident from the figure. This is in line with the human epidermal variation observed by other researchers (Vyumvuhore et al., 2014). Higher values of the AUC were confirmed for PG:LA (50:50) compared with neat PG, TC and the ternary solvent

systems ($p < 0.05$) while no difference was evident between the binary PG-LA and PG-OA systems ($p > 0.05$).

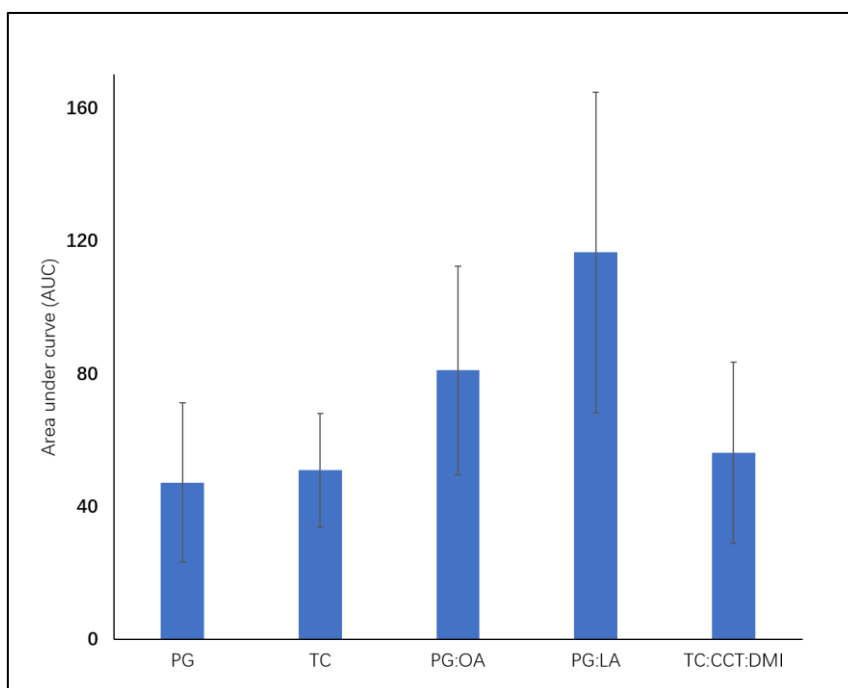


Figure 6. 6 Averaged AUC for NIA depth profiles for six volunteers after application of five tested solutions, namely PG, TC, PG:OA (oleic acid), PG:LA (linolenic acid) and TC:CCT:DMI. (mean \pm SD, $18 \leq n \leq 26$).

6.3.1.4 *In vivo* evaluation of solvents in NIA formulations using CRS

The depth profile of PG in the SC was determined. Fig 6.7 shows the results for NIA in neat PG solutions. The values for both active and solvent are exponential curves, reflecting the non-steady states of the diffusion of NIA and PG. Comparing the two curves, the profile of NIA decreased more rapidly than the profile of PG as a function of skin depth. At $x/h = 0.2$, the signal of PG decreased to 48.9 % of the signal at the skin surface ($x/h = 0$), while the signal of NIA decreased to 33.6 % of the signal at the skin surface ($P < 0.05$). For both NIA and PG, the signal intensities were < 10 % of the signal at the skin surface between $0.5 < x/h < 1.0$.

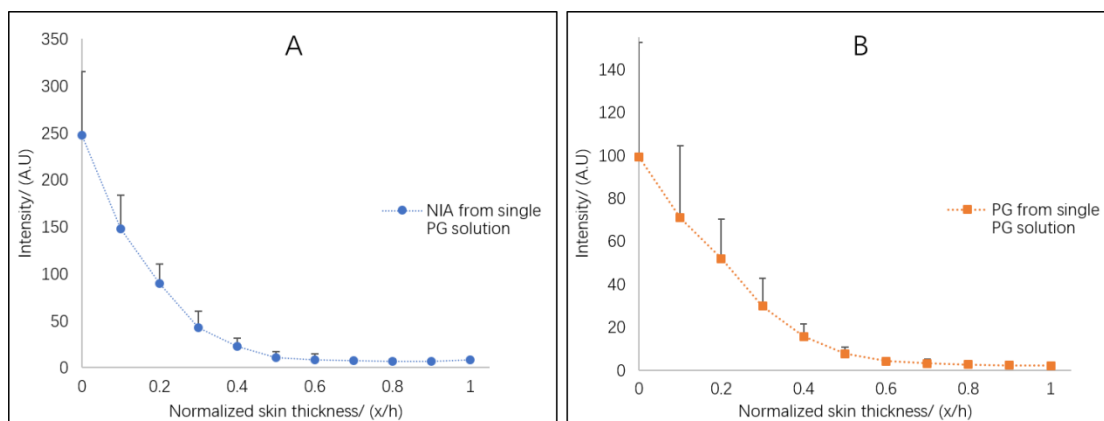


Figure 6. 7 The depth profile of NIA (A) and PG (B) in the SC after application of NIA in neat PG.

To examine the correlation between the distribution of vehicle and the active, the signals of NIA at various skin depths were plotted against the corresponding values of PG. As shown in Fig 6.8, a linear correlation between the intensity of NIA and PG in SC was evident ($R^2=0.97$). The correlation between the solvent and active was consistent with the results reported by other researchers. Mohammed et al. (2014b) performed a proof-of-concept study to assess the feasibility of CRS as an approach to evaluate *in vivo* permeation of NIA within the same volunteer. In their study, monitoring of the vehicles (PG, DMI) as well as the active (NIA) was performed. The authors reported a very good correlation between the signal intensity of NIA and signal intensities of PG and DMI in the SC ($R^2=0.99$).

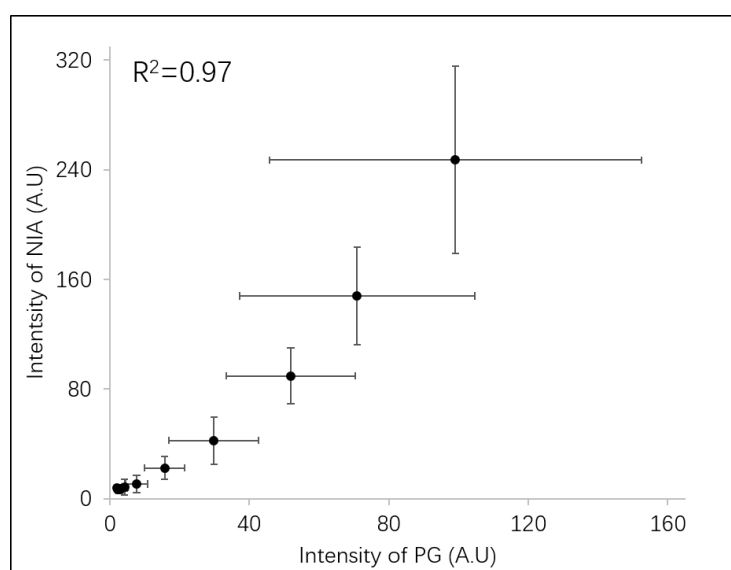


Figure 6. 8 Correlation between the signal intensity of NIA and signal intensity of PG in the SC with depth ($x/h=1, 0.9, 0.8, 0.7, 0.6, 0.5, 0.4, 0.3, 0.2, 0.1$ and 0).

The depth profiles of the active and solvents following the application of binary PG:LA (50:50) systems are shown in Fig 6.9. Compared to the result following the application of neat PG (Fig 6.7 B), PG in the binary PG-LA system acted differently in the skin. As shown in Fig 6.9, similar to the depth profile of NIA (Fig 6.9A), a lower signal of PG was observed in the upper layers of the skin (Fig 6.9B), which could reflect the depletion of PG in the applied formulation. On the contrary, a higher signal of the fatty acid, LA, was observed at the surface of the SC (Fig 6.9C). The intensity of LA at $x/h=0.2$ decreased to 35.6 ± 8.7 % of the signal intensity detected at the skin surface ($x/h=0$). The results indicated that PG:LA (50:50) affected the barrier function of the SC and diffusion of NIA was increased.

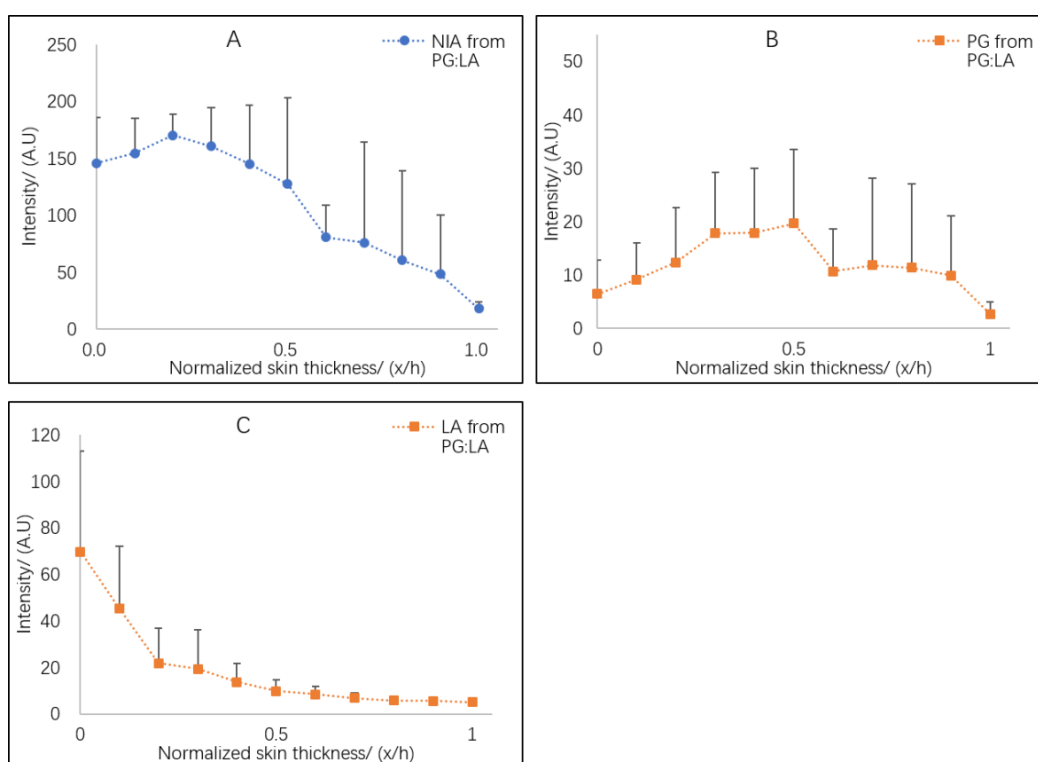


Figure 6. 9 The depth profiles of NIA (A), PG (B) and LA (C) in the SC after the application of binary PG:LA (50:50) systems.

The depth profiles of NIA, PG and OA after the application of PG:OA (10:90) are shown in Fig 6.10. A lower intensity of NIA was detected at $x/h = 0.8$ compared to the skin surface ($p<0.05$). The depth profile of PG is shown in Fig 6.10B and the signal intensity of PG following the application of PG:OA (10:90) was similar as compared to the result observed

for PG:LA (50:50). No difference was evident for the signal intensity of PG at different depths ($p>0.05$). As shown in Fig 6.10C, higher amounts of OA were distributed in the upper layers of the SC with significantly greater values detected at the skin surface compared with the values at $x/h = 0.6$ ($p<0.05$).

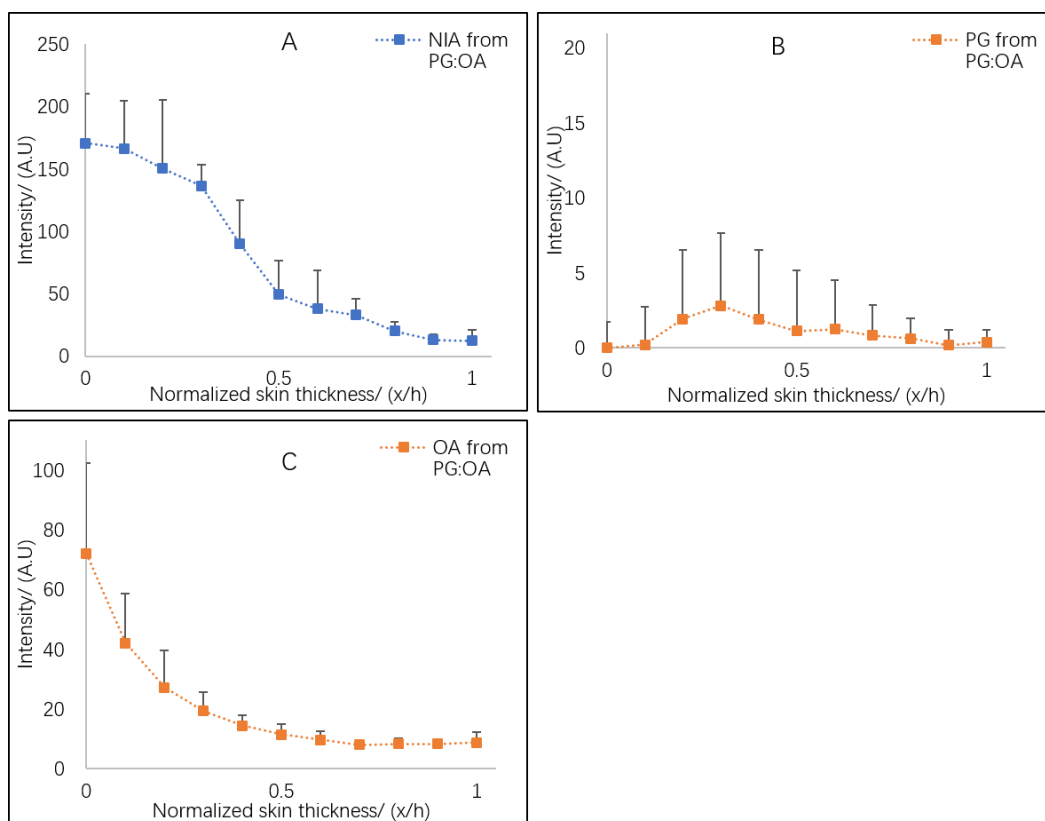


Figure 6. 10 The depth profiles of NIA (A), PG (B) and OA (C) in the SC after the application of binary PG:OA (10:90) systems.

The permeation of the solvent TC was also investigated. The depth profiles of TC for neat TC and CCT:DMI:TC (50:25:25) are shown in Fig 6.11. The depth profile of TC obtained from the neat solvent was similar to that for the ternary system. The low signals of the solvent were observed for both measurements. The rapid penetration of TC was also reported by other researchers. Haque et al. (2017b) investigated the *in vitro* permeation behavior of TC and anthramycin (ANT) using heat-separated human epidermis under finite dose conditions. The authors reported that 10 % of the applied TC was delivered through the skin at 5 h post application and about 1 % of ANT had permeated at that time point. The skin penetration of TC was more rapid compared with the other vehicles investigated, namely PG,

1,3-butanediol (BD) and dipropylene glycol (DPG).

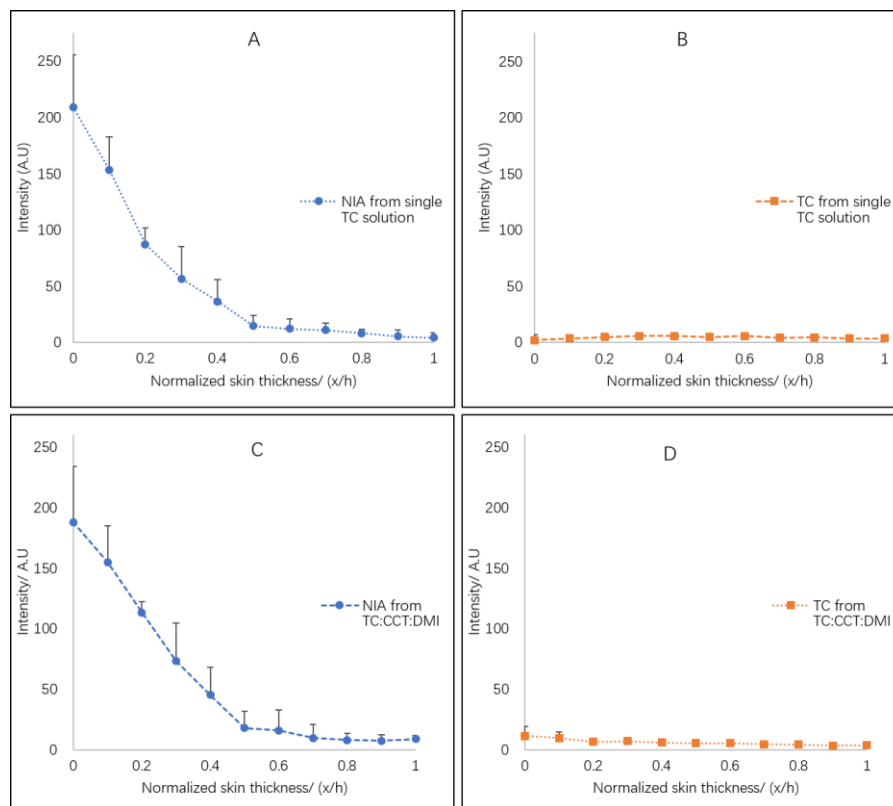


Figure 6. 11 The depth profiles of NIA (A) and TC (B) in the SC after the application of neat TC; The depth profiles of NIA (C) and TC (D) in the SC 1 h after the application of ternary TC:CCT:DMI (50:25:25) solution.

6.3.1.5 *In vivo* evaluation of PR using CRS

In vivo penetration of PR from neat PG, TC, OSaI, TC-IPM and PG-TC-IPM was evaluated 1 h post application. Figure 6.12 shows the averaged depth profiles of PR in the skin.

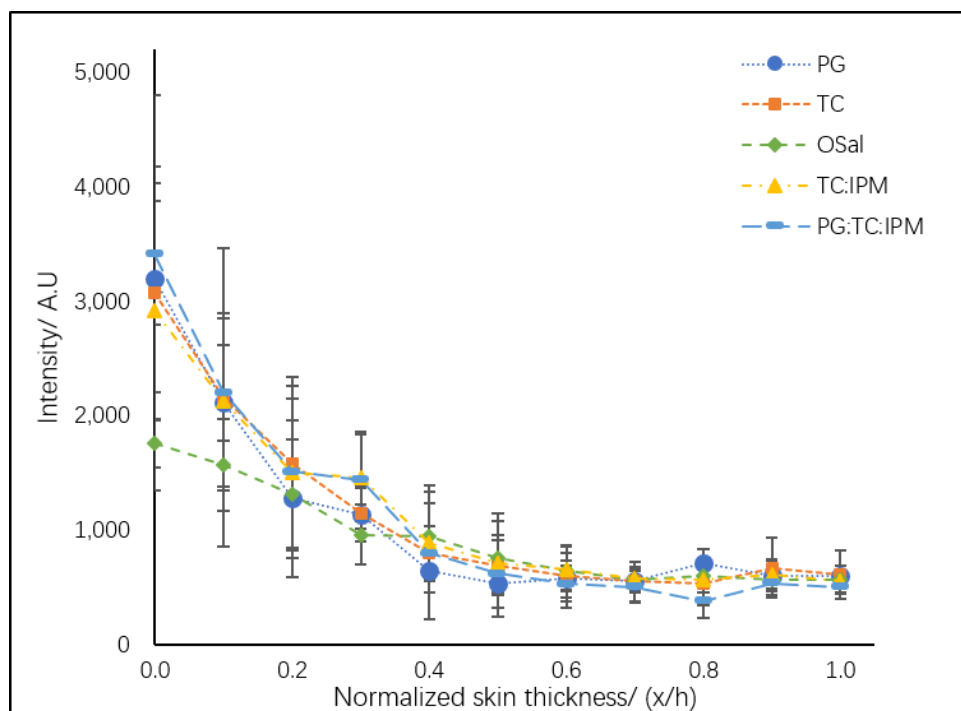


Figure 6.12 PR depth profiles in the skin 1 h post application of five systems, namely PG, TC, OSaI, TC:IPM (50:50) and PG:TC:IPM (50:25:25). (mean \pm SD, n=6).

For the five PR systems, there was no significant difference for the signal intensity of PR at each normalized skin depth interval ($p > 0.05$). For PR in neat PG, the intensity of PR measured at the skin surface ($x/h=0$) was significantly higher as compared to the intensity at $x/h=0.5$ ($p < 0.05$). Similarly, a greater intensity of PR from the neat OSaI solution was detected at the skin surface ($x/h=0$) than the intensity measured at $x/h=0.3$ ($p < 0.05$). AUC values were calculated for each volunteer and Fig 6.13 shows the averaged results of AUC and no significant difference was evident ($p > 0.05$).

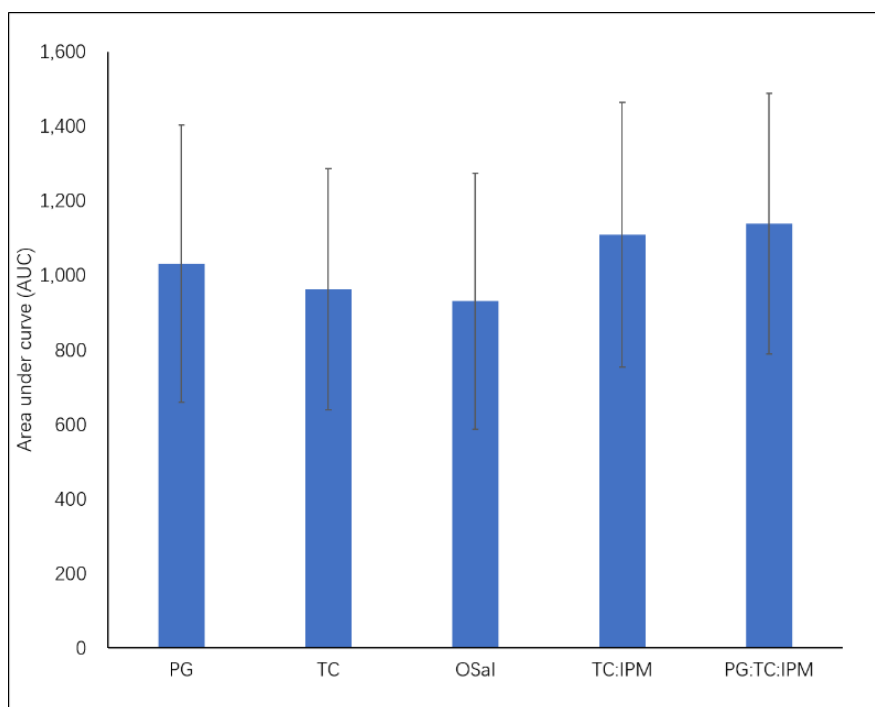


Figure 6. 13 Averaged AUC for PR depth profiles measured for each volunteer after application of five systems containing 5 % (w/v) of PR, namely neat PG, TC, OSaI, TC:IPM (50:50) and PG:TC:IPM (50:25:25) (mean \pm SD, $18 \leq n \leq 24$)

6.3.1.6 *In vivo* evaluation of solvents in PR formulations using CRS

The depth profiles of PG in the SC were determined using the reference spectra (Fig 6.14). The signals of both active and solvent decreased with the increase of SC depth. For PG, statistical analysis confirmed there was no difference for the signal intensity of PG measured at the $x/h = 0$ to $x/h = 0.6$ ($p > 0.05$). A higher intensity of PG was evident at the skin surface compared to $x/h = 0.7$ ($p < 0.05$).

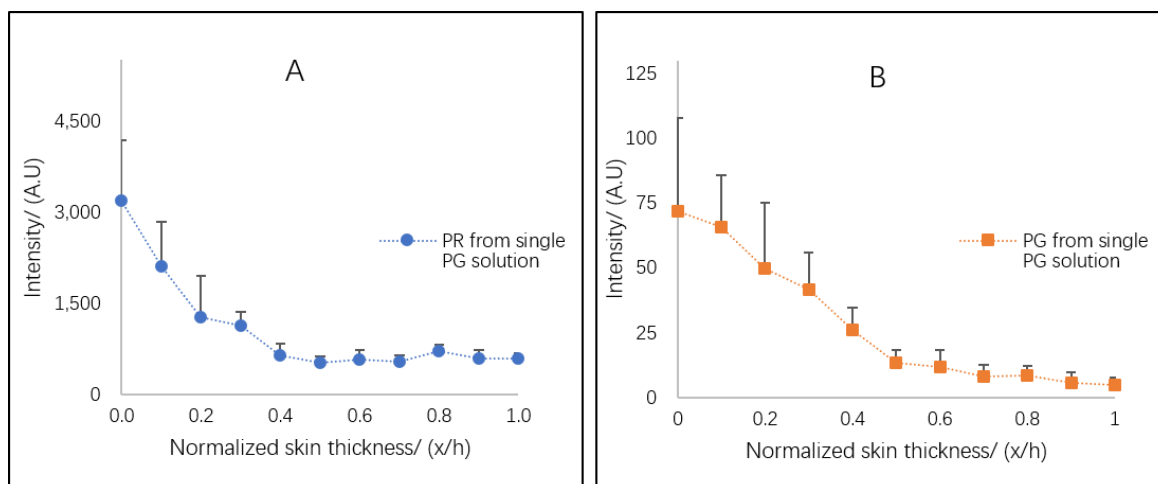


Figure 6. 14 The depth profile of PR (A) and PG (B) in the SC after application of PR in neat PG solutions.

The intensity of PR in the SC after the application of neat PG solution was plotted against the corresponding values of the solvent (Fig 6.15). A correlation coefficient (R^2) of 0.83 was determined for the signal intensity of PR and signal intensity of PG.

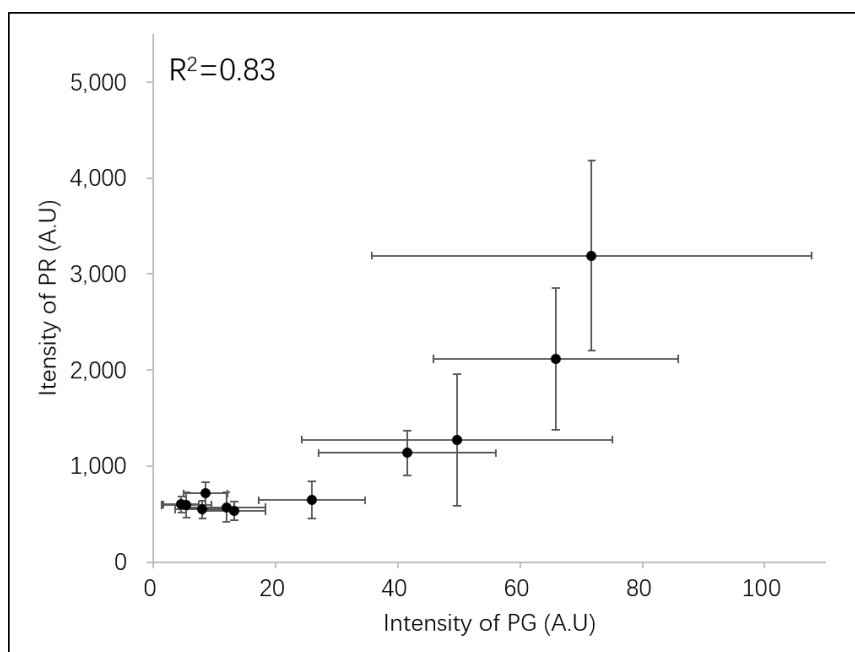


Figure 6. 15 Correlation between the signal intensity of PR and signal intensity of PG in the SC with depth ($x/h=1, 0.9, 0.8, 0.7, 0.6, 0.5, 0.4, 0.3, 0.2, 0.1$ and 0).

A similar correlation between the signal of PG and the permeant was also observed earlier for NIA (Fig 6.7). It is hypothesized that the permeants “tracked” the penetration of PG into the SC. Haque et al. (2017b) proposed a similar theory for *in vitro* permeation of PG

and anthramycin (ANT), where the author monitored the penetration behavior of both the active and solvent. It was reported that ANT was delivered through human skin with the active “tracking” the permeation of PG.

The permeation behavior of the solvent TC was also evaluated. Fig 6.16 illustrates the depth profiles of the solvent and active in the SC from neat TC solution. The signal intensity of TC was low, and no difference was observed between the intensity of TC measured at different SC depths ($p>0.05$). This result was consistent with the earlier findings for the NIA formulations.

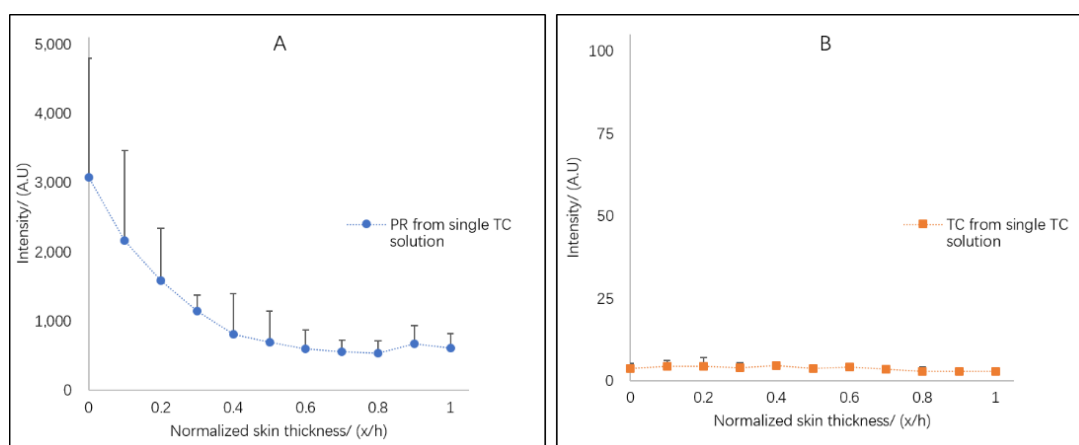


Figure 6. 16 The depth profiles of PR (A) and TC (B) in SC after the application of PR in neat TC solutions.

Fig 6.17 shows the depth profiles of PR and the solvent after the application of OSal formulations. At 1 h, OSal was detected in the SC (Fig 6.17B). OSal is a lipophilic solvent. Santos et al. (2012) investigated the effects of this solvent on the penetration enhancement of fentanyl with different concentrations of OSal. The authors found that a concentration of 25 % (v/v) OSal significantly improved drug delivery compared with the formulations containing 5 or 10 % OSal. The authors proposed that the increased permeability was caused by the solvent uptake in skin. It was also observed that OSal had a longer residence time in the skin than PG. This result was not observed in the present study, as only one sampling time point was monitored.

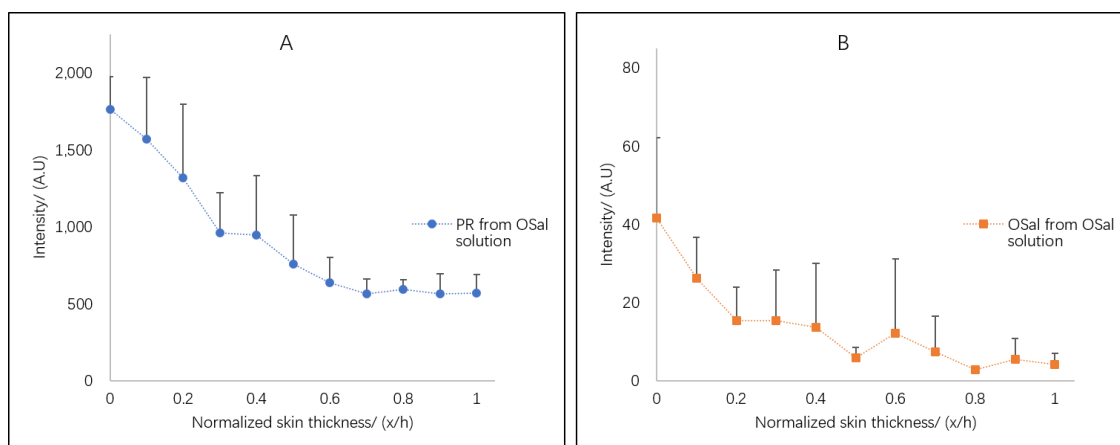


Figure 6. 17 The depth profile of PR (A) and OSal (B) in the SC after the application of neat OSal formulations (mean \pm SD, $n=6$).

The permeation behavior of TC from the binary TC-IPM systems was also monitored. The depth profile is shown in Fig 6.18. As shown in Fig 1.18B, the signal intensity of IPM decreased with the increase of SC depth. Interestingly, the depth profile of TC from the binary system was different from the results measured for the neat solution (Fig 6.18C).

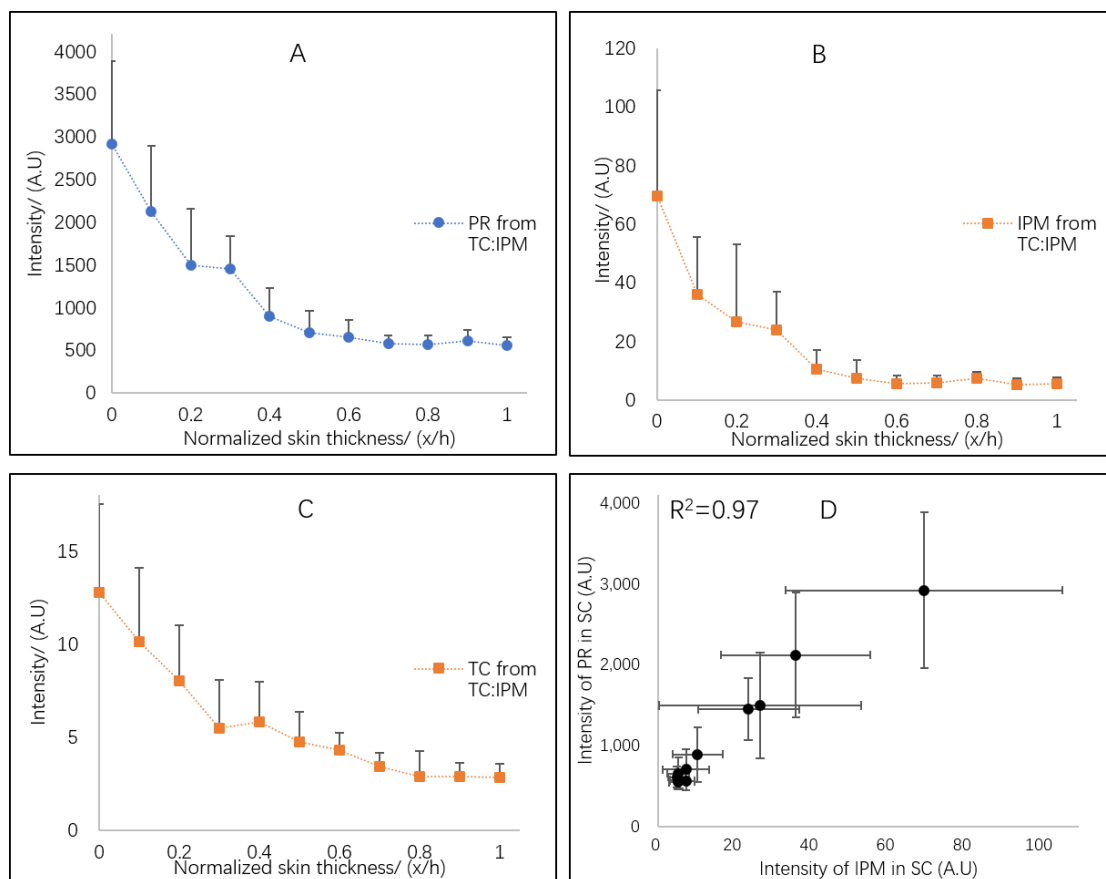


Figure 6.18 The depth profiles of PR (A), IPM (B) and TC (C) in the SC after the application of the TC-IPM system. Figure 6.17 (D) shows the correlation between the signal intensity of PR and signal intensity of IPM in the SC with depth ($x/h=1, 0.9, 0.8, 0.7, 0.6, 0.5, 0.4, 0.3, 0.2, 0.1$ and 0).

IPM is a fatty acid ester penetration enhancer with a $\text{Log}K_{\text{oct/wat}}$ value of 5.02 (Santos et al., 2012). On the other hand, the $\text{Log}K_{\text{oct/wat}}$ value of TC was reported to be -0.54 (Hansch, 1995). Based on the results observed for IPM and TC in this study, it could be proposed that the lipid environment was affected by IPM which leads to a decreased permeation of its cosolvent, TC. Furthermore, the residence time of TC could be extended by the attendance of IPM. The correlation between the signal intensity of IPM in the SC was compared with the corresponding signal intensity of PR at each normalized skin depth interval (Fig 1.17D). A correlation was evident between PR and IPM with a coefficient of 0.97 (R^2).

Solvent penetration was also evaluated for the ternary PG:TC:IPM (50:25:25) system (Fig 6.19). The depth profile of PG from the ternary system is different from the result obtained for the single solvent system (Fig 6.14B). A low value of signal intensity was observed at the

skin surface ($x/h=0$) and this could be indicative of depletion of the formulation (Fig 6.19B). As for the results obtained for the binary system, an excellent agreement between the signal intensity of PR and IPM was evident ($R^2=0.99$).

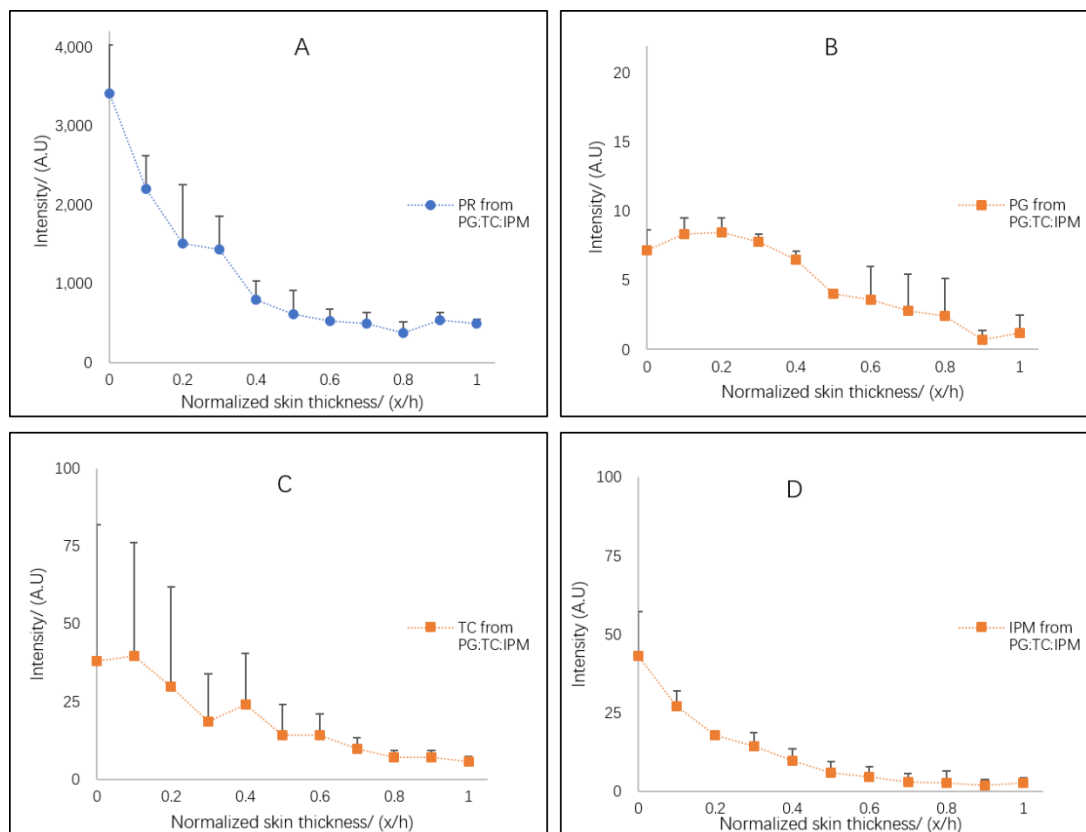


Figure 6. 19 The depth profiles of PR (A), PG (B), TC (C) and IPM (D) in the SC after application of the PG-TC-IPM system.

6.3.2 Tape stripping studies

6.3.2.1 Stratum corneum thickness

The inverse TEWL values were plotted against the cumulative protein content in Fig 6.20. The theoretical total protein content in the SC was determined. Accordingly, the total protein amount in the SC on the tested volar forearm site was determined as $790.5 \mu\text{g cm}^{-2}$ which corresponds to an estimated thickness of $15.0 \mu\text{m}$ (Boncheva et al., 2009; Guneri et al., 2018). The determined SC thickness fell in the range of the SC thickness obtained in the CRS studies (Session C.6.3.1.2). 15 tape strips only removed a thickness of $3.7 \mu\text{m}$ SC, corresponding to

0.24 of normalized skin thickness (x/h).

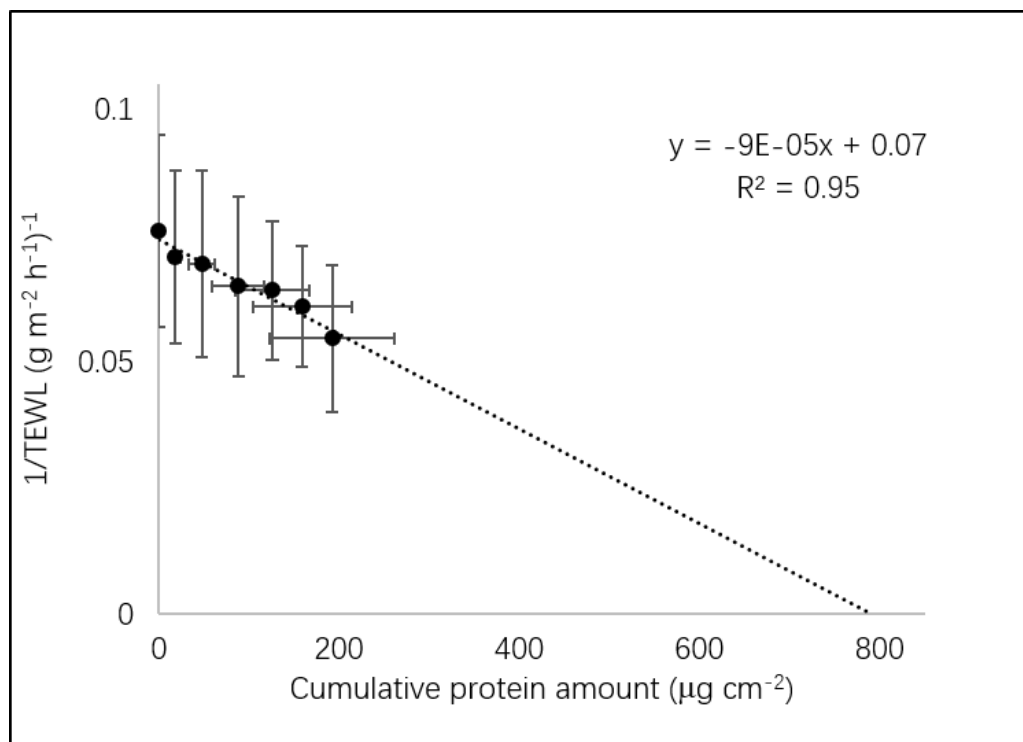


Figure 6. 20 Determination of the theoretical SC thickness. The total amount of SC protein content can be determined at the x-intercept. The estimated SC protein content was $790.5 \mu\text{g cm}^{-2}$ (mean \pm SD, n=12)

6.3.2.2 *In vivo* permeation of NIA evaluated using tape stripping

The penetration of NIA from neat PG and neat TC solutions, binary PG-OA and PG-LA systems and the ternary TC-CCT-DMI system was evaluated using tape stripping. The depth profiles of NIA in the SC are shown in Fig 6.21. In general, higher amounts of NIA were collected from the upper layers of the SC. For PG:OA (10:90), $20.7 \pm 6.1 \mu\text{g/cm}^2$ of NIA was recovered from the first tape strip ($x/h=0.02$), which was significantly higher compared with the amount of NIA recovered for TC and CCT:TC:DMI (50:25:25) ($p<0.05$). No significant difference was evident between the amount of NIA recovered from any depth intervals for the two binary systems composed of PG and fatty acids, PG:OA (10:90) and PG:LA (50:50) ($p>0.05$). Higher amounts of NIA were extracted from the second and the third tape strips ($x/h= 0.04, 0.06$) for PG:OA (10:90) compared with TC ($p<0.05$), and no statistical difference was evident comparing the amounts of NIA delivered into any deeper layers of the SC ($x/h =$

0.08 – 0.24) ($p>0.05$).

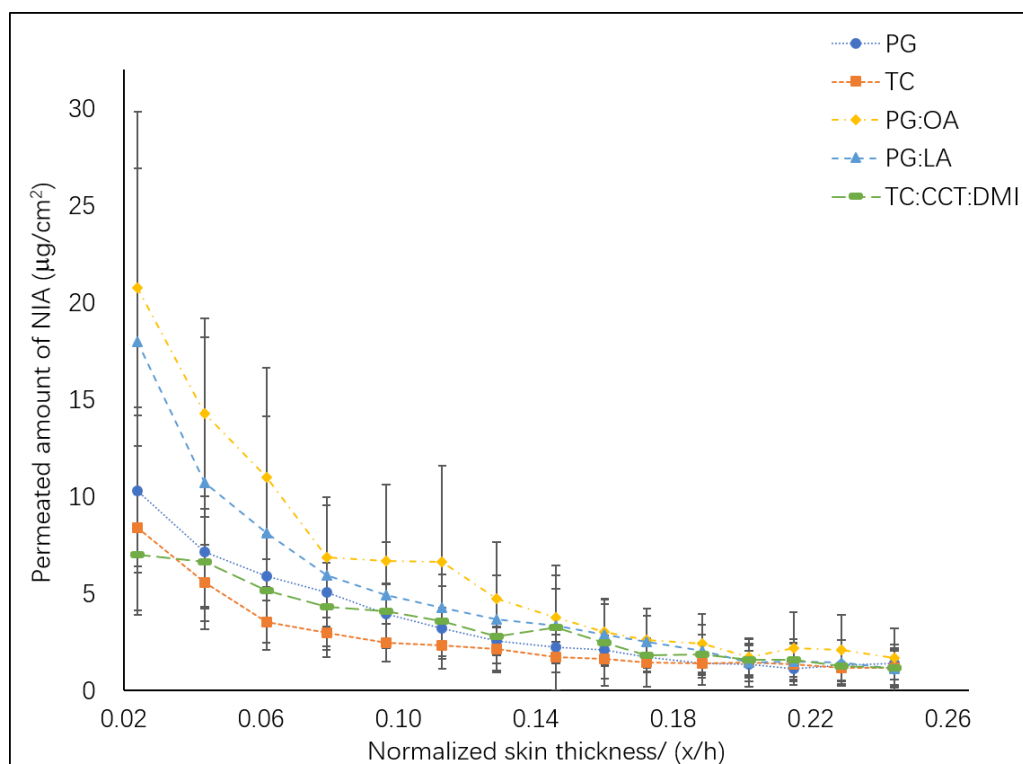


Figure 6. 21 Depth profiles of NIA in the SC after application of PG, TC, PG:OA (10:90), PG:LA (50:50) and TC:CCT:DMI (50:25:25) evaluated using tape stripping.

The area under the curve was calculated for the depth profiles of NIA determined using tape stripping for each volunteer. Fig 6.22 shows the averaged values of the AUC calculated for the five assessed systems. Although high values were observed for PG:OA (10:90) and PG:LA (50:50), statistical analysis confirmed there was no significant difference among the AUC values obtained for all assessed systems ($p>0.05$).

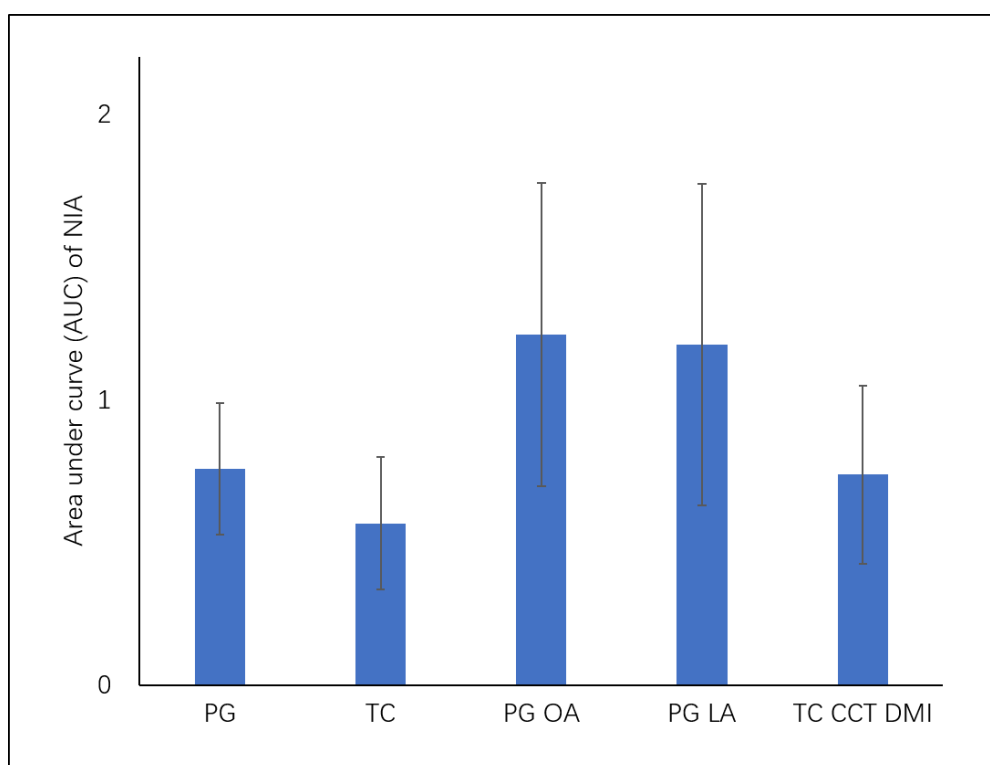


Figure 6. 22 Averaged AUC values for NIA depth profiles measured in tape stripping studies (mean \pm SD, n=6)

6.3.2.3 *In vivo* permeation of PR evaluated using tape stripping

The *in vivo* penetration of PR from five delivery systems was determined using tape stripping. Fig 6.23 shows the depth profiles of PR in the SC after 1 h of formulation application. As for the results observed for NIA, the amounts of PR recovered from tape strips decreased as a function of the depth. For the five assessed systems, the amounts of PR recovered from the first tape strip ranged from 8.1 to 11.2 $\mu\text{g}/\text{cm}^2$ ($p>0.05$) and the amounts ranged from 3.9 to 6.6 $\mu\text{g}/\text{cm}^2$ for the second tape strip ($p>0.05$).

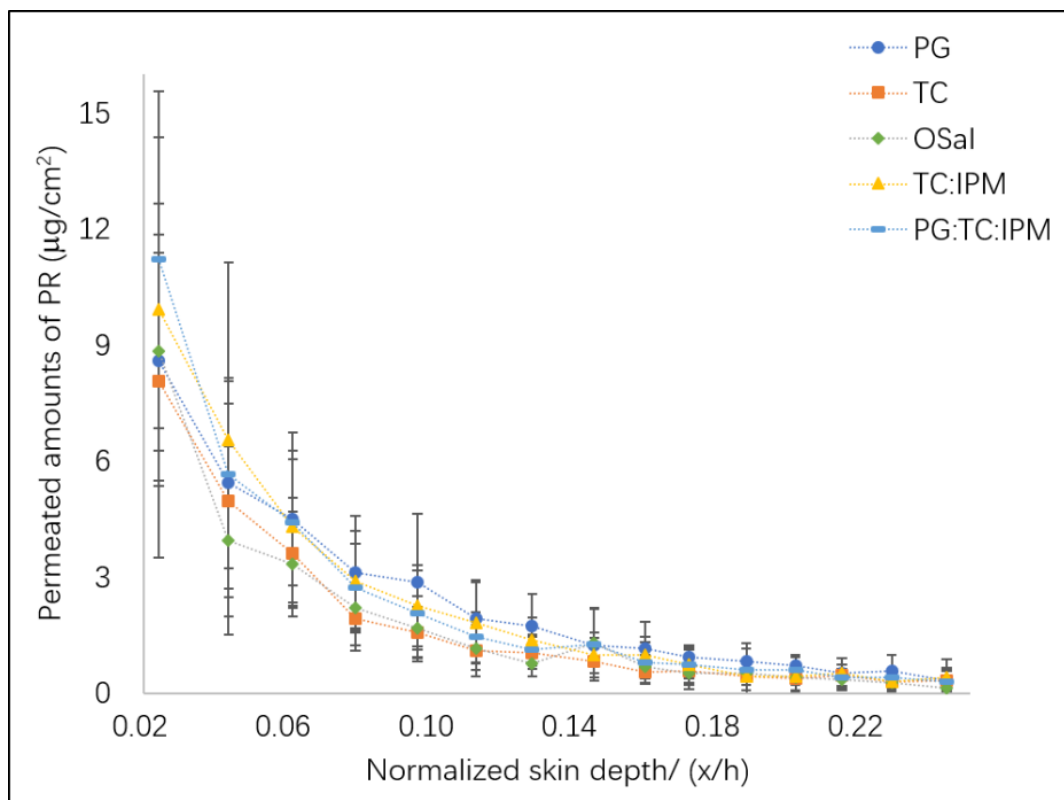


Figure 6.23 Depth profiles of PR in the SC after application in PG, TC, OSaI, TC:IPM (50:50) and PG:TC:IPM (50:25:25) evaluated using tape stripping.

The area under the curve was calculated for each volunteer and Fig 6.24 summarizes the average values. The AUC values determined for the binary TC-IPM and ternary PG-TC-IPM systems were greater compared with the corresponding values for OSaI ($p < 0.05$).

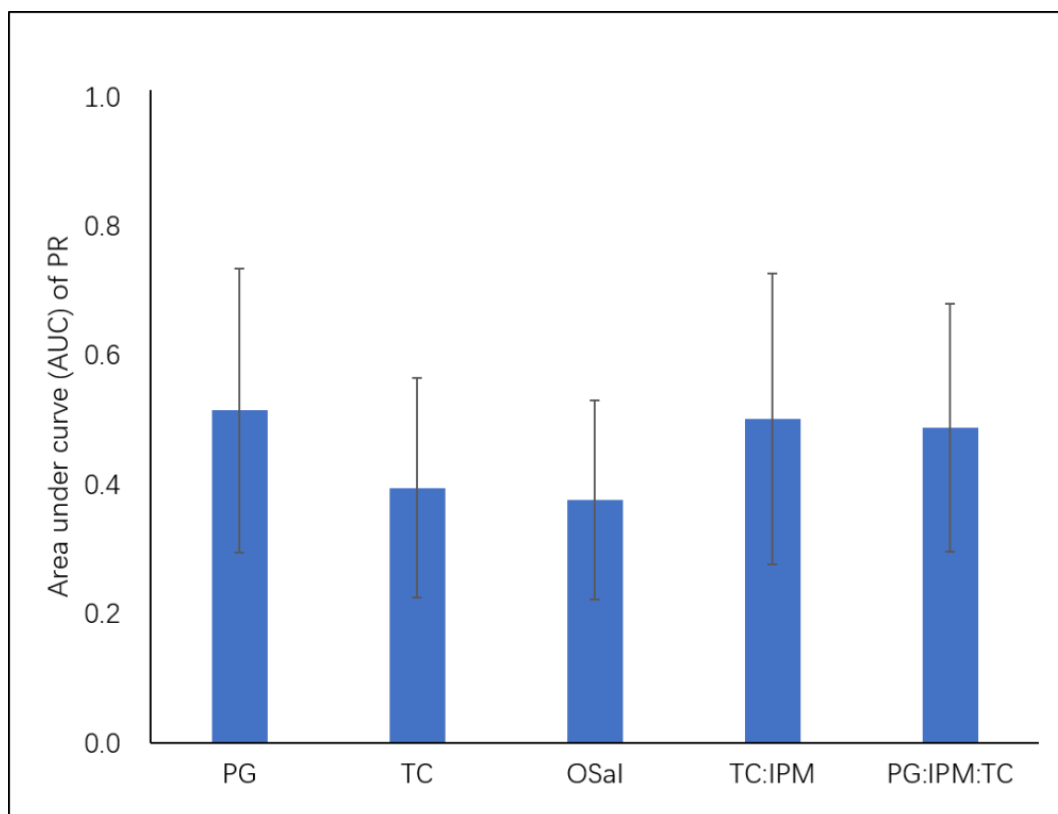


Figure 6. 24 Averaged AUC values for PR depth profiles measured in tape stripping studies (mean \pm SD, n=6)

6.3.3 *In vivo* - *in vitro* correlation in skin permeation

The correlation between *in vitro* permeation studies using human skin and *in vivo* topical delivery of NIA was investigated. The area under the curve (AUC) of each CRS depth profile was plotted against the *in vitro* cumulative permeation of NIA in heat separated human epidermis at 24 h (Fig 6.25A). The correlation coefficient was determined (R^2) as 0.84. The AUC values for NIA depth profiles determined in tape stripping studies are plotted against the cumulative amounts permeated of NIA in Fig 6.25B and the correlation coefficient (R^2) was determined as 0.86. The finding is in agreement with the results published by Mohammed et al. (2014b). The authors investigated the *in vivo* permeation behavior of NIA using CRS on one human volunteer. The signal intensity obtained for NIA in the SC at 4 μm *in vivo* was correlated with the *in vitro* flux of NIA under infinite dose conditions, and the R^2 was reported as 0.96. As *in vitro* permeation studies were conducted under finite dose conditions in this work, the cumulative amount permeated at 24 h instead

of flux values was selected as the indicator of the ability of the formulation to deliver NIA. As the CRS depth profile of NIA determined for PG:LA (50:50) reflected possible depletion of the formulations, the AUC value of PG:LA (50:50) determined after 1 h of treatment may have been underestimated. This is the limitation caused by only monitoring one time point for NIA penetration. Multiple sampling times could be considered in future studies.

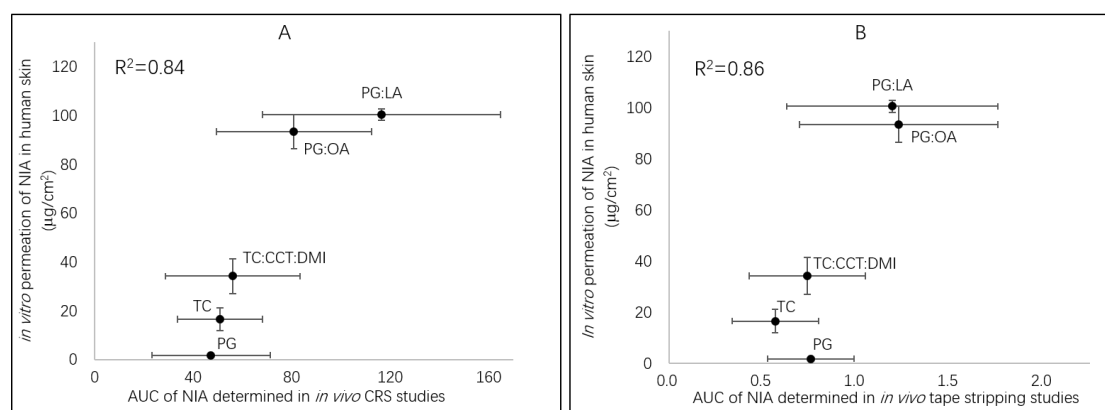


Figure 6.25 (A) Correlation of the *in vivo* area under curve (AUC) of the depth profiles determined in CRS studies and *in vitro* cumulative permeation of NIA at 24 h in human skin ($R^2=0.84$). (B) Correlation of the *in vivo* AUC values of the depth profiles determined in tape stripping studies and *in vitro* cumulative permeation of NIA at 24 h in human skin ($R^2=0.86$). (mean \pm SD, $4 \leq n \leq 24$)

As for the results observed for PR, although attempts were made to determine the R^2 for *in vivo* data and corresponding cumulative permeation at 24 h in *in vitro* human skin, no correlation was observed. As shown in Fig 6.26, the results of PR delivered by OSal using *in vivo* assessment were not in agreement with the results obtained *in vitro*. The mechanism of skin penetration enhancement of OSal is not fully understood (Lane, 2013). Walters et al. (1997) reported the low human skin permeability of OSal. The authors have reported 0.6 % absorption of OSal at 24 h following the application of $5 \mu\text{L}/\text{cm}^2$ of an ethanol solution containing 5 % (w/w) of OSal. The results observed in the CRS study suggested that OSal permeated into the SC at 1 h (Fig 6.15). OSal demonstrated promising potential in dermal delivery in earlier *in vitro* permeation studies in porcine skin and human epidermis under varying dose conditions (Chapter 3). *In vitro* human skin penetration of PR from the OSal formulation was detectable from 4 h after application. However, the low permeation of PR observed in the present *in vivo* studies suggested the enhancement action of OSal was not

evident at 1 h. Longer intervals should be considered to understand the role of OSal in skin permeation enhancement. Excluding the results of OSal, the *in vivo-in vitro* correlation (R^2) was determined as 0.62 for CRS studies and 0.68 for tape stripping studies (data not shown).

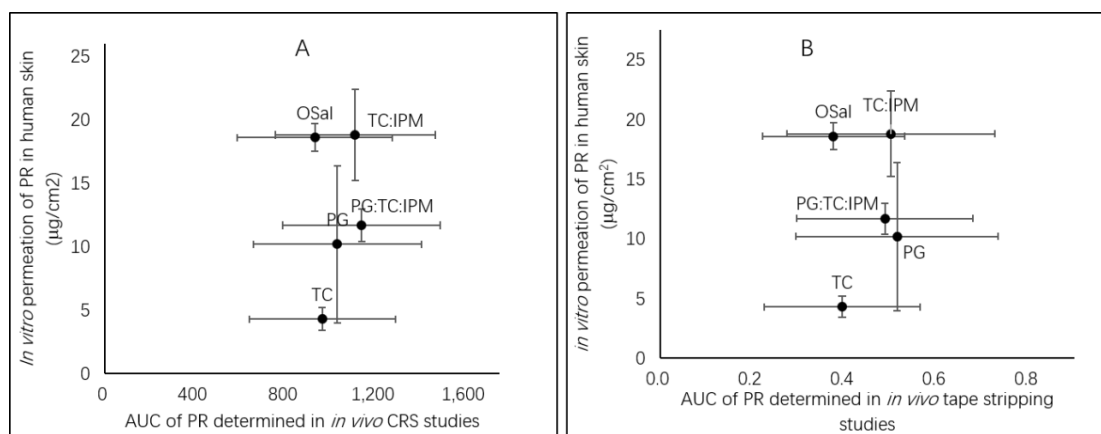


Figure 6. 26 The *in vitro* permeation data of PR plotted against the AUC values of the depth profiles determined in CRS studies (A) and in tape stripping studies (B) *in vivo*. (mean \pm SD, $4 \leq n \leq 24$)

On the other hand, a correlation between the data obtained in the two *in vivo* studies was observed. The measured penetration depths differed for these two techniques (Fig 6.12 and 6.23). However, when the AUC values obtained in CRS studies were plotted against the corresponding AUC values obtained in tape stripping studies, a correlation of 0.68 (R^2) was determined (Fig 6.27). The result was in line with the correlation observed for NIA, an R^2 value of 0.72 was calculated for the data obtained in CRS studies and tape stripping studies (data not shown). Tape stripping is one of the permeation kinetics studies considered appropriate for equivalence testing (Wiedersberg and Nicoli, 2012). The correlation observed here supports the feasibility of CRS for *in vivo* assessment of skin delivery from topical formulations.

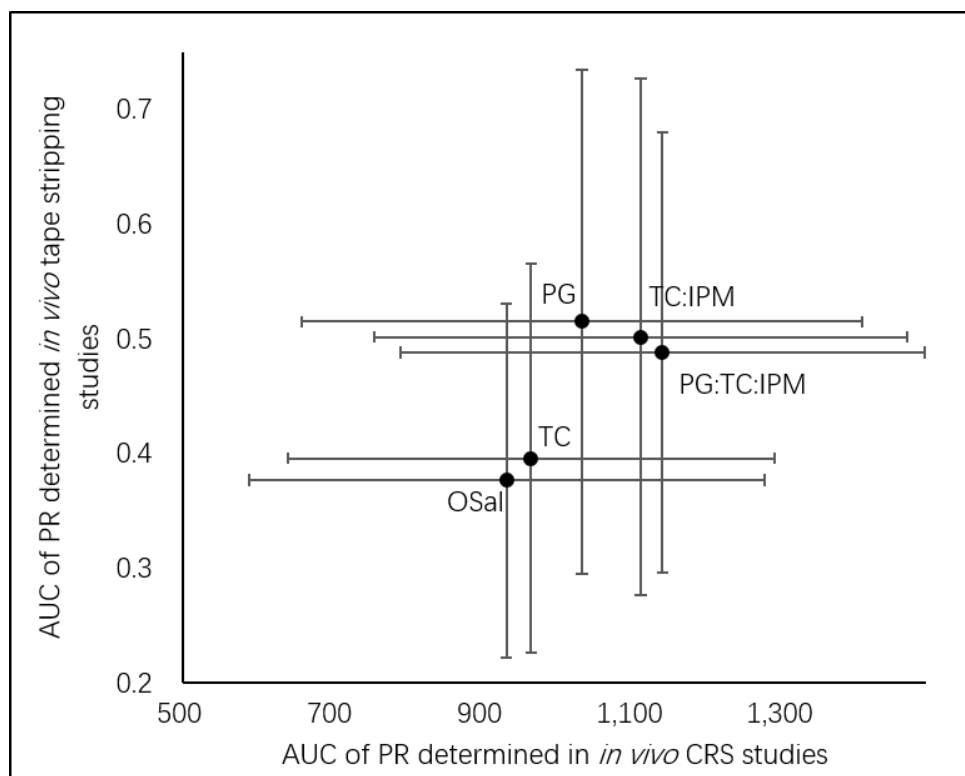


Figure 6. 27 The AUC values of PR determined in *in vivo* CRS studies plotted against the data determined in *in vivo* tape stripping studies ($R^2=0.68$) (mean \pm SD, $6 \leq n \leq 24$).

6.4 Conclusions

The solvents investigated in the present work have been studied extensively as skin penetration enhancers in topical and transdermal products. For the five NIA formulations examined in CRS studies, similar depth profiles of NIA were observed for neat PG and neat TC solutions. PG and TC were both taken up by the skin at 1 h, but different depth profiles were determined. There was a good correlation between the signal intensity of PG and NIA was observed at each depth interval. However, rapid penetration of TC was evident for both single TC and ternary TC-CCT-DMI systems. For the two binary systems combining PG and fatty acids, the depth profiles determined in CRS studies indicated the penetration of NIA was promoted compared to other systems. For the five assessed NIA formulations, the *in vivo* data correlated very well with *in vitro* human skin permeation data.

As for the results obtained in PR studies, the rapid permeation of TC was also observed after the application of single TC solutions. The results for the ternary PG-TC-IPM system suggested that IPM affects the lipid environment in the SC and extends the residence time of

TC in the skin. The PR penetration enhancement of OSal was not clearly observed at 1 h. Longer *in vivo* experimental time points are needed to fully explore the influence of OSal on skin permeation. Chemical penetration enhancers modulate skin permeation by changing the partition of the substance into, and/or diffusion through the skin membrane (Wiechers et al., 2004; Lane, 2013). It is crucial to understand how penetration enhancers act within the skin. The CRS technique allows monitoring of the active as well as the solvents. A suitable Raman signal and intensity are required for investigated actives and solvents.

Tape stripping experiments were performed to evaluate the efficacy of the same NIA and PR systems investigated using CRS. TEWL measurements were performed to determine the SC thickness. The averaged SC thickness was determined as 15.0 μm , and the value was consistent with the results determined using CRS. The results for NIA obtained in the tape stripping studies correlated well with the *in vitro* permeation data. As for the five PR formulations investigated using tape stripping, agreement of *in vivo* and *in vitro* permeation data was lacking. The results for PR suggested multiple sampling time points are necessary to further monitor the penetration behavior of OSal *in vivo*.

To conclude, the *in vivo-in vitro* correlation observed here shows both CRS and tape stripping could serve as suitable methods for measuring dermal formulation efficacy. CRS is a non-invasive and highly efficient technique. Application of this technique could facilitate the investigation of skin delivery and would generate great benefits for researchers, scientists, government, patients and consumers.

Chapter 7.

Conclusions and future work

7.1 Conclusions

This work focuses on the rational design of topical delivery systems containing different model actives. The two model actives, NIA and PR, have different physicochemical properties. Both actives are suitable for dermal delivery. The benefits of their dermal application have been reported and rational formulations are desirable to improve the skin delivery of NIA and PR. Human skin is considered as the “gold standard” when evaluating formulation efficacy *in vitro*. However, there are issues regarding difficulty of sourcing and laboratory conditions restricting the application of human skin. Therefore, the feasibility of a possible surrogate, the Skin PAMPA model for prediction of human skin permeability was also investigated.

The development and validation of the analytical method of NIA was included in Chapter 2. Solubility of NIA in a series of solvents were investigated with the use of the solubility parameter. Followed by the stability studies, permeation studies of NIA were initially performed in full thickness porcine skin and heat separated human epidermis under two dosing conditions, an infinite dose ($50 \mu\text{L}/\text{cm}^2$) and a finite dose ($5 \mu\text{L}/\text{cm}^2$) using various single solvents. NIA solutions were then evaluated using the Skin PAMPA models. The permeation studies were first conducted up to 6 h for three different doses, corresponding to 3, 51 and $90 \mu\text{L}/\text{cm}^2$. Subsequently, the Skin PAMPA experimental time period was identified as 2.5 h, and the application of $3 \mu\text{L}/\text{cm}^2$ was confirmed to match the intended clinical dosage application. Of all the vehicles, high permeation of NIA was observed for t-butyl alcohol (T-BA) in human skin. A linear correlation ($R^2=0.71$) between the Skin PAMPA model and human skin was observed for the cumulative amount of NIA that permeated under finite dose condition. These results highlight the potential of the Skin PAMPA model as a screening tool for simple solution formulations containing NIA.

A comprehensive characterization of PR was included in Chapter 3. The melting point of PR was determined using differential scanning calorimetry (DSC) and thermogravimetric analysis (TGA) as 79.13°C . The measured log P (octanol water partition coefficient) at 21°C was 3.35 ± 0.03 . A new HPLC method was developed and validated, and the solubility studies were conducted with the use of the solubility parameter. The 72 h stability of PR in

TC, IPM, PG, OSaI, DMI, glycerol, PEG400 and the receptor medium PBS were confirmed. The dermal delivery of PR from selected single solvents was measured in porcine skin under both infinite and finite dose conditions. The effects of solvents on dermal delivery of PR were evaluated using human skin ($5 \mu\text{L}/\text{cm}^2$) and the Skin PAMPA model (3, 50 and $90 \mu\text{L}/\text{cm}^2$). OSaI emerged as the most efficient solvent for PR delivery to human skin compared with other solvents ($p < 0.05$). A linear correlation ($R^2 = 0.70$) was observed between the permeation data obtained in the Skin PAMPA model and human skin under finite dose conditions.

The model active NIA was formulated in binary and ternary solvent systems in Chapter 4 using a rational formulation design strategy. The effects of solvent combination on the distribution of the active in the skin were investigated using porcine skin, heat separated human epidermis and the Skin PAMPA model. A positive synergistic effect on NIA delivery was evident for the systems composed of PG and fatty acids (PG-OA and PG-LA) in human skin. However, no significant enhancement of NIA delivery by the PG-fatty acid systems was observed in the Skin PAMPA model. Therefore, Skin PAMPA model may not be suitable for screening formulations containing fatty acids. A good correlation ($R^2 = 0.70$) was obtained for permeation data from the Skin PAMPA and porcine skin. However, data from the Skin PAMPA model and from human epidermis could only be correlated when the PG-fatty acid systems were excluded. The two PG-fatty acid binary systems and one ternary TC-CCT-DMI system were selected for further *in vivo* evaluation.

The model active PR was formulated in binary and ternary solvent systems in Chapter 5. The formulation efficacy was evaluated in porcine skin, human epidermis and the Skin PAMPA model. The combination of TC:IPM (50:50) was identified as the most efficient binary system ($p < 0.05$), while no significant difference was evident between TC-IPM and neat OSaI ($p > 0.05$). No correlation was observed for permeation data of PR in the Skin PAMPA model and mammalian skin. PG:TC:IPM (50:25:25) system delivered the highest amount of PR among the three assessed ternary solvent systems. The binary TC-IPM and ternary PG-TC-IPM systems were taken forward for *in vivo* evaluation.

In vivo assessment of formulation efficacy involving 12 healthy human volunteers was described in Chapter 6. The effect of solvents on the distribution of active in the SC under

finite dose conditions ($2.6 \mu\text{L}/\text{cm}^2$) was measured using two techniques, tape stripping and CRS. In this work, monitoring of the solvents and the actives in the SC was conducted using CRS. Permeation of NIA was observed 1 h after the application of NIA in neat PG and neat TC solutions. A good correlation between the signal intensity of PG and the intensity of NIA was observed at all measured depth intervals in CRS studies. Rapid penetration of TC was evident for both single TC and ternary TC-CCT-DMI systems. A good correlation was observed for the *in vivo* CRS AUC values and the values for cumulative permeation of NIA obtained from *in vitro* human skin permeation studies ($R^2=0.84$).

Rapid penetration of TC was also observed in the CRS study after the application of PR in neat TC solutions. It was proposed that the application of IPM could lead to changes of the lipid environment in the SC and extend the residence time of TC in the skin. No penetration enhancement of PR was observed for OSal and no *in vivo-in vitro* correlation in skin permeation of PR could be determined.

Subsequently, the formulations were assessed using the tape stripping technique. In tape stripping studies, the average SC thickness was determined as $15.0 \mu\text{m}$. This value was consistent with the results obtained in CRS studies (11.6 to $24.6 \mu\text{m}$, with a $4.2 \mu\text{m}$ SD value at most for any subject). In this part of the work, 15 adhesive tapes removed 24 % of the total SC. Therefore, only actives distributed in the upper layer of SC were recovered using tape stripping. Statistical analysis confirmed no significant difference was obtained for all assessed NIA systems in tape stripping studies. The *in vivo* AUC values determined in tape stripping studies also correlated well with the *in vitro* permeated amounts of NIA ($R^2=0.86$). As for the investigation of PR formulations, statistical analysis confirmed there was no significant difference for the five assessed systems in tape stripping studies. Although no *in vivo-in vitro* correlation was observed, a correlation between the AUC values of PR depth profiles using tape stripping and CRS techniques was established ($R^2=0.68$). OSal was confirmed as a promising solvent for dermal delivery of PR in *in vitro* assessments, while no permeation enhancement was observed at 1 h post application *in vivo*. The results suggest longer intervals should be considered to fully understand the role of OSal *in vivo*. These results confirmed that CRS and tape stripping could serve as suitable methods for assessment of

dermal formulation efficacy. CRS is a non-invasive and efficient technique as no additional collection procedures of SC layers are required. Therefore, any further application of this technique should potentially deliver great benefits to the researcher, scientists, government, patients and consumers.

7.2 Future work

In Chapter 2 and Chapter 4, the Skin PAMPA model was confirmed as a useful screening tool for topical formulations of NIA. However, the skin penetration enhancement of formulations containing fatty acids was not observed in the Skin PAMPA model. The proposed potential interaction between the Skin PAMPA membrane and the fatty acids OA and LA will be probed in future studies. In Chapter 3, a correlation of PR permeation from single solvent systems in the Skin PAMPA model and *in vitro* human epidermis was established. However, no correlation was observed for the permeation of PR from binary and ternary solvent systems. It was hypothesized that the Skin PAMPA model could be more suitable in screening of hydrophilic compounds than lipophilic compounds. A wider range of substances with varying physicochemical properties should be investigated to probe this hypothesis.

In Chapter 6, various formulations containing PR or NIA were tested *in vivo* on human volunteers. *In vivo* – *in vitro* correlation in NIA skin permeation was observed. However, the depth profiles of NIA after application of the two binary systems PG-OA, PG-LA indicated that the diffusion of NIA is increased to the extent that steady state is reached. These results suggested that some applied NIA has passed through the SC. The AUC values calculated from the depth profiles of NIA in the SC recorded at 1 h may have been underestimated. Therefore, consistent measurement of NIA after application up to 2 h using the CRS technique will be considered. For the tape stripping studies, the formulations should be compared at different time points. More detailed studies comparing both CRS and tape stripping with other actives would add further value to the use of CRS as a tool to probe percutaneous absorption.

Appendices

Appendix 1. TEWL measurement of porcine skin after the application of T-BA

Of all the vehicles, and for all models examined, a significantly higher amount of NIA was delivered by t-butyl alcohol (T-BA). There is limited information about the action of T-BA in skin penetration enhancement. The TEWL of porcine skin was measured after the application of T-BA.

Fresh porcine skin was used as the model membrane. After skin preparation, Franz diffusion cells were set up and maintained following the procedure described in Chapter 2. The initial porcine skin integrity was confirmed by electrical resistance testing. The TEWL values were measured at 0, 1, 2, 15, 21 and 24 h after the application of formulations. 20 μ L of T-BA solvent was applied on the skin surface for the test group, and no application was performed for the Franz cells in the control group. The differences between the measured TEWL readings at different time intervals and the TEWL reading at time 0 were calculated. Fig A1.1 shows the results. For the skin treated with T-BA, low values of TEWL were observed at 1 and 2 h compared with the TEWL value at time 0, while no significant difference was evident ($p>0.05$). Low TEWL values were observed at 1 and 2 h after the application of T-BA compared with the initial TEWL reading at time 0, while no significant difference was evident ($p>0.05$). This may reflect skin dehydration caused by evaporation of T-BA. At 18 h, a lower TEWL value was evident for skin treated with T-BA compared with the control group ($p<0.05$). Statistical analysis confirmed no significant difference was evident for the TEWL values between T-BA and the control group at 21 and 24 h ($p>0.05$).

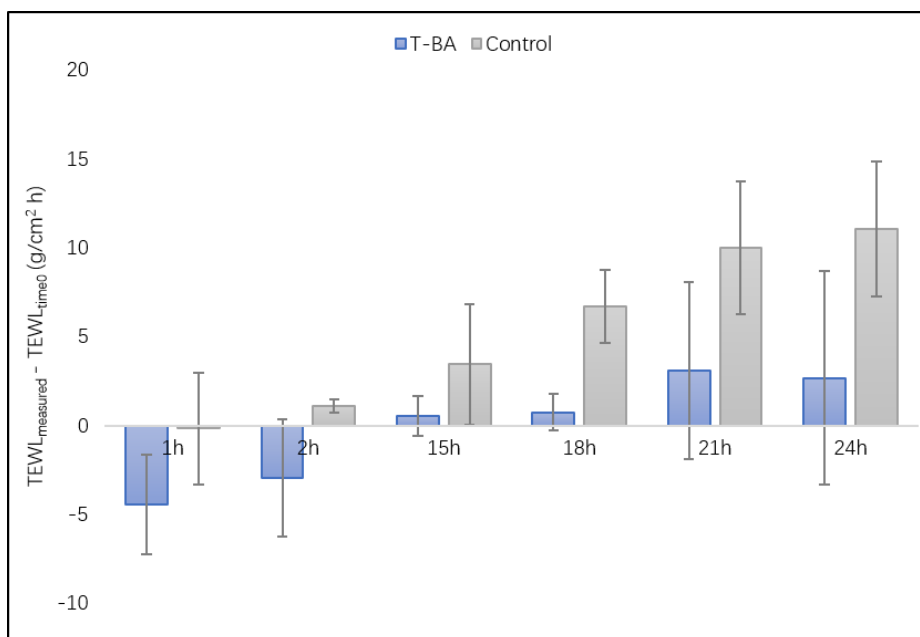


Figure A1.1 The differences between the TEWL values measured at different intervals and the TEWL values measured at time 0 (mean \pm SD, $n=3$).

Appendix 2. DVS measurement of TC under infinite dose conditions

To investigate the evaporation of TC under infinite dose conditions, the DVS measurement of neat TC solvent was performed following the application of 50 μL for 24 h at $32 \pm 1^\circ\text{C}$ and 50 % RH. Fig A2.1 shows the results. The initial increase in mass could be explained by the hygroscopic nature of TC. At 24h, 80.7 ± 0.5 % of the applied TC solvent was recovered.

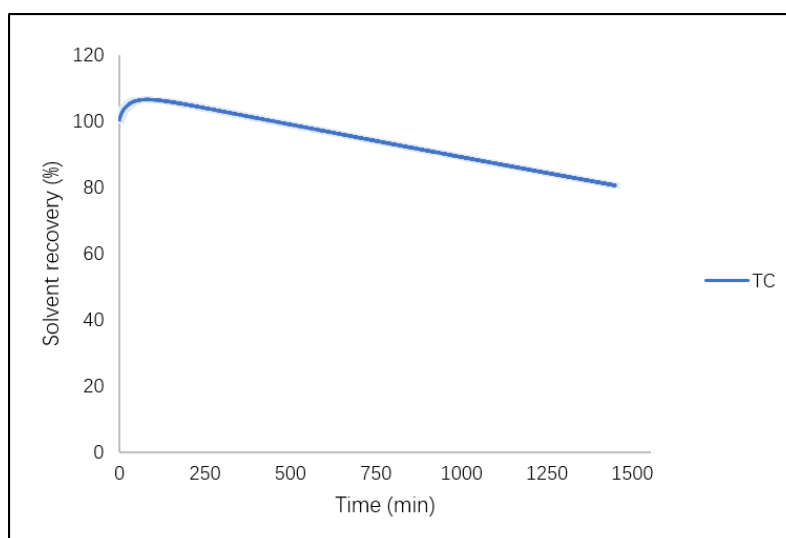


Figure A2.1 Percentage weight loss over 1440 min (24 h) for neat TC solvent ($n=3$, mean \pm SD).

Appendix 3. Miscibility determination of binary and ternary vehicle systems

The miscibility studies of varying vehicles were performed prior to optional formulation development. Miscibility studies of binary solvents were conducted in the ratios of 10:90, 20:80, 30:70, 40:60, 50:50, 60:40, 70:30, 80:20 and 90:10. For ternary systems, three vehicles were mixed in different percentages (varying every 10 %). For each estimated system, an appropriate volume of vehicle was added to make up a final volume of 2 mL in glass specimen tubes. Glass tubes were manually mixed for 1 min and placed in an incubator held at 32 ± 1 °C overnight. The standards for the visual inspection of miscibility were as following. The tested vehicles were considered as miscible if a clear solution was evident; the tested vehicles were considered as immiscible if a cloudy emulsion or phase separation was observed. A ternary phase diagram was constructed using Origin[®] 8.0 software (OriginLab Cooperation, USA)

Table A 3.1 summarizes the miscibility results observed for binary solvent systems. The hydrophilic vehicle, TC, was miscible with all assessed vehicles in all ratios. The hydrophobic ingredients, CCT and Bosal were immiscible with PG and PEG 400 in all ratios. PG was miscible in OA only at the 10:90 ratio.

Table A3.1 Miscibility table of binary solvent systems

Binary solvent systems	Observation	Binary solvent systems	Observation	Binary solvent systems	Observation
PG:TC	M	TC:DMI	M	TC:T-BA	M
PG:DMI	M	TC:OSal	M	DMI:CCT	M
PG:LA	M	TC:CCT	M	DMI:OSal	M
PG:T-BA	M	TC:BG	M	DMI:T-BA	M
PG:PEG400	M	TC:PEG400	M	PEG400:OSal	IM
PG:OA	M/IM	TC:IPM	M	PEG400:IPM	IM
PG:CCT	IM	PG:OSal	IM	PEG400:CCT	IM

*M = miscible, **IM = immiscible, *** M/IM indicates that PG-OA were only miscible at 10:90 ratios.

To prepare ternary solvent formulations of NIA and PR, miscibility studies with ternary systems were conducted. The ternary solvent systems of TC-CCT-DMI and TC-PG-DMI were fully miscible at all mixed ratios. The phase diagrams indicate regions of miscibility and immiscibility of the ternary solvent systems of PG-TC-IPM (Fig A 3.1).

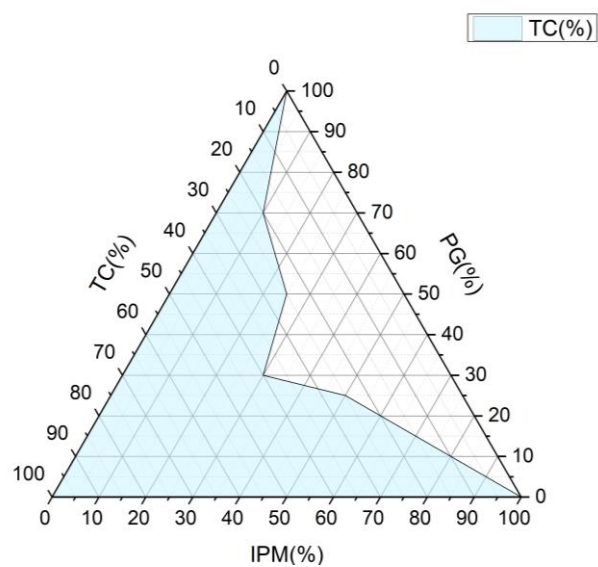


Figure A3.1 Ternary phase diagram for PG:TC:IPM. The light blue region indicates the miscible regions.

Appendix 4. Consent form used in the *in vivo* study

CONSENT FORM FOR VOLUNTEERS IN RESEARCH STUDIES

Please complete this form after you have read the Information Sheet and/or listened to an explanation about the research.

Title of Study:

The influence of excipients on transport of model compounds through human skin

Department:

School of Pharmacy

Name and Contact Details of the Researcher(s):

Yanling Zhang, email: yanling.zhang.15@ucl.ac.uk

Name and Contact Details of the Principal Researcher:

Dr. Majella Lane, email: m.lane@ucl.ac.uk

Contact Details of the UCL Data Protection Officer: data-protection@ucl.ac.uk

This study has been approved by the UCL Research Ethics Committee (Project ID number:13271/001). Thank you for considering taking part in this research. The person organising the research must explain the project to you before you agree to take part. If you have any questions arising from the Information Sheet or explanation already given to you, please ask the researcher before you decide whether to join in. You will be given a copy of this Consent Form to keep and refer to at any time.

I confirm that I understand that by ticking/initialling each box below I am consenting to this element of the study. I understand that it will be assumed that unticked/initialled boxes means that I DO NOT consent to that part of the study. I understand that by not giving consent for any one element that I may be deemed ineligible for the study.

		Tick Box
1.	*I confirm that I have read and understood the Information Sheet for the above study. I have had an opportunity to consider the information and what will be expected of me. I have also had the opportunity to ask questions which have been answered to my satisfaction and would like to take part in this <i>in vivo</i> study	
2.	*I understand that I will be able to withdraw my data at any stage during the course of the study	
3.	*I consent to the processing of my personal information (<i>age, email</i>) for	

	the purposes explained to me. I understand that such information will be handled in accordance with all applicable data protection legislation.	
4.	<p>Use of the information for this project only</p> <p>*I understand that all personal information will remain confidential and that all efforts will be made to ensure I cannot be identified</p> <p>I understand that my data gathered in this study will be stored anonymously and securely. It will not be possible to identify me in any publications.</p>	
5.	*I understand that my information may be subject to review by responsible individuals from the University (to include sponsors and funders) for monitoring and audit purposes.	
6.	*I understand that my participation is voluntary and that I am free to withdraw at any time without giving a reason, I understand that if I decide to withdraw, any personal data I have provided up to that point will be deleted unless I agree otherwise.	
7.	I understand the potential risks of participating and the support that will be available to me should I become distressed during the course of the research.	
8.	I understand the direct/indirect benefits of participating.	
9.	I understand that the data will not be made available to any commercial organisations but is solely the responsibility of the researcher(s) undertaking this study.	
10.	I understand that I will not benefit financially from this study or from any possible outcome it may result in in the future.	
11.	I agree that my research data may be used by others for future research. [No one will be able to identify you when this data is shared.]	
12.	I understand that the information I have submitted will be published as a poster or papers on science journals.	
13.	I hereby confirm that I understand the inclusion criteria as detailed in the Information Sheet and explained to me by the researcher.	
14.	<p>I hereby confirm that:</p> <p>(a) I understand the exclusion criteria as detailed in the Information Sheet and explained to me by the researcher; and</p> <p>(b) I do not fall under the exclusion criteria.</p>	

15.	I agree that my GP may be contacted if any unexpected results are found in relation to my health.	
16.	I have informed the researcher of any other research in which I am currently involved or have been involved in during the past 12 months.	
17.	I am aware of who I should contact if I wish to lodge a complaint.	
18.	I voluntarily agree to take part in this study.	
19.	<p>Use of information for this project and beyond</p> <p>I would be happy for the data I provide to be archived at papers on science journals.</p> <p>I understand that other authenticated researchers will have access to my anonymised data.</p>	

If you would like your contact details to be retained so that you can be contacted in the future by UCL researchers who would like to invite you to participate in follow up studies to this project, or in future studies of a similar nature, please tick the appropriate box below.

<input type="checkbox"/>	Yes, I would be happy to be contacted in this way	
<input type="checkbox"/>	No, I would not like to be contacted	

Name of participant

Date

Signature

Name of witness
(If applicable)

Date

Signature

Researcher

Date

Signature

References

- Abd, E., Yousef, S.A., Pastore, M.N., Telaprolu, K., Mohammed, Y.H., Namjoshi, S., Grice, J.E., Roberts, M.S., 2016. Skin models for the testing of transdermal drugs. *Clin. Pharmacol.* 8, 163-176.
- Albery, W., Hadgraft, J., 1979. Percutaneous absorption: in vivo experiments. *J. Pharm. Pharmacol.* 31, 140-147.
- Alkilani, A.Z., McCrudden, M.T.C., Donnelly, R.F., 2015. Transdermal Drug Delivery: Innovative Pharmaceutical Developments Based on Disruption of the Barrier Properties of the stratum corneum. *Pharmaceutics* 7, 438-470.
- Amnuakit, T., Limsuwan, T., Khongkow, P., Boonme, P., 2018. Vesicular carriers containing phenylethyl resorcinol for topical delivery system; liposomes, transfersomes and invasomes. *Asian J. Pharm. Sci.*
- Andersen, F.A., 1994. Final report on the safety assessment of propylene-glycol and polypropylene glycols. *J Am Coll Toxicol* 13, 437-491.
- Ando, H., Kondoh, H., Ichihashi, M., Hearing, V.J., 2007. Approaches to Identify Inhibitors of Melanin Biosynthesis via the Quality Control of Tyrosinase. *J. Invest. Dermatol.* 127, 751-761.
- Avdeef, A., Tsinman, O., 2006. PAMPA—a drug absorption in vitro model: 13. Chemical selectivity due to membrane hydrogen bonding: in combo comparisons of HDM-, DOPC-, and DS-PAMPA models. *Eur. J. Pharm. Sci.* 28, 43-50.
- Balazs, B., Vizserálek, G., Berkó, S., Budai-Szűcs, M., Kelemen, A., Sinkó, B., Takács-Novák, K., Szabó-Révész, P., Csányi, E., 2016. Investigation of the Efficacy of Transdermal Penetration Enhancers Through the Use of Human Skin and a Skin Mimic Artificial Membrane. *J. Pharm. Sci.* 105, 1134-1140.
- Barbero, A.M., Frasc, H.F., 2009. Pig and guinea pig skin as surrogates for human in vitro penetration studies: A quantitative review. *Toxicol. In Vitro* 23, 1-13.
- Barry, B.W., 1991. Lipid-Protein-Partitioning theory of skin penetration enhancement. *J. Control. Release* 15, 237-248.
- Barry, B.W., 2001. Novel mechanisms and devices to enable successful transdermal drug delivery. *Eur. J. Pharm. Sci.* 14, 101-114.
- Ben-Shabat, S., Baruch, N., Sintov, A.C., 2007. Conjugates of Unsaturated Fatty Acids with Propylene Glycol as Potentially Less-Irritant Skin Penetration Enhancers. *Drug Dev. Ind. Pharm.* 33, 1169-1175.
- Benson, H.A.E., 2005. Transdermal Drug Delivery: Penetration Enhancement Techniques. *Curr.*

Drug Deliv. 2, 23-33.

Benson, H.A.E., 2012. Skin Structure, Function, and Permeation, Topical and Transdermal Drug Delivery. John Wiley & Sons, Inc., pp. 1-22.

Bielfeldt, S., Schoder, V., Ely, U., Van Der Pol, A., De Sterke, J., Wilhelm, K.-P., 2009. Assessment of human stratum corneum thickness and its barrier properties by in-vivo confocal Raman spectroscopy. *Int. J. Cosmet. Sci.* 31, 479-480.

Binder, L., Kulovits, E.M., Petz, R., Ruthofer, J., Baurecht, D., Klang, V., Valenta, C., 2018. Penetration monitoring of drugs and additives by ATR-FTIR spectroscopy/tape stripping and confocal Raman spectroscopy – A comparative study. *Eur. J. Pharm. Biopharm.* 130, 214-223.

Bjorklund, S., Engblom, J., Thuresson, K., Sparr, E., 2013. Glycerol and urea can be used to increase skin permeability in reduced hydration conditions. *Eur. J. Pharm. Sci.* 50, 638-645.

Boncheva, M., De Sterke, J., Caspers, P.J., Puppels, G.J., 2009. Depth profiling of Stratum corneum hydration in vivo: a comparison between conductance and confocal Raman spectroscopic measurements. *Exp. Dermatol.* 18, 870-876.

Breternitz, M., Flach, M., Präßler, J., Elsner, P., Fluhr, J.W., 2007. Acute barrier disruption by adhesive tapes is influenced by pressure, time and anatomical location: integrity and cohesion assessed by sequential tape stripping; a randomized, controlled study. *Br. J. Dermatol.* 156, 231-240.

Brinkmann, I., Müller-Goymann, C., 2005. An attempt to clarify the influence of glycerol, propylene glycol, isopropyl myristate and a combination of propylene glycol and isopropyl myristate on human stratum corneum. *Pharmazie.* 60, 215-220.

Brinkmann, I., Müller-Goymann, C.C., 2003. Role of Isopropyl Myristate, Isopropyl Alcohol and a Combination of Both in Hydrocortisone Permeation across the Human Stratum corneum. *Skin Pharmacol. Physiol.* 16, 393-404.

Bronaugh, R.L., Franz, T.J., 1986. Vehicle effects on percutaneous absorption: in vivo and in vitro comparisons with human skin. *Br. J. Dermatol.* 115, 1-11.

Cázares-Delgadillo, J., Naik, A., Kalia, Y.N., Quintanar-Guerrero, D., Ganem-Quintanar, A., 2005. Skin permeation enhancement by sucrose esters: A pH-dependent phenomenon. *Int. J. Pharm.* 297, 204-212.

Carrara, D., 2001. Composition for controlled and sustained transdermal administration, US6231885B1.

Caspers, P., Lucassen, G., Bruining, H.A., Puppels, G., 2000. Automated depth-scanning confocal

Raman microspectrometer for rapid in vivo determination of water concentration profiles in human skin. *J. Raman Spectrosc* 31, 813-818.

Caspers, P.J., Bruining, H.A., Puppels, G.J., Lucassen, G.W., Carter, E.A., 2001. In Vivo Confocal Raman Microspectroscopy of the Skin: Noninvasive Determination of Molecular Concentration Profiles. *J. Invest. Dermatol.* 116, 434-442.

Chen, M., 2005. Amended Final Report of the Safety Assessment of t-Butyl Alcohol as Used in Cosmetics. *Int. J. Toxicol.* 24, 1-20.

CIRP, C.I.R.E.P., 2003. Caprylic/Capric Triglyceride. *Int. J. Toxicol.* 22, 4-5.

CIRP, C.I.R.E.P., 2019. Safety assessment of fatty acids and fatty acid salts as used in cosmetics.

Cooper, E.R., 1984. Increased Skin Permeability for Lipophilic Molecules. *J. Pharm. Sci.* 73, 1153-1156.

Coulman, S.A., Birchall, J.C., Alex, A., Pearton, M., Hofer, B., O'Mahony, C., Drexler, W., Považay, B., 2011. In Vivo, In Situ Imaging of Microneedle Insertion into the Skin of Human Volunteers Using Optical Coherence Tomography. *Pharm. Res.* 28, 66-81.

Coulman, S.A., David, B., Alexander, A., Chris, G., Anthony, M., Nicolle, W., Chris, A., Keith, B., James, C.B., 2006. Minimally Invasive Cutaneous Delivery of Macromolecules and Plasmid DNA Via Microneedles. *Curr. Drug Deliv.* 3, 65-75.

Crowther, J.M., Sieg, A., Blenkiron, P., Marcott, C., Matts, P.J., Kaczvinsky, J.R., Rawlings, A.V., 2008. Measuring the effects of topical moisturizers on changes in stratum corneum thickness, water gradients and hydration in vivo. *Br. J. Dermatol.* 159, 567-577.

D'souza, A.A., Shegokar, R., 2016. Polyethylene glycol (PEG): a versatile polymer for pharmaceutical applications. *Expert Opin. Drug Deliv.* 13, 1257-1275.

Dąbrowska, A.K., Adlhart, C., Spano, F., Rotaru, G.-M., Derler, S., Zhai, L., Spencer, N.D., Rossi, R.M., 2016. In vivo confirmation of hydration-induced changes in human-skin thickness, roughness and interaction with the environment. *Biointerphases* 11, 031015.

Das, C., Olmsted, P.D., 2016. The physics of stratum corneum lipid membranes. *Philos Trans A Math Phys Eng Sci.* 374, 20150126.

Davies, D.J., Ward, R.J., Heylings, J.R., 2004. Multi-species assessment of electrical resistance as a skin integrity marker for in vitro percutaneous absorption studies. *Toxicol. In Vitro* 18, 351-358.

Deng, J., Lin, J., Xiao, J., 2012. Transdermal patch containing rasagiline for treatment or prophylaxis of nervous system disease and its preparation process, EP2011488A1.

Dias, M., Hadgraft, J., Lane, M.E., 2007a. Influence of membrane-solvent-solute interactions on solute permeation in skin. *Int. J. Pharm.* 340, 65-70.

Dias, M., Hadgraft, J., Lane, M.E., 2007b. Influence of membrane-solvent-solute interactions on solute permeation in model membranes. *Int. J. Pharm.* 336, 108-114.

Dick, I.P., Scott, R.C., 1992. Pig ear skin as an in-vitro model for human skin permeability. *J. Pharm. Pharmacol.* 44, 640-645.

Diegel, K.L., Danilenko, D.M., Wojcinski, Z.W., 2013. Chapter 55 - Integument, in: Haschek, W.M., Rousseaux, C.G., Wallig, M.A. (Eds.), *Haschek and Rousseaux's Handbook of Toxicologic Pathology* (Third Edition). Academic Press, Boston, pp. 2219-2275.

Donnelly, R.F., Singh, T.R.R., Garland, M.J., Migalska, K., Majithiya, R., McCrudden, C.M., Kole, P.L., Mahmood, T.M.T., McCarthy, H.O., Woolfson, A.D., 2012. Hydrogel-Forming Microneedle Arrays for Enhanced Transdermal Drug Delivery. *Adv. Funct. Mater.* 22, 4879-4890.

Donnelly, R.F., Singh, T.R.R., Woolfson, A.D., 2010. Microneedle-based drug delivery systems: Microfabrication, drug delivery, and safety. *Drug Delivery* 17, 187-207.

Dragicevic, N., Atkinson, J.P., Maibach, H.I., 2015. Chemical Penetration Enhancers: Classification and Mode of Action, in: Nina Dragicevic, H.I.M. (Ed.), *Percutaneous Penetration Enhancers Chemical Methods in Penetration Enhancement: Modification of the Stratum Corneum*. Springer.

Dreher, F., Draelos, Z.D., Gold, M.H., Goldman, M.P., Fabi, S.G., Puissegur Lupo, M.L., 2013. Efficacy of hydroquinone-free skin-lightening cream for photoaging. *J. Cosmet. Dermatol.* 12, 12-17.

DrugBank, 2015. Octisalate.

DrugBank, 2018. phenylethyl resorcinol.

Egawa, M., Hirao, T., Takahashi, M., 2007. In vivo Estimation of Stratum Corneum Thickness from Water Concentration Profiles Obtained with Raman Spectroscopy. *Acta Derm. Venereol.* 87, 4-8.

El Nagar, M.H., Mahdy, M., Selem, M., El Maghraby, G., 2016. Transdermal delivery of kojic acid from microemulgel. *J Appl Pharm Sci* 6, 008-016.

Elshafeey, A.H., Hamza, Y.E., Amin, S.Y., Zia, H., 2012. In vitro transdermal permeation of fenoterol hydrobromide. *J. Adv. Res.* 3, 125-132.

EMA, 2018. Draft guideline on quality and equivalence of topical products, in: (CHMP), C.f.M.P.f.H.U. (Ed.). European Medicines Agency.

Epstein, M.E., 2015. Chapter 9 - Opioids, in: Gaynor, J.S., Muir, W.W. (Eds.), *Handbook of Veterinary Pain Management* (Third Edition). Mosby, St. Louis, pp. 161-195.

Erdal, M.S., Özdin, D., Güngör, S., 2014. Synergistic Effects of Transcutol and Terpenes as Penetration Enhancers: In Vitro and In Vivo ATR-FTIR Spectroscopic Imaging Studies, *Advances in Dermatological Sciences*. The Royal Society of Chemistry, pp. 113-123.

Fan, H., Liu, G., Huang, Y., Li, Y., Xia, Q., 2014. Development of a nanostructured lipid carrier formulation for increasing photo-stability and water solubility of Phenylethyl Resorcinol. *Appl. Surf. Sci.* 288, 193-200.

FDA, 2015. *Analytical Procedures and Methods Validation for Drugs and Biologics*

Feldmann, R.J., Maibach, H.I., 1970. Absorption of Some Organic Compounds Through the Skin in Man. *J. Invest. Dermatol.* 54, 399-404.

Fenner, J., Clark, R.A.F., 2016. Chapter 1 - Anatomy, Physiology, Histology, and Immunohistochemistry of Human Skin, in: Albanna, M.Z., Holmes Iv, J.H. (Eds.), *Skin Tissue Engineering and Regenerative Medicine*. Academic Press, Boston, pp. 1-17.

Finnin, B., Walters, K.A., Franz, T.J., 2012. *In Vitro Skin Permeation Methodology, Topical and Transdermal Drug Delivery*. John Wiley & Sons, Inc., pp. 85-108.

Fitzpatrick, T.B., Breathnach, A., 1963. The epidermal melanin unit system. *Dermatol. Wochenschr.* 147, 481-489.

Fiume, M.M.B., W.F.; Belsito, D. V.; Hill, R. A.; Klaassen, C. D.; Liebler, D. C.; Marks, J.G.; Shank, R.C.; Slaga, T.J.; Snyder, P. W., 2014. Safety Assessment of PEGylated Alkyl Glycerides as Used in Cosmetics. CIR.

Flaten, G.E., Palac, Z., Engesland, A., Filipović-Grčić, J., Vanić, Ž., Škalko-Basnet, N., 2015. In vitro skin models as a tool in optimization of drug formulation. *Eur. J. Pharm. Sci.* 75, 10-24.

Forbat, E., Al-Niimi, F., Ali, F.R., 2017. Use of nicotinamide in dermatology. *Clin. Exp. Dermatol.* 42, 137-144.

Francesco, C., Antonella, C., Francesca, S., Paola, M., 2015. Supersaturation as a Tool For Skin Penetration Enhancement. *Curr. Pharm. Des.* 21, 2733-2744.

Franz, T.J., 1975. Percutaneous absorption. On the relevance of in vitro data. *J. Invest. Dermatol.* 64, 190-195.

Fruijtier-Pölloth, C., 2005. Safety assessment on polyethylene glycols (PEGs) and their derivatives as used in cosmetic products. *Toxicology* 214, 1-38.

Gay, C.L., Murphy, T.M., Hadgraft, J., Kellaway, I.W., Evans, J.C., Rowlands, C.C., 1989. An electron spin resonance study of skin penetration enhancers. *Int. J. Pharm.* 49, 39-45.

Giridhar, G., Manepalli, R.R.K.N., Gudimalla, A., 2017. Confocal Raman Spectroscopy, in: Thomas, S., Thomas, R., Zachariah, A.K., Kumar, R. (Eds.), pp. 141-161.

Goates, C.Y., Knutson, K., 1994. Enhanced permeation of polar compounds through human epidermis. I. Permeability and membrane structural changes in the presence of short chain alcohols. *Biochim Biophys Acta.* 1195, 169-179.

Godin, B., Touitou, E., 2007. Transdermal skin delivery: predictions for humans from in vivo, ex vivo and animal models. *Adv. Drug Delivery Rev.* 59, 1152-1161.

Gohara, M., Yagami, A., Suzuki, K., Morita, Y., Sano, A., Iwata, Y., Hashimoto, T., Matsunaga, K., 2013. Allergic contact dermatitis caused by phenylethyl resorcinol [4-(1-phenylethyl)-1, 3-benzenediol], a skin-lightening agent in cosmetics. *Contact Dermatitis* 69, 319-320.

Gold, M.H., Biron, J., 2011. Efficacy of a novel hydroquinone-free skin-brightening cream in patients with melasma. *J. Cosmet. Dermatol.* 10, 189-196.

Gould, J., 2018. Superpowered skin. *Nature* 563, S84.

Gray, G.M., Yardley, H.J., 1975. Lipid compositions of cells isolated from pig, human, and rat epidermis. *J. Lipid Res.* 16, 434-440.

Green, J.M., 1996. Peer reviewed: a practical guide to analytical method validation. *Anal. Chem.* 68, 305A-309A.

Grumetto, L., Russo, G., Barbato, F., 2016. Immobilized Artificial Membrane HPLC Derived Parameters vs PAMPA-BBB Data in Estimating in Situ Measured Blood-Brain Barrier Permeation of Drugs. *Mol. Pharm.* 13, 2808-2816.

Gureri, D., Voegeli, R., Gurgul, S.J., Munday, M.R., Lane, M.E., Rawlings, A.V., 2018. A new approach to assess the effect of photodamage on corneocyte envelope maturity using combined hydrophobicity and mechanical fragility assays. *Int. J. Cosmet. Sci.* 40, 207-216.

Hadgraft, J., 1983. Percutaneous absorption: possibilities and problems. *Int. J. Pharm.* 16, 255-270.

Hadgraft, J., 2001. Skin, the final frontier. *Int. J. Pharm.* 224, 1-18.

Hadgraft, J., 2004. Skin deep. *Eur. J. Pharm. Biopharm.* 58, 291-299.

- Hadgraft, J., Lane, M.E., 2005. Skin permeation: The years of enlightenment. *Int. J. Pharm.* 305, 2-12.
- Hadgraft, J., Lane, M.E., 2011. Skin: the ultimate interface. *Phys. Chem. Chem. Phys.* 13, 5215-5222.
- Hadgraft, J., Lane, M.E., 2016. Advanced topical formulations (ATF). *Int. J. Pharm.* 514, 52-57.
- Hadgraft, J., Walters, K., 1994. Skin penetration enhancement. *J. Dermatol.* 5, 43-47.
- Hadgraft, J.W., Somers, G.F., 1956. PERCUTANEOUS ABSORPTION. *J. Pharm. Pharmacol.* 8, 625-634.
- Hansch, C., 1995. Exploring QSAR. Hydrophobic, Electronic, and Steric Constants. Amer Chem Soc, Washington, DC.
- Haque, T., ME, L., BS, S., Crowther, J.M., Moore, D.J., 2017a. In vitro permeation and disposition of niacinamide in silicone and porcine skin of skin barrier-mimetic formulations. *Int. J. Pharm.* 520, 158-162.
- Haque, T., Rahman, K.M., Thurston, D.E., Hadgraft, J., Lane, M.E., 2017b. Topical delivery of anthramycin I. Influence of neat solvents. *Eur. J. Pharm. Sci.* 104, 188-195.
- Harrison, J.E., Watkinson, A.C., Green, D.M., Hadgraft, J., Brain, K., 1996. The Relative Effect of Azone® and Transcutol® on Permeant Diffusivity and Solubility in Human Stratum Corneum. *Pharm. Res.* 13, 542-546.
- Haskell, H., 2010. Introduction, in: Busam, K.J. (Ed.), *Dermatopathology*. W.B. Saunders, Philadelphia, pp. 1-8.
- Herkenne, C., Naik, A., Kalia, Y.N., Hadgraft, J., Guy, R.H., 2006. Pig Ear Skin ex Vivo as a Model for in Vivo Dermatopharmacokinetic Studies in Man. *Pharm. Res.* 23, 1850-1856.
- Higuchi, W.I., Higuchi, T., 1960. Theoretical analysis of diffusional movement through heterogeneous barriers. *J. Am. Pharm. Assoc.* 49, 598-606.
- Hille, T., Babriel, W., Kevin, J.S., Gillian, E.M., Helen, E.J., 2017. Transdermal delivery system comprising buprenorphine, US9549903B2.
- Hirata, K., Helal, F., Hadgraft, J., Lane, M.E., 2013. Formulation of carbenoxolone for delivery to the skin. *Int. J. Pharm.* 448, 360-365.
- Hollricher, O., 2011. Raman Instrumentation for Confocal Raman Microscopy. Springer Series in Optical Sciences, vol 158, Springer, Berlin, Heidelberg.

Honari, G., Maibach, H., 2014. Chapter 1 - Skin Structure and Function, Applied Dermatotoxicology. Academic Press, Boston, pp. 1-10.

Ibrahim, S.A., Li, S.K., 2010. Efficiency of Fatty Acids as Chemical Penetration Enhancers: Mechanisms and Structure Enhancement Relationship. *Pharm. Res.* 27, 115-125.

ICH, 2005. Validation of analytical procedures: text and methodology, ICH Harmonised Tripartite Guideline. ICH, Geneva, Switzerland, pp. 1-13.

Iwai, I., Han, H., Hollander, L.d., Svensson, S., Öfverstedt, L.-G., Anwar, J., Brewer, J., Bloksgaard, M., Laloëuf, A., Nosek, D., Masich, S., Bagatolli, L.A., Skoglund, U., Norlén, L., 2012. The Human Skin Barrier Is Organized as Stacked Bilayers of Fully Extended Ceramides with Cholesterol Molecules Associated with the Ceramide Sphingoid Moiety. *J. Invest. Dermatol.* 132, 2215-2225.

J, J.N., Breslawec, H., 2014. International Cosmetic Ingredient Dictionary and Hnadbook, 15 ed. Personal Care Products Council, Washington, DC.

Jacobi, U., Kaiser, M., Toll, R., Mangelsdorf, S., Audring, H., Otberg, N., Sterry, W., Lademann, J., 2007. Porcine ear skin: an in vitro model for human skin. *Skin Res Technol* 13, 19-24.

Jiang, R., Roberts, M.S., Prankerd, R.J., Benson, H.A.E., 1997. Percutaneous Absorption of Sunscreen Agents from Liquid Paraffin: Self-Association of Octyl Salicylate and Effects on Skin Flux. *J. Pharm. Sci.* 86, 791-796.

Jones, K., Hughes, J., Hong, M., Jia, Q., Orndorff, S., 2002. Modulation of Melanogenesis by Aloesin: A Competitive Inhibitor of Tyrosinase. *Pigm. Cell Res.* 15, 335-340.

Jones, T.M., 2018. Chapter 1 Preformulation Studies, Pharmaceutical Formulation: The Science and Technology of Dosage Forms. The Royal Society of Chemistry, pp. 1-41.

Jung, E.C., Maibach, H.I., 2014. Animal models for percutaneous absorption. *J. Appl. Toxicol.* 35, 1-10.

Köpke, D., Müller, R.H., Pyo, S.M., 2019. Phenylethyl resorcinol smartLipids for skin brightening – Increased loading & chemical stability. *Eur. J. Pharm. Sci.* 137, 104992.

Kang, M., Park, S.-H., Park, S.J., Oh, S.W., Yoo, J.A., Kwon, K., Kim, J., Yu, E., Cho, J.Y., Lee, J., 2019. p44/42 MAPK signaling is a prime target activated by phenylethyl resorcinol in its anti-melanogenic action. *Phytomedicine* 58, 152877.

Kansy, M., Senner, F., Gubernator, K., 1998. Physicochemical high throughput screening: parallel artificial membrane permeation assay in the description of passive absorption processes. *J. Med. Chem.* 41, 1007-1010.

Karande, P., Mitragotri, S., 2009. Enhancement of transdermal drug delivery via synergistic action of chemicals. *Biochim Biophys Acta*. 1788, 2362-2373.

Kasting, G.B., Francis, W.R., Roberts, G.E., 1993. Skin Penetration Enhancement of Triprolidine Base by Propylene Glycol. *J. Pharm. Sci.* 82, 551-552.

Katz, M., Poulsen, B.J., 1971. Absorption of drugs through the skin, *Concepts in Biochemical Pharmacology*. Springer, pp. 103-174.

Kezic, S., 2008. Methods for measuring in-vivo percutaneous absorption in humans. *Hum. Exp. Toxicol.* 27, 289-295.

Klang, V., Schwarz, J.C., Lenobel, B., Nadj, M., Auböck, J., Wolzt, M., Valenta, C., 2012. In vitro vs. in vivo tape stripping: Validation of the porcine ear model and penetration assessment of novel sucrose stearate emulsions. *Eur. J. Pharm. Biopharm.* 80, 604-614.

Kligman, A.M., Christophers, E., 1963. Preparation of isolated sheets of human stratum corneum. *Arch. Dermatol.* 88, 702-705.

Krevelent†, D.W.v., Nijenhuis, K.t., 2009. 7.1 Introduction, Properties of Polymers - Their Correlation with Chemical Structure; Their Numerical Estimation and Prediction from Additive Group Contributions (4th, Completely Revised Edition). Elsevier, p. 189.

Lai-Cheong, J.E., McGrath, J.A., 2009. Structure and function of skin, hair and nails. *Medicine (Baltimore)* 37, 223-226.

Lane, M.E., 2013. Skin penetration enhancers. *Int. J. Pharm.* 447, 12-21.

Lane, M.E., Hadgraft, J., Oliveira, G., Vieira, R., Mohammed, D., Hirata, K., 2012a. Rational formulation design. *Int. J. Cosmet. Sci.* 34, 496-501.

Lane, M.E., Santos, P., Watkinson, A.C., Hadgraft, J., 2012b. Passive Skin Permeation Enhancement, in: Benson, H.A., Watkinson, A.C. (Eds.), *Topical and Transdermal Drug Delivery*, pp. 23-42.

Law, A.W.L., Ahmed, R., Cheung, T.W., Mak, C.Y., Lau, C., 2017. In situ cellular level Raman spectroscopy of the thyroid. *Biomed. Opt. Express* 8, 670-678.

Lawrence, J.N., 1997. Electrical resistance and tritiated water permeability as indicators of barrier integrity of in vitro human skin. *Toxicol. In Vitro* 11, 241-249.

Leopold, C.S., Lippold, B.C., 1995a. An attempt to clarify the mechanism of the penetration enhancing effects of lipophilic vehicles with differential scanning calorimetry (DSC). *J. Pharm. Pharmacol.* 47, 276-281.

Leopold, C.S., Lippold, B.C., 1995b. Enhancing Effects of Lipophilic Vehicles on Skin Penetration of Methyl Nicotinate in Vivo. *J. Pharm. Sci.* 84, 195-198.

Li, Y., Igne, B., Drennen, J.K., Anderson, C.A., 2016. Method development and validation for pharmaceutical tablets analysis using transmission Raman spectroscopy. *Int. J. Pharm.* 498, 318-325.

Limsuwan, T., Boonme, P., Khongkow, P., Amnuait, T., 2017. Ethosomes of Phenylethyl Resorcinol as Vesicular Delivery System for Skin Lightening Applications. *Biomed Res Int* 2017.

Luo, L., Patel, A., Sinko, B., Bell, M., Wibawa, J., Hadgraft, J., Lane, M.E., 2016. A comparative study of the in vitro permeation of ibuprofen in mammalian skin, the PAMPA model and silicone membrane. *Int. J. Pharm.* 505, 14-19.

Müller, J., Esső, K., Dargó, G., Könczöl, Á., Balogh, G.T., 2015. Tuning the predictive capacity of the PAMPA-BBB model. *Eur. J. Pharm. Sci.* 79, 53-60.

Mélot, M., Pudney, P.D.A., Williamson, A.-M., Caspers, P.J., Van Der Pol, A., Puppels, G.J., 2009. Studying the effectiveness of penetration enhancers to deliver retinol through the stratum corneum by in vivo confocal Raman spectroscopy. *J. Control. Release* 138, 32-39.

Machado, M., Salgado, T.M., Hadgraft, J., Lane, M.E., 2010. The relationship between transepidermal water loss and skin permeability. *Int. J. Pharm.* 384, 73-77.

Maghraby, G.M.M.E., Campbell, M., Finnin, B.C., 2005. Mechanisms of action of novel skin penetration enhancers: Phospholipid versus skin lipid liposomes. *Int. J. Pharm.* 305, 90-104.

Mateus, R., Abdalghafor, H., Oliveira, G., Hadgraft, J., Lane, M.E., 2013. A new paradigm in dermatopharmacokinetics - Confocal Raman spectroscopy. *Int. J. Pharm.* 444, 106-108.

Mateus, R., Moore, D.J., Hadgraft, J., Lane, M.E., 2014. Percutaneous absorption of salicylic acid – in vitro and in vivo studies. *Int. J. Pharm.* 475, 471-474.

Mathes, S.H., Ruffner, H., Graf-Hausner, U., 2014. The use of skin models in drug development. *Adv Drug Deliv Rev* 69-70, 81-102.

Matts, P., Oblong, J., Bissett, D.L., 2002. A Review of the range of effects of niacinamide in human skin. *Int Fed Soc Cosmet Chem Mag* 5, 285-289.

Maurya, A., Lili, C., Murthy, S.N., 2015. Magnetophoresis and Electret-Mediated Transdermal Delivery of Drugs, in: Donnelly, R.F., Singh, T.R. (Eds.), *Novel Delivery Systems for Transdermal and Intradermal Drug Delivery*, pp. 147-162.

Menon, G.K., Cleary, G.W., Lane, M.E., 2012. The structure and function of the stratum corneum.

Int. J. Pharm. 435, 3-9.

Menon, G.K., Feingold, K.R., Elias, P.M., 1992. Lamellar body secretory response to barrier disruption. *J. Invest. Dermatol.* 98, 279-289.

Michaels, A.S., Chandrasekaran, S.K., Shaw, J.E., 1975. Drug permeation through human skin: Theory and invitro experimental measurement. *AIChE J.* 21, 985-996.

Mishima, Y., Hatta, S., Ohyama, Y., Inazu, M., 1988. Induction of Melanogenesis Suppression: Cellular Pharmacology and Mode of Differential Action. *Pigm. Cell Res.* 1, 367-374.

Mishima, Y., Kondoh, H., 2000. Dual Control of Melanogenesis and Melanoma Growth: Overview: Molecular to Clinical Level and the Reverse. *Pigm. Cell Res.* 13, 10-22.

Mittal, A., V S Sara, U., Ali, A., Aqil, M., 2009. Status of Fatty Acids as Skin Penetration Enhancers-A Review. *Curr Drug Deliv.* 6, 274-279.

Moffat, A.C., Osselton, M.D., Widdop, B., 2010. *Clarke's Analysis of Drugs and Poisons*. Sage Publications, London.

Mohammed, D., Crowther, J.M., Matts, P.J., Hadgraft, J., Lane, M.E., 2013. Influence of niacinamide containing formulations on the molecular and biophysical properties of the stratum corneum. *Int. J. Pharm.* 441, 192-201.

Mohammed, D., Hirata, K., Hadgraft, J., Lane, M.E., 2014a. Influence of skin penetration enhancers on skin barrier function and skin protease activity. *Eur. J. Pharm. Sci.* 51, 118-122.

Mohammed, D., Matts, P.J., Hadgraft, J., Lane, M.E., 2011. Influence of Aqueous Cream BP on corneocyte size, maturity, skin protease activity, protein content and transepidermal water loss. *Br. J. Dermatol.* 164, 1304-1310.

Mohammed, D., Matts, P.J., Hadgraft, J., Lane, M.E., 2014b. In Vitro–In Vivo Correlation in Skin Permeation. *Pharm. Res.* 31, 394-400.

Mohammed, D., Yang, Q., Guy, R.H., Matts, P.J., Hadgraft, J., Lane, M.E., 2012. Comparison of gravimetric and spectroscopic approaches to quantify stratum corneum removed by tape-stripping. *Eur. J. Pharm. Biopharm.* 82, 171-174.

Morgan, T.M., Reed, B.L., Finnin, B.C., 1998. Enhanced Skin Permeation of Sex Hormones with Novel Topical Spray Vehicles. *J. Pharm. Sci.* 87, 1213-1218.

Moss, G.P.J., 2015. Introduction, in: Donnelly, R.F., Singh, T.R.R. (Eds.), *Novel Delivery Systems for Transdermal and Intradermal Drug Delivery*. John Wiley & Sons, Ltd., Queen's University Belfast, UK, pp. 1-40.

Mura, P., Faucci, M.T., Bramanti, G., Corti, P., 2000. Evaluation of transcutol as a clonazepam transdermal permeation enhancer from hydrophilic gel formulations. *Eur. J. Pharm. Sci.* 9, 365-372.

Nemanic, M.K., Elias, P.M., 1980. In situ precipitation: a novel cytochemical technique for visualization of permeability pathways in mammalian stratum corneum. *J. Histochem. Cytochem.* 28, 573-578.

Ng, K.W., Lau, W.M., 2015. Skin deep: the basics of human skin structure and drug penetration, in: Dragicevic N, HI, M. (Eds.), *Percutaneous penetration enhancers: chemical methods in penetration enhancement*. Heidelberg: Springer-Verlag. , Berlin, pp. 3-11.

Ng, K.W., Lau, W.M., Williams, A., 2015. Synergy Between Chemical Penetration Enhancers, pp. 373-385.

O'Neil, M.J., Heckelman, P.E., Dobbelaar, P.H., Roman, K.J., M., K.C., S., K.L., 2013. *The Merck Index An Encyclopedia of Chemicals. Drugs. and Biologicals*, 15 ed. The Royal Society of Chemistry, Cambridge.

OECD, 1995. Test No. 107: Partition Coefficient (n-octanol/water): Shake Flask Method.

OECD, 2004a. Guidance Document for the Conduct of Skin Absorption Studies.

OECD, 2004b. Test No. 428: Skin Absorption: In Vitro Method.

Oh, H.-J., Oh, Y.-K., Kim, C.-K., 2001. Effects of vehicles and enhancers on transdermal delivery of melatonin. *Int. J. Pharm.* 212, 63-71.

Oliveira, G., Beezer, A.E., Hadgraft, J., Lane, M.E., 2010. Alcohol enhanced permeation in model membranes. Part I. Thermodynamic and kinetic analyses of membrane permeation. *Int. J. Pharm.* 393, 61-67.

Oliveira, G., Hadgraft, J., Lane, M.E., 2012. The influence of volatile solvents on transport across model membranes and human skin. *Int. J. Pharm.* 435, 38-49.

Osborne, D.W., Musakhanian, J., 2018. Skin Penetration and Permeation Properties of Transcutol®—Neat or Diluted Mixtures. *AAPS PharmSciTech* 19, 3512-3533.

Ottaviani, G., Martel, S., Carrupt, P.-A., 2006. Parallel artificial membrane permeability assay: a new membrane for the fast prediction of passive human skin permeability. *J. Med. Chem.* 49, 3948-3954.

Otto, A., Du Plessis, J., Wiechers, J.W., 2009. Formulation effects of topical emulsions on transdermal and dermal delivery. *Int. J. Cosmet. Sci.* 31, 1-19.

- Pagliaro, M., Rossi, M., 2010. Glycerol: properties and production. The future of glycerol, 20-21.
- Parisi, N., Matts, P.J., Lever, R., Hadgraft, J., Lane, M.E., 2015. Preparation and characterisation of hexamidine salts. *Int. J. Pharm.* 493, 404-411.
- Patel, D., Welsh, D., Baker, M., 1985. Comparative study of propylene glycol and caprylic/capric triglyceride vehicles for topical application. *J. Soc. Cosmet. Chem.* 303-311.
- Paz-Alvarez, M., Pudney, P.D.A., Hadgraft, J., Lane, M.E., 2018. Topical delivery of climbazole to mammalian skin. *Int. J. Pharm.* 549, 317-324.
- Pellett, M.A., Roberts, M.S., Hadgraft, J., 1997. Supersaturated solutions evaluated with an in vitro stratum corneum tape stripping technique. *Int. J. Pharm.* 151, 91-98.
- Pham, Q.D., Björklund, S., Engblom, J., Topgaard, D., Sparr, E., 2016. Chemical penetration enhancers in stratum corneum — Relation between molecular effects and barrier function. *J. Control. Release* 232, 175-187.
- Pillaiyar, T., Manickam, M., Jung, S.-H., 2017. Recent development of signaling pathways inhibitors of melanogenesis. *Cell. Signal.* 40, 99-115.
- Polat, B.E., Hart, D., Langer, R., Blankschtein, D., 2011. Ultrasound-mediated transdermal drug delivery: Mechanisms, scope, and emerging trends. *J. Control. Release* 152, 330-348.
- Potts, R.O., Francoeur, M.L., 1991. The Influence of Stratum Corneum Morphology on Water Permeability. *J. Invest. Dermatol.* 96, 495-499.
- Praça, F.S.G., Medina, W.S.G., Eloy, J.O., Petrilli, R., Campos, P.M., Ascenso, A., Bentley, M.V.L.B., 2018. Evaluation of critical parameters for in vitro skin permeation and penetration studies using animal skin models. *Eur. J. Pharm. Sci.* 111, 121-132.
- Pudney, P., Mélot, M., Caspers, P., Pol, A., Puppels, G., 2007. An In Vivo Confocal Raman Study of the Delivery of Trans Retinol to the Skin. *Appl. Spectrosc.* 61, 804-811.
- Pugh, W.J., Degim, I.T., Hadgraft, J., 2000. Epidermal permeability–penetrant structure relationships: 4, QSAR of permeant diffusion across human stratum corneum in terms of molecular weight, H-bonding and electronic charge. *Int. J. Pharm.* 197, 203-211.
- Puppels, G.J., Colier, W., Olminkhof, J.H.F., Otto, C., de Mul, F.F.M., Greve, J., 1991. Description and performance of a highly sensitive confocal Raman microspectrometer. *J. Raman Spectrosc.* 22, 217-225.
- Quinn, H.L., Courtenay, A.J., Kearney, M.C., Donnelly, R.F., 2015. Microneedle Technology, in: Donnelly, R.F., Singh, T.R.R. (Eds.), *Novel Delivery Systems for Transdermal and Intradermal Drug Delivery*. John Wiley & Sons, Ltd., Queen's University Belfast, UK, pp. 179-208.

Raghavan, S.L., Kiepfer, B., Davis, A.F., Kazarian, S.G., Hadgraft, J., 2001. Membrane transport of hydrocortisone acetate from supersaturated solutions; the role of polymers. *Int. J. Pharm.* 221, 95-105.

Ramalingam, S., Periandy, S., Govindarajan, M., Mohan, S., 2010. FT-IR and FT-Raman vibrational spectra and molecular structure investigation of nicotinamide: A combined experimental and theoretical study. *Spectrochim. Acta A* 75, 1552-1558.

Raney, S.G., Franz, T.J., Lehman, P.A., Lionberger, R., Chen, M.-L., 2015. Pharmacokinetics-Based Approaches for Bioequivalence Evaluation of Topical Dermatological Drug Products. *Clin. Pharmacokinet.* 54, 1095-1106.

Roberts, M.S., Cross, S.E., Pellett, M.A., 2002. Skin Transport, in: Walters, K.A. (Ed.), *Dermatological and Transdermal Formulations*. CRC Press.

Rolfe, H.M., 2014. A review of nicotinamide: treatment of skin diseases and potential side effects. *J. Cosmet. Dermatol.* 13, 324-328.

Sandby-Moller, J., Poulsen, T., Wulf, H.C., 2003. Epidermal thickness at different body sites: relationship to age, gender, pigmentation, blood content, skin type and smoking habits. *Acta Derm. Venereol.* 83, 410-413.

Santos, P., Watkinson, A.C., Hadgraft, J., Lane, M.E., 2011. Formulation issues associated with transdermal fentanyl delivery. *Int. J. Pharm.* 416, 155-159.

Santos, P., Watkinson, A.C., Hadgraft, J., Lane, M.E., 2012. Influence of penetration enhancer on drug permeation from volatile formulations. *Int. J. Pharm.* 439, 260-268.

SCCP, 2006. The Scientific Committee on Consumer Products. Opinion on Diethylene Glycol Monoethyl Ether. Updated 19th December 2006. SCCP/1044/06.

SCCS, 2010. The Scientific Committee on Consumer Safety. Opinion on Basic Criteria for the In Vitro Assessment of Dermal Absorption of Cosmetic Ingredients. Updated 22nd June 2010. SCCS/1358/10.

Schaefer, U.F., 2008. Models for skin absorption and skin toxicity testing, *Drug Absorption Studies*. Springer, pp. 3-33.

Sil, B.C., Moore, D.J., Lane, M.E., 2018. Use of LC-MS analysis to elucidate by-products of niacinamide transformation following in vitro skin permeation studies. *Int. J. Cosmet. Sci.* 40, 525-529.

Singh, A., Gangopadhyay, D., Nandi, R., Sharma, P., Singh, R.K., 2016. Raman signatures of strong and weak hydrogen bonds in binary mixtures of phenol with acetonitrile, benzene and

orthodichlorobenzene. *J. Raman Spectrosc.* 47, 712–719.

Singh, S., Zhao, K., Singh, J., 2002. In vitro permeability and binding of hydrocarbons in pig ear and human abdominal skin. *Drug Chem. Toxicol.* 25, 83–92.

Sinkó, B., Garrigues, T.M., Balogh, G.T., Nagy, Z.K., Tsinman, O., Avdeef, A., Takács-Novák, K., 2012. Skin–PAMPA: A new method for fast prediction of skin penetration. *Eur. J. Pharm. Sci.* 45, 698–707.

Sinkó, B., Vizserálek, G., Krisztina, T.-N., 2015. Skin PAMPA: Application in practice. *ADMET & DMPK* 2, 191–198.

Small, D.M., 1984. Lateral chain packing in lipids and membranes. *J. Lipid Res.* 25, 1490–1500.

Snaidr, V.A., Damian, D.L., Halliday, G.M., 2019. Nicotinamide for photoprotection and skin cancer chemoprevention: A review of efficacy and safety. *Exp. Dermatol.* 28, 15–22.

Socrates, G., 2012. Infrared and Raman characteristics group frequencies—tables and charts. 68.

Solassol, I., Caumette, L., Bressolle, F., Garcia, F., Thezenas, S., Astre, C., Culine, S., Coulouma, R., Pinguet, F., 2005. Inter- and intra-individual variability in transdermal fentanyl absorption in cancer pain patients. *Oncol. Rep.* 14, 1029–1036.

Sorg, O., Kasraee, B., Salomon, D., Saurat, J.H., 2013. The Combination of a Retinoid, a Phenolic Agent and an Antioxidant Improves Tolerance while Retaining an Optimal Depigmenting Action in Reconstructed Epidermis. *Dermatology* 227, 150–156.

Sotoodian, B., Maibach, H.I., 2012. Noninvasive test methods for epidermal barrier function. *Clin. Dermatol.* 30, 301–310.

Spruit, D., Malten, K., 1965. Epidermal water-barrier formation after stripping of normal skin. *J. Invest. Dermatol.* 45, 6–14.

Stecco, C., Hammer, W., Vleeming, A., De Caro, R., 2015. 2 - Subcutaneous Tissue and Superficial Fascia, in: Stecco, C., Hammer, W., Vleeming, A., De Caro, R. (Eds.), *Functional Atlas of the Human Fascial System*. Churchill Livingstone, pp. 21–49.

Sullivan, D.W., Gad, S.C., Julien, M., 2014. A review of the nonclinical safety of Transcutol®, a highly purified form of diethylene glycol monoethyl ether (DEGEE) used as a pharmaceutical excipient. *Food Chem. Toxicol.* 72, 40–50.

Suzuki, E., Okuda, H., Nishida, K., Fujimoto, S., Nagasawa, K., 2010. Protective effect of nicotinamide against poly(ADP-ribose) polymerase-1-mediated astrocyte death depends on its transporter-mediated uptake. *Life Sci.* 86, 676–682.

Thakur, R.R.S., Martin, J.G., Corona, M.C., Katarzyna, M., Yusuf, K.D., Sharif, A., Elizabeth, R., David, W., Ryan, F.D., 2010. Microporation Techniques for Enhanced Delivery of Therapeutic Agents. *Recent Pat Drug Deliv Formul.* 4, 1-17.

Thijs, H.M.L., Becer, C.R., Guerrero-Sanchez, C., Fournier, D., Hoogenboom, R., Schubert, U.S., 2007. Water uptake of hydrophilic polymers determined by a thermal gravimetric analyzer with a controlled humidity chamber. *J. Mater. Chem.* 17, 4864-4871.

Trommer, H., Neubert, R.H.H., 2006. Overcoming the Stratum Corneum: The Modulation of Skin Penetration. *Skin Pharmacol. Physiol.* 19, 106-121.

Trottet, L., Merly, C., Mirza, M., Hadgraft, J., Davis, A.F., 2004. Effect of finite doses of propylene glycol on enhancement of in vitro percutaneous permeation of loperamide hydrochloride. *Int. J. Pharm.* 274, 213-219.

van Zyl, L., du Preez, J., Gerber, M., du Plessis, J., Viljoen, J., 2016. Essential Fatty Acids as Transdermal Penetration Enhancers. *J. Pharm. Sci.* 105, 188-193.

Vielhaber, G., Schmaus, G., Jacobs, K., Franke, H., Lange, S., Herrmann, M., Joppe, H., Koch, O., 2007. 4-(1-Phenylethyl) 1, 3-Benzenediol: A New, Highly Efficient Lightening Agent. *Int. J. Cosmet. Sci.* 29, 65-66.

Vizserálek, G., Berkó, S., Tóth, G., Balogh, R., Budai-Szűcs, M., Csányi, E., Sinkó, B., Takács-Novák, K., 2015. Permeability test for transdermal and local therapeutic patches using Skin PAMPA method. *Eur. J. Pharm. Sci.* 76, 165-172.

Voegeli, R., Heiland, J., Doppler, S., Rawlings, A.V., Schreier, T., 2007a. Efficient and simple quantification of stratum corneum proteins on tape strippings by infrared densitometry. *Skin Res Technol* 13, 242-251.

Voegeli, R., Rawlings, A.V., Doppler, S., Heiland, J., Schreier, T., 2007b. Profiling of serine protease activities in human stratum corneum and detection of a stratum corneum tryptase-like enzyme. *Int. J. Cosmet. Sci.* 29, 191-200.

Vyumvuhore, R., Tfayli, A.M., Piot, O., Guillou, M.L., Guichard, N., Manfait, M., Baillet-Guffroy, A., 2014. Raman spectroscopy: in vivo quick response code of skin physiological status. *J. Biomed. Opt.* 19, 1-14, 14.

Walters, K.A., 2002. Structure and function of the skin, in: Walters, K.A. (Ed.), *Dermatological and Transdermal Formulations*. CRC Press.

Walters, K.A., Brain, K.R., Howes, D., James, V.J., Kraus, A.L., Teetsel, N.M., Toulon, M., Watkinson, A.C., Gettings, S.D., 1997. Percutaneous penetration of octyl salicylate from representative sunscreen formulations through human skin in vitro. *Food Chem. Toxicol.* 35, 1219-1225.

Watkinson, R.M., Herkenne, C., Guy, R.H., Hadgraft, J., Oliveira, G., Lane, M.E., 2009. Influence of Ethanol on the Solubility, Ionization and Permeation Characteristics of Ibuprofen in Silicone and Human Skin. *Skin Pharmacol. Physiol.* 22, 15-21.

Welker, R.W., 2012. Chapter 1 - Basics and Sampling of Particles for Size Analysis and Identification, in: Kohli, R., Mittal, K.L. (Eds.), *Developments in Surface Contamination and Cleaning*. William Andrew Publishing, Oxford, pp. 1-80.

Wiechers, J.W., 2008. Avoiding Transdermal Cosmetic Delivery, in: Wiechers, J.W. (Ed.), *Skin Barrier: Chemistry of Skin Delivery Systems*. Allured.

Wiechers, J.W., Kelly, C.L., Blease, T.G., Dederen, J.C., 2004. Formulating for efficacy. *Int. J. Cosmet. Sci.* 26, 173-182.

Wiechers, J.W., Watkinson, A.C., Cross, S.E., Roberts, M.S., 2012. Predicting skin penetration of actives from complex cosmetic formulations: an evaluation of inter formulation and inter active effects during formulation optimization for transdermal delivery. *Int. J. Cosmet. Sci.* 34, 525-535.

Wiedersberg, S., Nicoli, S., 2012. Skin Permeation Assessment: Tape Stripping, in: Benson, H.A.E., Watkinson, A.C. (Eds.), *Topical and Transdermal Drug Delivery*. Wiley, pp. 109-130.

Williams, A.C., Barry, B.W., 2004. Penetration enhancers. *Adv. Drug Delivery Rev.* 56, 603-618.

Williams, A.C., Barry, B.W., 2012. Penetration enhancers. *Adv. Drug Delivery Rev.* 64, 128-137.

Williams, A.C., Edwards, H.G.M., Barry, B.W., 1992. Fourier transform Raman spectroscopy a novel application for examining human stratum corneum. *Int. J. Pharm.* 81, R11-R14.

Wohlrab, J., Kreft, D., 2014. Niacinamide-mechanisms of action and its topical use in dermatology. *Skin Pharmacol. Physiol.* 27, 311-315.

Yoshimatsu, H., Ishii, K., Konno, Y., Satsukawa, M., Yamashita, S., 2017. Prediction of human percutaneous absorption from in vitro and in vivo animal experiments. *Int. J. Pharm.* 534, 348-355.

Zhou, F., Xu, H., Song, Z., Zhu, L., Feng, S., Feng, R., 2019. α -Linolenic acid-modified pluronic 127-CS copolymeric micelles for the skin targeted delivery of amphotericin B. *New J. Chem.* 43, 444-453.

Zia, H., Ma, J.K.H., O'donnell, J.P., Luzzi, L.A., 1991. Cosolvency of dimethyl isosorbide for steroid solubility. *Pharm. Res.* 8, 502-504.

Zidan, A.S., Kamal, N., Alayoubi, A., Seggel, M., Ibrahim, S., Rahman, Z., Cruz, C.N., Ashraf, M., 2017. Effect of Isopropyl Myristate on Transdermal Permeation of Testosterone From Carbopol

Gel. J. Pharm. Sci. 106, 1805-1813.

Zimmerman, A., Bai, L., Ginty, D.D., 2014. The gentle touch receptors of mammalian skin. Science 346, 950-954.